# MECHANISM OF ACTION OF TYPE I AND TYPE II COMBI-MOLECULES DESIGNED TO TARGET DNA AND EPIDERMAL GROWTH FACTOR RECEPTOR IN SOLID TUMOURS

By

Margarita Todorova

Department of Medicine
Division of Experimental Medicine
McGill University
Montreal, Canada

October, 2010

A thesis submitted to the Faculty of Graduate Studies and Research in partial fulfillment of the requirements of the degree of Doctor of Philosophy

Copyright © Margarita Todorova, 2010

#### **ABSTRACT**

The overexpression of several receptors and dysfunction of signal transduction pathways characterize the heterogeneity of many solid tumours. Targeted therapies against epidermal growth factor receptor (EGFR)-overexpressing tumours involve well tolerated EGFR inhibitors. However, the potency of these inhibitors is mitigated by several factors including mutations in signaling pathways and receptor heterogeneity. To circumvent this problem, we recently designed a novel strategy that seeks to synthesize molecules "programmed" to release an EGFR inhibitor and a cytotoxic DNA-damaging agent. This led to mixed EGFR-DNA targeting agents, termed "type I combi-molecules". Previous work demonstrated that these compounds: (1) inhibited EGFR and (2) damaged DNA. However, the correlation of their degradation, localization and distribution in the cell with their mechanism of action remained elusive. In this thesis, we designed a fluorescence-labeled combi-molecule AL237 "programmed" to release a blue fluorescent EGFR inhibitor and a green DNA targeting species. The results showed that AL237 blocked EGFR phosphorylation and downstream MAPK pathway, subsequently leading to downregulation of XRCC1 and ERCC1, two DNA repair enzymes. Following demonstration of the ability of AL237 to fully block the MAPK pathway, we studied its localization in the tumour cells by fluorescence microscopy. The results showed that the released quinazoline colocalized with EGFR in the perinuclear region and the green fluorescence was detected in isolated nuclei. This led to a model whereby combimolecule entered the cell, bind to the EGFR at the plasma membrane to prevent signal transduction and abundantly localized in the perinuclear region from where the released alkylating species could diffuse to the nucleus. This mechanism explained the significantly high levels of DNA damaging species in the nuclei of cells expressing EGFR. Further studies exploiting AL237 fluorescence properties demonstrated that its potency did not depend on the P-gp status of the cells. The P-gp independence of AL237 effect was explained by its intracellular degradation that prevented the efflux of the intact structure. Further studies on combi-molecules that do not require hydrolysis to generate the two targeting species (type II combi-molecules) showed that they exhibited potency in the submicromolar range. Studies designed to elucidate the mechanism underlying the exquisite potency of ZR2008 showed that it induced significant levels of apoptosis, independently of the AKT status of the cells. A constant in its potency was its ability to block cells in G1/S and to downregulate the antiapoptotic protein survivin. Our findings suggest that pathways leading to the inhibition of survivin could be a major molecular determinant for the cytotoxicity of ZR2008. The results from this work *in toto* contributed to the elucidation of the mechanism of action of two classes of combi-molecules: type I and type II.

### **RÉSUMÉ**

L'hétérogénéité de la plupart des tumeurs solides est caractérisée par la surexpression de plusieurs récepteurs et le disfonctionnement des voies de transduction des signaux. Les thérapies actuelles contre les tumeurs surexprimant le récepteur du facteur de croissance épidermique (EGFR) utilisent des inhibiteurs de l'EGFR, agents relativement bien tolérés en clinique. Cependant, l'efficacité de ces inhibiteurs est atténuée par plusieurs facteurs tels que les mutations dans les voies de signalisation et par l'hétérogénéité des récepteurs. Pour palier ce problème, nous avons récemment conçu une stratégie basée sur la synthèse des molécules «programmées» pour libérer un inhibiteur de l'EGFR et un agent cytotoxique capable d'endommager l'ADN. Ces molécules, combinant des agents ciblant l'EGFR et l'ADN, sont dénommées «combi-molécules de type I». Les travaux réalisés précédemment au laboratoire ont démontré que ces composés (1) inhibent la phosphorylation de l'EGFR et (2) endommagent l'ADN. Cependant, la corrélation entre leur dégradation, leur localisation et leur distribution au sein de la cellule et leur mécanisme d'action n'a pas encore été élucidée. Au cours de cette thèse de doctorat, nous avons élaboré une combi-molécule, AL237, marquée d'un groupe fluorescent et « programmée» pour libérer un inhibiteur de l'EGFR fluorescant dans le bleu et une entité fluorescant dans le vert ciblant l'ADN. Les résultats ont démontré que AL237 bloque la phosphorylation de l'EGFR et de la voie de signalisation des MAP kinases, accompagnée par la réduction sousjacente de l'expression de XRCC1 et ERCC1: deux enzymes impliquées dans la réparation de l'ADN. Après avoir démontré la capacité de AL237 à bloquer entièrement la voie de signalisation des MAP kinases, nous avons étudié la localisation de cette molécule dans des cellules cancéreuses par microscopie en fluorescence. Les résultats ont montré que la quinazoline libérée est colocalisée avec l'EGFR dans la région périnucléaire et que le signal de fluorescence vert est détecté dans les noyaux isolés. Ces résultats mettent en valeur un modèle ou la combi-molécule entre dans la cellule, s'associe au REGF au niveau de la membrane plasmique, empêchant ainsi la transduction des signaux, puis se localise abondamment dans la région périnucléaire où les espèces alkylantes sont libérées et peuvent ainsi diffuser dans le noyau. Ce mécanisme permet d'expliquer la forte concentration d'espèces ciblant l'ADN observée dans les noyaux des cellules exprimant l'EGFR. D'autre part, des études utilisant les propriétés de fluorescence de AL237 ont démontré que la toxicité de cette molécule n'est pas affectée par la présence de la P-glycoprotéine (P-gp) dans les cellules. Cette observation peut être expliquée par le fait que, AL237 se dégrade intracellulairement en deux petites molécules empêchant ainsi l'efflux de la macrostructure intacte.

Au cours de cette thèse, d'autres travaux ont été réalisés sur des combi-molécules, dites de type II, qui ne nécessitent pas d'hydrolyse pour générer les deux espèces actives et montrent une toxicité élevée à des concentrations submicromolaires. Les études élaborées pour élucider le mécanisme de l'exceptionnelle activité de ZR2008, une combi-molécule exemple de type II, ont montré qu'elle induit des niveaux significatifs d'apoptose indépendamment du statut d'AKT dans les cellules. Une constante dans son activité est sa capacité à bloquer les cellules dans les phases G1/S du cycle cellulaire et à inhiber le niveau de la survivine, une protéine antiapoptotique. Nos résultats suggèrent que les voies de signalisation, menant à l'inhibition de la survivine, pourraient jouer un rôle déterminant pour la cytotoxicité de ZR2008.

En conclusion, les travaux de cette thèse ont contribué à l'élucidation des mécanismes d'action des deux classes de combi-molécules : type I et type II.

#### **ACKNOWLEDGMENTS**

I have been thinking about this moment for a long time. Reaching the destination is nothing compared to the moments I had the chance to experience. As said by a great Chinese spiritual teacher:

"A journey of a thousand miles starts from beneath one's feet."

My gratitude starts with you Dr. Jean-Claude. Thank you for accepting me in your laboratory, for believing in me, giving me the chance to expand my scientific curiosity and to gain invaluable experience. Your supportive and guiding mentorship pushed me to better myself. The generous manner in which you have taught me in research is precious to me, but I am exceptionally grateful for the invaluable life lessons you have provided me, to chase my dreams, be strong and persevering. Thank you for all the uplifting moments that I will cherish forever. It is rare to have a supervisor so devoted to his students and passionate about science, with a generous mind, full of optimism and great ideas. No matter how unsolvable a situation can be, you were always there to shed some light and turn the obstacles into achievements.

Next, I would like to extend my appreciation to all my lab members past and present. Since it has been an amazingly long research journey, it will be hard to name you all, dear friends and colleagues. You will be always in my memories. I am thankful to all of you for being part of this great experience. Thank you for cheering me on, for sharing the moments of sorrow and happiness, for the advice and fruitful discussions and for helping me to carry the load along the way. I will guard forever all the fond memories that made this transition so much easier and enjoyable.

Thank you for everything!

I will end with this quote,

"To attain knowledge, add things every day. To attain wisdom, remove things every day."

Lao-tse, Tao te Ching

### **CONTRIBUTIONS OF AUTHORS**

This manuscript-based thesis is composed of four manuscripts. The contributions of each author are described below.

Chapter 2: This paper was published in Molecular Cancer Therapeutics: 2010, 9 (4) p. 869-882. The chemical synthesis and purification of AL237 were performed by Dr. Anne-Laure Larroque, post-doctoral fellow in our laboratory. The first set of data for fluorescence drug cellular accumulation (Fig. 2.5C) were generated by Sabine Dauphin-Pierre and EGFR binding *in vitro* enzyme assay (Fig. 2.2A) was performed by Dr.You-Qiang Fang. I performed the rest of the experiments and helped with the preparation of the manuscript. Dr Bertrand Jean-Claude revised the manuscript.

Chapter 3: The paper was published in the Journal of Medicinal Chemistry: 2010, 53 (5): p. 2104-13. Compounds chemical synthesis and purification were carried by Dr. Anne-Laure Larroque. AL194 and AL237 compounds degradation was performed by Nahid Golabi by HPCL analysis (Table 3.1). Molecular modeling was done by Dr. Christopher Williams from Chemical Computing Group Inc. (Fig. 3.5). The chemistry synthesis and analysis were performed by Dr. Larroque, as well as the chemistry sections described in the paper. I performed all *in vitro* biology experiments. The manuscript was written by Dr. Larroque and I, and both as co-authors contributed equally for the preparation of the manuscript. Dr Bertrand Jean-Claude made the necessary corrections and revised the manuscript.

Chapter 4: The manuscript is accepted for publication in the Journal of Chemical Biology and Drug Design. The compounds AL414 and AL232 were synthesized by Dr. Anne-Laure Larroque. *In vivo* design of the study and the preparation of the samples were performed by Dr. Qiu Qyiu. Studies of *in vivo* samples were completed by LC/MS and HPLC analyses

performed by Dr. Anne-Laure Larroque. My contribution was the rest of *in vitro* biology experiments. The manuscript is a joint contribution of Dr. Anne-Laure and me. Dr. Bertrand Jean-Claude revised the manuscript.

**Chapter 5:** The manuscript is under revision for publication in the Journal of Cancer Biology and Therapy. All the compounds tested: ZR2003, ZR2008 and ZRMS were synthesized by Dr. Zakaria Rachid. I designed and performed the experiments and contributed with the first draft of the manuscript. Dr. Jean-Claude made the necessary revisions and corrections of the manuscript.

### CONTRIBUTIONS NOT INCLUDED IN THIS THESIS

In addition to the manuscripts included in this thesis, I contributed to the following studies, which have been published:

Rachid Z, MacPhee M, Williams C, **Todorova M** and Bertrand Jean-Claude (2009). Design and synthesis of new stabilized combi-triazenes for targeting solid tumors expressing the epidermal growth factor receptor (EGFR) or its closest homologue HER2. <u>Bioorg Med Chem Lett.</u> **19** (18): 5505-5509.

Banerjee R, Huang Y, McNamee J, **Todorova M** and Bertrand Jean-Claude (2010). The combi-targeting concept: selective targeting of the epidermal growth factor receptor- and Her2-expressing cancer cells by the complex combi-molecule RB24. <u>J Pharmacol Exp Ther</u> **334** (1):9-20.

MacPhee M, Rachid Z, **Todorova M,** Qiu Qiyu, Belinsky G and Bertrand Jean-Claude (2010). Characterization of the potency of epidermal growth factor (EGFR)-DNA targeting combimolecules containing a hydrolabile carbamate at the 3-position of the triazene chain, <u>Investigational New Drugs</u>: 1-13.

### TABLE OF CONTENTS

ABSTRACT	ii
RÉSUMÉ	iv
ACKNOWLEDGMENTS	vi
CONTRIBUTIONS OF AUTHORS	viii
CONTRIBUTIONS NOT INCLUDED IN THIS THESIS	X
TABLE OF CONTENTS	xi
LIST OF FIGURES	xix
LIST OF TABLES	xxi
LIST OF ABBREVIATIONS	xxii
CHAPTER 1: INTRODUCTION	
1.1. PREFACE	
1.2. RECEPTOR TYROSINE KINASES (RTKS)	3
1.3. EGFR FAMILY OF RTKS	3
1.3.1. ROLE OF EGFR IN CANCER	7
1.3.1.1. Aberrations in EGFR expression	
1.3.2. EGFR CRYSTAL STRUCTURE	
1.3.3. EGFR-ACTIVATED SIGNALING PATHWAYS	10
1.3.3.1. Ras/Raf/MEK/ERK cascade	12
1.3.3.2. The lipid kinase cascade-PI3K/AKT/mTOR	
1.3.3.3. JNK/SAPK and p38 kinase signaling cascade	13
1.3.3.4. Phospholipase C (PLCγ) cascade	
1.3.3.5. The JAK/Signal transducers and activator of transcription (STAT) case	
1.3.3.6. EGFR and Src non-receptor tyrosine kinase: special interaction	
1.3.3.7. EGFR and cross-talks	
1.3.4. EGFR INTERNALIZATION	18

1.3.4.1. EGFR degradation through the endosomal pathway	18
1.3.4.1.1. Ligand-dependent	18
1.3.4.1.2. Ligand-independent	20
1.3.4.2. Perinuclear EGFR localization	20
1.3.4.3. Nuclear EGFR localization	21
1.3.4.3.1. Nuclear EGFR and resistance	23
1.4. TARGETED THERAPY FOR CANCER TREATMENT	23
1.4.1. EGFR-targeted agents	23
1.4.1.1. Anti-EGFR antibody	24
1.4.1.2. Small molecules approach	24
1.4.2. DNA TARGETING	26
1.4.2.1. Classical DNA damaging agents	26
1.4.2.1.1. DNA monoalkylating agents and triazenes	27
1.4.2.1.2. Cyclic Triazenes	29
1.4.2.1.3. Nitrosoureas	29
1.4.2.1.4. Nitrogen mustards and crosslinking agents	29
1.4.2.1.5. Platinum agents (cisplatin, carboplatin, oxaliplatin, lipoplatin)	30
1.4.2.2. Types of DNA damage	31
1.4.3. CELL RESPONSE TO DNA DAMAGE	31
1.4.3.1. Phosphoinositide 3-kinase related kinases (PIKKs)	31
1.4.3.2. Induction of cell cycle checkpoints	32
1.4.3.3. p53-mediated cell cycle arrest	34
1.4.3.4. p53-independent mechanism	34
1.4.3.5. Stress-response via JNK/SAPK	35
1.4.3.6. yH2AX as a marker of DNA damage	35
1.4.4. DNA REPAIR ENZYMES	36
1.4 4.1. AGT/MGMT	38
1.4.4.2. Base-excision repair (BER)	38
1.4.4.2.1. Poly (ADP-ribose) polymerase (PARP)	40
1.4.4.2.2. APE1 (apurinic/apyramidinic endonuclease 1/Redox factor-1)	40
1.4.4.2.3. X-ray cross complementing-1 (XRCC1)	41
1 4 4 3 Nucleotide-excision renair (NFR)	41

1.4.4.4. Mismatch repair (MMR)	43
1.4.4.5. Homologous recombination (HR) and non-homologous end-joining (NHEJ)	)45
1.4.4.5.1. Non-homologous end-joining (NHEJ).	45
1.4.4.5.2. Homologous recombination (HR).	45
1.4.4.6. Summary on DNA repair enzymes	47
1. 5. CELL DEATH MECHANISMS	47
1.5.1. EXTRINSIC APOPTOTIC PATHWAY	48
1.5.2. Intrinsic mitochondria-mediated apoptosis	48
1.5.3. AKT ANTI-APOPTOTIC TARGETS	49
1.5.3.1. Member of IAP family, survivin	50
1.6. RESISTANCE TO CANCER THERAPY	51
1.6.1. MULTI-DRUG RESISTANCE (MDR)	51
1.6.2. P-GLYCOPROTEINS	52
1.7. COMBINATION THERAPY FOR TREATMENT OF SOLID TUMOURS	53
1.7.1. CLASSICAL COMBINATIONS	53
1.7.1.1. DNA-damaging agents and their limitations	53
1.7.1.2. Limitations of tyrosine kinase inhibitors	53
1.7.1.3. Advances with multi-drug combination strategy	54
1.7.2. COMBI-TARGETING APPROACH	54
1.7.2.1. First generation of combi-molecules	56
1.7.2.2. Combi-molecules with improved water solubility, stability and EGFR binding	<b>g</b> .56
1.7.2.3. Cascade-release targeting combi-molecules	57
1.7.2.4. Combi-nitrosoureas	58
1.7.2.5. Classes of combi-molecules-type I and type II	58
1.7.2.6. Examples of type II combi-molecules	59
1.7.2.7. Labeling combi-molecules for cellular distribution	59
1.8 RESEARCH OBJECTIVES	61
1.8.1. Project outline	61
1 0 DEFEDENCES	63

CHAPTER 2:SUBCELLULAR DISTRIBUTION OF A FLUORESCENCE-LABE	LED
COMBI-MOLECULE DESIGNED TO BLOCK EGFR TYROSINE KINASE AND	D
DAMAGE DNA WITH A GREEN FLUORESCENT SPECIES	84
2.1. ABSTRACT	85
2.2. INTRODUCTION	86
2.3. MATERIALS AND METHODS	88
2.3.1. CELL CULTURE	88
2.3.2. Drug treatment	88
2.3.3. GROWTH INHIBITION ASSAY	91
2.3.4. IN VITRO ENZYME ASSAY	91
2.3.5. WESTERN BLOT ANALYSIS	92
2.3.6. ALKALINE COMET ASSAY	93
2.3.7. NEUTRAL COMET ASSAY	93
2.3.8. Intracellular fluorescence by UV flow cytometry	93
2.3.9. NUCLEAR FLUORESCENCE UV FLOW CYTOMETRY	94
2.3.10. IMMUNOFLUORESCENCE OF EGFR AND PHOSPHO-TYROSINE	94
2.3.11. LIVE CELL FLUORESCENCE IMAGING OF AL237 IN NIH 3T3 CELLS	95
2.3.12. Immunofluorescence of phospho-γH2AX	95
2.3.13. ANNEXIN V/PI BINDING ASSAY	96
2.4. RESULTS	96
2.4.1. Analysis of binary EGFR-DNA targeting potentials	96
2.4.1.1. Inhibition of EGFR phosphorylation	96
2.4.1.2. Inhibition of downstream signaling	99
2.4.1.3. Induction of DNA damage in MDA-MB-468 breast cancer cells	99
2.4.1.4. Induction of apoptosis in MDA-MB-468 breast cancer cells	100
2.4.2. IMAGING OF AL237 IN MDA-MB-468 HUMAN BREAST CANCER CELLS AND N	Н 3Т3
TRANSFECTANTS	104
2.4.2.1. Imaging of MDA-MB-468 cells treated with AL237	104
2.4.2.2. Qualitative analyses of isogenic NIH 3T3 EGFR/ErbB2 transfectants	104
2.4.2.3. Co-localization of EGFR and AL237 in MDA-MB-468 cells	108

2.4.3. SELECTIVE NUCLEAR LOCALIZATION AND GROWTH INHIBITION	109
2.4.3.1. Quantitative and qualitative nuclear analysis	109
2.4.3.2. Selective growth inhibition of EGFR expressing MDA-MB-468 and NIH	3 <i>T3</i>
cells	112
2.5. DISCUSSION	112
2.6. ACKNOWLEDGMENTS	117
2.7. CONNECTING TEXT	117
2.8 REFERENCES	119
CHAPTER 3: SYNTHESIS AND UPTAKE OF FLUORESCENCE-LABELED	
COMBI-MOLECULES BY P-GLYCOPROTEIN-PROFICIENT AND -DEFICIEN	T
UTERINE SARCOMA CELLS MES-SA AND MES-SA/DX5	123
3.1. ABSTRACT	124
3.2. INTRODUCTION	125
3.3. RESULTS AND DISCUSSION	126
3.3.1. CHEMISTRY	126
3.3.2. HALF-LIFE IN A SERUM-CONTAINING MEDIUM	127
3.3.3. DIFFERENTIAL GROWTH INHIBITORY ACTIVITY	130
3.3.4. CELLULAR UPTAKE	132
3.3.5. DNA DAMAGE	135
3.4. CONCLUSION	139
3.5. EXPERIMENTAL SECTION	139
3.5.1. CHEMISTRY	139
3.5.1.1. Compound 1, 2-dansyl-9-fluorenylmethyl N-(2-aminoethyl)carbamate	140
3.5.1.2. Compound 2, Dansyl-N-(2-aminoethyl)amide	140
3.5.1.3. Compound 5, Dansyl-N-(2-[(2-aminoethyl)-N-methylamino]-ethyl)amide .	141
3.5.1.4. Compound 4	141
3.5.1.5. Compound 6	142
3.5.2. HALF-LIVES	143
3.5.3. MOLECHLAR MODELING	143

3.5.4. BIOLOGY	144
3.5.4.1. Cell culture	144
3.5.4.2. Drug treatment	144
3.5.4. BIOLOGY 3.5.4.1. Cell culture 3.5.4.2. Drug treatment 3.5.4.3. Growth inhibition assay 3.5.4.4. DNA damage by alkaline comet assay 3.5.4.5. Fluorescence microscopy 3.5.4.6. Flow cytometry analysis of intracellular drug fluorescence 3.6. ACKNOWLEDGMENTS 3.7. CONNECTING TEXT 3.8. REFERENCES CHAPTER 4: SYNTHESIS AND STUDIES ON 3-COMPARTEMENT FLAVO CONTAINING COMBI-MOLECULES DESIGNED TO TARGET EGFR, DNA MEK 4.1 ABSTRACT 4.2 INTRODUCTION 4.3 RESULTS 4.3.1. CHEMISTRY 4.3.2. DNA DAMAGE. 4.3.3.1. EGFR phosphorylation 4.3.3.2 MEK/ERKI,2 inhibition 4.3.3.2 MEK/ERKI,2 inhibition 4.3.4. SELECTIVE GROWTH INHIBITION AND CELL DEATH BY APOPTOSIS 4.3.5. IN VIVO METABOLISM 4.3.6. ACTIVITY OF SPECIES 1 (COMPOUND 9) 4.4. DISCUSSION AND CONCLUSION 4.5.1. CHEMISTRY 4.5.1.1. Compound 7a (AL232)	144
3.5.4.1. Cell culture 3.5.4.2. Drug treatment. 3.5.4.3. Growth inhibition assay. 3.5.4.4. DNA damage by alkaline comet assay. 3.5.4.5. Fluorescence microscopy 3.5.4.6. Flow cytometry analysis of intracellular drug fluorescence. 3.6. ACKNOWLEDGMENTS. 3.7. CONNECTING TEXT. 3.8. REFERENCES. CHAPTER 4: SYNTHESIS AND STUDIES ON 3-COMPARTEMENT FLAVO CONTAINING COMBI-MOLECULES DESIGNED TO TARGET EGFR, DNA MEK. 4.1 ABSTRACT. 4.2 INTRODUCTION. 4.3 RESULTS. 4.3.1. CHEMISTRY 4.3.2. DNA DAMAGE. 4.3.3. EGFR AND MEK TARGETING. 4.3.3.1. EGFR phosphorylation. 4.3.3.2 MEK/ERK1,2 inhibition. 4.3.4. SELECTIVE GROWTH INHIBITION AND CELL DEATH BY APOPTOSIS. 4.3.5. IN VIVO METABOLISM. 4.3.6. ACTIVITY OF SPECIES 1 (COMPOUND 9). 4.4. DISCUSSION AND CONCLUSION.	145
3.5.4.5. Fluorescence microscopy	146
3.5.4.1. Cell culture 3.5.4.2. Drug treatment 3.5.4.3. Growth inhibition assay 3.5.4.4. DNA damage by alkaline comet assay 3.5.4.5. Fluorescence microscopy 3.5.4.6. Flow cytometry analysis of intracellular drug fluorescence 3.6. ACKNOWLEDGMENTS 3.7. CONNECTING TEXT 3.8. REFERENCES CHAPTER 4: SYNTHESIS AND STUDIES ON 3-COMPARTEMENT FLAVICONTAINING COMBI-MOLECULES DESIGNED TO TARGET EGFR, DNAMEK 4.1 ABSTRACT 4.2 INTRODUCTION 4.3 RESULTS 4.3.1. CHEMISTRY 4.3.2. DNA DAMAGE 4.3.3.1. EGFR phosphorylation 4.3.3.2 MEK/ERK1,2 inhibition 4.3.4. SELECTIVE GROWTH INHIBITION AND CELL DEATH BY APOPTOSIS 4.3.5. IN VIVO METABOLISM 4.3.6. ACTIVITY OF SPECIES 1 (COMPOUND 9) 4.4. DISCUSSION AND CONCLUSION 4.5. EXPERIMENTAL SECTION 4.5.1.1. Compound 7a (AL232)	146
3.6. ACKNOWLEDGMENTS	147
3.7. CONNECTING TEXT	147
3.8. REFERENCES	149
CHAPTER 4: SYNTHESIS AND STUDIES ON 3-COMPARTEMENT FLA	VONE-
CONTAINING COMBI-MOLECULES DESIGNED TO TARGET EGFR, D	NA AND
MEK	152
4.1 ABSTRACT	153
4.2 INTRODUCTION	154
4.3 RESULTS	155
4.3.1. CHEMISTRY	155
4.3.2. DNA DAMAGE	158
4.3.3. EGFR AND MEK TARGETING	158
4.3.3.1. EGFR phosphorylation	158
4.3.3.2 MEK/ERK1,2 inhibition	161
4.3.4. SELECTIVE GROWTH INHIBITION AND CELL DEATH BY APOPTOSIS	161
4.3.5. IN VIVO METABOLISM	166
4.3.6. ACTIVITY OF SPECIES 1 (COMPOUND 9)	166
4.4. DISCUSSION AND CONCLUSION	166
4.5. EXPERIMENTAL SECTION	169
4.5.1. CHEMISTRY	169
4.5.1.1. Compound 7a (AL232)	169
4512 Compound 7h (AI 414)	169

4.5.1.3. Compound 9	
4.5.2 BIOLOGY	171
4.5.2.1. Cell culture	171
4.5.2.2. Drug treatment	171
4.5.2.3. Growth inhibition assay	171
4.5.2.4. DNA damage by alkaline comet assay	172
4.5.2.5. In vitro Enzyme Assay	172
4.5.2.6. Western blot analysis	173
4.5.2.7. Annexin V/PI binding assay	174
4.5.2.8. In vivo analysis by LC/MS	174
4.6. CONNECTING TEXT	175
4.7. REFERENCES	176
CHAPTER 5: CYTOKINETICS OF POTENT TYPE II EGFR-DNA TA	RGETING
COMBI-MOLECULES IN OVARIAN CANCER CELLS	179
5.1. ABSTRACT	
5.2. INTRODUCTION	181
5.3. MATERIAL AND METHODS	183
5.3.1. CELL CULTURE	183
5.3.2. DRUG TREATMENT	183
5.3.3. GROWTH INHIBITION ASSAY	183
5.3.4. IN VITRO ENZYME ASSAY	184
5.3.5. DNA DAMAGE BY ALKALINE COMET ASSAY	184
5.3.6. ANNEXIN V/ PROPIDIUM IODIDE BINDING ASSAY	185
5.3.7. FLOW CYTOMETRY CELL CYCLE DISTRIBUTION ANALYSIS	185
5.3.8. WESTERN BLOT ANALYSIS	186
5.4. RESULTS	187
5.4.1. GROWTH INHIBITORY ACTIVITY	187
5.4.2. EGFR SIGNALING	187
5.4.2.1. Inhibition of EGFR TK activity	187
5.4.2.2. EGFR. ERK1.2 and AKT phosphorylation in whole cells	189

5.4.3. DNA DAMAGE	
5.4.3.1. Alkaline comet assay	189
5.4.3.2. Phosphorylation of histone H2AX	192
5.4.4. CELL CYCLE ARREST AND APOPTOTIC RESPONSE	192
5.4.4.1. Cell Cycle Perturbation	192
5.4.4.2. Activation of the stress response pathway	192
5.4.4.3. PARP1 cleavage as an indicator of apoptosis	197
5.4.4.4. Induction of p53 in TOV21G cells	197
5.4.4.5. Apoptosis by Annexin V binding	197
5.4.4.6. Survivin accumulation	203
5.4.3.1. Alkaline comet assay	203
5.6. ACKNOWLEDGMENTS	206
5.7. REFERENCES	207
CHAPTER 6: GENERAL DISCUSSION AND CONTRIBUTION TO	O KNOWLEDGE
•••••	212
6.1 GENERAL DISCUSSION AND CONTRIBUTION	213
6.1.1. CONTRIBUTION 1	214
6.1.2. CONTRIBUTION 2	217
6.1.3. CONTRIBUTION 3	218
6.1.4. CONTRIBUTION 4	220
6.2 CONCLUSIONS	221
6.3. REFERENCES	222
APPENDIY	226

### LIST OF FIGURES

<u>CHAPTER 1</u>
$\textbf{Figure 1.1}. \ \textbf{Structural motifs, regulatory elements and important residues for EGFR function}5$
Figure 1.2. Downstream signaling pathways of EGFR activation
<b>Figure 1.3.</b> Steps in EGFR recycling or degradation
Figure 1.4. Cell cycle checkpoints and regulators in response to DNA damage33
<b>Figure 1.5.</b> Type of DNA damage, DNA repair pathways and enzymes involved37
<b>Figure 1.6.</b> The three main DNA repair pathways induced by monoalkylating agents39
<b>Figure 1.7.</b> DNA repair of O <sup>6</sup> -meG in AGT-deficient cells
Figure 1.8. Steps and proteins involved in NHEJ (A) and HR (B) DNA repair pathways46
Figure 1.9. Principle of combi-targeting and combi-molecule distribution in the cell55
Figure 1.10. Type I and type II combi-molecules
CHAPTED 2
CHAPTER 2
<b>Figure 2.1</b> . Structure and stepwise decomposition of AL23790
<b>Figure 2.2</b> . AL237 inhibits EGFR phosphorylation and downstream signaling98
Figure 2.3. DNA damage induced by AL237 in MDA-MB-468.
Figure 2.4. Annexin V binding in MDA-MB-468 cells
Figure 2.5. Cellular fluorescence of AL237 and EGFR in MDA-MB-468 and NIH 3T3, NIH
3T3her14, NIH 3T3neu cells
Figure 2.6. Nuclear accumulation of AL237 and N-dansylaziridine in NIH 3T3, NIH 3T3her14
and NIH 3T3neu cells
<b>Figure 2.7.</b> Selective growth inhibition by AL237 in NIH 3T3 and MDA-MB-468 cells113
CHAPTER 3
Figure 3.1. Synthesis of compound 4
Figure 3.2. Synthesis of compound 6
Figure 3.3. Degradation pathway of compound 6 in physiological conditions131
<b>Figure 3.4.</b> Degradation pathway of compound <b>4</b> in physiological conditions
<b>Figure 3.5</b> . Molecular modeling using AM1 semi-empirical calculation of 6

Figure 3.6. Growth inhibition of doxorubicin, 4 and 6 by SRB assay.	134
Figure 3.7. Cellular fluorescence and DNA damage by doxorubicin	136
Figure 3.8. Cellular uptake of 4 and 6 by fluorescence microscopy and FACS	137
Figure 3.9. DNA damage induced by 4 and 6.	138
CHAPTER 4	
<b>Figure 4.1.</b> Biodegradation of the combi-molecule AL414	156
<b>Figure 4.2.</b> Synthesis pathway of AL232 and AL414.	157
<b>Figure 4.3.</b> Synthesis pathway of compound <b>9</b> .	157
Figure 4.4. DNA damage by AL414 in MDA-MB-468, DU145 and MES-SA cells	160
Figure 4.5. Inhibition of EGFR phosphorylation and downstream activation.	163
<b>Figure 4.6.</b> Selective growth inhibition by AL414, AL232 and Iressa	164
<b>Figure 4.7.</b> Apoptosis by Annexin V binding assay in DU145 cells.	165
<b>Figure 4.8.</b> LC/MS spectrum of AL414 metabolites observed in mouse plasma	167
CHAPTER 5	
<b>Figure 5.1.</b> Antiproliferative effects of ZR2003, ZR2008, ZRMS and gefitinib on four hum	nan
ovarian cancer cells with different levels of EGFR expression	188
<b>Figure 5.2.</b> Inhibition of EGF-induced EGFR phosphorylation and downstream signaling.	191
<b>Figure 5.3.</b> Quantitation of DNA damage induced by ZR2008 the panel of ovarian cells	194
<b>Figure 5.4.</b> Cell cycle distribution after 24 h treatment with ZR2008	196
<b>Figure 5.5.</b> Activation of apoptotic and stress-induced proteins by ZR2008	198
<b>Figure 5.6.</b> Induction of cell death by apoptosis in the ovarian cell lines.	202
CHAPTER 6	
<b>Figure 6.1.</b> Degradation of type I combi-molecules at the perinuclear region	216

### LIST OF TABLES

### CHAPTER 1

Table 1.1. Association of intracellular proteins with EGFR tyrosine residues	6
Table 1.2. Increased EGFR expression in tumours.	8
<b>Table 1.3.</b> Chemical structures of clinically approved ErbB family tyrosine kinase	
inhibitors	25
<b>Table 1.4.</b> Clinical DNA damaging agents and DNA repair responses	28
CHAPTER 3	
Table 3.1 Half-life of compound 4 and 6 in a serum-containing medium	129
<u>CHAPTER 4</u>	
<b>Table 4.1.</b> Growth inhibitory potency of AL414 on a panel of EGFR and non-EGFR	
expressing cancer cell lines.	167

### LIST OF ABBREVIATIONS

ABC ATP-binding cassette

AGT O<sup>6</sup>-alkylguanine transferase

AIF apoptosis-inducing factor

Alk alkylating species

AP-1 clathrin-associated protein complex from the trans-golgi network

APAF-1 apoptosis protease activating factor 1

APE1 apurinic/apyramidinic endonuclease 1

ASK<sup>a</sup> activator of S-phase kinase group

ASK1<sup>b</sup> apoptosis signal-regulating kinase 1

ATF activating transcription factor

ATM ataxia-telangiectasia, mutated

ATR ataxia telangiectasia and Rad3-related

BAD Bcl-2 antagonist of cell death

BID BH3-interacting domain death agonist

BAX Bcl-2 associated protein X

Bcl B-cell lymphoma 2

BCTIC 5-[3,3-bis(2-chloroethyl)-1-triazene] imidazole-carboxamide

BCNU 1,3-bis(2-chloroethyl)-1-nitrosourea

BER base excision DNA repair pathway

BG O6-benzylguanine

BRAC breast cancer susceptibility gene

BTG O6-bromotenyl guanine

Cdc cell division cycle

Cdk cyclin-dependent kinase

CHK checkpoint kinase

COX-2 cyclooxygenase-2

DDB2 DNA damage binding protein

DNA-PK DNA-dependent protein kinase

DMEM dulbecco's modified eagle medium

DMF dimethyl fluoride

DMSO dimethyl sulfoxide

DSB double strand break

EGF epidermal growth factor

EGFR/ErbB1/HER1 epidermal growth factor receptor

ELISA enzyme-linked immunosorbent assay

ErbBs epidermal growth factor receptors

ERCC1 excision repair cross-complementation group 1

ERGs early response genes

ERK extracellular signal-regulated kinase

FACS fluorescence-activated cell sorting

FANC fanconi anemia complementation group

FAK focal adhesion kinase

FBS fetal bovine serum

FGFR fibroblast growth factor receptors

FITC fluorescein isothiocyanate

GADD45 Growth Arrest and DNA Damage

GF growth factor

GPCR G-protein coupled receptor

Grb2 growth factor receptor binding protein 2

HER2/neu/ErbB2 human epidermal growth factor receptor 2

H2AX histone H2A variant

HGFR hepatocyte growth factor receptor

HIF-1α hypoxia-inducible factor-1-alpha

HPLC high pressure liquid chromatography

HR homologous recombination

HRP horseradish peroxidise

Hsp heat shock protein

I inhibitor (ErbB1 TKI)

IAP inhibitor of apoptosis protein

IC<sub>50</sub> 50 % of inhibitory concentration

IGF insulin-like growth factor

IGFR insulin growth factor receptors

iNOS inducible nitric oxide synthase

JNK c-jun-N-terminal protein kinase

MAP mitogen-activated protein

MAPK mitogen-activated protein kinase

Mcl-1 myeloid cell leukaemia-1

MDC1 mediator of DNA damage checkpoint protein 1

MDR multi-drug resistance

MDM2 mouse double mutant 2

MEK MAPK/ERK kinase

MGMT O6-methyl-guanine-DNA methyl-transferase

MSH-MLH MutS homolog-MutL homolog complex

MMR mismatch repair

MRP multidrug resistance-related protein

MTIC 5-(3-methyltriazin-1-yl) imidazole-4-carbomide

mTOR mammalian target of rapamycin

MVB multivesicular bodies

NER nucleotide excision repair

NF-κB nuclear factor kappa-light-chain-enhancer of activated B cells

NHEJ non-homologous end-joining

NOVA neuro-oncological ventral antigen

NSCLC non-small-cell lung cancer

PARP poly (ADP-ribose) polymerase

PBS phosphate-buffer saline

PCNA proliferating cell nuclear antigen

PDGFR platelet-derived growth factor receptor

PE pycoerythrin

P-gp P-glycoprotein

PGT poly(L-glutamic acid-L-tyrosine,4:1)

PH phospholipid

PI propidium iodide

PI3K phosphatidylinositol 3-kinase

PIKK phosphoinositide 3-kinase related kinases

PKB protein kinase B

PKC protein kinase C

PLC phospholipase C

PTB phosphotyrosine-binding domains

PtdIns phosphatidylinositol triphosphate

PUMA p53 upregulated modulator of apoptosis

Rb retinoblastoma

RTK receptor tyrosine kinase

SAPK stress-activated protein kinase

SAR structure activity relationship

SH2 Src homology 2

SMAC second mitochondria-derived activator of caspases

SMG1 suppressor with morphological effect on genitalia 1

SRB sulforhodamine B

SSB single strand break

STAT signal transducers and activator of transcription

TEM temozolomide, Temodal<sup>TM</sup>

TF transcription factor

TGF-α transforming growth factor-alpha

TK tyrosine kinase

TKI tyrosine kinase inhibitors

TRRAP transformation/transcription domain-associated protein

TZ triazene (DNA damaging moiety)

VEGF vascular endothelial growth factor

VEGFR vascular endothelial growth factor receptor

XIAP X-linked mammalian inhibitor of apoptosis protein

XP xeroderma pigmentosum

XRCC1 X-ray repair cross-complementing group

## Chapter 1

INTRODUCTION

#### 1.1. PREFACE

The response rate to chemotherapy for most advanced solid tumour is about 50% in first-line treatments and about 10-15% in second- or third-line treatments [1, 2]. Despite the improved response rate with the advances in chemotherapy, no major difference in long-term survival has been achieved in many cancers including lung, pancreatic, brain, ovarian and melanoma. The success rate of single-targeted anti-cancer agents is extremely low and this debility is believed to be due to targeted heterogeneity of solid tumours at the advanced stages [3, 4]. In order to increase response rates in several tumours, classical DNA-damaging agents are combined with other agents with different mechanism of action (e.g., anti-tubulin, topoisomerase inhibitors and anti-metabolites) [5, 6].

Recently, with the emergence of several kinase inhibitors, which are mostly cytostatic agents, novel combinations directed at interactions with cell signaling mechanisms are being developed. One such mechanism is growth signaling induced by growth factors, such as epidermal growth factor (EGF). The EGF receptor (EGFR) is known to be overexpressed in many solid tumours including lung, breast, ovarian, prostate and brain. Currently, several trials are ongoing involving the combinations of classical DNA alkylators (Temozolomide, Cyclophosphamide) with EGFR inhibitors (Iressa<sup>TM</sup>, Tarceva<sup>TM</sup>, lapatinib) [7-12].

Recently, with the purpose of directly targeting cytotoxic agents to EGFR-overexpressing tumour, our laboratory designed a novel strategy that sought to combine a DNA alkylating function with EGFR-targeting warheads in order to selectively target tumours with EGFR-related disordered signaling [13-16]. The purpose of the current work being to investigate the mechanism of action of these novel agents, here we will review the biology of EGFR and responses associated with DNA damage and repair.

### 1.2. RECEPTOR TYROSINE KINASES (RTKs)

The most important requirement for normal cell function in the context of a multicellular organism is the ability of each individual cell to be part of a cellular network. By responding to external signals and connecting with the surrounding cell environment, cells are enabled to perform important functions. For an extracellular message to be transmitted in response to growth factors (GFs), it requires activation of various cell surface receptors including receptor tyrosine kinases (RTKs). By transmitting the extracellular signal across the membrane and through the intracellular signaling cascades, RTKs elicit signals for proliferation, growth, survival, cell-cell interactions, cell differentiation and development [17, 18]. Some of the most important RTKs include the following families of receptors: vascular endothelial growth factor receptors (VEGFRs), fibroblast growth factor receptors (FGFR), insulin growth factor receptors (IGFRs), platelet-derived growth factor receptors (PDGFRs), hepatocyte growth factor receptors (c-Met, HGFRs), neurotrophin receptors and epidermal growth factor receptors (EGFRs). Since the EGFR family of receptors is the main focus of this thesis, normal and mutagenic signaling pathways originating from the activation of these receptors will be discussed [18, 19].

### 1.3. EGFR FAMILY OF RTKs

EGFR (ErbB) family of RTKs consists of four human epidermal receptors (HER1-4). EGFR, also known as HER1 or ErbB1, is a 170-kD glycoprotein that consists of an extracellular ligand-binding domain, a hydrophobic transmembrane region, and an intracellular tyrosine kinase (TK) domain (Fig. 1.1). Ligands for EGFR include EGF, transforming growth factoralpha (TGF-α), amphiregulin, heparin-binding EGF, β-cellulin, and epiregulin [7, 20]. Existing as an inactive monomer on the cell membrane, each of these four HER transmembrane proteins

clusters on the cell surface to facilitate interactions between each other upon ligand binding. EGFR homo- or hetero-dimerization with other receptors from ErbB family (eg, HER2/neu, HER3, or HER4) results in TK activation and autophosphorylation of key tyrosine residues, followed by recruitment of a myriad of intracellular proteins initiating downstream signaling [19, 21, 22]. The C-terminus kinase domain of EGFR contains several important tyrosine residues with the most common phosphorylation sites listed (Y845, Y992, Y1068, Y1086, Y1101, Y1148, Y1173) [19, 23, 24]. These sites can be either auto- or trans-phosphorylated upon dimerization and serve as substrates for other tyrosine kinases (TKs) to transmit the signal. A schematic diagram of the phosphorylated tyrosine residues on the C-terminus of the receptor (Fig. 1.1) with the characterized adaptor proteins recruited at specific sites are summarized in Table 1.1. The modular nature of interactions of proteins at these phosphorylated residues via phosphotyrosine-Src homology 2 (SH2) and phosphotyrosinebinding (PTB) domains defines the specificity of signal transduction [25]. From the extracellular GF stimulation, the protein signaling network enables the activation of the downstream components that transduce the signals down to the nucleus for tightly regulated transcription of a group of genes termed early response genes (ERGs, e.g., c-jun, c-fos, c-myc, c-myb, egr-1) [19].

While EGFR stimulation is required for normal cell growth, cell division and cell viability, abnormal EGFR expression and signaling lead to cell transformation and tumorigenesis [26, 27].

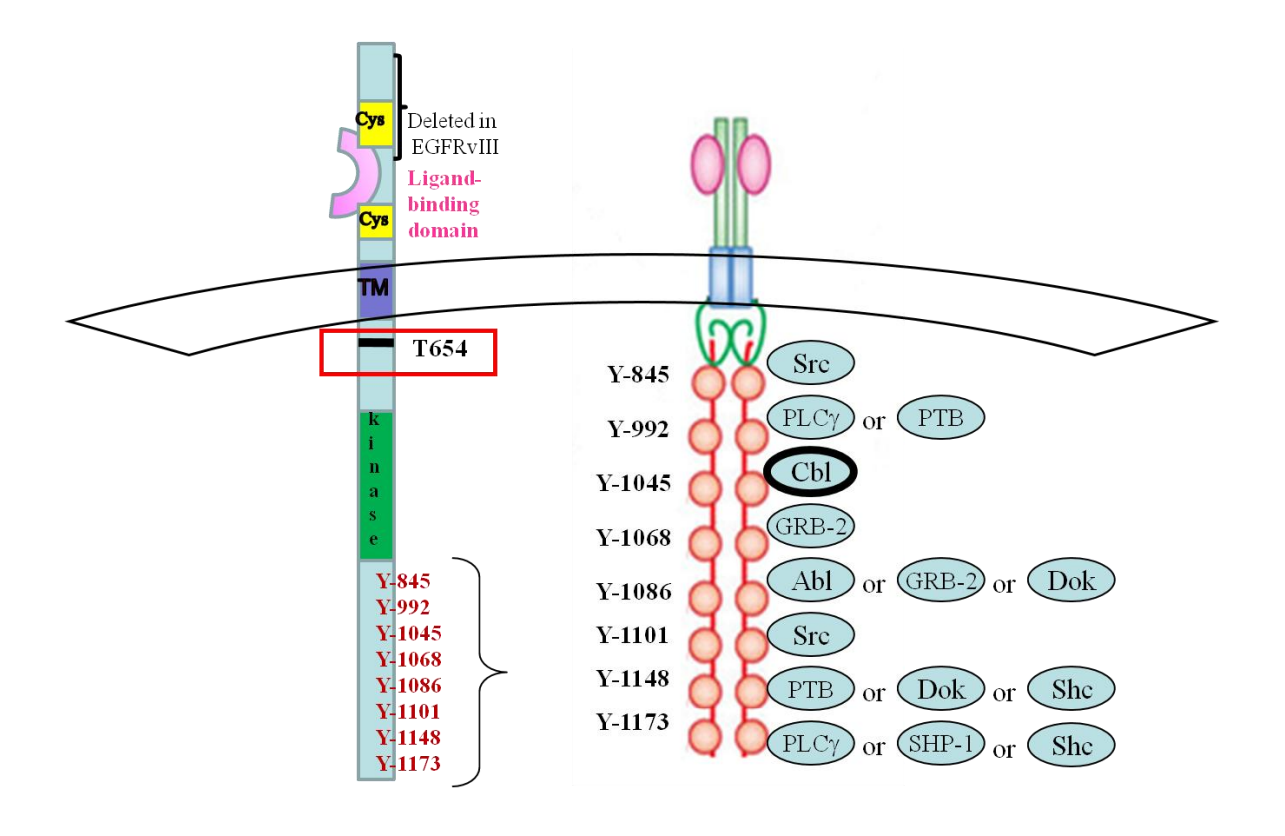


Figure 1.1. Structural motifs, regulatory elements and important residues for EGFR function.

The extracellular domain of the receptor consists of two cystein-rich domains (Cys) surrounding the ligand binding domain. The transmemembrane (TM) domain, followed by the intracellular kinase domain encompasses several tyrosine residues (Y) important for receptor phosphorylation and recruitment of specific adaptor proteins (Table 1.1). Threonine 654 (T-654) is important for protein kinase C interaction and mediates nuclear localization of the receptor. c-Cbl recruitment at Y-1045 with several other important residues triggers EGFR internalization in endosomes for receptor recycling or degradation [28-30].

**Table 1.1.** Association of intracellular proteins with EGFR tyrosine residues.

Intracellular Proteins	Docking sites on EGFR	Reference
Grb2	pY-1068, pY-1086	[31]
Nck	pY-992, pY-1086	[32]
Crk	pY-1068	[33]
Dok	pY-1086, pY-1148	[34]
Ras	pY-992	[35]
PTB-1B	pY-992, pY-1148	[36]
SHP1	pY-1173	[37]
Abl	pY-1086	[38]
c-Src	Y-845, pY-891, pY-920, Y-1086, Y-1101	[24, 39-42]
Shc	pY-1148, pY-1173	[43]
PLCγ	Y-1173, pY-992	[44]
PKC	Thr-645	[45]

#### 1.3.1. Role of EGFR in cancer

The link between EGFR and cancer was established in the early 1980s by the characterization of the avian erythroblastosis virus v-erbB gene. EGFR is the cellular homolog (proto-oncogene) of the viral v-erbB (oncogene) which is a truncated form of EGFR that lacks the extracellular domain and exhibits several intracellular mutations at the C-terminus, resulting in ligand-independent dimerization and receptor phosphorylation [46]. The oncogenic properties of EGFR have been demonstrated by Velu et al. [47] with the observation that cells overexpressing the receptor became transformed when grown in the presence of EGF. Thereafter, the oncogenicity of EGFR has been confirmed by a large number of animal studies [48]. Since EGFR is expressed normally in a broad range of cell types throughout development, any aberrant expression and regulation results in constitutive signaling for growth and cell tumorigenesis [49]. The average percentage of EGFR overexpressing solid tumours from different tissues (e.g., prostate, breast, ovarian, brain, colorectal, non-small-cell lung, head and neck) are summarized in the Table 1.2 [50].

The oncogenic potentials of EGFR are clearly and concisely defined by Khazaie *et al.* [49]: "The receptor can transmit signals to cells: i) upon interaction with ligands such as EGF, TGF alpha, amphiregulin or heparin binding EGF, ii) upon truncation or mutation of extracellular and/or intracellular domains, iii) upon amplification of a basal receptor activity (in the absence of ligand) through cooperation with other cellular signaling pathways or nuclear events (e.g. expression of *v-erbB*). The activated EGFR can exert pleiotropic functions on cells, depending on their tissue origin and state of differentiation. Under certain conditions it can also contribute to neoplasia and development of metastases. Such conditions can exist upon aberrant receptor/ligand expression and activation."

**Table 1.2.** Increased EGFR expression in tumours.

Increased EGFR observed in tumours	Percentage expression
Head and Neck	80-100
Breast	14-91 (~35 %)
Kidney	50-90
Uterus, cervix	90
Oesophagus	43-89
Lung (NSCLC)	40-80
Colon-Rectum	25-77
Stomach	33-74
Ovaries	35-70
Prostate	65
Glioma	40-63
Pancreas	30-50
Bladder	31-48

### 1.3.1.1. Aberrations in EGFR expression

The most common abnormalities leading to constitutive EGFR activation are: (1) accumulation of active mutations, (2) deletions of domains that cause ligand-independent constitutive activation, (3) transcriptional or translational changes that lead to EGFR overexpression, (4) mutations that prevent EGFR internalization and receptor inactivation [51, 52]. The most common mutant form of EGFR, known as EGFRvIII deletion (in frame deletion of exons 2 to 7 spanning the extracellular ligand-binding domain) is amplified in about 45% in glioblastomas.

The EGFRvIII form is also observed in head and neck squamous cell carcinoma, non-small-cell lung cancer (NSCLC), breast and ovarian cancer. Specific point mutations of EGFR are common for NSCLC, while EGFR gene amplifications are characteristic for breast carcinomas. In many cases where no gene amplification is observed, EGFR overexpression leads to transcriptional and translational changes that result from increased activation of EGFR promoter or dysregulation at a translational level [53]. Multiple EGFR mutations are also detected in human head and neck, prostate and colon cancers. These mutations occur either in: (1) the extracellular domain, (2) the intracellular domain, (3) specific residues at the tyrosine kinase domain, and (4) loss of sensitivity to its ligand [51, 54].

The interest in EGFR as a good anti-cancer target began more than 20 years ago [55, 56]. Recognising the central role of EGFR and ErbB2 in broad range of tumours marked these receptors as good molecular targets for anti-cancer therapy. Blocking the pleiotropic signals originating from EGFR/ErbB2 receptors' activation would disrupt the signals for cell proliferation, resistance to cell death, cell migration and invasion leading to cancer progression. Moreover, better understanding of the signaling pathways downstream of mutant EGFR variants could be beneficial to assign the right treatment, to predict and evaluate correctly a therapeutic response. Therefore, to improve current EGFR targeting strategies and develop new drug design approaches for selectively targeting EGFR and its downstream signaling are the primary focus of this thesis.

### 1.3.2. EGFR crystal structure

With the three-dimensional structure of EGFR resolved in the early 2000, a major advancement in the understanding of many other receptors has been achieved [57, 58]. Using point mutants or deletion mutants of EGFR significantly advanced our understanding about the mechanisms

regulating EGFR activity with the key amino acid residues involved [59]. More importantly, the atomic structure obtained permitted a large number of structure-activity studies with a series of EGFR tyrosine kinase inhibitors (TKI) [60-63]. The two types of inhibitors (e.g., anilinoquinazoline, pyrido[d]pyrimidines) have been crystallized with the receptor demonstrating Met-769 and Thr-766 residues at the active ATP site of EGFR as the key residues involved in hydrogen bonding with N1 and N3 of the quinazoline respectively. Moreover, quinazolines with a reactive group coupled at the 6- and 7-position on the ring can covalently interact with Cys-773 of EGFR, thus irreversibly inhibiting the receptor [61, 62]. These findings greatly advanced our understanding of interactions between inhibitors and the ATP site of EGFR.

# 1.3.3. EGFR-activated signaling pathways

Upon binding of a ligand to EGFR, followed by dimerization and phosphorylation of the critical tyrosine residues, different adaptor proteins are recruited [19, 25]. Through these adaptor proteins, various effector proteins coordinate, amplify and transmit multiple signal transduction pathways. The diverse recruitment and specific protein interactions define the signals downstream and the activation of target genes [64-66]. The following four canonical pathways, resulting from EGF stimulation, are illustrated in a schematic diagram (Fig. 1.2) and described briefly. Due to the synchronized and coordinated activation of these downstream pathways they should not be considered in an isolated context, but for purpose of simplicity, will be discussed individually.

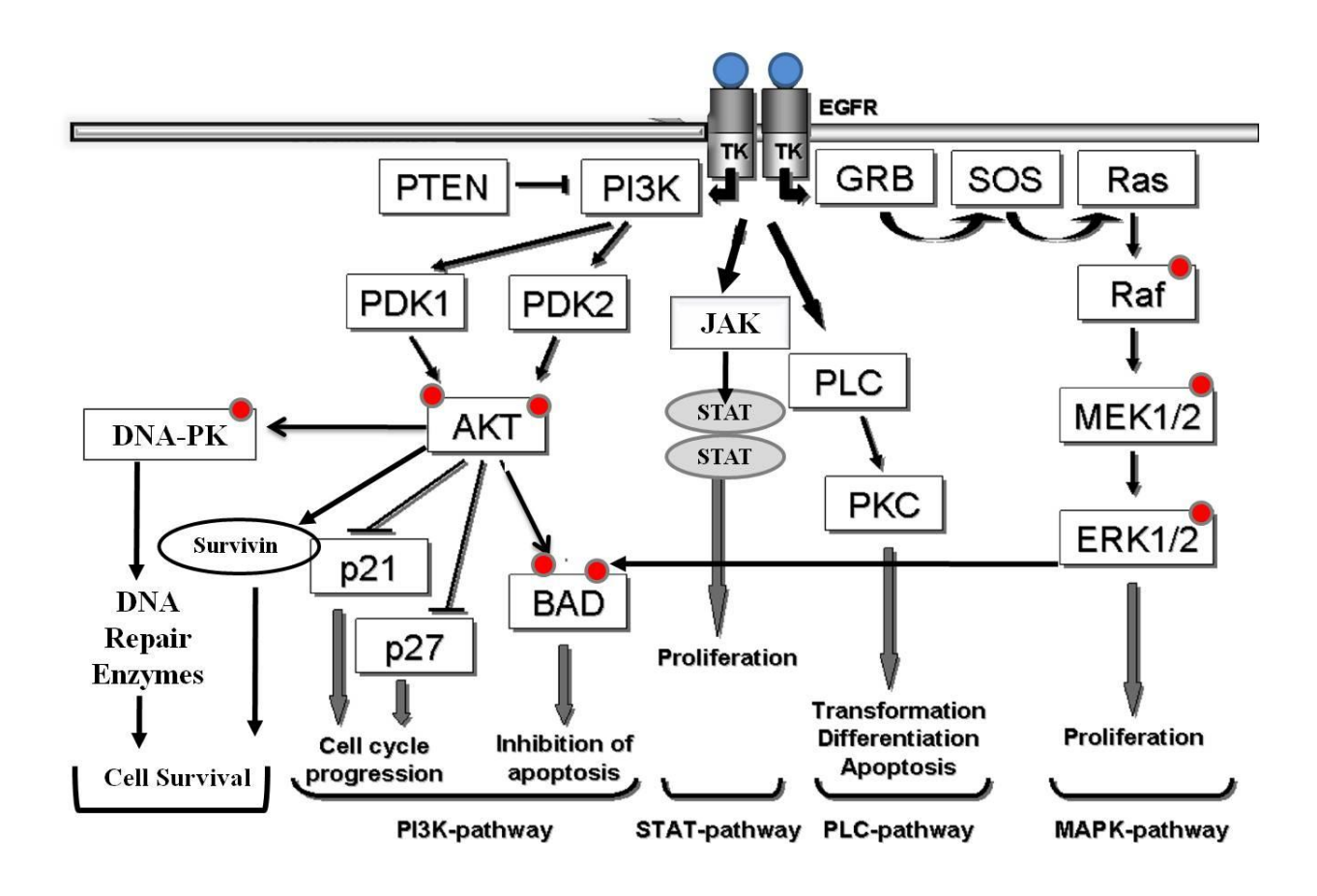


**Figure 1.2.** Downstream signaling pathways of EGFR activation.

### 1.3.3.1. Ras/Raf/MEK/ERK cascade

The signaling resulting from the mitogen-activated protein kinases (MAPKs) is the most extensively studied cell signaling [67]. The first layer of MAPK cascade events, which connects extracellular signals and allow their intracellular transmission to occur, are Ras family of small GTP-binding proteins [35, 43]. When recruited at the plasma membrane, Ras co-localizes with many proteins and facilitates the interactions between several cascades, thus transmitting signals for proliferation, differentiation, sustained growth and survival. GTP-bound active Ras, phosphorylates the serine/threonine kinase Raf, which propagates the signal via dual-specificity MAPK kinases, MEK1 and MEK2 [68]. Depending on which kinase acts as a final substrate to propagate the signal to the nucleus the pathways are named as following: extracellular signalregulated kinases (ERK1/2), ERK5, Jun NH2-terminal kinases JNK1-JNK3, and p38 kinases,  $\alpha$ ,  $\beta$ ,  $\gamma$ , and  $\delta$  isoforms [69]. While ERK1/2 are strictly regulated by RTK activation in a GFdependent manner, ERK5 kinase responds to both stress and GF activation, and the other two kinases are primarily considered stress-induced signals. Overall, regardless of the exact route, the common feature of all these kinases is their ability to translocate to the nucleus upon activation and phosphorylate nuclear regulatory proteins (e.g., Sp1, E2F, Elk-1 and AP-1) important for transcriptional activation of early response genes (e.g., c-jun, c-fos, egr-1, c-myc, c-myb) [67, 70].

### 1.3.3.2. The lipid kinase cascade-PI3K/AKT/mTOR

One of the major pathways by which EGFR triggers signals for survival occurs through Ras as well as with the recruitment of phosphatidylinositol 3-kinase (PI3K) at the plasma membrane. These interactions lead to the activation of the lipid PI3K/AKT cascade [71]. PI3K is a

heterodimeric lipid kinase that contains two subunits, the p85 regulatory subunit with two SH2-domains and the p110 catalytic subunit. Once recruited to the plasma membrane, either though its regulatory subunit or through the small G protein Ras, the lipid kinase changes into an active conformation and together with phosphatidylinositol (PtdIns 3,4,5) triphosphate serves as a docking site for other regulatory proteins with phospholipid (PH)-binding domains. The downstream effectors of the PI3K pathway are PDK1 (phosphorylates Thr-308 residue of AKT) and PDK2 (Ser-473 of AKT). The phosphorylation of these sites are essential for maximal AKT activation [72]. The family of AKT/protein kinase B (PKB) serine/threonine kinases are composed of three members: AKT1/PKBα, AKT2/PKBβ, AKT3/PKBγ [73]. Activated AKT modulates the activity of many proteins involved in cell cycle progression, cellular growth and sustained survival [72]. The magnitude and the length of the signals mediated by PI3K/AKT is regulated by the lipid phosphatase PTEN, which by dephosphorylating PtdIns 3,4,5 triphosphate, prevents AKT activation. Frequent mutations or full inactivation in PTEN activity are often observed in many human cancers, which results in constitutive AKT activation [74].

# 1.3.3.3. JNK/SAPK and p38 kinase signaling cascade

The activation of this cascade, aside from classical growth factors stimulation, results from other stimuli such as mitogens, inflammatory cytokines, DNA damage by UV irradiation, genotoxic agents and oxidants. JNK activation, in response to a specific stimulus, is achieved through dual phosphorylation of Thr-183 and Tyr-185 residues by various protein kinases [69]. In addition to its activation via the Ras/Raf/MEK cascade, three other groups of kinases, the TGFβ-activated kinase-1, mixed lineage kinase group and the activator of S-phase kinase group (ASK<sup>a</sup>) can stimulate the effector kinases, MAK2K4 and MAK2K7, responsible for JNK phosphorylation [75]. The activated JNK in the nucleus leads to phosphorylation of c-Jun,

JunA, JunB, ATF2, Elk and several other transcriptional regulators, while accumulation of JNK in the cytoplasm promotes cytochrome c release and apoptosis [76]. Overall, JNK role is a little controversial since this kinase can enable cell survival and tumour progression under certain conditions, but in most cases of cellular stress and DNA damage, it predominantly results in JNK activation leading to cell death [75, 77].

In analogy to the JNK cascade, p38 kinase primary role is to respond to stress conditions, inflammatory cytokines and growth factors starvation. An important connection between p38 activation and EGFR, that has recently been demonstrated, is that DNA damage induced by platinum agents or UV irradiation triggers p38-kinase—dependent endocytosis of EGFR [78, 79]. Unlike the ligand-induced endocytosis and degradation of EGFR, this signal results in receptor temporal inactivation by stress [78]. Therefore, inhibiting receptor activation and inflicting DNA damage could be potentiated by the addition of p38 kinase inhibitors.

# 1.3.3.4. Phospholipase C (PLCy) cascade

Another signaling pathway activated as a result of EGF stimulation and receptor phosphorylation is PLCγ [20]. In a similar manner, PLCγ is recruited at specific phosphorylated receptor tyrosine residues through its SH2-binding domain and after being phosphorylated, it translocates to the plasma membrane [45]. The recruitment of specific adaptor proteins together with other PLCγ-binding proteins initiates the signaling cascade. In general, PLC enzyme activation results in hydrolysis of PtdIns (4,5) biphosphate into two second messenger molecules: 1,2-diacylglycerol and inositol 1,4,5-triphosphate. Their function is to activate calcium channels at the endoplasmic reticulum membrane, raise the levels of free cytosolic Ca<sup>2+</sup> and together with diacylglycerol to activate the calcium-dependent families of kinases such as: protein kinases C (PKCs), calcium/calmodulin-dependent kinases (CD) and CD-phosphatases

[80, 81]. Various adaptor proteins once phosphorylated via PKCs can serve as point of conversion between other signaling pathways involved in: (i) signal transduction (Ras, GAP, Raf), (ii) motility (e.g., fak, profilin), (iii) cell migration (e.g., c-Src, actin modifying proteins) [45, 82]. EGFR itself is a substrate of PKC by being phosphorylated at Thr-654. This has been demonstrated to serve as a feedback loop for signal attenuation by decreasing binding affinity of the receptor for ligands, diminishing the activation of Ras/MAPK cascade, thus favoring cell motility rather than mitogenesis [45, 67]. A recent study by Dittmann group, exploring the mechanism of EGFR nuclear shuffling, observed that deletion of this Thr-654 residue blocked EGFR nuclear transport and accumulation, thereby showing an alternative pathway as a result of this phosphorylation [83].

# 1.3.3.5. The JAK/Signal transducers and activator of transcription (STAT) cascade

Activated EGFR triggers the association of both JAK and STAT and subsequently the recruitment of many of the STAT members (e.g., STAT1, STAT3, STAT5a, STAT5b). STAT and JAK phosphorylation promotes STAT-dimerization and translocation to the nucleus, where they activate genes involved in cell proliferation [84]. Even though STAT family of transcription factors have been shown to undergo phosphorylation and activation in response to cytokines, several STAT members may be directly phosphorylated by EGFR in a ligand-dependent manner [85-87]. STAT3 and STAT5 activation by EGFR is involved in c-Src-mediated processes of cytoskeleton remodelling, critical for cell migration and invasion [64, 88]. Since these cytosolic transcription factors can directly transmit signals from the plasma membrane to the nucleus, any aberrant tyrosine kinase activities is propagated efficiently and results in constitutive gene activation.

### 1.3.3.6. EGFR and Src non-receptor tyrosine kinase: special interaction

The Src family of kinases is composed of several non-RTKs (e.g., c-Src, c-Yes, Fyn, Lyn, Hck, Blk, Fgr and Yrk) [89, 90]. A critical player with an important role in transducing mitogenic signals downstream of EGFR is c-Src tyrosine kinase. c-Src controls two mechanisms in the cell: (1) modulates EGFR function by enhancing signals downstream of the receptor and regulating its endocytosis; (2) affects cell motility by phosphorylating proteins that are involved in actin cytoskeleton remodelling [91, 92]. The special interaction between EGFR and c-Src is due to its ability to phosphorylate EGFR in a ligand-independent fashion, which confers to c-Src a potent role in activating ErbB family of receptors. Parsons group [93] extensively studied c-Src activities and were the first to report c-Src-mediated phosphorylation of EGFR at Tyr-845 and Tyr-1101. Several other EGFR residues such as Tyr-891 and Tyr-920 were also phosphorylated by c-Src and were characterised to be cell-type specific and ligand independent [40, 41]. Thus, without extracellular signals, c-Src can phosphorylate EGFR and transmit signals involved in cell proliferation, migration and invasion [94].

In addition to the mitogenic signals elicited from c-Src-EGFR interaction, c-Src plays a role in receptor degradation. c-Src mediated involvement in EGFR endocytosis results in EGFR being predominantly recycled by sequestration in perinuclear/recycling endosomes instead of being targeted to multivesicular bodies (MVB) and lysosomal degradation (see section on EGFR internalization) [95]. These findings expand the previous observations about c-Src involvement in increased perinuclear localization and enhanced EGFR translocation to the nucleus [96]. Overall, these examples suggest special interactions between EGFR and c-Src critical for tumorigenesis. Thus, activation of both kinases results in increased signal propagation, receptor stability and nuclear localization, overall highly synergistic mitogenic effects. In addition,

activation of c-Src by other GFs, cytokine receptors, G-protein coupled receptors and integrins enhances c-Src- and EGFR-mediated signals for proliferation, cell survival, motility and invasion [92, 97]. Thus, c-Src has pleiotropic effects on many cellular processes for normal and more importantly on cancer cells by modulating the action of multiple growth-promoting receptors.

#### 1.3.3.7. EGFR and cross-talks

Enhanced EGFR signaling often escalates into cross-talks between several of the upper mentioned pathways which increases mitogenic effects of the receptor [98]. The divergence between EGFR family members at the C-terminus and the possible combinations of EGFR heterodimeric complexes allows for a great number of interactions among the proteins recruited in order to elicit multiple intracellular responses. The adaptor proteins associate via their SH2 and SH3 domains with different EGFR phosphotyrosine residues and modify the signals transmitted downstream (Fig.1.1, Table 1.1). They serve as docking proteins to mediate the interactions between EGFR and other downstream proteins for the activation of different signal transduction pathways. Importantly, c-Src-EGFR interaction is among the most potent due to their bi-directional kinase activity and reciprocal phosphorylation. Overall, the two major pathways important for the work described in this thesis include the MAPK and PI3K/AKT pathways. The Ras-Raf-MEK-MAPK pathway leads to cell proliferation, angiogenesis, and metastasis [67]. The PI3K/AKT pathway affects cell survival, metabolism, proliferation, and blockade of apoptotic proteins [71]. Even though the signaling cascades described above appear to be unidirectional, the shared effector proteins establish cross-talks between downstream proteins and enable transversal activations. On the other hand, an attenuation of signal activation in one cascade often results in compensatory activation of another cascade in order to sustain propagation of mitogenic signals [27].

### 1.3.4. EGFR internalization

Internalization of RTKs is a tightly regulated mechanism of temporal desensitization or full inactivation of receptors which influence many downstream cell signaling events [52, 99].

# 1.3.4.1. EGFR degradation through the endosomal pathway

# 1.3.4.1.1. Ligand-dependent

It is now recognized that receptor signaling and receptor internalization by endocytosis are two interconnected, tightly linked processes and that ligand-induced receptor downregulation requires the kinase activity of EGFR [52]. The direct evidence that endocytosis requires receptor kinase activation is the fact that the Cbl E3 ubiquitin ligase is recruited only upon EGF-stimulation and phosphorylation. Cbl ubiquitylates the receptor and initiates its internalization into endosomes [100]. The trafficking of EGFR from the membrane into clathrin-coated pits, early endosomes and MVB, where sorting of receptors occurs, is accompanied by a series of ubiquitin-dependent steps (Fig. 1.3) [101, 102]. From these late endosomes where sorted receptors are marked by poly-ubiquitin chains, they are transferred in lysosomes for proteolytic degradation [52]. The alternative pathway is receptor temporal desensitization which defines the strength and duration of signal propagation. EGFR, marked by mono-ubiquitylated moieties, leaves the endosomes to be recycled back to the plasma membrane [103]. In addition, other studies have shown that endosomes can serve as compartments that enable the assembly of EGFR signaling complexes with other adaptor proteins [104, 105].

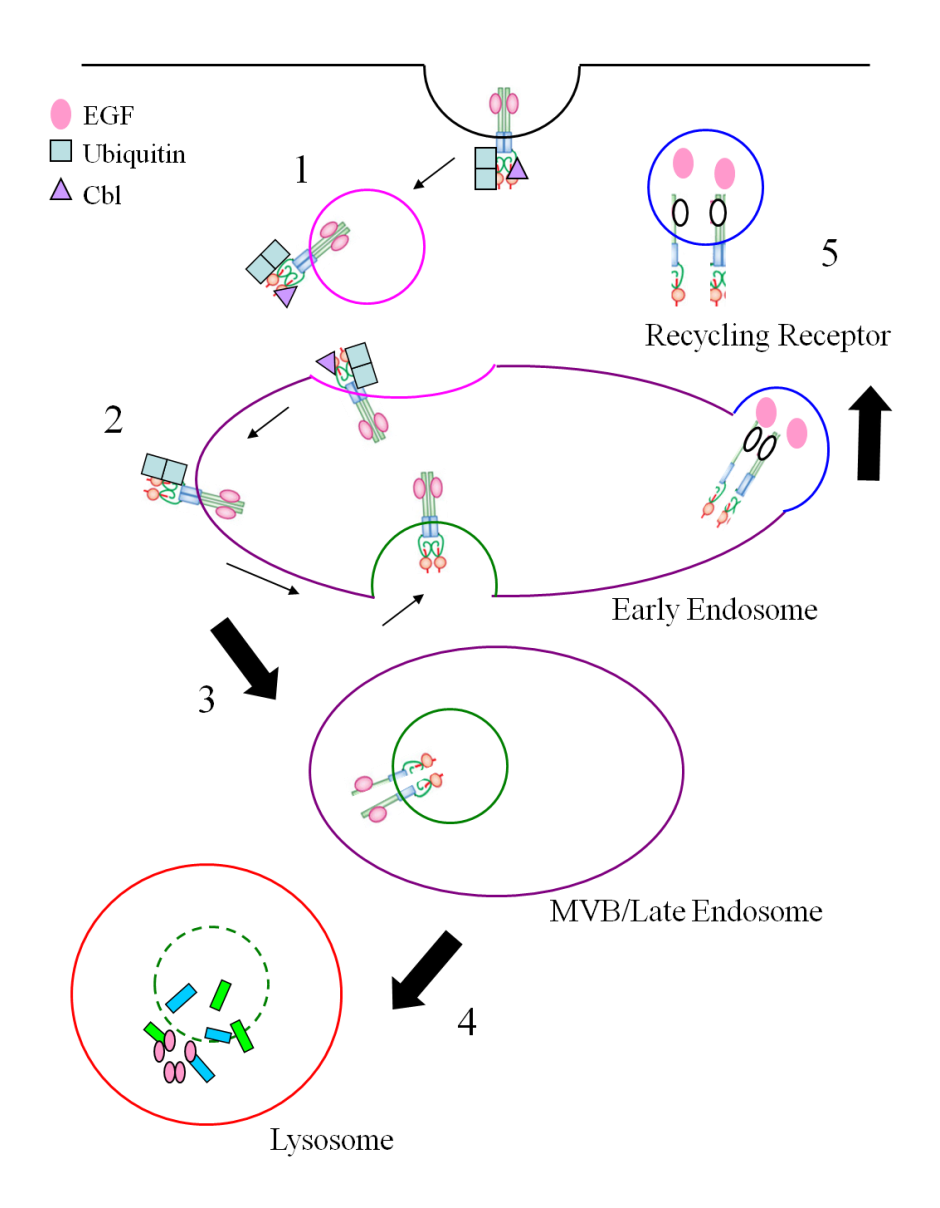


**Figure 1.3.** Steps in EGFR recycling or degradation. **Step 1:** Cbl ubiquitin ligase recruitment and initiation of clathrin-mediated internalization of receptor. **Step 2:** receptors move along the membrane of the clathrin-coated vesicles, which fuse and give rise to an early endosome. **Step 3:** late endosomes or multivesicular bodies (MVBs), where receptors are sorted based on either mono- or poly-ubiquitinated modifications. The major regulatory proteins in MVB required for sorting are ESCRTI, ESCRTII, ESCRTIII. **Step 4:** receptors directed toward lysosomes for proteasomal degradation. **Step 5:** the alternative pathway where EGFR is recycled back to the plasma membrane.

Studies with EGFR deletion mutants which cannot be internalized in endosomes, and which have a constitutive activity, have defined the protein regions critical for receptor desensitization and inactivation [52]. Cells expressing the mutant versions have elevated levels of ERK1/2, a constitutive PI3K/AKT activation and upregulation of several anti-apoptotic proteins [106, 107].

### 1.3.4.1.2. Ligand-independent

In contrast to ligand-induced receptor dimerization, EGFR can be activated by oxidative stress, interactions with G-proteins coupled receptors (GPCRs), radiation, estrogen receptors [48, 49]. The fate of the receptor after ligand-independent activation involves either receptor internalization and the proteasomal degradation described above, or a caveolin-driven pathway with EGFR localized in caveolae structures [96, 108, 109]. The second, recently characterized mechanism of EGFR internalization into caveolae in response to treatment to oxidants or radiation, leads to receptor trafficking toward the nucleus as observed by EGFR perinuclear and nuclear localization [96, 110]. C-Src-mediated activation of EGFR after exposure to H<sub>2</sub>O<sub>2</sub> and radiation, stimulates caveolae formation, ongoing signaling from these vesicles in order to facilitates nuclear shuttling and nuclear accumulation of EGFR [96, 109, 111]. The observation that inhibition of c-Src TK activity (either with its known inhibitor PP2 or with specific siRNAs) blocks caveolin-1 driven EGFR internalization and subsequently prevents EGFR nuclear translocation, demonstrates another important role of c-Src on EGFR signaling.

#### 1.3.4.2. Perinuclear EGFR localization

Murthy et al. [112] were the first to demonstrate EGFR perinuclear localization using immunofluorescence. Stimulated receptor migrates to the perinuclear region in a ligand

dependent fashion and upon ligand withdrawing it is rapidly recycled back to the plasma membrane. They suggest that perinuclear observation of EGFR is primarily due to recycled receptor rather than to newly synthesized EGFR in response to EGF. In addition, in highly EGFR-expressing cells but not in their wild type counterpart cells, the fluorescent quinazoline EGFR inhibitor was observed preferentially in the perinuclear region [13, 113]. The TK inhibitor distribution was not diffused in the cytoplasm, but rather concentrated at the perinuclear region, most likely co-distributed and colocalized with EGFR.

### 1.3.4.3. Nuclear EGFR localization

Findings from the last ten years clearly demonstrated the accumulation of EGFR in the nucleus [114, 115]. Even though nuclear EGFR activity has not been well understood, its translocation was strongly associated with response to DNA damage and resistance to chemo- and radiation therapy [116, 117]. Several reports by Dittmann *et al.* [109, 118] demonstrated that EGFR translocated to the nucleus in response to radiation-induced DNA lesions. Nuclear EGFR abundance has also been observed to lower the therapeutic response to anti-EGFR antibody therapy (Erbitux®, cetuximax) and correlates with resistance [116].

The presence of EGFR accumulation in the nucleus has been first detected in regenerating liver tissue by Marti *et al.* [119] and since then many reports have demonstrated its nuclear function in a variety of normal and cancer cells [117, 120, 121]. More recent evidence supports the finding that EGFR is involved in (1) transcriptional regulation, (2) phosphorylation and activation of nuclear proteins, (3) association in complex with DNA repair proteins [70, 111, 115, 122, 123]. The fact that nuclear EGFR retains its tyrosine kinase activity and phosphorylates proliferating cell nuclear antigen (PCNA), raises the possibility of EGFR activating other proteins involved in cell proliferation and DNA repair [117]. It has been shown

to interact with DNA-dependent protein kinase (DNA-PK), as well as to stimulate complex formation between p53 and another essential protein for the recruitment of DNA repair foci, MDC1 (mediator of DNA damage checkpoint protein 1) following radiation [111, 117]. The genes that have been shown to be activated by EGFR as part of a transcriptional activation complex are cyclin D1, inducible nitric oxide synthase (iNOS), b-myb, aurora A and cyclooxygenase-2 (COX-2) [70, 115, 121, 122, 124]. Other candidate genes, which are currently being validated, will help better understand normal versus pathological functions of nuclear EGFR [121]. The challenge to understand this unexpected mode of EGFR signaling has initiated an active research on nuclear EGFR activities. It is important for the work described in this thesis to appreciate the localization of EGFR not only in the perinuclear region but in the nucleus as well when the effect of DNA damaging agents are studied.

While the results on EGFR nuclear translocation are controversial when cells are treated with EGFR antibody, the effect of lapatinib (Tykerb®) on inhibiting its nuclear localization has been confirmed [12]. The inhibition of nuclear EGFR transport and nuclear EGFR-induced DNA repair with an anti-inflammatory drug celecoxib (Celebrex®) has been shown to improve tumour response to radiation [125]. Therefore, it would be plausible to propose that inhibition of nuclear EGFR accumulation upon combinations of EGFR TK inhibitors with DNA-damaging agents would bring a synergistic effect and improved response in tumours. Although EGFR nuclear mechanism of action is just at the beginning of its elucidation, it is considered an important prognostic marker in breast and ovarian cancer [124, 126]. Blockade of nuclear EGFR accumulation and its function in the nucleus may be a new strategy to overcome treatment resistance.

#### 1.3.4.3.1. Nuclear EGFR and resistance

The observation that EGFR translocates to the nucleus following radiation therapy, where it interacts with DNA-PK and plays a role in radiation-induced DNA repair raises the question about possible response upon treatment with DNA damaging agents [111]. Indeed, another study confirmed the negative impact of nuclear EGFR on DNA damage response induced by cisplatin and the development of tumour resistance when nuclear EGFR accumulation increases [117]. Collectively, these studies demonstrate the effect of nuclear EGFR on a lack of response to radiation and DNA-damaging agents, thereby raising the question about plausible improved effect when these therapies are combined with EGFR TK inhibitors.

### 1.4. TARGETED THERAPY FOR CANCER TREATMENT

# 1.4.1. EGFR-targeted agents

As seen from the increased EGFR expression in different tumours, the design and development of agents that aim at targeting malignant EGFR expressing cells versus non malignant cells is very rational but extremely challenging [127, 128]. The two targeted strategies developed for blocking abnormal EGFR activation are designed toward inhibiting: (1) the extracellular ligand binding domain with anti-EGFR antibody and (2) the intracellular tyrosine kinase domain with small molecules EGFR-TK inhibitors. Both approaches result in blockade of signal transduction, thereby preventing the downstream effects normally associated with EGFR activation as discussed previously.

### 1.4.1.1. Anti-EGFR antibody

The humanized anti-EGFR agents, Cetuximab (Erbitux®) and Panitumumab (Vectibix®), are currently the only two clinically approved antibodies for patients with EGFR-expressing aggressive metastatic cancers [129]. Cetuximab is a mouse/human chimeric monoclonal antibody that recognizes the extracellular domain of the EGFR and competes with its ligands for binding with the receptor. Cetuximab induces receptor endocytosis and downregulation by a variety of mechanism, but most importantly, it exerts a synergistic effect in combination with other chemotherapeutic agents and enhances response to radiation therapy [130-132]. Panitumumab is a fully humanized monoclonal antibody that is approved for the treatment of advanced and metastatic colorectal cancer patients [133]. Overall, the anti-EGFR therapies are less toxic but still not fully tolerable. Adverse skin rash reactions and dermatologic toxicities are among the most frequently reported side effects in addition to infusion reactions unique to monoclonal antibodies, which require intravenous administration.

### 1.4.1.2. Small molecules approach

Selective small-molecule tyrosine kinase inhibitors (TKI) are an important class of anti-cancer agents. For the last ten years, they have demonstrated great efficacy in the treatment of cancer. TKIs are designed to bind to the ATP-binding site of the receptor tyrosine kinase and block its ability to phosphorylate tyrosine residues on its own kinase domain or to phosphorylate the receptor dimer in trans. Quinazolines are a class of kinase inhibitors that share structural similarity with ATP [134]. Structure activity relationship (SAR) of quinazoline derivatives (shown in Table 1.3) elucidates the structural requirements essential for inhibition. In the case of EGFR, the three critical residues required for anilinoquinazoline binding at the ATP binding

**Table 1.3.** Chemical structures of clinically approved ErbB family tyrosine kinase inhibitors.

Quinazoline-based inhibitors of EGFR	Name, company	Known targets	IC <sub>50</sub> , μΜ	Indications Clinical Trial	Ref.
HN N	Erlotinib (Tarceva: OSI-774 Pharmaceauticals/ Genentech/Roche	EGFR (irr), ErbB2	0.02 0.35	NSCLC, pancreas cancer, Phase III	[135, 136]
O HN CI	Gefitinib (Iressa; ZD 1839 AstraZeneca)	EGFR (r), ErbB2, HER4	0.023 3.7	NSCLC Phase III	[137, 138]
O S N N N N N N N N N N N N N N N N N N	Lapatinib (Tykerb; GW-2016 GlaxoSmith Kline)	EGFR ErbB2 (r),	0.01	Breast cancer Phase II	[139, 140]
HIN CN CN	Pelitinub EKB-569 (Wyeth)	EGFR (irr) ErbB2	0.039	Pancreas Colon Phase I	[141, 142]
HN CI N 2HCI	Canertinib (CI-1033 /PD183805) Pfizer	EGFR (irr), ErbB2	0.0014 0.0074	Phase I	[143, 144]

pocket of the receptor are (1) Met-769, (2) Thr-766 (3) Asp-776 while a bridge with Cys-773 is critical for irreversible inhibition of the receptor [62].

In the last 20 years, multiple EGFR/ErB2 TKIs have been developed, evaluated and their potent antitumour effects validated in multiple preclinical studies and then moved into clinic [137, 145].

The three small molecule inhibitors currently approved for use in patients are gefitinib, erlotinib, and lapatinib. Despite great advances made in this field, EGFR-targeted therapy has shown only modest results. The treatment effect has been minimal across most cancers except being successful for only a small number of specific gain-of-function mutations in NSCLC [146, 147]. Despite being the most extensively studied family of growth factor-activated receptors, there is still an increasing need for novel EGFR-targeting strategies against EGFR expressing tumours.

# 1.4.2. DNA targeting

DNA damaging agents are the classical agents for cancer therapy. Despite the progress made toward developing such agents, the major downside of cytotoxic therapy is that DNA alkylating agents are not cancer cell selective. Unfortunately, classical DNA targeting agents are still used today as first line chemotherapeutic agents regardless of their strong toxicity and the above mentioned lack of selectivity.

## 1.4.2.1. Classical DNA damaging agents

The development of alkylating agents and their biological application started since 1950s, with the discovery of the molecular structure of DNA [148]. Thereafter, a series of reports about reactivity of nitrogen mustard and of mono- and bi-functional alkylating agents with nucleic

acid and their biological effects were published [149-152]. All this early work has established a deep understanding on the types of DNA adducts formed, the types of alkylation among different agents, and expanded into *in vivo* studies in mice. To put this into a clinical contest, the first cytotoxic effect of nitrogen mustard (2-chloroethyl-sulfide) on blood and bone marrow cells was reported early in 1919 by Krumbhaar [153], followed by the lethal effect of nitrogen mustard observed in 1946 during the second World War reported by Goodman [154]. Thereafter, started the real interest in alkylating agents for the treatment of malignancies and the first clinical trial in 1963 with a nitrogen mustard was reported [155]. Since then, many different type of DNA targeting agents were developed and the one used currently in the clinic are summarized in Table 1.4. These DNA damaging agents can be grouped into monoalkylating agents (temozolomide, dacarbazine, adozelesin), bifunctional alkylating and crosslinking agents like nitrosoureas (BCNU, lomustine, mitomycin C, streptozotocin) or nitrogen mustards (cyclophosphamide, chlorambucil, ifosfamide, mechlorethamine, bendamustine).

# 1.4.2.1.1. DNA monoalkylating agents and triazenes

Triazenes are a group of alkylating agents containing as the name implies three adjacent nitrogen atoms [156]. The N=N-N linkage can be attached to various aromatic carbon-containing compounds and it can be easily hydrolysed under physiological pH to give the core chemical species and a methyldiazonium ion. These DNA reactive methylating species are the most accepted class of alkylators with the best examples of triazenes in the clinic being temozolomide (TEM), dacarbazine, procarbazine [157, 158]. Their use in the clinic dates from the mid-70s when approved for the treatment of advanced metastatic melanoma, sarcoma, some forms of lymphoma and malignant gliomas [159, 160]. They are preferred for their excellent pharmacokinetic properties, great bioavailability, uptake, distribution and limited toxicity.

 Table 1.4. Clinical DNA damaging agents and DNA repair responses.

DNA-damage agents	Type of damage	DNA repair pathway	Ref				
Direct and Indirect		(enzymes)					
Temozolomide	O <sup>6</sup> -meG, N <sup>3</sup> -meA, N <sup>7</sup> -meG	AGT and BER	[161]				
Dacarbazine/imidazole	O <sup>6</sup> -meG, N <sup>7</sup> -meG	AGT and BER	[162]				
BCNU/carmustine	Chloroethyl adduct at O <sup>6-</sup> G DNA cross-links	AGT NER and HR	[163]				
Streptozotocin	O <sup>6</sup> -meG, N <sup>3</sup> -meA, N <sup>7</sup> -meG	AGT and BER	[163]				
Mechlorethamine	N <sup>3</sup> -meA, N <sup>7</sup> -meG	BER					
Melphalan	N <sup>3</sup> -meA, N <sup>7</sup> -meG DNA cross-links	BER and NER	[164]				
Bendamustine	N <sup>3</sup> -meA, N <sup>7</sup> -meG DNA cross-links	BER and NER	[165]				
Platinum Agents							
Cisplatin/Oxaliplatin	Inter- and Intra- strand DNA cross-links	NER/MMR/HR/BER	[166, 167]				
Anthracyclines							
Doxorubicin/Epirubicin Daunorubicin	ROS	BER	[168]				
Nucleoside Analogs							
Gemcitabine/Troxacitabine	L-configuration analogs	BER	[169]				
Radiation	SSBs, DSBs, ROS	BER/HR/NHEJ	[170]				

Methyldiazonium ion, the active product of most methylating agents reacts with several nucleophilic sites in DNA to give: (1)  $O^6$ -methyl guanine (~8%), (2)  $N^7$ -methyl guanine (~65-80%), (3)  $N^3$ -methyl adenine (~8-12%).

### 1.4.2.1.2. Cyclic Triazenes

The 5-[3,3-bis(2-chloroethyl)-1-triazene] imidazole-carboxamide (BCTIC) is one such agent previously reported to have *in vivo* activity. The latter drug contains a triazene chain capped with a nitrogen mustard moiety that is believed to be oxidized *in vivo* into monochloroethyltriazene moiety, a species known to be prone to further hydrolyze to the DNA alkylating chloroethylating species [171].

#### 1.4.2.1.3. *Nitrosoureas*

The nitrosoureas are among the most potent alkylating agents used. They can alkylate DNA (primarily N-base alkylation) and in addition, the modified bases can form inter- or intrastrand cross-links. Unfortunately, despite their potency and spectrum of activities, nitrosoureas are inactive against tumours expressing the O<sup>6</sup>-methyl-guanine methyl-transferase (MGMT) and are very short-lived. Bis-chloroethyl-nitrosourea (BCNU/Carmustine), Mitomycin C and streptozotocin are some currently used nitrosoureas. Streptozotocin is originally identified as an antibiotic naturally produced by bacteria. This glucosamine nitrosourea is transported by the glucose transporter, it is primarily used for pancreatic carcinomas and unlike other nitrosoureas, streptozocin causes little myelosuppression.

### 1.4.2.1.4. Nitrogen mustards and crosslinking agents

Nitrogen mustards (e.g., chlorambucil, ifosfamide, bendamustine, mechlorethamine, melphalan, N-acetyl-aziridine) are highly reactive compounds. They can alkylate DNA, RNA and proteins,

form cross-links, thus prevent DNA replication, cause cell cycle arrest, and lead to apoptosis. They can form cyclic aminium ions (aziridinium rings) by intramolecular displacement of the chloride by the amine. Due to the strain in the aziridinium ring, aziridines have enhanced reactivity and tendency to undergo ring-opening reaction with nucleophiles. The work in this thesis exploits the aziridine moiety conjugated to a fluorescent tag in order to expand our understanding by imaging the DNA-alkylating species in the nucleus.

Another nitrogen mustard with unusual properties is bendamustine with three active moieties: an alkylating group, a benzimidazole ring, which may act as a purine analogue and a butyric acid side chain. In addition, due to the fact that it activates the base excision DNA repair pathway (BER) rather than the MGMT repair mechanism, it can be less susceptible to cell-developed resistance [172]. Other more therapeutically useful alkylating agents are the ones with more than one alkylating group per molecule, these are the di- or polyalkylating agents with a potent "radiomimetic" effect.

# 1.4.2.1.5. Platinum agents (cisplatin, carboplatin, oxaliplatin, lipoplatin)

Platinum agents cause toxic lesions by interstrand DNA bridges in a very unselective fashion, but they still continue to play a central role in cancer chemotherapy. They are used as first-line chemotherapy against epithelial malignancies of lung, ovarian, bladder, testicular, head and neck, esophageal, gastric, colon and pancreatic but also as second- and third-line treatment against a number of metastatic malignancies including cancers of the breast, melanoma, prostate, malignant gliomas and others. Recently, lipoplatin, cisplatin encapsulated into liposomes version, has been developed to overcome its major drawback, high cytotoxicity, in the therapy of many solid tumours. It is currently under Phase III clinical evaluation for lung, pancreatic, head and neck carcinomas [173].

# 1.4.2.2. Types of DNA damage

Depending on the nature and extent of DNA damage, the lesions observed are either single strand brakes (SSBs) or double strand brakes (DSBs). Monoalkylation of O<sup>6</sup>-meG, N<sup>3</sup>-meA and N<sup>7</sup>-meG are the most common modifications. These lesions result in SSBs due to loss of the modified base and disruption of the DNA backbone. Breaking of the parallel DNA strand can occur if alkylation on each strand is at nearly opposite sites giving DSBs.

In contrast, di-alkylating and cross-linking agents produce bulky DNA adducts and DNA cross-links which result in frequent DSBs. Moreover, when the two adjacent alkylated guanines form covalent bridges, the DNA lesions are termed intrastrand cross-links and when the alkylated bases are from the opposite strands, these interstrand cross-links are much more deleterious lesions. The latter greatly inhibits the replication process due to the extent of covalent bridges formed along DNA.

The DNA damage resulting from either natural exposure to environmental toxins, oxidative stress, replication stress, UV light or from exposure to DNA damaging agent and ionizing radiation can activate any of the five DNA repair mechanisms in the cell discussed below.

### 1.4.3. Cell response to DNA damage

Understanding how DNA repair is coordinated according to cell cycle phases has important impact on therapy of cancer. The phosphoinositide 3-kinase related kinases (PIKKs) have a central role in the organization of repair complexes.

### 1.4.3.1. Phosphoinositide 3-kinase related kinases (PIKKs)

The PIKKs family of signaling proteins play a central role in the control of cell growth, gene expression, genome surveillance and DNA repair in eukaryotic cells. Mammalian cells express

six PIKK family members [174]. There are five serine-threonine kinases: Ataxiatelangiectasia mutated (ATM), Ataxia telangiectasia and Rad3 related (ATR), mammalian target of Rapamycin (mTOR), DNA-PKs, suppressor with morphological effect on genitalia 1 (SMG1), and the sixth one: a transformation/transcription domain-associated protein (TRRAP) which functions as an adaptor protein in various chromatin complexes, for detection and repair of DSBs, mitotic checkpoint and normal cell cycle progression [174]. ATM responds mainly to DSBs whereas ATR is activated by SSBs and stalled forks during replication [175]. ATM/ATR executes three crucial functions: (1) cell cycle arrest, (2) DNA repair and (3) apoptosis [176]. Depending on the downstream ATM and ATR targets, cells will trigger a specific signaling response. ATM through the adaptor protein nibrin activates CHK2, then cdc25A [176] while ATR via CHK1 and cdc25C has been recently recognized with its involvement in activating and regulating proteins uniquely in a S phase-specific manner [177]. Other substrates common for ATM/ATR are p53, its E3 ubiquitin ligase MDM2, CHK1/2, H2AX and BRCA1/2 (Fig. 1.4) [174, 176, 178].

# 1.4.3.2. Induction of cell cycle checkpoints

Upon DNA damage, cells are arrested in G1, S or G2-M, as illustrated in figure 1.4, to allow time for DNA repair and to minimize the replication and segregation of DNA. The G1-S checkpoint is in part dependent on the p53-regulated transcription of p21, which is the potent inhibitor of cyclin E and cyclin-dependent kinase 2 (CDK2) [179]. Likewise, p53 exerts effect on G2/M arrest by p21 in coordination with 14-3-3-σ, which through cdc25C inactivation disrupts cdc2/cyclin B1 complex to prevent cells from going through mitosis [180]. In contrast to G1-S and G2-M checkpoints, the S-phase checkpoint is believed to be p53-independent, which serves to prevent replication from continuing before repair is efficiently executed [181].

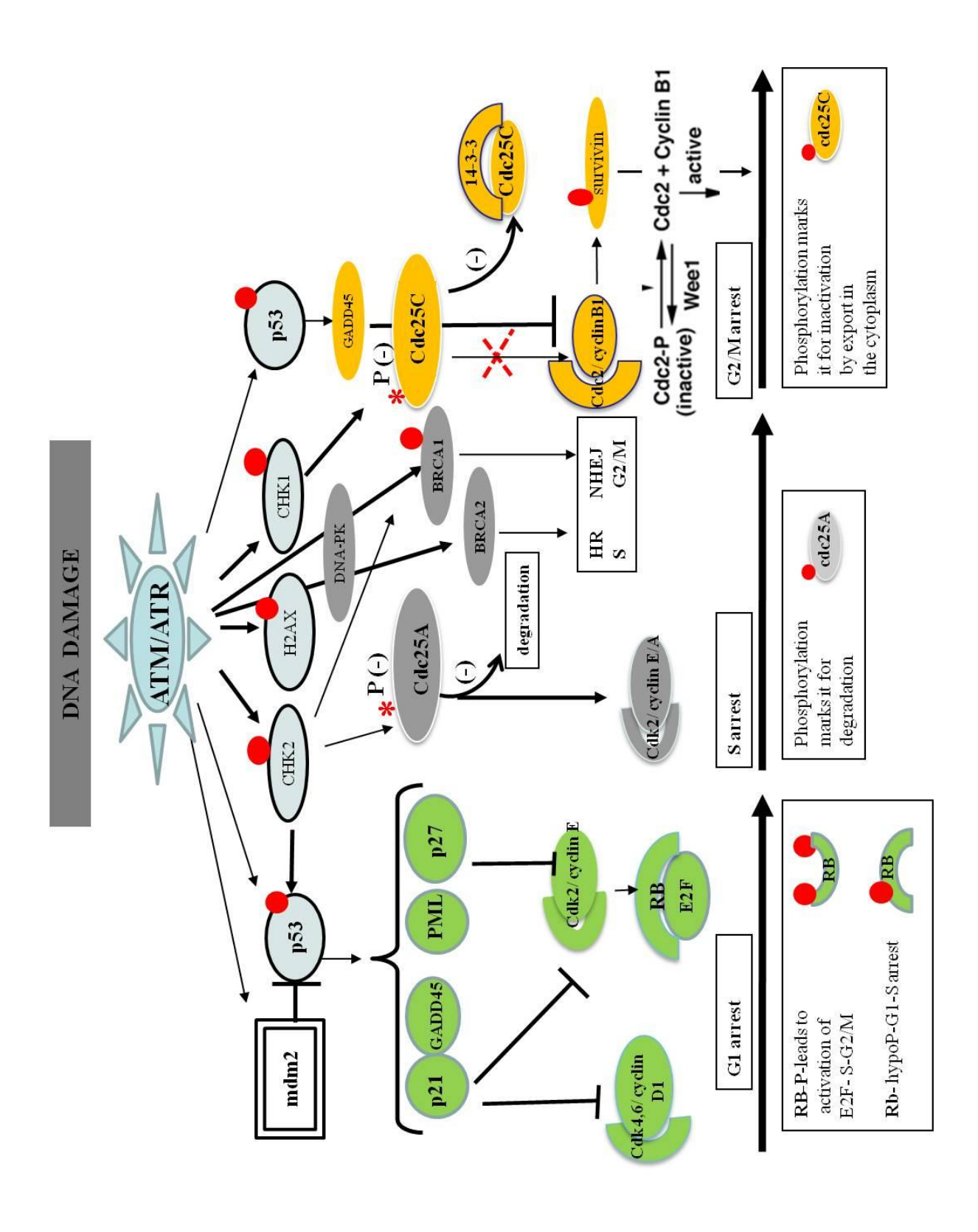


Figure 1.4. Cell cycle checkpoints in response to DNA damage.

Cyclins, differentially expressed during each cell cycle phase, together with the CDKs either activated by their cyclin subunits or inhibited by the specific cell cycle inhibitors (e.g., p15, p16, p21, p27, p53, p73) ensure the coordinated progression through each cell cycle phase.

# 1.4.3.3. p53-mediated cell cycle arrest

The extent of DSBs is considered the triggering event in the decision of apoptosis versus repair. As mentioned above, SSBs or DSBs via the activation of ATM, ATR or DNA-PK phosphorylate one of its target p53 [176]. When the damage is minor and repairable, only low level of p53 accumulation is sufficient to trigger cell cycle arrest. When phosphorylated and stabilized, p53 activates p21, which then triggers gene expression of cell-cycle regulatory proteins to execute G1-S arrest and initiate DNA repair via upregulation of DNA damage binding protein (DDB2), xeroderma pigmentosum complement (XPC) and AGT. With high DNA lesions inflicted, p53 accumulates to a threshold level that initiates the transcriptional activation of proapoptotic factors such as Fas-death receptor, PUMA (p53 upregulated modulator of apoptosis), p21, Bcl2-associated X protein (BAX) and growth arrest and DNA damage (GADD45) [182, 183].

# 1.4.3.4. p53-independent mechanism

In case of p53 mutation, deletion or inactivation, which is frequently observed in tumour cells, a p53-independent alternative pathway is activated. A central player, which is activated upon DNA damage through ATM/ATR and downstream CHK1/2 phosphorylation is E2F1 [184]. This in turn transactivates two of the p53 homologues p63 and p73, which are known to trigger apoptosis in the absence of p53 [185]. p73-mediated apoptosis was shown to involve transcriptional activation of PUMA, NOVA and BAX genes, or causing their translocation to

mitochondria and the ultimate cytochrome c release [186]. It is interesting to mention that p73 is rarely mutated, but on the contrary, it is often overexpressed in tumours [185]. This might be one of the reasons which cause tumours to be vulnerable to genotoxic agents even in the absence of functional p53. Another factor implicated in p53-independent apoptosis is NF- $\kappa$ B, which has been shown to switch from an activator of anti-apoptotic genes into a transcriptional regulator with pro-apoptotic activity [182, 187]. The mechanism underlying such swich is not fully elucidated.

# 1.4.3.5. Stress-response via JNK/SAPK

Additional mechanism involves the activation of SAPK, known as well as JNK and p38 kinase [188]. During the genotoxic stress sustained activation of JNK and subsequently c-jun/c-fos (AP-1) activation leads to the stimulation of DNA repair genes or/and the genes for the death receptor Fas and its ligand [189, 190]. One of the earliest cellular responses upon exposure to DNA-damaging agents is the induction of c-fos, which subsequently activates genes important in cellular protection against genotoxic agents and UV radiation [191, 192].

# 1.4.3.6. yH2AX as a marker of DNA damage

If p53 is considered the "cell guardian" of the genome, H2AX is the "histone guardian" of the genome [193]. When DNA damage comes to a serious point and high levels of DSBs are generated, affecting the structural integrity of the DNA, histone variant H2AX is at the center of cellular DNA repair response [193]. It is phosphorylated by either ATM/ATR-dependent or DNA-dependent PKs on Ser-139 and Tyr-142 [194, 195]. The significance of serine-139 phosphorylation of  $\gamma$ H2AX and foci immunodetection is well documented and generally accepted as consistent and quantitative markers of DSBs [196, 197].

This routine practice of  $\gamma$ H2AX foci detection led to the observations that DNA lesions with mono-functional alkylating agents (eg., adozelesin, MNNG) also result in DSBs and foci formation [196]. Exposure to DNA cross-linking agents (e.g., chlorombucil, melphalan) also results in the production of DSBs and increases  $\gamma$ H2AX phosphorylation [198, 199]. Overall, regardless of the mode of action of some DSB-inducing agents which act by forming free radicals (eg., bleomycin, tirapazamine) or topoisomerase II inhibitors (eg., etoposide, doxorubicin, mitoxantrone), which prevent TopoII-mediated DNA re-ligation, they all lead to induction of  $\gamma$ H2AX phosphorylation and foci detection [200, 201]. Therefore, it is broadly used for evaluating the degree of DNA damage induced by many different DNA-targeting agents at a single cell level. The observation that induction of  $\gamma$ H2AX foci occurs only in S-phase is due to the fact that these drugs primarily interfere with DNA replication causing stalling of the replication fork [181].

# 1.4.4. DNA repair enzymes

The DNA repair enzymes form an important network responsible for maintaining genome integrity. They are immediately recruited and activated to neutralize the DNA damage induced by normal exposure or treatment to various physical and chemical agents [187, 202]. The major DNA repair pathways that cells use to repair lesions induced by alkylating-agents are: (1) O<sup>6</sup>-alkylguanine-DNA-alkyltransferase (AGT/MGMT), (2) mismatch repair (MMR), (3) base excision repair (BER) and nucleotide excision repair (NER), (4) homologous recombination (HR) repair and (5) non-homologous end-joining (NHEJ). Each pathway will be described briefly with some of the important proteins in the context of this thesis with more details. All five pathways with the specific enzymes recruited in DNA repair complexes are summarized in figure 1.5.

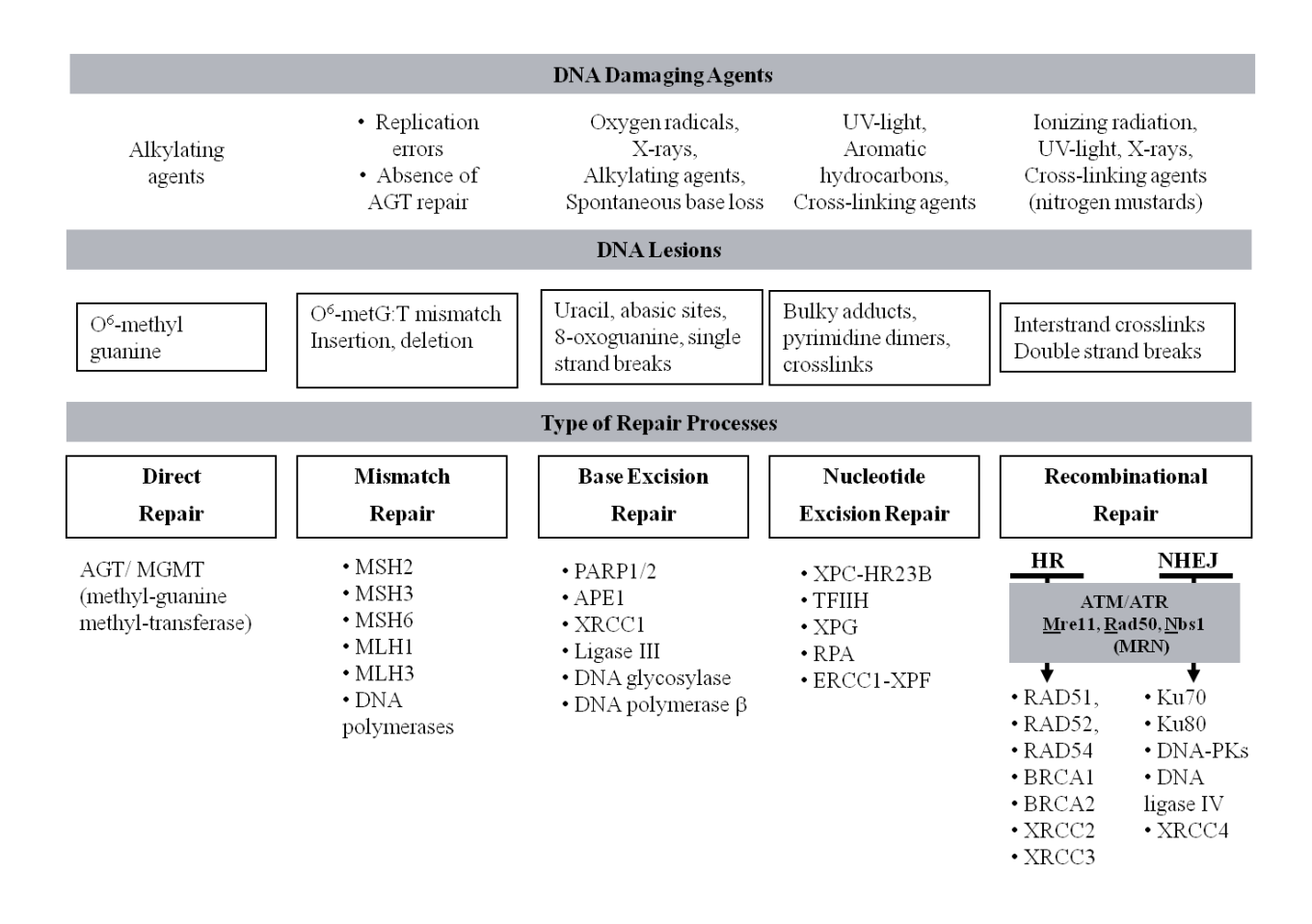


**Figure 1.5.** Type of DNA damage, DNA repair pathways and enzymes involved.

### 1.4 4.1. AGT/MGMT

AGT is a small nuclear protein with its unique function to repair specific of O<sup>6</sup>-meG lesions and upon alkylating itself it is degraded. This protein is the only one involved in the repair of this type of DNA lesions, which despite being the least abundant are the most cytotoxic DNA adducts. While AGT expression is critical for normal cells, the observed overexpression in cancer cells is undesirable since it is involved in resistance to alkylating agents and decreases their therapeutic effect [191]. For this reason AGT is considered a predictive marker and a key factor determining the response to alkylating agents-based therapy [187]. The enzyme is able to remove the alkyl group from O<sup>6</sup>-meG by transferring it onto its own cysteine residue. This alkylated form of AGT is not able to execute more rounds of repair by transferring the alkyl group to another substrate and being regenerated, but after being utilized once it is ubiquitylated and degraded. For this unique nature, it is considered a "suicidal" protein. It cannot be reutilized after the repair process, but has to be synthesized de novo. AGT mutations greatly reduce the capacity to repair the O<sup>6</sup>-meG and sensitize tumours to alkylating agents. For the same reason, the development and applications of AGT inhibitors is important. The two currently used AGT inhibitors, O<sup>6</sup>-benzylguanine (BG) and O<sup>6</sup>-bromotenyl guanine (BTG) are evaluated in the clinic in combination with alkylating DNA damaging agents [167].

# 1.4.4.2. Base-excision repair (BER)

BER removes lesions on the DNA bases resulting from normal cellular metabolism, physical or chemical damage [203]. In the case of N<sup>3</sup>-meA and N<sup>7</sup>-meG lesions formed by the alkylating agents, they can be very efficiently repaired by an intact BER system consisting of the

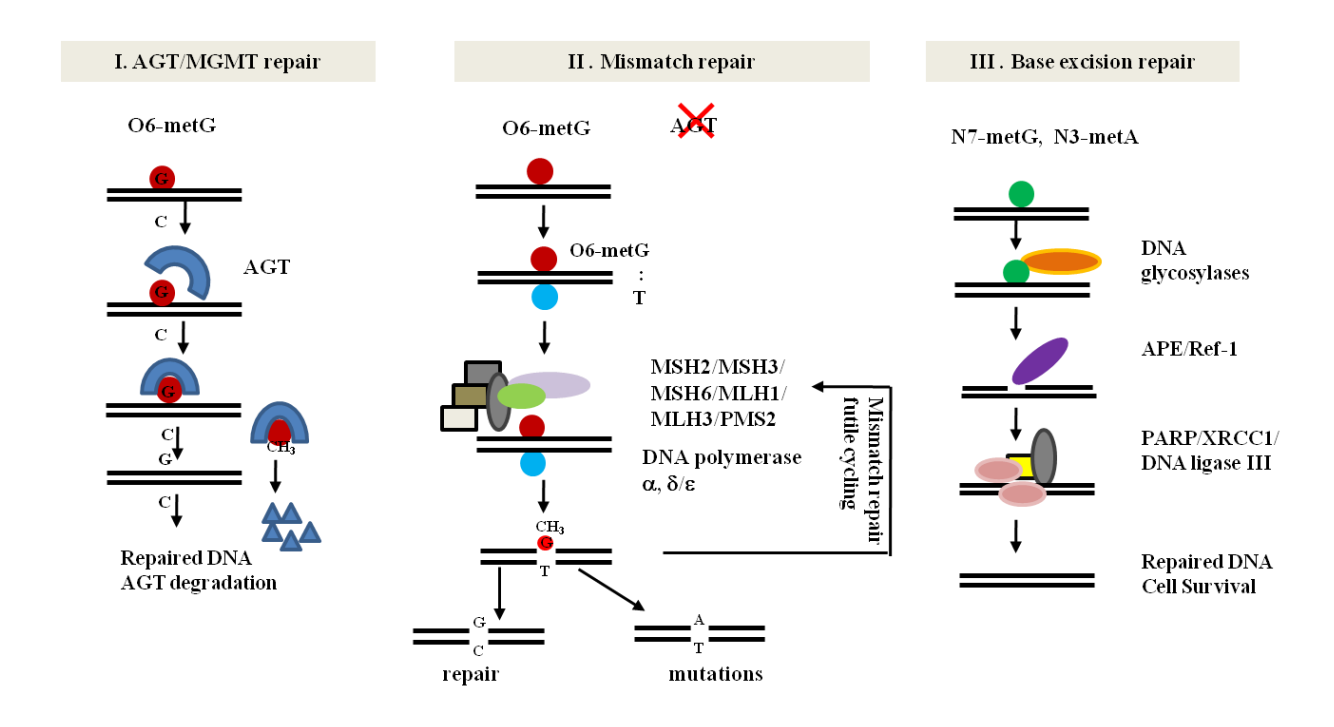


Figure 1.6. The three main DNA repair pathways induced by monoalkylating agents.

DNA alkylating agents generate O<sup>6</sup>-meGuanine, N<sup>7</sup>-meGuanine, N<sup>3</sup>-meAdenine adducts.

I) AGT/MGMT direct repair; II) Mismatch repair is activated when no AGT activity is present to remove the O<sup>6</sup>-meG lesion (e.g., AGT-deficient cells or cells treated with AGT inhibitors); III) Base excision repair enzymes (DNA glycosylases, APE/Ref-1, PARP1/XRCC1/DNA ligase III) are recruited for the removal of N<sup>3</sup>-meA and N<sup>7</sup>-meG adducts.

following enzymes: DNA glycosylases, APE1/Ref-1 endonuclease, DNA polymerase β,PARP1 and XRCC1/DNA ligase III (Fig. 1.6).

# 1.4.4.2.1. Poly (ADP-ribose) polymerase (PARP)

Interestingly, PARP1 was purified and identified from chronic lymphocytic leukemia cells which were treated with melphalan and then analyzed for the accumulation of DNA repair proteins. Damaged DNA served as a probe to identified proteins involved in the repair of nitrogen mustard lesions [204]. PARP1 is a cytosolic protein but is well known for its recruitment in the nucleus upon DNA damage to facilitate short patch base excision [205]. It has a very important role in recognizing both SSBs and DSBs. On the other hand, at high levels of DNA damage, cells eliminate PARP1 by proteolytic cleavage in order to minimize NAD consumption and save ATP for apoptosis, which is a high energy consumption process [206]. PARP1 is able to modulate the switch between DNA repair and cell survival versus the apoptosis response when DNA damage is excessive and cannot be repaired by the cell.

# 1.4.4.2.2. APE1 (apurinic/apyramidinic endonuclease 1/Redox factor-1)

This is an important multifunctional protein, absence of which seriously affects survival of cells due to the increased incidence of abasic sites [207, 208]. It is responsible for the repair of DNA damage induced by oxidants and alkylating agents, therefore is essential for neutralizing the effect of endogenous and exogenous genotoxic agents. There are two ways of executing BER, short-patch repair and long-patch repair, for the initiation of which APE1 is required (see Fig. 1.6). As a critical enzyme involved in the initiation of BER, disrupting its function affects the activity of all downstream member of BER pathway. Furthermore, APE1 is involved not only in DNA repair but in the activation of reduction-oxidation-sensitive transcription factors (TFs)

such as AP-1 (fos/jun), p53, NF-κB, HLF, HIF-1α, CREB, ATF, Egr-1, PAX [207, 208]. The deregulation of reduction-oxidation control of TFs leads to critical changes in genes which are implicated in important aspects of cancer such as angiogenesis and tumour progression.

# 1.4.4.2.3. X-ray cross complementing-1 (XRCC1)

XRCC1 is implicated in both pathways of BER, single-nucleotide (short-patch) and long-patch repair. The most striking feature of XRCC1 is that although lacking any enzymatic activity itself, XRCC1 interacts with the enzymatic components at each stage of BER (Fig. 1.6). Via its specific protein domains, serving as protein-protein interaction modules, XRCC1 recruits all the members of BER, PARP1, DNA polymerase β and ligase III in a complex [209, 210]. Defect in XRCC1 activity directly reflects on the function of each one of these proteins, but most critically on ligase III activity [211, 212]. A low residual ligase activity was detected in XRCC1 deficient cells, thus compromising seriously BER repair. Therefore, targeting XRCC1 downregulation would translate into decreased DNA ligase III activity as well. Overall, the severity of XRCC1 deficiency is revealed by the fact that XRCC1 knockout mice are lethal, whereas PARP1 knockout is viable and fertile [206, 213]. More importantly, aside from demonstrating an increase in XRCC1 upon radiation-induced DNA damage, changes in XRCC1 expression are observed in response to EGFR activation [214, 215].

# 1.4.4.3. Nucleotide-excision repair (NER)

NER pathway evolved as a more complex mechanism to correctly repair DNA lesions caused by cross-linking agents, reactive oxygen species, radiation, and polycyclic aromatic hydrocarbons [216]. Bulky adducts inflicted anywhere in the genome, activate the global-genomic NER, while lesions at genes being actively transcribed activate transcription-coupled

NER [217, 218]. Mechanistically, the steps and DNA repair enzymes involved are: (1) damage recognition, (2) binding of a multiprotein complex, (3) double incision of the damaged strand several nucleotides 5' and 3' away on both sides, (4) removal of the damage-containing nucleotides, (5) filling the resulting gap by DNA polymerase and (6) ligation [219]. The complex consists of XPC-HR23B, TFIIH, XPG, RPA (replication protein A) and ERCC1/XPF (Fig. 1.5). Individuals with mutations in any of the seven proteins involved (XPA-XPG), named after the characterization of the syndrome Xeroderma pigmentosum (XP), are severely compromised in DNA repair [187, 220]. One of the most critical proteins, involved in recognizing DNA lesions, recruiting proteins and stabilizing the repair complex is ERCC1. Panasci's group was the first to observe and report a correlation between increased ERCC1 levels and decreased response to platinum and chlorombucil [221, 222]. Furthermore, the ability of cells to highly activate DNA repair response and to overcome genotoxic stress was shown to be mediated by the activation of the stress response pathway [223]. This led to the interest in inhibiting signaling proteins which are involved in activation of DNA repair enzymes. Studies on DNA-damaging agents (e.g., cisplatin, radiation, alkylating agents) in combination with EGFR inhibitors (e.g., Iressa, tyrphostin) and MEK inhibitors (e.g., PD98059, U0126) have supported this important combination by demonstrating that decreased ERCC1mediated repair significantly enhanced drug cytotoxicity [215, 224]. More importantly, in the context of this thesis, is previous work by Banerjee et al. [224] demonstrating enhanced potency of DNA-EGFR dual targeting agents in combination with MEK inhibitors. By inhibiting the stress response pathway, a significant down regulation in the two components of the NER (ERCC1) and BER (XRCC1) was observed. Thus, MEK, with its significant involvement at a cross-talk between mitogenic, apoptotic and stress signaling pathways, appears as a critical target for enhancing potency of DNA damaging agents.

### 1.4.4.4. Mismatch repair (MMR)

MMR is a large protein complex, strictly regulated to result in high fidelity and error-free DNA repairs [225]. As the name implies the specificity of MMR is primarily for any base-pairing mismatches, deletion or insertion. Mispaired bases detected or generated during DNA replication and recombination activate the recruitment of the MMR proteins listed in figures 1.5 and 1.6.

The O<sup>6</sup>-MeG lesions, if not repaired first by AGT enzyme, result in the mismatch pairing of O<sup>6</sup>-MeG with thymine. This absence of AGT activity subsequently triggers the activation of the MMR pathway [225]. However, MMR is primarily acting on the newly synthesized strand where it removes the incorrectly paired pyrimidines to reinsert again a thymine or a cytosine opposite to O<sup>6</sup>-MeG. This persists in repeated futile MMR cycles which eventually provoke DNA nicks with the induction of apoptosis or replication arrest shown in figure 1.7. In addition, in the absence MMR activity or partial inactivation of these enzymes, cancer cells become tolerant to O<sup>6</sup>-MeG lesions [206]. In these settings, the inhibition of AGT activity, which usually enhances cell killing by methylating agents, is no longer able to potentiate the apoptotic effect of the latter DNA-damaging species [206, 226]. This aspect of combining AGT inhibitors with DNA-damaging drugs is very important for the cytotoxic effect of these compounds. Therefore, the MMR status of the cancer cells is a determinant for the response to afore mentioned combinations. This needs to be taken in consideration in order to avoid the unfavorable outcome of increasing the mutagenic activity of these compounds, the chance to introduce additional mutations and elevate the risk of developing secondary tumours. Overall, MMR-deficient tumours are resistant not only to methylating agents but to most of the DNAdamaging drugs used for the treatment of solid or hematological malignancies.

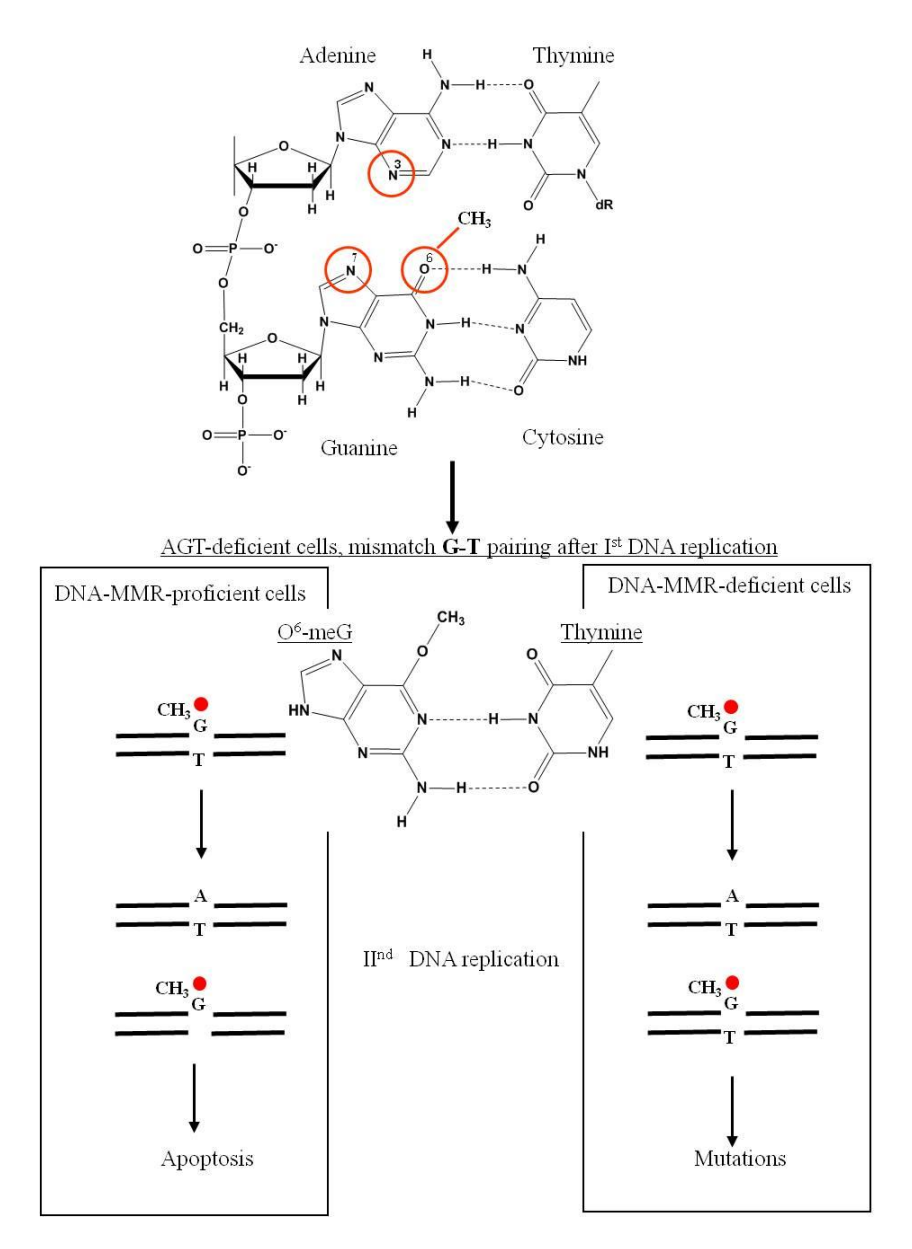


**Figure 1.7.** DNA repair of O<sup>6</sup>-meG in AGT-deficient cells.

MMR complex (see Fig. 1.6) has high recognition ability but less efficient removal. The outcomes in MMR-proficient cells are: (1) removal of the mispaired thymidine and futile MMR cycles until the methyl-guanine is either repaired leading to cell survival or not repaired leading to apoptosis. In the case of MMR-deficient cells the G-T mispaired bases lead to incorporation of wrong A-T propagation of mutation in the second round of replication.

# 1.4.4.5. Homologous recombination (HR) and non-homologous end-joining (NHEJ)

To protect DNA integrity, cells have developed two major DNA repair pathways: homologous recombination (HR) and non-homologous end-joining (NHEJ). The key component common for both NHEJ and HR pathways is the Mre11-Rad50-Nbs1 (MRN) complex which has important exonuclease and endonuclease activities [227, 228].

1.4.4.5.1. Non-homologous end-joining (NHEJ). As depicted in figure 1.8A, the NHEJ repair pathway is initiated by the MRN complex, followed by the recruitment of Ku70/80 heterodimers at the DSBs [229]. The latter heterodimers serving as a regulatory subunit of DNA-PK together with its catalytic subunit trigger the phosphorylation of several other DNA binding proteins and the typical H2AX DSB foci formation [199, 230]. The latter macromolecular complex recruits XRCC4/DNA ligase 4/XLF, which terminates the repair by rejoining the DNA ends. Due to the nature of NHEJ repair, which is a straightforward religation of broken DNA ends without any requirement for a template, this pathway is much highly error-prone but it is still very efficient DSBs repair mechanism.

1.4.4.5.2. Homologous recombination (HR). In contrast to NHEJ, HR is an error-free high fidelity rejoining of damaged DNA, which requires a homologous DNA strand as a template [175]. As illustrated in figure 1.8B, the HR repair pathway is initiated by ATM/ATR activation, through the recruitment of MRN complex at the DSBs. It requires DNA end-resection to generate 3' overhangs prior to homologous pairing and strand invasion. The recruitment of Rad51 onto the 3' overhang is assisted by BRCA2, Rad52 and Rad54 [231]. The DNA protein complex formed initiates strand invasion into an intact DNA strand in search for DNA homology. The structures formed, known as Holliday junctions, facilitate the invasion of the damaged DNA strand into the complementary sister chromatid strand, allowing for gap-filling and correct replication of the lost DNA. The repaired sequences are terminated with a final

# A. Non-homologous end-joining

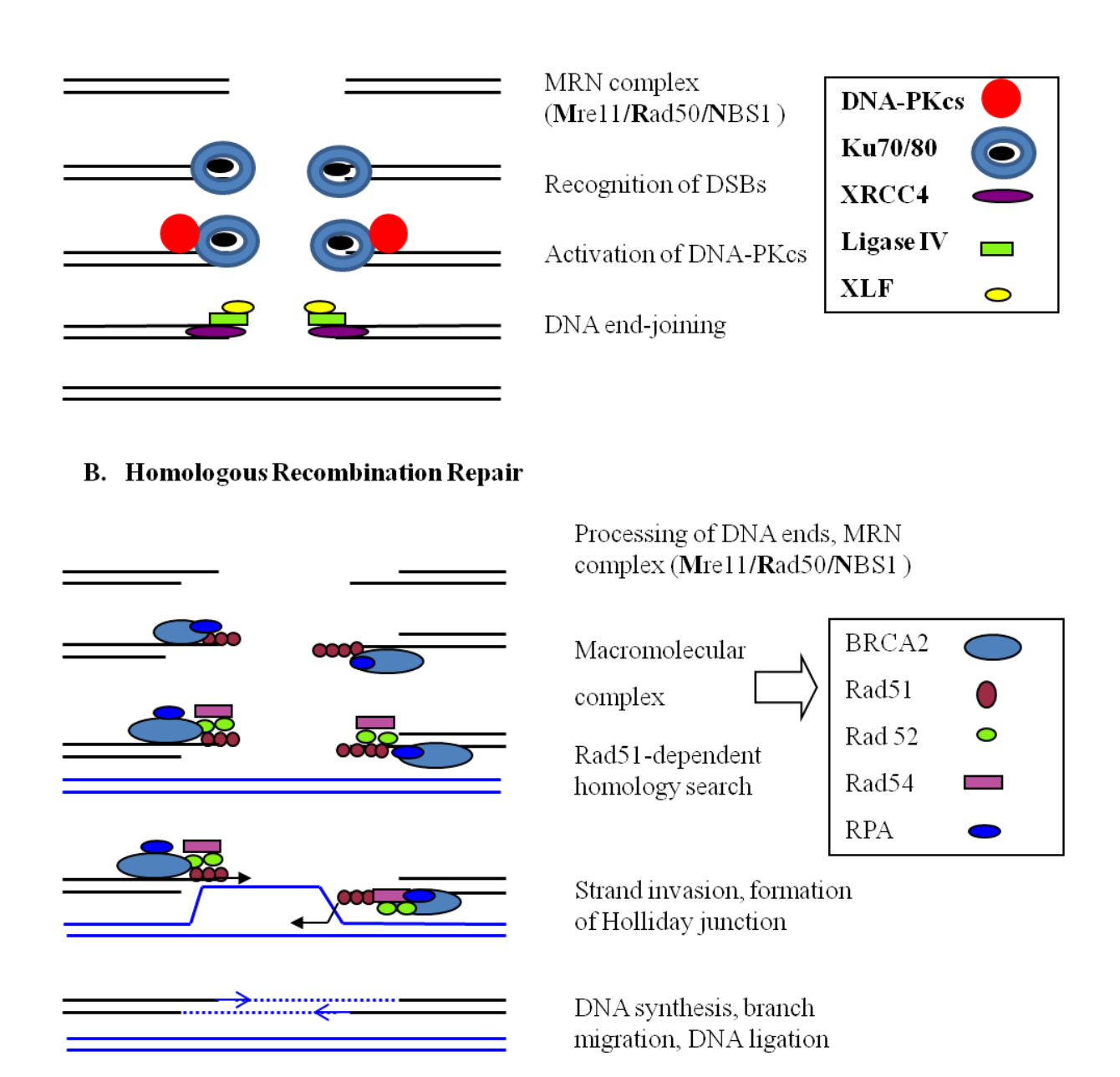


Figure 1.8. Steps and proteins involved in NHEJ (A) and HR (B) DNA repair pathways.

resolution of the Holliday junctions and ligation of the copied DNA strands, leading to crossover and non-crossover products. Cells defective in any of these DNA repair proteins are exquisitely sensitive not only to DNA-damaging agents, but to normal DNA damage occurring during cell division and metabolism.

### 1.4.4.6. Summary on DNA repair enzymes

On one side, the critical importance of these enzymes is to maintain DNA repair and to ensure DNA integrity. On the other, the efficiency of these enzymes to dictate the responsiveness to DNA damaging agents is a drawback. The challenge is how to develop these repair mechanisms to target for selective therapeutic intervention against cancer cells. The fact that some extremely resistant cells are still able to survive (TEM treated AGT negative cells or PARP1 treated BRCA1/BRCA2 negative cells), outlines nature of cancer cells and the capability of these cells to find alternative means to resist therapies. Thus, finding combinations of DNA damaging agents with DNA repair enzyme inhibitors (e.g., PARP1, AGT) with synergistic effects are the ultimate solution to the problem.

#### 1. 5. CELL DEATH MECHANISMS

Many DNA repair proteins have a dual function: (1) to be involved in DNA repair response and (2) to initiate apoptosis [174]. Germline mutations in these proteins result in high incidence of cancer and some of them are well known: BRCA1, ATM, ATR, p53, PARP1, XPB, XPD, MSH6, MLH1 involved at different steps in DNA repair complexes. For that reason, an inefficient DNA repair mechanism coupled with the inability to activate apoptotic machinery lead to mutations and cell tumorigenesis. Recently, this new post-translational modification of H2AX phosphorylation at Tyr-142 was characterized and is proposed to act as a switch in DNA

damage recognition. Cells either proceed toward recruitment of DNA repair enzymes or undergo activation of pro-apoptotic factors in response to DNA damage [232]. The classical response of most genotoxic agents discussed above involves two major apoptotic pathways: (1) extrinsic which is triggered by an external stimulus via the death receptor, (2) intrinsic executed by an internal trigger via activation of the mitochondrial factors forming the apoptosome. Even though they are triggered by totally different mechanisms, both pathways have common points of convergence and several cross-talks involving caspases activation.

## 1.5.1. Extrinsic apoptotic pathway

The signaling through Fas ligand and death receptor activation, known also as CD-95, Apo-1 and FasR, triggers the extrinsic mechanism of program cell death [233]. DNA damage caused by alkylating agents strongly induces Fas ligand (FasL) expression, the central pro-apoptotic protein involved in death receptor activation [234]. Even though different agents initiate different cell-type specific responses, the cascade downstream of CD-95 is executed by the release of cleaved caspase-8 from the death receptor complex. When accumulated in the cytoplasm it subsequently cleaves and activates other effector caspases, eventually leading to nuclear membrane degradation and DNA fragmentation.

#### 1.5.2. Intrinsic mitochondria-mediated apoptosis

Mitochondria are very sensitive to drug-induced DNA damage and are known to act as central regulators of cell death activation. Several pro-apoptotic signals converge to the mitochondria to initiate mitochondrial membrane permeabilization [235, 236]. The balance between the pro-apoptotic (e.g., BAD, BAK, BAX, tBID, BIM) and anti-apoptotic (e.g., A1, Bcl-2, Bcl-w, Bcl-X<sub>L</sub>) proteins activation and inhibition is what influences the apoptotic response [237-239]. This

triggers the release of mitochondrial apoptogenic factors from the intermembrane space and initiates coordinated events of caspase-dependent apoptotic machinery, known as apoptosome [240]. This large protein complex consists of the three major components: procaspase-9, **A**poptosis **P**rotease **A**ctivating **F**actor 1(APAF-1), and cytochrome *c*. The release of the latter from the mitochondria triggers the proteolytic maturation of caspases. On the other hand, a large group of regulatory proteins, identified as **I**nhibitors of **A**poptosis **P**roteins (IAPs) bind to the catalytic sites of caspases-3, -6, -7, -9 to keep them in their inactive state. When procaspase-9 is activated to caspase-9, it sequesters the IAPs, cleaves procaspase-3, -6, -7 and induces full activation of these effector caspases [241]. Other caspase activators in addition to caspase-9 include Hsp10 (stimulates the apoptosome), Smac and HtrA2 (both inhibit the caspase-inhibitory IAP members). Finally, the mitochondria release **A**poptosis-**I**nducing **F**actor (AIF) and endonuclease G, two proteins that translocate to the nucleus and cooperate in the induction of DNA fragmentation and DNA ladder formation during apoptosis [242, 243].

### 1.5.3. AKT anti-apoptotic targets

The central role of AKT in the anti-apoptotic network is defined by its interaction with several proteins executing apoptotic responses. AKT directly suppresses the mitochondria apoptotic pathway by phosphorylating the following targets. First, phosphorylation of BAD (Bclantagonist of cell death) by AKT at Ser-136 is a key modification at the intersection point between pro- and anti-apoptotic regulatory proteins. This inactivation of BAD to form BAD/Bcl-2 and BAD/Bcl-XL hetero-dimers promotes cell survival, thus restoring the anti-apoptotic functions of free Bcl-2 and Bcl-X<sub>L</sub> [239]. Second, the direct involvement of AKT in blocking cell death responses is by phosphorylating caspase-9 and attenuating its ability to act on downstream caspases. Third, AKT inhibits apoptosis signal-regulating kinase 1 (ASK1<sup>b</sup>) by

phosphorylating it and inactivating its pro-apoptotic effect [244]. ASK1 acts via JNK and p38, which trigger BID cleavage, BAX translocation and cytochrome c release. In addition, AKT activates the smallest member of the IAP family, the anti-apoptotic protein survivin [78]. The AKT response to EGF-stimulation is the classical pro-survival trigger. Furthermore, AKT is able to transmit signals resulting from various cellular stresses and DNA damage. This occurs via AKT phosphorylation of MDM2, its translocation to the nucleus, and subsequent ubiquitination and degradation of p53 [239].

## 1.5.3.1. Member of IAP family, survivin

Cancer cells have developed mechanisms to bypass normal apoptotic signals and to sustain high proliferative capacity even in more cytotoxic environment. One such anti-apoptotic protein which is overexpressed in cancer cells is the smallest member of IAP family, survivin [245, 246]. Normally it is expressed in cell cycle-dependent manner during G2/M phase, under E2F regulation which acts downstream of EGFR activation, through PI3K/AKT pathway, rather than MEK/ERK1/2 signaling [247]. Analysis of breast cancer tissues with high EGFR/ERbB2 levels showed a strong correlation between the level of receptor overexpression and survivin expression [248]. Survivin is stabilized by the mitotic kinase complex cdc2/cyclin B1 by phosphorylation at Thr-34 which protects it from proteasomal degradation. This process is inhibited and leads to a decrease in survivin levels by the use of either cdc25 phosphatase or cdc2 kinase inhibitors [249]. When inhibited it disrupts normal chromosome segregation, while when overexpressed it leads to cellular transformation and tumorigenesis [250]. The cyclindependent kinase inhibitor, flavopiridol, is a pan-CDK inhibitor of CDK2, CDK4, and CDK6 at nanomolar concentrations, resulting in cell cycle arrest at both the G1/S and the G2/M transition. It inhibits as well cdc2-mediated survivin phosphorylation, which results in growth inhibition, promotes apoptosis, and suppresses tumour growth *in vitro* and *in vivo* [249, 251]. While in most cell lines survivin expression is upregulated in an AKT-dependent manner, in some other cancer cell types survivin induction depends strongly on STAT3-mediated activation [252, 253]. Several important proteins (e.g., Hsp90, XIAP, cIAP1, Smac, Aurora B) have been shown to interact directly with survivin and modulate its functions [254]. All together these observations help us appreciate the functional diversity of survivin in tumour versus normal tissue, provide important clues for the control of survivin and direct us toward possible strategies for targeting its inhibition [246].

#### 1.6. RESISTANCE TO CANCER THERAPY

### 1.6.1. Multi-drug resistance (MDR)

As discussed in the previous sections most of the agents used in the clinic induced acquired resistance. A number of different mechanisms can trigger a unique protection system in cancer cells, referred to as multidrug resistance (MDR): (a) activation of detoxification enzymes to alter or inactivate drug activity, (b) alteration in apoptotic pathways, (c) increase in DNA repair pathways, (d) decreased uptake by carrier transporter proteins which mediates the cellular uptake of anticancer drugs, and (e) increased activity of the ATP-dependent efflux pump which flushes the toxic chemotherapeutic drugs outside the cells [255]. Until now, the classical theory for MDR accepted is the overexpression of ATP-binding cassette (ABC) family of transporters such as P-glycoprotein/ABCB1/MDR1, the group of multidrug resistance-related proteins (MRP) such as MRP1/ABCC1, MRP2/ABCC2 and half-transporter breast cancer resistance protein (BCRP/MXR/ABCG2) [255]. These ATP-dependent transporters, can efflux without selectivity for any compound with large molecular weights [256]. MDR phenomenon can be either due to intrinsic expression of the latter proteins without previous exposure to

chemotherapeutic agents or to the development of an acquired-resistance to a range of compounds after long-term exposure. A wide variety of solid tumours and hematological malignancy have increased levels of P-glycoproteins (P-gp), the ABCB1 member of the ABC membrane transporter family [257, 258]. Since P-gp expression represents the most common feature and the best understood form of MDR, its role will be described here in details.

### 1.6.2. P-glycoproteins

P-gps are one group of membrane transporters which act as pumps by effluxing the toxic compounds outside the cell. There are two MDR genes in humans but only the expression of mdr1 gene has been shown to be involved in drug resistance [255, 259]. This gene is expressed under normal conditions in liver and kidney cells and it is regulated in response to various xenobiotics and hormones. The product of this gene is a large 170-kDa plasma membrane protein, which is phosphorylated and highly glycosylated [260, 261]. The overexpression of these proteins represents a major hurdle in cancer drug therapy due to cells ability to acquire resistance during the course of drug treatment. Cells with abundant expression of P-gp develop a long term protection and confer to them the MDR phenotype. P-gp is usually highly expressed in tumours (e.g., kidney, pancreas, liver, colon) as part of various xenobiotics and hormones active transport regulation. In addition, many MDR tumours from epithelial origin often overexpress EGFR and P-gp [261]. Moreover, it has been demonstrated that EGFR activation can modulate the P-gp function through PLC activity [262]. Thus, further understanding of these membrane protein interactions would bring insight in P-gp-mediated drug resistance in EGFR-overexpressing cancers.

#### 1.7. COMBINATION THERAPY FOR TREATMENT OF SOLID TUMOURS

### 1.7.1. Classical combinations

#### 1.7.1.1. DNA-damaging agents and their limitations

Over the past 30 years, treatment with DNA targeting agents for various solid tumours (breast, prostate, lung, ovarian, colon, brain) and haematological malignancies has encountered serious limitations. As previously described, various DNA damaging compounds are used in the clinic, but their broad cell targeting spectrum resulted in high toxicity. Therefore, current therapies with DNA-damaging drugs often involve the combination of two or more cytotoxic agents.

## 1.7.1.2. Limitations of tyrosine kinase inhibitors

As an alternative to DNA-damaging therapeutic, a more "targeted approach" was developed that involved inhibiting receptor tyrosine kinases (e.g., EGFR, VEGFR, c-kit) or other downstream signaling proteins (e.g., Bcr-abl, c-Src, MAPK, AKT, mTOR) overexpressed in tumour cells. Blockade of these TKs, which have been described earlier, resulted in strong antitumour activity *in vivo*. The research and clinical applications of kinase inhibitors (e.g., Gleevec, Iressa, Tarceva, Sorafenib, Dasatinib) rapidly expanded over the last 20 years. Targeting RTK signaling has mainly achieved a cytostatic effect. Therefore, the growth promoting and survival mechanisms triggered by the receptor are often reactivated. In addition, the inhibition of EGFR signaling cannot attenuate all cell mitogenic-inducing signals. Thus, inhibition of one pathway results in compensatory response via the activation of an alternative pathway. Growth inhibitory properties of RTK inhibitors are not sufficient to eradicate the tumour and they often result in mutations with more aggressive and resistant tumours. To

improve treatment efficacy, targeted TK inhibitors are combined with classical DNA damaging agents.

#### 1.7.1.3. Advances with multi-drug combination strategy

Multi-drug combination strategy designed to minimize drug toxicity and to increase selectivity for cancer cells, has been explored for more than 15 years. However, these combinations involve two or three drugs, with their major disadvantage being systemic drug toxicity. Moreover, since the two agents are administered as two separate entities, it is not possible to control, influence and target a more selective distribution of both agents in the tumour.

#### 1.7.2. Combi-targeting approach

Based on its targeted nature, it is plausible to believe that a single compound with multiple intracellular targets would be a more effective agent against advanced and resistant tumours than their classical counterparts or corresponding combinations. It is in this context that a novel tumour targeting strategy termed "combi-targeting" was developed in the years 2000. These novel compounds termed "combi-molecules" were designed to hit several targets in the cells. This principle is illustrated in figure 1.9, where a combi-molecule, designated as EGFR-I-DNA, is designed to inhibit EGFR TK activity and to damage DNA. These agents carry two bioactive moieties that are used in the clinic: the Iressa-like structure of the aminoquinazoline moiety (I) and the DNA-targeting triazene moiety (TZ, Alk), capable of alkylating DNA. The entire combi-molecule is designed to diffuse into the cell, bind to one of its target, EGFR, before and after decomposing inside the cells. The quinazoline moiety, known to have a high affinity for the ATP-binding site of EGFR, is proposed to target the combi-molecule to EGFR and to hydrolyze either in situ or in the intracellular milieu into another EGFR inhibitor and a DNA

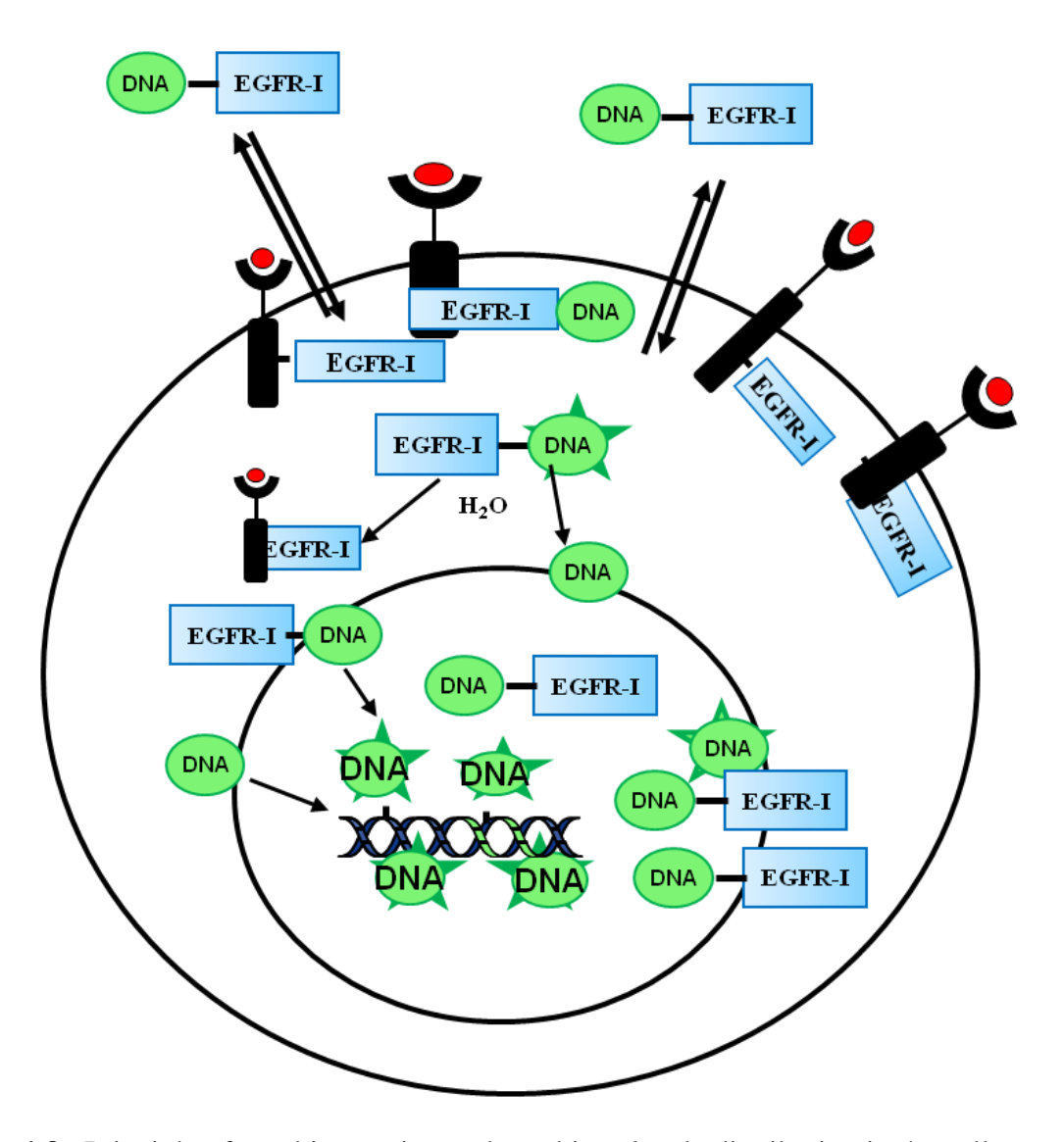


Figure 1.9. Principle of combi-targeting and combi-molecule distribution in the cell.

damaging species. This second DNA damaging moiety of the combi-molecule will diffuse towards the nuclear DNA. This strategy was designed to synthesize molecules that can mimic the targeting mechanism of classical alkylating agents, (e.g., Temozolomide, dacarbazine) and EGFR TK inhibitors (e.g., Iressa, Tarceva).

### 1.7.2.1. First generation of combi-molecules

For the last ten years, multiple aspects of combi-targeting have been explored *in vitro* and *in vivo*. Initially the feasibility of the combi-molecule strategy was proven by the first prototype of combi-molecules SMA41 [14] and BJ2000 [16]. The first single agent SMA41, contained the pharmacophore of the potent quinazoline class of EGFR TK inhibitors, and the active metabolite 3-alkyltriazene of the DNA-damaging agent Temozolomide [136, 263, 264]. The chimeric molecule is able to interact with the receptor on its own and upon hydrolysis to liberate the quinazoline moiety of EGFR TK inhibitor and the methyldiazonium DNA-damaging species. The high affinity of the molecule for EGFR, when delivered in EGFR-overexpressing cells was able to promote higher intracellular retention, thereby favouring more intracellular-than extracellular-degradation.

With these agents exhibiting reversible versus partially irreversible inhibition of EGFR respectively potent anti-proliferative activity and strong EGFR inhibition were demonstrated. The validity of this novel concept was supported by several publications [265-267]. The superior activity of combi-molecules was demonstrated when compared with its two identical moieties given in combination in several *in vitro* experiments.

### 1.7.2.2. Combi-molecules with improved water solubility, stability and EGFR binding

The challenge with SMA41, the first prototype combi-molecule, was: (1) poor water solubility, (2) decreased potency observed in AGT-expressing cells and (3) very short half-life. This was

further addressed with the synthesis of new prototype combi-triazene ZRBA1 [268]. With ZRBA1, we have successfully demonstrated the potency of a stable dimethyaminoethyl triazene ZRBA1 with a half-life of 108 min and a greater potency *in vivo* in MDA-MB-468 xenograft model than the first combi-triazene, SMA41 [265, 268]. The appendage of N,N-dimethylaminoethyl group at the 6-position of the quinazoline ring led to ZRBA1, a more water soluble molecule than SMA41. Moreover, the increased length of the spacer with a protonated central nitrogen was positioned at a distance that allowed: (a) an extra hydrogen bond with the acidic Asp-776 residue at the ATP site of EGFR and (b) an increase of the stability of the molecule [268, 269]. The third advantage over the observed hydrosolubility, stability and binding to EGFR, was the greater potency of ZRBA1 in cells that harbour high AGT levels. This was most likely due to the N,N-dimethylaminoethyl-guanine lesions formed, which are believed not to be the preferred substrate for AGT, O<sup>6</sup>-meG.

### 1.7.2.3. Cascade-release targeting combi-molecules

In order to further augment and sustain the inhibition of EGFR inhibitor, a novel approach was pursued to develop combi-molecules capable of degrading into multiple inhibitors of EGFR, generating highly reactive electrophiles in a stepwise fashion, a model termed "cascade release" [266]. The cascade release model slightly prolonged the half-life of 6-triazeno-quinazolines, but significantly increased water solubility of the resulting acetoxymethylene compounds. RB24 and RB107 were synthesized to prove the feasibility of the cascade release model. Indeed, these combi-molecules generated multiple EGFR inhibitors during the degradation steps and released the methyldiazonium DNA damaging species at the final stage of hydrolysis [266]. The formation of several intermediates with high irreversible binding affinity for EGFR resulted in much stronger receptor inhibition and sustained anti-prolifrative activity [270]. The rapid

hydrolysis of the masking acetoxy group of RB24 and RB107 accelerated their degradation *in vitro* and *in vivo*. To circumvent the problems associated with the instability of RB107 and enhance the bioavailability of combi-triazene molecules, a new series of quinazoline-based triazene containing a hydrolabile carbamate were synthesized and evaluated *in vitro* for antiproliferative activity and *in vivo* for antitumour efficacy [271]. Antitumour activities of two such compounds with carbamate moieties, ZRL1 and ZRS1, showed greated stability than RB107 and strong potency against MDA-MB-435 EGFR-expressing tumour models [271].

#### 1.7.2.4. Combi-nitrosoureas

Nitrosoureas are another class of potent DNA damaging agents with chloroalkylating and cross-linking activity. When conjugated to aminoquinazoline, the resulting combi-nitrosoureas are the most stable type I combi-molecule with an average half-life of 20 hours *ex vivo*. FD137 is an example of a potent and stable combi-nitrosourea studied *in vitro* and *in vivo* [272]. While the parent combi-molecule exerted only a moderate activity to block EGFR phosphorylation, upon hydrolysis, it released a strong secondary EGFR inhibitor and a damaging chloroethydiazonium species [273].

In search for a combi-nitrosourea with an improved EGFR TK inhibitory activity, 12 new combi-nitrosoureas were designed and evaluated based on their SAR [274]. From that series of molecules tested on the basis of its stability, EGFR TK inhibitory potency and selective EGFR targeting, JDA58 was considered to have the structural requirements for further development [275].

### 1.7.2.5. Classes of combi-molecules: type I and type II

The first generation of combi-molecules, which were described above, was designed to hydrolyze in cell culture medium. We demonstrated that these molecules after penetration in

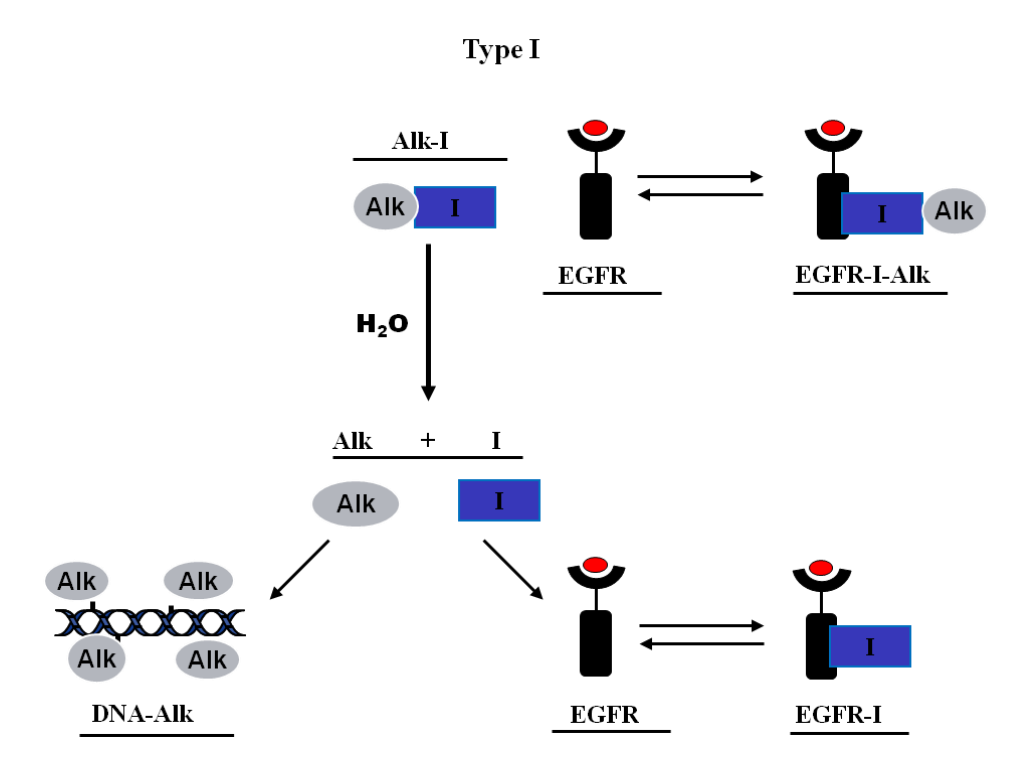
the cell, required hydrolytic scission to generate the cytotoxic function [16, 264]. Based on the ability of combi-molecules to either hydrolyze or remain intact in order to exert their binary or tertiary property, they are classified into two classes, termed type I and type II, respectively. Type I combi-molecules require hydrolysis to generate the DNA reactive species, versus type II have binary EGFR-DNA targeting function imprinted into the entire molecule. As demonstrated in figure 1.10 (top), the entire combi-molecule designated with *Alk-I* can inhibit the receptor or upon hydrolysis to generate the quinazoline-like EGFR inhibitor (*I*) and a DNA damaging moiety (*Alk*). On the other hand, type II combi-molecules *Alk-I* (Fig 1.10, bottom) exert their inhibition on EGFR (*Alk-I*) and on damaging DNA (*Alk-I*) while remaining intact [276, 277].

## 1.7.2.6. Examples of type II combi-molecules

The first prototypes of combi-molecules, capable of generating the mixed EGFR and DNA targeting properties without the requirement for hydrolysis, are ZR2002 and ZR2003. These are a series of hemi-mustard compounds that contain a chloroethyl group appended to the quinazoline. Thus, being partially irreversible EGFR inhibitors with a potent DNA damaging function, these type II combi-molecules induced significantly higher toxicity and strong apoptosis at a very low concentration [276, 277].

#### 1.7.2.7. Labeling combi-molecules for cellular distribution

The quinazoline fluorescence property was exploited to determine combi-molecule degradation in the cell and intracellular distribution of only the EGFR moiety. In order to trace the alkylating species released from the combi-molecule, radioactive <sup>14</sup>C-labeled methyl triazene species was used [278]. This was the first evidence that the drug was capable of alkylating all



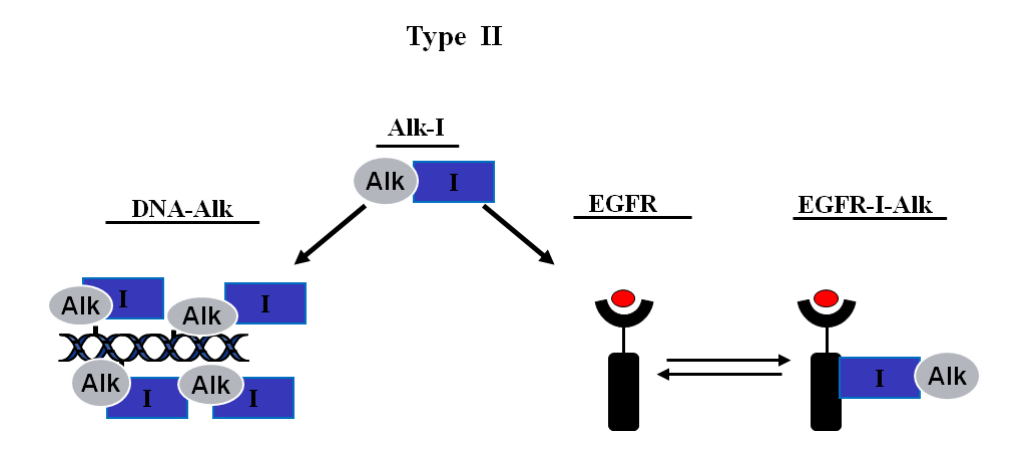


Figure 1.10. Type I and type II combi-molecules.

three macromolecules in the cell, proteins, RNA and DNA. However, fluorescence microscopy showed that the released inhibitor *I* was primarily localized in the perinuclear region. Even though the main receptor localization is at the plasma membrane, its concentration was not sufficiently high to detect the molecule associated with EGFR at the plasma membrane. Higher abundance of EGFR at the perinuclear region was reported in several studies, which can result from the association of the combi-molecules with EGFR in that area of the cells [13, 15].

#### 1.8 RESEARCH OBJECTIVES

The primary goal of this thesis was to define the potency and demonstrate the mechanism of action of: (1) type I combi-molecules, which are designed to hydrolyze in order to generate the DNA damaging moiety and (2) type II combi-molecules, which can induce the binary targeting mechanism without the requirement for hydrolysis. The prototype of combi-molecules used for probing intracellular distribution and targeting the combi-targeting principle, AL237 and AL194, for type I combi-molecule and ZR2008, for type II combi-molecule. Furthermore, with the purpose of adding a third target to the EGFR-DNA we designed and analyzed the mechanism of action of AL414 which was programmed to release EGFR inhibitor, DNA-damaging species and a flavone-containing MEK inhibitor.

### 1.8.1. Project outline

The following objectives were pursued in order to achieve the goals of this thesis:

**Objective 1:** To probe the subcellular distribution of specifically fluorescence-labeled type I combi-molecule, AL237, designed to release a blue fluorescent EGFR inhibitor and a green fluorescent DNA-damaging species.

**Objective 2:** To use the fluorescence probes developed in Objective 1 for determining whether P-glycoprotein was a determinant for the cytotoxic potentials of combi-molecules.

**Objective 3:** To increase the targeting spectrum of combi-molecules by synthesizing tricompartment combi-molecules designed to contain in addition to an EGFR-DNA targeting moiety a flavone-based MEK inhibitor.

**Objective 4:** To study the EGFR-DNA targeting mechanism of a type II combi-molecule, ZR2008, designed to damage DNA without requirement for hydrolysis.

The work *in toto* was designed to elucidate the mechanisms underlying the potency of EGFR-DNA targeting molecules of the two classes: type I and type II.

#### 1.9. REFERENCES

- 1. Brawley, O.W. and M.Z. Berger, *Cancer and disparities in health: perspectives on health statistics and research questions.* Cancer, 2008. **113**(7 Suppl): p. 1744-54.
- 2. Jemal, A., R. Siegel, E. Ward, et al., *Cancer statistics*, 2008. CA Cancer J Clin, 2008. **58**(2): p. 71-96.
- 3. Gibbs, J.B., Mechanism-based target identification and drug discovery in cancer research. Science, 2000. **287**(5460): p. 1969-73.
- 4. Pauwels, E.K., P. Erba, G. Mariani, et al., *Multidrug resistance in cancer: its mechanism and its modulation*. Drug News Perspect, 2007. **20**(6): p. 371-7.
- 5. Bianco, R., V. Damiano, T. Gelardi, et al., *Rational combination of targeted therapies* as a strategy to overcome the mechanisms of resistance to inhibitors of EGFR signaling. Curr Pharm Des, 2007. **13**(33): p. 3358-67.
- 6. Chen, H., *Optimising strategies for clinical development of combinations of targeted agents*. European Journal of Cancer Supplements, 2007. **5**(9): p. 3-5.
- 7. Arteaga, C.L., Overview of epidermal growth factor receptor biology and its role as a therapeutic target in human neoplasia. Semin Oncol, 2002. **29**(5 Suppl 14): p. 3-9.
- 8. Newlands, E.S., G.R. Blackledge, J.A. Slack, et al., *Phase I trial of temozolomide* (*CCRG 81045: M&B 39831: NSC 362856*). Br J Cancer, 1992. **65**(2): p. 287-91.
- 9. Newlands, E.S., M.F. Stevens, S.R. Wedge, et al., *Temozolomide: a review of its discovery, chemical properties, pre-clinical development and clinical trials.* Cancer Treat Rev, 1997. **23**(1): p. 35-61.
- 10. Quinn, J.A., S.X. Jiang, D.A. Reardon, et al., *Phase II trial of temozolomide plus O6-benzylguanine in adults with recurrent, temozolomide-resistant malignant glioma*. J. Clin. Oncol., 2009. **27**(8): p. 1262-1267.
- 11. Albanell, J. and P. Gascon, *Small molecules with EGFR-TK inhibitor activity*. Current Drug Targets, 2005. **6**(3): p. 259-274.
- 12. Kim, H.P., Y.K. Yoon, J.W. Kim, et al., *Lapatinib, a dual EGFR and HER2 tyrosine kinase inhibitor, downregulates thymidylate synthase by inhibiting the nuclear translocation of EGFR and HER2*. PLoS One, 2009. **4**(6): p. e5933.
- 13. Matheson, S.L., F. Brahimi, and B.J. Jean-Claude, *The combi-targeting concept: intracellular fragmentation of the binary epidermal growth factor (EGFR)/DNA targeting "combi-triazene" SMA41*. Biochemical Pharmacology, 2004. **67**(6): p. 1131-1138.

- 14. Matheson, S.L., J.P. McNamee, and B.J. Jean-Claude, *Differential responses of EGFR-AGT-expressing cells to the "combi-triazene" SMA41*. Cancer Chemoth. Pharm., 2003. **51**(1): p. 11-20.
- 15. Banerjee, R., Y. Huang, J.P. McNamee, et al., *The combi-targeting concept: selective targeting of the epidermal growth factor receptor- and Her2-expressing cancer cells by the complex combi-molecule RB24*. J Pharmacol Exp Ther, 2010. **334**(1): p. 9-20.
- 16. Brahimi, F., S.L. Matheson, F. Dudouit, et al., *Inhibition of epidermal growth factor receptor-mediated signaling by "Combi-Triazene" BJ2000, a new probe for Combi-Targeting postulates.* J. Pharmacol. Exp. Ther., 2002. **303**(1): p. 238-246.
- 17. Schlessinger, J. and A. Ullrich, *Growth factor signaling by receptor tyrosine kinases*. Neuron, 1992. **9**(3): p. 383-91.
- 18. Fantl, W.J., D.E. Johnson, and L.T. Williams, *Signalling by receptor tyrosine kinases*. Annu Rev Biochem, 1993. **62**: p. 453-81.
- 19. Jorissen, R.N., F. Walker, N. Pouliot, et al., *Epidermal growth factor receptor:* mechanisms of activation and signalling. Exp Cell Res., 2003. **284**(1): p. 31-53.
- 20. Wells, A., *EGF receptor*. Int J Biochem Cell Biol, 1999. **31**(6): p. 637-43.
- 21. Salomon, D.S., R. Brandt, F. Ciardiello, et al., *Epidermal growth factor-related peptides and their receptors in human malignancies*. Crit Rev Oncol Hematol, 1995. **19**(3): p. 183-232.
- 22. Moghal, N. and P.W. Sternberg, *Multiple positive and negative regulators of signaling by the EGF-receptor*. Curr Opin Cell Biol, 1999. **11**(2): p. 190-6.
- 23. Bishayee, A., L. Beguinot, and S. Bishayee, *Phosphorylation of tyrosine 992, 1068, and 1086 is required for conformational change of the human epidermal growth factor receptor c-terminal tail.* Mol Biol Cell, 1999. **10**(3): p. 525-36.
- 24. Lombardo, C.R., T.G. Consler, and D.B. Kassel, *In vitro phosphorylation of the epidermal growth factor receptor autophosphorylation domain by c-src: identification of phosphorylation sites and c-src SH2 domain binding sites.* Biochemistry, 1995. **34**(50): p. 16456-66.
- 25. Pawson, T., Specificity in Signal Transduction: From Phosphotyrosine-SH2 Domain Interactions to Complex Cellular Systems. Cell, 2004. **116**(2): p. 191-203.
- 26. Normanno, N., C. Bianco, L. Strizzi, et al., *The ErbB receptors and their ligands in cancer: an overview.* Curr Drug Targets, 2005. **6**(3): p. 243-57.
- 27. Blume-Jensen, P. and T. Hunter, *Oncogenic kinase signalling*. Nature, 2001. **411**(6835): p. 355-365.

- 28. de Diesbach, P., T. Medts, S. Carpentier, et al., *Differential subcellular membrane recruitment of Src may specify its downstream signalling*. Exp Cell Res, 2008. **314**(7): p. 1465-79.
- 29. Donepudi, M. and M.D. Resh, *c-Src trafficking and co-localization with the EGF receptor promotes EGF ligand-independent EGF receptor activation and signaling*. Cell Signal, 2008. **20**(7): p. 1359-67.
- 30. Lo, H.W., M. Ali-Seyed, Y. Wu, et al., *Nuclear-cytoplasmic transport of EGFR involves receptor endocytosis, importin beta1 and CRM1*. J Cell Biochem, 2006. **98**(6): p. 1570-83.
- 31. Okutani, T., Y. Okabayashi, Y. Kido, et al., *Grb2/Ash binds directly to tyrosines 1068 and 1086 and indirectly to tyrosine 1148 of activated human epidermal growth factor receptors in intact cells.* Journal of Biological Chemistry, 1994. **269**(49): p. 31310-31314.
- 32. McCarty, J.H., *The Nck SH2/SH3 adaptor protein: a regulator of multiple intracellular signal transduction events.* Bioessays, 1998. **20**(11): p. 913-921.
- 33. Hashimoto, Y., H. Katayama, E. Kiyokawa, et al., *Phosphorylation of CrkII Adaptor Protein at Tyrosine 221 by Epidermal Growth Factor Receptor*. Journal of Biological Chemistry, 1998. **273**(27): p. 17186-17191.
- 34. Jones, N. and D.J. Dumont, Recruitment of Dok-R to the EGF receptor through its PTB domain is required for attenuation of Erk MAP kinase activation. Curr Biol, 1999. **9**(18): p. 1057-60.
- 35. Serth, J., W. Weber, M. Frech, et al., *Binding of the H-ras p21 GTPase activating protein by the activated epidermal growth factor receptor leads to inhibition of the p21 GTPase activity in vitro*. Biochemistry, 1992. **31**(28): p. 6361-5.
- 36. Milarski, K.L., G. Zhu, C.G. Pearl, et al., Sequence specificity in recognition of the epidermal growth factor receptor by protein tyrosine phosphatase 1B. Journal of Biological Chemistry, 1993. **268**(31): p. 23634-23639.
- 37. Keilhack, H., T. Tenev, E. Nyakatura, et al., *Phosphotyrosine 1173 Mediates Binding of the Protein-tyrosine Phosphatase SHP-1 to the Epidermal Growth Factor Receptor and Attenuation of Receptor Signaling*. Journal of Biological Chemistry, 1998. **273**(38): p. 24839-24846.
- 38. Zhu, G., S.J. Decker, D. Maclean, et al., Sequence specificity in the recognition of the epidermal growth factor receptor by the abl Src homology 2 domain. Oncogene, 1994. 9(5): p. 1379-85.
- 39. Stover, D.R., M. Becker, J. Liebetanz, et al., Src phosphorylation of the epidermal growth factor receptor at novel sites mediates receptor interaction with Src and P85 alpha. J Biol Chem, 1995. **270**(26): p. 15591-7.

- 40. Stover, D.R., P. Furet, and N.B. Lydon, *Modulation of the SH2 binding specificity and kinase activity of Src by tyrosine phosphorylation within its SH2 domain.* J Biol Chem, 1996. **271**(21): p. 12481-7.
- 41. Biscardi, J.S., M.-C. Maa, D.A. Tice, et al., *c-Src-mediated phosphorylation of the epidermal growth factor receptor on Tyr845 and Tyr1101 is associated with modulation of receptor function.* Journal of Biological Chemistry, 1999. **274**(12): p. 8335-8343.
- 42. Sato, K., A. Sato, M. Aoto, et al., *c-Src phosphorylates epidermal growth factor receptor on tyrosine 845*. Biochem Biophys Res Commun, 1995. **215**(3): p. 1078-87.
- 43. Sakaguchi, K., Y. Okabayashi, Y. Kido, et al., Shc Phosphotyrosine-Binding Domain Dominantly Interacts with Epidermal Growth Factor Receptors and Mediates Ras Activation in Intact Cells. Mol Endocrinol, 1998. 12(4): p. 536-543.
- 44. Chattopadhyay, A., M. Vecchi, Q.-s. Ji, et al., *The Role of Individual SH2 Domains in Mediating Association of Phospholipase C-gamal with the Activated EGF Receptor.* Journal of Biological Chemistry, 1999. **274**(37): p. 26091-26097.
- 45. Chen, P., H. Xie, and A. Wells, *Mitogenic signaling from the egf receptor is attenuated by a phospholipase C-gamma/protein kinase C feedback mechanism.* Mol Biol Cell, 1996. **7**(6): p. 871-81.
- 46. Downward, J., Y. Yarden, E. Mayes, et al., *Close similarity of epidermal growth factor receptor and v-erb-B oncogene protein sequences*. Nature, 1984. **307**(5951): p. 521-7.
- 47. Velu, T.J., L. Beguinot, W.C. Vass, et al., *Epidermal-growth-factor-dependent transformation by a human EGF receptor proto-oncogene*. Science, 1987. **238**(4832): p. 1408-10.
- 48. Arteaga, C.L., The epidermal growth factor receptor: from mutant oncogene in nonhuman cancers to therapeutic target in human neoplasia. J Clin Oncol, 2001. **19**(18 Suppl): p. 32S-40S.
- 49. Khazaie, K., V. Schirrmacher, and R.B. Lichtner, *EGF receptor in neoplasia and metastasis*. Cancer Metastasis Rev, 1993. **12**(3-4): p. 255-74.
- 50. Ciardiello, F. and F. De Vita, *Epidermal growth factor receptor (EGFR) inhibitors in cancer therapy*. Prog Drug Res, 2005. **63**: p. 93-114.
- 51. Pines, G., W.J. Kostler, and Y. Yarden, *Oncogenic mutant forms of EGFR: lessons in signal transduction and targets for cancer therapy.* FEBS Lett, 2010. **584**(12): p. 2699-706.
- 52. Sorkin, A. and M. von Zastrow, *Endocytosis and signalling: intertwining molecular networks*. Nat Rev Mol Cell Biol, 2009. **10**(9): p. 609-22.

- 53. Gu, D., W.A. Scaringe, K. Li, et al., *Database of somatic mutations in EGFR with analyses revealing indel hotspots but no smoking-associated signature*. Human Mutation, 2007. **28**(8): p. 760-770.
- 54. Zandi, R., A.B. Larsen, P. Andersen, et al., *Mechanisms for oncogenic activation of the epidermal growth factor receptor*. Cellular Signalling, 2007. **19**(10): p. 2013-2023.
- 55. Mendelsohn, J. and J. Baselga, *Status of epidermal growth factor receptor antagonists in the biology and treatment of cancer.* J Clin Oncol, 2003. **21**(14): p. 2787-99.
- 56. Mendelsohn, J., *Anti-epidermal growth factor receptor monoclonal antibodies as potential anti-cancer agents*. J Steroid Biochem Mol Biol, 1990. **37**(6): p. 889-92.
- 57. Ogiso, H., R. Ishitani, O. Nureki, et al., Crystal structure of the complex of human epidermal growth factor and receptor extracellular domains. Cell., 2002. **110**(6): p. 775-87.
- 58. Garrett, T.P., N.M. McKern, M. Lou, et al., Crystal structure of a truncated epidermal growth factor receptor extracellular domain bound to transforming growth factor alpha. Cell, 2002. **110**(6): p. 763-73.
- 59. Decker, S.J., Transmembrane signaling by epidermal growth factor receptors lacking autophosphorylation sites. Journal of Biological Chemistry, 1993. **268**(13): p. 9176-9179.
- 60. Bridges, A.J., H. Zhou, D.R. Cody, et al., *Tyrosine kinase inhibitors: unusually steep structure-activity relationship for analogs of 4-(3-bromoanilino)-6,7-dimethoxyquinazoline (PD 153035), a potent inhibitor of the epidermal growth factor receptor.* Journal of Medicinal Chemistry, 1996. **39**(1): p. 267-76.
- 61. Rewcastle, G.W., W.A. Denny, A.J. Bridges, et al., Tyrosine kinase inhibitors. 5. Synthesis and structure-activity relationships for 4-[(phenylmethyl)amino]- and 4-(phenylamino)quinazolines as potent adenosine 5'-triphosphate binding site inhibitors of the tyrosine kinase domain of the epidermal growth factor receptor. J. Med. Chem., 1995. **38**(18): p. 3482-7.
- 62. Rewcastle, G.W., D.K. Murray, W.L. Elliott, et al., Tyrosine Kinase Inhibitors. 14. Structure-Activity Relationships for Methyl- amino-Substituted Derivatives of 4-[(3-Bromophenyl)amino]-6-(methylamino)- pyrido[3,4-d]pyrimidine (PD 158780), a Potent and Specific Inhibitor of the Tyrosine Kinase Activity of Receptors for the EGF Family of Growth Factors. J. Med. Chem., 1998. 41(5): p. 742-751.
- 63. Stamos, J., M.X. Sliwkowski, and C. Eigenbrot, Structure of the Epidermal Growth Factor Receptor Kinase Domain Alone and in Complex with a 4-Anilinoquinazoline Inhibitor. J. Biol. Chem., 2002. 277(48): p. 46265-46272.
- 64. Yarden, Y. and B.Z. Shilo, *SnapShot: EGFR signaling pathway*. Cell, 2007. **131**(5): p. 1018.

- 65. Hackel, P.O., E. Zwick, N. Prenzel, et al., *Epidermal growth factor receptors: critical mediators of multiple receptor pathways.* Curr Opin Cell Biol, 1999. **11**(2): p. 184-9.
- 66. Pawson, T. and M. Kofler, *Kinome signaling through regulated protein-protein interactions in normal and cancer cells.* Curr Opin Cell Biol, 2009. **21**(2): p. 147-53.
- 67. Katz, M., I. Amit, and Y. Yarden, *Regulation of MAPKs by growth factors and receptor tyrosine kinases*. Biochim Biophys Acta, 2007. **1773**(8): p. 1161-76.
- 68. Jaiswal, R.K., S.A. Moodie, A. Wolfman, et al., *The mitogen-activated protein kinase cascade is activated by B-Raf in response to nerve growth factor through interaction with p21ras*. Mol. Cell. Biol., 1994. **14**: p. 6944-6953.
- 69. Kyriakis, J.M., P. Banerjee, E. Nikolakaki, et al., *The stress-activated protein kinase subfamily of c-Jun kinases*. Nature, 1994. **369**(6476): p. 156-160.
- 70. Hanada, N., H.W. Lo, C.P. Day, et al., *Co-regulation of B-Myb expression by E2F1 and EGF receptor.* Mol Carcinog, 2006. **45**(1): p. 10-7.
- 71. Fruman, D.A., R.E. Meyers, and L.C. Cantley, *Phosphoinositide kinases*. Annu Rev Biochem, 1998. **67**: p. 481-507.
- 72. Vara, J.Á.F., E. Casado, J. de Castro, et al., *PI3K/Akt signalling pathway and cancer*. Cancer Treatment Reviews, 2004. **30**(2): p. 193-204.
- 73. Bellacosa, A., J.R. Testa, S.P. Staal, et al., *A retroviral oncogene, akt, encoding a serine-threonine kinase containing an SH2-like region.* Science, 1991. **254**(5029): p. 274-7.
- 74. Yuan, T.L. and L.C. Cantley, *PI3K pathway alterations in cancer: variations on a theme*. Oncogene., 2008. **27**(41): p. 5497-510.
- 75. Davis, R.J., Signal transduction by the JNK group of MAP kinases. Cell, 2000. **103**(2): p. 239-52.
- 76. Tournier, C., P. Hess, D.D. Yang, et al., Requirement of JNK for Stress- Induced Activation of the Cytochrome c-Mediated Death Pathway. Science, 2000. **288**(5467): p. 870-874.
- 77. Xia, Z., M. Dickens, J. Raingeaud, et al., *Opposing Effects of ERK and JNK-p38 MAP Kinases on Apoptosis*. Science, 1995. **270**(5240): p. 1326-1331.
- 78. Zwang, Y. and Y. Yarden, p38 MAP kinase mediates stress-induced internalization of EGFR: implications for cancer chemotherapy. EMBO J, 2006. **25**(18): p. 4195-206.
- 79. Vergarajauregui, S., A. San Miguel, and R. Puertollano, *Activation of p38 mitogen-activated protein kinase promotes epidermal growth factor receptor internalization*. Traffic, 2006. **7**(6): p. 686-98.

- 80. Hug, H. and T.F. Sarre, *Protein kinase C isoenzymes: divergence in signal transduction?* Biochem J, 1993. **291** ( **Pt 2**): p. 329-43.
- 81. Dekker, L.V. and P.J. Parker, *Protein kinase C--a question of specificity*. Trends Biochem Sci, 1994. **19**(2): p. 73-7.
- 82. Kharait, S., R. Dhir, D. Lauffenburger, et al., *Protein kinase Cdelta signaling downstream of the EGF receptor mediates migration and invasiveness of prostate cancer cells.* Biochem Biophys Res Commun, 2006. **343**(3): p. 848-56.
- 83. Dittmann, K., C. Mayer, B. Fehrenbacher, et al., *Nuclear EGFR shuttling induced by ionizing radiation is regulated by phosphorylation at residue Thr654*. FEBS Lett, 2010.
- 84. Levy, D.E., *The house that Jak/Stat built*. Cytokine Growth Factor Rev, 1997. **8**(1): p. 81-90.
- 85. Levy, D.E. and J.E. Darnell, *STATs: transcriptional control and biological impact*. Nat Rev Mol Cell Biol, 2002. **3**(9): p. 651-662.
- Wang, Y. and D.E. Levy, *C. elegans STAT: evolution of a regulatory switch.* FASEB J, 2006. **20**(10): p. 1641-52.
- 87. O'Shea, J.J., Y. Kanno, X. Chen, et al., *Cell signaling. Stat acetylation--a key facet of cytokine signaling?* Science, 2005. **307**(5707): p. 217-8.
- 88. David, M., L. Wong, R. Flavell, et al., STAT activation by epidermal growth factor (EGF) and amphiregulin. Requirement for the EGF receptor kinase but not for tyrosine phosphorylation sites or JAK1. J Biol Chem, 1996. 271(16): p. 9185-8.
- 89. Thomas, S.M. and J.S. Brugge, *Cellular functions regulated by Src family kinases*. Annu Rev Cell Dev Biol, 1997. **13**: p. 513-609.
- 90. Yeatman, T.J., *A renaissance for SRC*. Nat Rev Cancer, 2004. **4**(6): p. 470-80.
- 91. Biscardi, J.S., D.A. Tice, and S.J. Parsons, *c-Src*, receptor tyrosine kinases, and human cancer. Adv Cancer Res, 1999. **76**: p. 61-119.
- 92. Ishizawar, R. and S.J. Parsons, *c-Src and cooperating partners in human cancer*. Cancer Cell, 2004. **6**(3): p. 209-14.
- 93. Tice, D.A., J.S. Biscardi, A.L. Nickles, et al., *Mechanism of biological synergy between cellular Src and epidermal growth factor receptor*. Proceedings of the National Academy of Sciences of the United States of America, 1999. **96**(4): p. 1415-1420.
- 94. Belsches, A.P., M.D. Haskell, and S.J. Parsons, *Role of c-Src tyrosine kinase in EGF-induced mitogenesis*. Front Biosci, 1997. **2**: p. d501-18.

- 95. de Diesbach, M.T., A. Cominelli, F. N'Kuli, et al., Acute ligand-independent Src activation mimics low EGF-induced EGFR surface signalling and redistribution into recycling endosomes. Exp Cell Res.
- 96. Khan, E.M., J.M. Heidinger, M. Levy, et al., *Epidermal growth factor receptor exposed to oxidative stress undergoes Src- and caveolin-1-dependent perinuclear trafficking*. J Biol Chem, 2006. **281**(20): p. 14486-93.
- 97. Summy, J.M. and G.E. Gallick, *Src family kinases in tumor progression and metastasis*. Cancer Metastasis Rev, 2003. **22**(4): p. 337-58.
- 98. Alaoui-Jamali, M.A. and H. Qiang, *The interface between ErbB and non-ErbB receptors in tumor invasion: clinical implications and opportunities for target discovery.* Drug Resist Updat, 2003. **6**(2): p. 95-107.
- 99. Bergeron, J.J., G.M. Di Guglielmo, P.C. Baass, et al., *Endosomes, receptor tyrosine kinase internalization and signal transduction*. Biosci Rep, 1995. **15**(6): p. 411-8.
- 100. Wiley, H.S., *Trafficking of the ErbB receptors and its influence on signaling*. Exp Cell Res, 2003. **284**(1): p. 78-88.
- 101. Felder, S., K. Miller, G. Moehren, et al., *Kinase activity controls the sorting of the epidermal growth factor receptor within the multivesicular body*. Cell, 1990. **61**(4): p. 623-634.
- 102. Vieira, A.V., C. Lamaze, and S.L. Schmid, *Control of EGF Receptor Signaling by Clathrin-Mediated Endocytosis*. Science, 1996. **274**(5295): p. 2086-2089.
- 103. Mosesson, Y., K. Shtiegman, M. Katz, et al., *Endocytosis of receptor tyrosine kinases is driven by monoubiquitylation, not polyubiquitylation.* J Biol Chem, 2003. **278**(24): p. 21323-6.
- 104. Jiang, X., F. Huang, A. Marusyk, et al., *Grb2 Regulates Internalization of EGF Receptors through Clathrin-coated Pits.* Mol. Biol. Cell, 2003. **14**(3): p. 858-870.
- 105. Di Guglielmo, G.M., P.C. Baass, W.J. Ou, et al., Compartmentalization of SHC, GRB2 and mSOS, and hyperphosphorylation of Raf-1 by EGF but not insulin in liver parenchyma. Embo J, 1994. **13**(18): p. 4269-77.
- 106. Antonyak, M.A., D.K. Moscatello, and A.J. Wong, *Constitutive Activation of c-Jun N-terminal Kinase by a Mutant Epidermal Growth Factor Receptor*. Journal of Biological Chemistry, 1998. **273**(5): p. 2817-2822.
- 107. Pedersen, M.W., M. Meltorn, L. Damstrup, et al., *The type III epidermal growth factor receptor mutation*. Annals of Oncology, 2001. **12**(6): p. 745-760.
- 108. Parton, R.G. and K. Simons, *The multiple faces of caveolae*. Nat Rev Mol Cell Biol, 2007. **8**(3): p. 185-94.

- 109. Dittmann, K., C. Mayer, R. Kehlbach, et al., *Radiation-induced caveolin-1 associated EGFR internalization is linked with nuclear EGFR transport and activation of DNA-PK*. Mol Cancer, 2008. **7**: p. 69.
- 110. Khan, E.M., R. Lanir, A.R. Danielson, et al., *Epidermal growth factor receptor exposed to cigarette smoke is aberrantly activated and undergoes perinuclear trafficking*. FASEB J, 2008. **22**(3): p. 910-7.
- 111. Dittmann, K., C. Mayer, and H.P. Rodemann, *Inhibition of radiation-induced EGFR nuclear import by C225 (Cetuximab) suppresses DNA-PK activity.* Radiother Oncol, 2005. **76**(2): p. 157-61.
- 112. Murthy, U., M. Basu, A. Sen-Majumdar, et al., *Perinuclear location and recycling of epidermal growth factor receptor kinase: immunofluorescent visualization using antibodies directed to kinase and extracellular domains.* J Cell Biol, 1986. **103**(2): p. 333-42.
- 113. Jean-Claude, B., F. Brahimi, and Z. Rachid, *Preparation of aminoquinazolines as fluorescent irreversible inhibitors of epidermal growth factor receptor with DNA targeting properties*. 2005, (McGill University, Can.). p. 63 pp.
- 114. Carpenter, G. and H.-J. Liao, *Trafficking of receptor tyrosine kinases to the nucleus*. Experimental Cell Research, 2009. **315**(9): p. 1556-1566.
- 115. Lin, S.Y., K. Makino, W. Xia, et al., *Nuclear localization of EGF receptor and its potential new role as a transcription factor*. Nat Cell Biol, 2001. **3**(9): p. 802-8.
- 116. Li, C., M. Iida, E.F. Dunn, et al., *Nuclear EGFR contributes to acquired resistance to cetuximab*. Oncogene, 2009. **28**(43): p. 3801-13.
- 117. Hsu, S.C., S.A. Miller, Y. Wang, et al., *Nuclear EGFR is required for cisplatin resistance and DNA repair*. Am J Transl Res, 2009. **1**(3): p. 249-58.
- 118. Wanner, G., C. Mayer, R. Kehlbach, et al., *Activation of protein kinase C[epsilon] stimulates DNA-repair via epidermal growth factor receptor nuclear accumulation.* Radiotherapy and Oncology, 2008. **86**(3): p. 383-390.
- 119. Marti, U., S.J. Burwen, A. Wells, et al., *Localization of epidermal growth factor receptor in hepatocyte nuclei*. Hepatology, 1991. **13**(1): p. 15-20.
- 120. Marti, U. and A. Wells, *The nuclear accumulation of a variant epidermal growth factor receptor (EGFR) lacking the transmembrane domain requires coexpression of a full-length EGFR*. Mol Cell Biol Res Commun, 2000. **3**(1): p. 8-14.
- 121. Lo, H.W., Nuclear mode of the EGFR signaling network: biology, prognostic value, and therapeutic implications. Discov Med, 2010. **10**(50): p. 44-51.

- 122. Hung, L.-Y., J.T. Tseng, Y.-C. Lee, et al., Nuclear epidermal growth factor receptor (EGFR) interacts with signal transducer and activator of transcription 5 (STAT5) in activating Aurora-A gene expression. Nucl. Acids Res., 2008. **36**(13): p. 4337-4351.
- 123. Wang, A.S., B. Ramanathan, Y.H. Chien, et al., *Comet assay with nuclear extract incubation*. Anal Biochem., 2005. **337**(1): p. 70-5.
- 124. Lo, H.W., S.C. Hsu, M. Ali-Seyed, et al., *Nuclear interaction of EGFR and STAT3 in the activation of the iNOS/NO pathway.* Cancer Cell, 2005. **7**(6): p. 575-89.
- 125. Dittmann, K.H., C. Mayer, P.A. Ohneseit, et al., *Celecoxib Induced Tumor Cell Radiosensitization by Inhibiting Radiation Induced Nuclear EGFR Transport and DNA-Repair: A COX-2 Independent Mechanism.* International Journal of Radiation Oncology\*Biology\*Physics, 2008. **70**(1): p. 203-212.
- 126. Xia, W., Y. Wei, Y. Du, et al., Nuclear expression of epidermal growth factor receptor is a novel prognostic value in patients with ovarian cancer. Mol Carcinog, 2009. **48**(7): p. 610-7.
- 127. Ciardiello, F. and G. Tortora, *Epidermal growth factor receptor (EGFR) as a target in cancer therapy: understanding the role of receptor expression and other molecular determinants that could influence the response to anti-EGFR drugs.* Eur J Cancer, 2003. **39**(10): p. 1348-54.
- 128. Bianco, R., T. Gelardi, V. Damiano, et al., *Rational bases for the development of EGFR inhibitors for cancer treatment.* Int J Biochem Cell Biol, 2007. **39**(7-8): p. 1416-31.
- 129. Herbst, R.S., *EGFR inhibition in NSCLC: the emerging role of cetuximab.* J Natl Compr Canc Netw, 2004. **2 Suppl 2**: p. S41-51.
- 130. Hirsch, F.R., R.S. Herbst, C. Olsen, et al., *Increased EGFR gene copy number detected by fluorescent in situ hybridization predicts outcome in non-small-cell lung cancer patients treated with cetuximab and chemotherapy*. J Clin Oncol, 2008. **26**(20): p. 3351-7.
- 131. Slovin, S.F., W.K. Kelly, A. Wilton, et al., *Anti-epidermal growth factor receptor monoclonal antibody cetuximab plus Doxorubicin in the treatment of metastatic castration-resistant prostate cancer*. Clin Genitourin Cancer, 2009. **7**(3): p. E77-82.
- 132. Wagner, T.D. and G.Y. Yang, *Cetuximab: its use in combination with radiation therapy and chemo-therapy in the multimodality treatment of head and neck cancer.* Recent Pat Anticancer Drug Discov, 2008. **3**(2): p. 76-83.
- 133. Mano, M. and Y. Humblet, *Drug Insight: panitumumab, a human EGFR-targeted monoclonal antibody with promising clinical activity in colorectal cancer.* Nat Clin Pract Oncol, 2008. **5**(7): p. 415-25.

- 134. Strawn, L.M. and L.K. Shawver, *Tyrosine kinases in disease: overview of kinase inhibitors as therapeutic agents and current drugs in clinical trials.* Expert Opinion on Investigational Drugs, 1998. **7**(4): p. 553-573.
- 135. Pollack, V.A., D.M. Savage, D.A. Baker, et al., *Inhibition of epidermal growth factor receptor-associated tyrosine phosphorylation in human carcinomas with CP-358,774: dynamics of receptor inhibition in situ and antitumor effects in athymic mice.* J Pharmacol Exp Ther, 1999. **291**(2): p. 739-48.
- 136. Moyer, J.D., E.G. Barbacci, K.K. Iwata, et al., *Induction of apoptosis and cell cycle arrest by CP-358774, an inhibitor of epidermal growth factor receptor tyrosine kinase.* Cancer Research, 1997. **57**(21): p. 4838-4848.
- 137. Baselga, J., D. Rischin, M. Ranson, et al., *Phase I safety, pharmacokinetic, and pharmacodynamic trial of ZD1839, a selective oral epidermal growth factor receptor tyrosine kinase inhibitor, in patients with five selected solid tumor.* Journal of Clinical Oncology, 2002. **20**(21): p. 4292-4302.
- 138. Barker, A.J., K.H. Gibson, W. Grundy, et al., Studies leading to the identification of ZD1839 (iressa): an orally active, selective epidermal growth factor receptor tyrosine kinase inhibitor targeted to the treatment of cancer. Bioorganic & Medicinal Chemistry Letters, 2001. 11(14): p. 1911-1914.
- 139. Spector, N.L., W. Xia, H. Burris, 3rd, et al., *Study of the biologic effects of lapatinib, a reversible inhibitor of ErbB1 and ErbB2 tyrosine kinases, on tumor growth and survival pathways in patients with advanced malignancies.* J Clin Oncol, 2005. **23**(11): p. 2502-12.
- 140. Xia, W., C.M. Gerard, L. Liu, et al., Combining lapatinib (GW572016), a small molecule inhibitor of ErbB1 and ErbB2 tyrosine kinases, with therapeutic anti-ErbB2 antibodies enhances apoptosis of ErbB2-overexpressing breast cancer cells. Oncogene, 2005. **24**(41): p. 6213-21.
- 141. Torrance, C.J., P.E. Jackson, E. Montgomery, et al., *Combinatorial chemoprevention of intestinal neoplasia*. Nat Med, 2000. **6**(9): p. 1024-8.
- 142. Erlichman, C., M. Hidalgo, J.P. Boni, et al., *Phase I study of EKB-569, an irreversible inhibitor of the epidermal growth factor receptor, in patients with advanced solid tumors.* J Clin Oncol, 2006. **24**(15): p. 2252-60.
- 143. Smaill, J.B., G.W. Rewcastle, J.A. Loo, et al., *Tyrosine kinase inhibitors. 17. Irreversible inhibitors of the epidermal growth factor receptor: 4-(Phenylamino)quinazoline- and 4-(Phenylamino)pyrido.* J Med Chem, 2000. **43**(16): p. 3199.
- 144. Smaill, J.B., H.D. Showalter, H. Zhou, et al., *Tyrosine kinase inhibitors*. 18. 6-Substituted 4-anilinoquinazolines and 4-anilinopyrido[3,4-d]pyrimidines as soluble,

- irreversible inhibitors of the epidermal growth factor receptor. J Med Chem, 2001. **44**(3): p. 429-40.
- 145. Janne, P.A., N. Gray, and J. Settleman, *Factors underlying sensitivity of cancers to small-molecule kinase inhibitors*. Nat Rev Drug Discov, 2009. **8**(9): p. 709-723.
- 146. Raben, D., B. Helfrich, F. Ciardiello, et al., *Understanding the mechanisms of action of EGFR inhibitors in NSCLC: what we know and what we do not know.* Lung Cancer, 2003. **41 Suppl 1**: p. S15-22.
- 147. Lynch, T.J., D.W. Bell, R. Sordella, et al., *Activating mutations in the epidermal growth factor receptor underlying responsiveness of non-small-cell lung cancer to gefitinib.* N. Eng. J. Med., 2004. **350**(21): p. 2129-2139.
- 148. Brookes, P., *The early history of the biological alkylating agents, 1918-1968.* Mutat Res, 1990. **233**(1-2): p. 3-14.
- 149. Elmore, D.T., J.M. Gulland, D.O. Jordan, et al., *The reaction of nucleic acids with mustard gas.* Biochem J, 1948. **42**(2): p. 308-16.
- 150. Biesele, J.J., F.S. Philips, J.B. Thiersch, et al., *Chromosome alteration and tumour inhibition by nitrogen mustards; the hypothesis of crosslinking alkylation.* Nature, 1950. **166**(4235): p. 1112-4.
- 151. Brookes, P. and P.D. Lawley, *The reaction of mono- and di-functional alkylating agents with nucleic acids.* Biochem J, 1961. **80**(3): p. 496-503.
- 152. Lawley, P.D. and P. Brookes, *The Action of Alkylating Agents on Deoxyribonucleic Acid in Relation to Biological Effects of the Alkylating Agents*. Exp Cell Res, 1963. **24**: p. SUPPL9:512-20.
- 153. Krumbhaar, E.B. and H.D. Krumbhaar, *The Blood and Bone Marrow in Yelloe Cross Gas (Mustard Gas) Poisoning: Changes produced in the Bone Marrow of Fatal Cases.*J Med Res, 1919. **40**(3): p. 497-508 3.
- 154. Goodman, L.S., M.M. Wintrobe, W. Dameshek, et al., Landmark article Sept. 21, 1946: Nitrogen mustard therapy. Use of methyl-bis(beta-chloroethyl)amine hydrochloride and tris(beta-chloroethyl)amine hydrochloride for Hodgkin's disease, lymphosarcoma, leukemia and certain allied and miscellaneous disorders. By Louis S. Goodman, Maxwell M. Wintrobe, William Dameshek, Morton J. Goodman, Alfred Gilman and Margaret T. McLennan. JAMA, 1984. 251(17): p. 2255-61.
- 155. Gilman, A., *The initial clinical trial of nitrogen mustard*. Am J Surg, 1963. **105**: p. 574-8.
- 156. Audette, R.C., T.A. Connors, H.G. Mandel, et al., *Studies on the mechanism of action of the tumour inhibitory triagenes*. Biochem Pharmacol, 1973. **22**(15): p. 1855-64.

- 157. Stevens, M.F., J.A. Hickman, R. Stone, et al., *Antitumor imidazotetrazines*. 1. Synthesis and chemistry of 8-carbamoyl-3-(2-chloroethyl)imidazo[5,1-d]-1,2,3,5-tetrazin-4(3 H)-one, a novel broad-spectrum antitumor agent. J Med Chem, 1984. **27**(2): p. 196-201.
- 158. Marchesi, F., M. Turriziani, G. Tortorelli, et al., *Triazene compounds: mechanism of action and related DNA repair systems*. Pharmacol Res, 2007. **56**(4): p. 275-87.
- 159. Middleton, M.R. and G.P. Margison, *Improvement of chemotherapy efficacy by inactivation of a DNA-repair pathway*. Lancet Oncol., 2003. **4**(1): p. 37-44.
- 160. Bleehen, N.M., E.S. Newlands, S.M. Lee, et al., *Cancer Research Campaign phase II trial of temozolomide in metastatic melanoma*. Journal of clinical oncology: official journal of the American Society of Clinical Oncology, 1995. **13**(4): p. 910-3.
- 161. Denny, B.J., R.T. Wheelhouse, M.F. Stevens, et al., *NMR* and molecular modeling investigation of the mechanism of activation of the antitumor drug temozolomide and its interaction with DNA. Biochemistry, 1994. **33**(31): p. 9045-51.
- 162. Pletsa, V., C. Valavanis, J.H. van Delft, et al., *DNA damage and mutagenesis induced by procarbazine in lambda lacZ transgenic mice: evidence that bone marrow mutations do not arise primarily through miscoding by O6-methylguanine*. Carcinogenesis, 1997. **18**(11): p. 2191-6.
- 163. Drablos, F., E. Feyzi, P.A. Aas, et al., *Alkylation damage in DNA and RNA--repair mechanisms and medical significance*. DNA Repair (Amst), 2004. **3**(11): p. 1389-407.
- 164. McHugh, P.J., R.D. Gill, R. Waters, et al., *Excision repair of nitrogen mustard-DNA adducts in Saccharomyces cerevisiae*. Nucleic Acids Res, 1999. **27**(16): p. 3259-66.
- 165. Gandhi, V., *Metabolism and mechanisms of action of bendamustine: rationales for combination therapies.* Semin Oncol, 2002. **29**(4 Suppl 13): p. 4-11.
- 166. Rabik, C.A. and M.E. Dolan, *Molecular mechanisms of resistance and toxicity associated with platinating agents*. Cancer Treat Rev, 2007. **33**(1): p. 9-23.
- 167. Rabik, C.A., M.C. Njoku, and M.E. Dolan, *Inactivation of O6-alkylguanine DNA alkyltransferase as a means to enhance chemotherapy*. Cancer Treat Rev, 2006. **32**(4): p. 261-76.
- 168. Alaoui Jamali, M.A., M.B. Yin, A. Mazzoni, et al., *Relationship between cytotoxicity, drug accumulation, DNA damage and repair of human ovarian cancer cells treated with doxorubicin: modulation by the tiapamil analog RO11-2933*. Cancer Chemother Pharmacol, 1989. **25**(2): p. 77-83.
- 169. Chou, K.M., M. Kukhanova, and Y.C. Cheng, *A novel action of human apurinic/apyrimidinic endonuclease: excision of L-configuration deoxyribonucleoside analogs from the 3' termini of DNA*. J Biol Chem, 2000. **275**(40): p. 31009-15.

- 170. Harrison, L., Z. Hatahet, and S.S. Wallace, *In vitro repair of synthetic ionizing radiation-induced multiply damaged DNA sites.* J Mol Biol, 1999. **290**(3): p. 667-84.
- 171. Shealy, Y.F., C.A. Krauth, S.J. Clayton, et al., *Imidazoles V. 5(or 4)-(3-alkyl-3-methyl-1-triazeno)imidazole-4(or 5)-carboxamides*. J Pharm Sci, 1968. **57**(9): p. 1562-8.
- 172. Cheson, B.D. and M.J. Rummel, *Bendamustine: rebirth of an old drug.* J Clin Oncol, 2009. **27**(9): p. 1492-501.
- 173. Boulikas, T., Clinical overview on Lipoplatin: a successful liposomal formulation of cisplatin. Expert Opin Investig Drugs, 2009. **18**(8): p. 1197-218.
- 174. Bernstein, C., H. Bernstein, C.M. Payne, et al., *DNA repair/pro-apoptotic dual-role proteins in five major DNA repair pathways: fail-safe protection against carcinogenesis.* Mutat Res, 2002. **511**(2): p. 145-78.
- 175. Branzei, D. and M. Foiani, *Regulation of DNA repair throughout the cell cycle*. Nat Rev Mol Cell Biol, 2008. **9**(4): p. 297-308.
- 176. Lavin, M.F., S. Kozlov, N. Gueven, et al., *Atm and cellular response to DNA damage*. Adv Exp Med Biol, 2005. **570**: p. 457-76.
- 177. Auclair, Y., R. Rouget, and E.A. Drobetsky, *ATR kinase as master regulator of nucleotide excision repair during S phase of the cell cycle*. Cell Cycle, 2009. **8**(12): p. 1865-71.
- 178. Kelley, M.R. and M.L. Fishel, *DNA repair proteins as molecular targets for cancer therapeutics*. Anticancer Agents Med Chem, 2008. **8**(4): p. 417-25.
- 179. el-Deiry, W.S., T. Tokino, V.E. Velculescu, et al., *WAF1*, a potential mediator of p53 tumor suppression. Cell, 1993. **75**(4): p. 817-25.
- 180. Lakin, N.D. and S.P. Jackson, *Regulation of p53 in response to DNA damage*. Oncogene, 1999. **18**(53): p. 7644-55.
- 181. Falck, J., J.H. Petrini, B.R. Williams, et al., *The DNA damage-dependent intra-S phase checkpoint is regulated by parallel pathways.* Nat Genet, 2002. **30**(3): p. 290-4.
- 182. Roos, W.P. and B. Kaina, *DNA damage-induced cell death by apoptosis*. Trends Mol Med, 2006. **12**(9): p. 440-50.
- 183. Lane, D.P., Cancer. p53, guardian of the genome. Nature, 1992. **358**(6381): p. 15-6.
- 184. Flinterman, M., L. Guelen, S. Ezzati-Nik, et al., *E1A activates transcription of p73 and Noxa to induce apoptosis*. J Biol Chem, 2005. **280**(7): p. 5945-59.
- 185. Melino, G., V. De Laurenzi, and K.H. Vousden, *p73: Friend or foe in tumorigenesis*. Nat Rev Cancer, 2002. **2**(8): p. 605-15.

- 186. Melino, G., F. Bernassola, M. Ranalli, et al., *p73 Induces apoptosis via PUMA transactivation and Bax mitochondrial translocation*. J Biol Chem, 2004. **279**(9): p. 8076-83.
- 187. Kaina, B., *DNA damage-triggered apoptosis: critical role of DNA repair, double-strand breaks, cell proliferation and signaling.* Biochem Pharmacol, 2003. **66**(8): p. 1547-54.
- 188. Alaoui-Jamali Moulay A., P.J.S., Martin Loignon, Stress-activated signal transduction pathways in DNA damage response: Implications for repair, arrest, and therapeutic interventions, in Cancer Drug Dicovery and Development: DNA Repair in Cancer Therapy, A.-J.M.A. Lawrence C. Panasci, Editor. 2004, Humana Press. p. 109-142.
- 189. Christmann, M., M.T. Tomicic, D. Aasland, et al., A role for UV-light-induced c-Fos: Stimulation of nucleotide excision repair and protection against sustained JNK activation and apoptosis. Carcinogenesis, 2007. **28**(1): p. 183-90.
- 190. Mansouri, A., L.D. Ridgway, A.L. Korapati, et al., Sustained activation of JNK/p38 MAPK pathways in response to cisplatin leads to Fas ligand induction and cell death in ovarian carcinoma cells. J Biol Chem, 2003. 278(21): p. 19245-56.
- 191. Kaina, B., G. Fritz, and T. Coquerelle, *Identification of human genes involved in repair and tolerance of DNA damage*. Radiat Environ Biophys, 1991. **30**(1): p. 1-19.
- 192. Kaina, B., S. Haas, and H. Kappes, *A general role for c-Fos in cellular protection against DNA-damaging carcinogens and cytostatic drugs*. Cancer Res, 1997. **57**(13): p. 2721-31.
- 193. Fernandez-Capetillo, O., A. Celeste, and A. Nussenzweig, *Focusing on foci: H2AX and the recruitment of DNA-damage response factors*. Cell Cycle, 2003. **2**(5): p. 426-7.
- 194. Xiao, A., H. Li, D. Shechter, et al., WSTF regulates the H2A.X DNA damage response via a novel tyrosine kinase activity. Nature, 2009. **457**(7225): p. 57-62.
- 195. Stiff, T., M. O'Driscoll, N. Rief, et al., *ATM and DNA-PK Function Redundantly to Phosphorylate H2AX after Exposure to Ionizing Radiation*. Cancer Research, 2004. **64**(7): p. 2390-2396.
- 196. Rogakou, E.P., W. Nieves-Neira, C. Boon, et al., *Initiation of DNA fragmentation during apoptosis induces phosphorylation of H2AX histone at serine 139*. J Biol Chem, 2000. **275**(13): p. 9390-5.
- 197. Sedelnikova, O.A., E.P. Rogakou, I.G. Panyutin, et al., *Quantitative detection of* (125)IdU-induced DNA double-strand breaks with gamma-H2AX antibody. Radiat Res, 2002. **158**(4): p. 486-92.
- 198. Huang, S., E.A. Armstrong, S. Benavente, et al., *Dual-agent molecular targeting of the epidermal growth factor receptor (EGFR): combining anti-EGFR antibody with tyrosine kinase inhibitor.* Cancer Res, 2004. **64**(15): p. 5355-62.

- 199. Mischo, H.E., P. Hemmerich, F. Grosse, et al., *Actinomycin D induces histone gamma-H2AX foci and complex formation of gamma-H2AX with Ku70 and nuclear DNA helicase II.* J Biol Chem, 2005. **280**(10): p. 9586-94.
- 200. Takahashi, A. and T. Ohnishi, *Does [gamma]H2AX foci formation depend on the presence of DNA double strand breaks?* Cancer Letters, 2005. **229**(2): p. 171-179.
- 201. Banáth, J.P. and P.L. Olive, *Expression of Phosphorylated Histone H2AX as a Surrogate of Cell Killing by Drugs That Create DNA Double-Strand Breaks*. Cancer Research, 2003. **63**(15): p. 4347-4350.
- 202. Karran, P. and M. Bignami, *DNA damage tolerance, mismatch repair and genome instability*. Bioessays, 1994. **16**(11): p. 833-9.
- 203. Sancar, A., L.A. Lindsey-Boltz, K. Unsal-Kacmaz, et al., *Molecular mechanisms of mammalian DNA repair and the DNA damage checkpoints*. Annu Rev Biochem., 2004. **73**: p. 39-85.
- 204. Bramson, J., J. Prevost, A. Malapetsa, et al., *Poly(ADP-ribose) polymerase can bind melphalan damaged DNA*. Cancer Res, 1993. **53**(22): p. 5370-3.
- 205. D'Amours, D., S. Desnoyers, I. D'Silva, et al., *Poly(ADP-ribosyl)ation reactions in the regulation of nuclear functions.* Biochem J, 1999. **342 ( Pt 2)**: p. 249-68.
- 206. Tentori, L. and G. Graziani, *Chemopotentiation by PARP inhibitors in cancer therapy*. Pharmacol Res, 2005. **52**(1): p. 25-33.
- 207. Tell, G., G. Damante, D. Caldwell, et al., *The intracellular localization of APE1/Ref-1: more than a passive phenomenon?* Antioxid Redox Signal, 2005. **7**(3-4): p. 367-84.
- 208. Larsen, E., T.J. Meza, L. Kleppa, et al., *Organ and cell specificity of base excision repair mutants in mice*. Mutat Res, 2007. **614**(1-2): p. 56-68.
- 209. Thompson, L.H. and M.G. West, *XRCC1 keeps DNA from getting stranded*. Mutat Res, 2000. **459**(1): p. 1-18.
- 210. Kubota, Y., R.A. Nash, A. Klungland, et al., *Reconstitution of DNA base excision-repair with purified human proteins: interaction between DNA polymerase beta and the XRCC1 protein.* Embo J, 1996. **15**(23): p. 6662-70.
- 211. Caldecott, K.W., J.D. Tucker, L.H. Stanker, et al., *Characterization of the XRCC1-DNA ligase III complex in vitro and its absence from mutant hamster cells.* Nucleic Acids Res, 1995. **23**(23): p. 4836-43.
- 212. Caldecott, K.W., *XRCC1* and *DNA* strand break repair. DNA Repair (Amst), 2003. **2**(9): p. 955-69.

- 213. Tebbs, R.S., M.L. Flannery, J.J. Meneses, et al., *Requirement for theXrcc1DNA Base Excision Repair Gene during Early Mouse Development*. Developmental Biology, 1999. **208**(2): p. 513-529.
- 214. Yacoub, A., J.S. Park, L. Qiao, et al., *MAPK dependence of DNA damage repair:* ionizing radiation and the induction of expression of the DNA repair genes XRCC1 and ERCC1 in DU145 human prostate carcinoma cells in a MEK1/2 dependent fashion. International journal of radiation biology, 2001. **77**(10): p. 1067-78.
- 215. Yacoub, A., R. McKinstry, D. Hinman, et al., *Epidermal growth factor and ionizing radiation up-regulate the DNA repair genes XRCC1 and ERCC1 in DU145 and LNCaP prostate carcinoma through MAPK signaling*. Radiation research, 2003. **159**(4): p. 439-52.
- 216. Batty, D.P. and R.D. Wood, *Damage recognition in nucleotide excision repair of DNA*. Gene, 2000. **241**(2): p. 193-204.
- 217. Shuck, S.C., E.A. Short, and J.J. Turchi, *Eukaryotic nucleotide excision repair: from understanding mechanisms to influencing biology*. Cell Res, 2008. **18**(1): p. 64-72.
- 218. Fousteri, M. and L.H. Mullenders, *Transcription-coupled nucleotide excision repair in mammalian cells: molecular mechanisms and biological effects*. Cell Res, 2008. **18**(1): p. 73-84.
- 219. Wood, R.D., S.J. Araujo, R.R. Ariza, et al., *DNA damage recognition and nucleotide excision repair in mammalian cells*. Cold Spring Harb Symp Quant Biol, 2000. **65**: p. 173-82.
- 220. Arora, S., A. Kothandapani, K. Tillison, et al., *Downregulation of XPF-ERCC1* enhances cisplatin efficacy in cancer cells. DNA Repair (Amst). **9**(7): p. 745-53.
- 221. Panasci, L. and V. Cohen, *ERCC1 and non-small-cell lung cancer*. N Engl J Med, 2007. **356**(24): p. 2540; author reply 2540-1.
- 222. Alaoui-Jamali, M., B.B. Loubaba, S. Robyn, et al., *Effect of DNA-repair-enzyme modulators on cytotoxicity of L-phenylalanine mustard and cis-diamminedichloroplatinum (II) in mammary carcinoma cells resistant to alkylating drugs*. Cancer Chemother Pharmacol, 1994. **34**(2): p. 153-8.
- 223. Lu, X., T.A. Nguyen, E. Appella, et al., *Homeostatic regulation of base excision repair* by a p53-induced phosphatase: linking stress response pathways with DNA repair proteins. Cell Cycle, 2004. **3**(11): p. 1363-6.
- 224. Banerjee, R., A novel small molecule-based multi-targeting approach for the selective therapy of epidermal growth factor receptor (EGFR)- or Her2-expressing carcinomas Ph. D. dissertation, Faculty of Medicine, 2006.
- 225. Stojic, L., R. Brun, and J. Jiricny, *Mismatch repair and DNA damage signalling*. DNA Repair (Amst). 2004. **3**(8-9): p. 1091-101.

- 226. Bignami, M., I. Casorelli, and P. Karran, *Mismatch repair and response to DNA-damaging antitumour therapies*. Eur J Cancer, 2003. **39**(15): p. 2142-9.
- 227. Helleday, T., J. Lo, D.C. van Gent, et al., *DNA double-strand break repair: From mechanistic understanding to cancer treatment.* DNA Repair, 2007. **6**(7): p. 923-935.
- 228. Takata, M., M.S. Sasaki, E. Sonoda, et al., *Homologous recombination and non-homologous end-joining pathways of DNA double-strand break repair have overlapping roles in the maintenance of chromosomal integrity in vertebrate cells.* EMBO J, 1998. **17**(18): p. 5497-508.
- 229. Hefferin, M.L. and A.E. Tomkinson, *Mechanism of DNA double-strand break repair by non-homologous end joining*. DNA Repair (Amst), 2005. **4**(6): p. 639-48.
- 230. Celeste, A., O. Fernandez-Capetillo, M.J. Kruhlak, et al., *Histone H2AX* phosphorylation is dispensable for the initial recognition of DNA breaks. Nat Cell Biol, 2003. **5**(7): p. 675-9.
- 231. Jean-Claude, B.J., Chemosensitization to Platinum-Based Anticancer Drugs: Current Trends and Future Prospects in DNA repair in cancer therapy, A.-J.M.A. Lawrence C. Panasci, Editor. 2004, Humana Press: Totowa, NJ. p. 51-72.
- 232. Cook, P.J., B.G. Ju, F. Telese, et al., *Tyrosine dephosphorylation of H2AX modulates apoptosis and survival decisions*. Nature, 2009. **458**(7238): p. 591-6.
- 233. Nagata, S., Fas and Fas ligand: a death factor and its receptor. Adv Immunol, 1994. **57**: p. 129-44.
- 234. Mo, Y.Y. and W.T. Beck, *DNA damage signals induction of fas ligand in tumor cells*. Mol Pharmacol, 1999. **55**(2): p. 216-22.
- 235. Kroemer, G. and J.C. Reed, *Mitochondrial control of cell death*. Nat Med, 2000. **6**(5): p. 513-9.
- 236. Vieira, H.L. and G. Kroemer, *Pathophysiology of mitochondrial cell death control*. Cell Mol Life Sci, 1999. **56**(11-12): p. 971-6.
- 237. Cheng, E.H., M.C. Wei, S. Weiler, et al., *BCL-2*, *BCL-X(L)* sequester *BH3* domain-only molecules preventing *BAX-* and *BAK-mediated* mitochondrial apoptosis. Mol Cell, 2001. **8**(3): p. 705-11.
- 238. Wei, M.C., W.X. Zong, E.H. Cheng, et al., *Proapoptotic BAX and BAK: a requisite gateway to mitochondrial dysfunction and death.* Science, 2001. **292**(5517): p. 727-30.
- 239. Yang, E., J. Zha, J. Jockel, et al., *Bad, a heterodimeric partner for Bcl-xL and Bcl-2, displaces bax and promotes cell death.* Cell, 1995. **80**(2): p. 285-291.
- 240. Budihardjo, I., H. Oliver, M. Lutter, et al., *Biochemical pathways of caspase activation during apoptosis*. Annu Rev Cell Dev Biol, 1999. **15**: p. 269-90.

- 241. Hakem, R., A. Hakem, G.S. Duncan, et al., *Differential requirement for caspase 9 in apoptotic pathways in vivo*. Cell, 1998. **94**(3): p. 339-52.
- 242. Cande, C., F. Cecconi, P. Dessen, et al., *Apoptosis-inducing factor (AIF): key to the conserved caspase-independent pathways of cell death?* J Cell Sci, 2002. **115**(Pt 24): p. 4727-34.
- 243. Cande, C., N. Vahsen, C. Garrido, et al., *Apoptosis-inducing factor (AIF): caspase-independent after all.* Cell Death Differ, 2004. **11**(6): p. 591-5.
- 244. Kim, G.-M., J. Xu, J. Xu, et al., *Tumor Necrosis Factor Receptor Deletion Reduces Nuclear Factor-{kappa}B Activation, Cellular Inhibitor of Apoptosis Protein 2 Expression, and Functional Recovery after Traumatic Spinal Cord Injury.* J. Neurosci., 2001. **21**(17): p. 6617-6625.
- 245. Mita, A.C., M.M. Mita, S.T. Nawrocki, et al., Survivin: key regulator of mitosis and apoptosis and novel target for cancer therapeutics. Clin Cancer Res, 2008. **14**(16): p. 5000-5.
- 246. Altieri, D.C., Survivin, cancer networks and pathway-directed drug discovery. Nat Rev Cancer, 2008. **8**(1): p. 61-70.
- 247. Wang, H., B. Rosidi, R. Perrault, et al., *DNA ligase III as a candidate component of backup pathways of nonhomologous end joining.* Cancer Res, 2005. **65**(10): p. 4020-30.
- 248. Asanuma, H., T. Torigoe, K. Kamiguchi, et al., Survivin Expression Is Regulated by Coexpression of Human Epidermal Growth Factor Receptor 2 and Epidermal Growth Factor Receptor via Phosphatidylinositol 3-Kinase/AKT Signaling Pathway in Breast Cancer Cells. Cancer Research, 2005. 65(23): p. 11018-11025.
- 249. O'Connor, D.S., N.R. Wall, A.C. Porter, et al., *A p34(cdc2) survival checkpoint in cancer*. Cancer Cell, 2002. **2**(1): p. 43-54.
- 250. Li, F. and M.G. Brattain, *Role of the Survivin gene in pathophysiology*. Am J Pathol, 2006. **169**(1): p. 1-11.
- Wall, N.R., D.S. O'Connor, J. Plescia, et al., *Suppression of survivin phosphorylation on Thr34 by flavopiridol enhances tumor cell apoptosis.* Cancer Res, 2003. **63**(1): p. 230-5.
- 252. Kanda, N., H. Seno, Y. Konda, et al., *STAT3 is constitutively activated and supports cell survival in association with survivin expression in gastric cancer cells.* Oncogene, 2004. **23**(28): p. 4921-9.
- 253. Diaz, N., S. Minton, C. Cox, et al., *Activation of stat3 in primary tumors from high-risk breast cancer patients is associated with elevated levels of activated SRC and survivin expression.* Clin Cancer Res, 2006. **12**(1): p. 20-8.
- 254. Li, F. and X. Ling, Survivin study: an update of "what is the next wave"? J Cell Physiol, 2006. **208**(3): p. 476-86.

- 255. Gottesman, M.M., *Mechanisms of cancer drug resistance*. Annu Rev Med, 2002. **53**: p. 615-27.
- 256. Fardel, O., V. Lecureur, and A. Guillouzo, *The P-glycoprotein multidrug transporter*. General Pharmacology: The Vascular System, 1996. **27**(8): p. 1283-1291.
- 257. Mahadevan, D. and N. Shirahatti, *Strategies for targeting the multidrug resistance-1* (MDR1)/P-gp transporter in human malignancies. Curr Cancer Drug Targets, 2005. **5**(6): p. 445-55.
- 258. Szakacs, G., J.K. Paterson, J.A. Ludwig, et al., *Targeting multidrug resistance in cancer*. Nat Rev Drug Discov, 2006. **5**(3): p. 219-34.
- 259. Loo, T.W. and D.M. Clarke, *Recent progress in understanding the mechanism of P-glycoprotein-mediated drug efflux.* J. Membr. Biol., 2005. **206**(3): p. 173-185.
- 260. Gros, P., Y.B. Ben Neriah, J.M. Croop, et al., *Isolation and expression of a complementary DNA that confers multidrug resistance*. Nature, 1986. **323**(6090): p. 728-31.
- 261. Endicott, J.A. and V. Ling, *The Biochemistry of P-Glycoprotein-Mediated Multidrug Resistance*. Annual Review of Biochemistry, 1989. **58**(1): p. 137-171.
- 262. Yang, J.M., G.F. Sullivan, and W.N. Hait, Regulation of the function of P-glycoprotein by epidermal growth factor through phospholipase C. Biochem Pharmacol, 1997. 53(11): p. 1597-604.
- 263. Ching, K.Z., E. Ramsey, N. Pettigrew, et al., *Expression of mRNA for epidermal growth factor, transforming growth factor-alpha and their receptor in human prostate tissue and cell lines.* Mol Cell Biochem, 1993. **126**(2): p. 151-8.
- 264. Matheson, S.L., J. McNamee, and B.J. Jean-Claude, *Design of a chimeric 3-methyl-1,2,3-triazene with mixed receptor tyrosine kinase and DNA damaging properties: a novel tumor targeting strategy.* J. Pharmacol. Exp. Ther., 2001. **296**(3): p. 832-840.
- 265. Merayo, N., Z. Rachid, Q. Qiu, et al., *The combi-targeting concept: evidence for the formation of a novel inhibitor in vivo*. Anti-Cancer Drugs, 2006. **17**(2): p. 165-171.
- 266. Banerjee, R., Z. Rachid, J. McNamee, et al., Synthesis of a Prodrug Designed To Release Multiple Inhibitors of the Epidermal Growth Factor Receptor Tyrosine Kinase and an Alkylating Agent: A Novel Tumor Targeting Concept. J. Med. Chem., 2003. 46(25): p. 5546-5551.
- 267. Matheson, S., Q. Qiu, F. Brahimi, et al., [Combi-molecules: a global approach towards better chemoselectivity and chemosensitivity]. Bull Cancer, 2004. **91**(12): p. 911-5.
- 268. Brahimi, F., Z. Rachid, J.P. McNamee, et al., *Mechanism of action of a novel "combitriazene" engineered to possess a polar functional group on the alkylating moiety:* Evidence for enhancement of potency. Biochem. Pharm., 2005. **70**(4): p. 511-519.

- 269. Rachid, Z., F. Brahimi, Q. Qiu, et al., Novel nitrogen mustard-armed combi-molecules for the selective targeting of epidermal growth factor receptor overexperessing solid tumors: discovery of an unusual structure-activity relationship. J Med Chem, 2007. 50(11): p. 2605-8.
- 270. Banerjee, R., Z. Rachid, Q. Qiu, et al., Sustained antiproliferative mechanisms by RB24, a targeted precursor of multiple inhibitors of epidermal growth factor receptor and a DNA alkylating agent in the A431 epidermal carcinoma of the vulva cell line. Bri. J. Cancer, 2004. **91**(6): p. 1066-1073.
- 271. MacPhee, M., Z. Rachid, M. Todorova, et al., *Characterization of the potency of epidermal growth factor (EGFR)-DNA targeting combi-molecules containing a hydrolabile carbamate at the 3-position of the triazene chain.* Investigational New Drugs, 2010: p. 1-13.
- 272. Qiu, Q., F. Dudouit, R. Banerjee, et al., *Inhibition of cell signaling by the combinitrosourea FD137 in the androgen independent DU145 prostate cancer cell line*. Prostate (New York, NY, United States), 2004. **59**(1): p. 13-21.
- 273. Qiu, Q., F. Dudouit, S.L. Matheson, et al., *The combi-targeting concept: a novel 3,3-disubstituted nitrosourea with EGFR tyrosine kinase inhibitory properties.* Cancer Chemother Pharmacol, 2003. **51**(1): p. 1-10.
- 274. Domarkas, J., F. Dudouit, C. Williams, et al., *The Combi-Targeting Concept: Synthesis of Stable Nitrosoureas Designed to Inhibit the Epidermal Growth Factor Receptor (EGFR)*. J. Med. Chem., 2006. **49**(12): p. 3544-3552.
- 275. Qiu, Q., J. Domarkas, R. Banerjee, et al., *The combi-targeting concept: in vitro and in vivo fragmentation of a stable combi-nitrosourea engineered to interact with the epidermal growth factor receptor while remaining DNA reactive.* Clin Cancer Res, 2007. **13**(1): p. 331-40.
- 276. Brahimi, F., Z. Rachid, Q. Qiu, et al., Multiple mechanisms of action of ZR2002 in human breast cancer cells: A novel combi-molecule designed to block signaling mediated by the ERB family of oncogenes and to damage genomic DNA. Int. J. Cancer, 2004. 112(3): p. 484-491.
- 277. Rachid, Z., F. Brahimi, J. Domarkas, et al., *Synthesis of half-mustard combi-molecules with fluorescence properties: correlation with EGFR status.* Bioorganic & Medicinal Chemistry Letters, 2005. **15**(4): p. 1135-1138.
- 278. Matheson, S.L., S. Mzengeza, and B.J. Jean-Claude, *Synthesis of 1-[4-(m-tolylamino)-6-quinazolinyl]-3-[14C]methyltriazene: a radiolabeled probe for the combi-targeting concept.* J. Labelled Comp. Rad., 2003. **46**(8): p. 729-735.

# Chapter 2

Subcellular Distribution of a Fluorescence-Labeled Combi-Molecule Designed To Block

EGFR Tyrosine Kinase and Damage DNA with a Green Fluorescent Species

Margarita I. Todorova<sup>1</sup>, Anne-Laure Larroque<sup>1</sup>, Sabine Dauphin-Pierre<sup>1</sup>, You-Qiang Fang<sup>1,2</sup>
and Bertrand J. Jean-Claude<sup>1</sup>

<sup>1</sup>Cancer Drug Research Laboratory, Department of Medicine, Division of Medical Oncology, McGill University/Royal Victoria Hospital, 687 Pine Avenue West, Montreal, Quebec, Canada, H3A 1A1.

<sup>2</sup>Department of Urology of the Third Affiliated Hospital, Sun Yat-Sen University, 600 Tianhe Road, Guangzhou, 510630, China.

#### 2.1. ABSTRACT

In order to monitor the subcellular distribution of mixed EGFR-DNA targeting drugs termed "combi-molecules", we designed AL237, a fluorescent prototype, to degrade into a green fluorescent DNA damaging species and FD105, a blue fluorescent EGFR inhibitor. Here we showed that AL237 damaged DNA in the 12.5-50 µM range. Despite its size, it blocked EGFR phosphorylation in an enzyme assay (IC<sub>50</sub>=0.27 μM) and in MDA-MB-468 breast cancer cells in the same concentration range as for DNA damage. This translated into inhibition of extracellular signal-regulated kinase (ERK1/2) or BAD phosphorylation and downregulation of DNA repair proteins (XRCC1, ERCC1). Having shown that AL237 was a balanced EGFR-DNA targeting molecule, it was used as an imaging probe to show that: (a) green and blue colors were primarily co-localized in the perinuclear and partially in the nucleus in EGFR- or ErbB2-expressing cells, (b) the blue fluorescence associated with FD105, but not the green, was co-localized with anti-EGFR red-labeled antibody, (c) the green fluorescence of nuclei was significantly more intense in NIH 3T3 cells expressing EGFR or ErbB2 than in their wild-type counterparts (P<0.05). Similarly, the growth inhibitory potency of AL237 was selectively stronger in the transfectants. In summary, the results suggest that AL237 diffuses into the cells and localizes abundantly in the perinuclear region and partially in the nucleus where it degrades into EGFR and DNA targeting species. This bystander-like effect, translates into high levels of DNA damage in the nucleus. Sufficient quinazoline levels are released in the cells to block EGF-induced activation of downstream signaling.

KEYWORDS: EGFR tyrosine kinase, DNA damage, combi-molecule, N-dansylaziridine, fluorescence microscopy

#### 2.2. INTRODUCTION

The epidermal growth factor receptor (EGFR) and its closest family member p185<sup>neu</sup>, the product of the HER2 gene, are transmembrane receptor tyrosine kinases (TKs), that transduce signals associated with tumour cell proliferation [1-4]. The variety of approaches currently used to target EGFR includes small monoclonal antibody strategy to block ligand binding and TK inhibitors [5-7]. Over the past 10 years, molecules that inhibit receptor autophosphorylation and downstream intracellular signaling have been developed and have shown significant antitumour activity in vitro [8-12]. Several of them including gefitinib (Iressa®), erlotinib (Tarceva®) and lapatinib (Tykerb®/Tyverb®) have been approved for clinical use [13, 14]. However, none of these drugs are used in the clinic as single agents in the therapy of advanced cancers [15, 16]. Despite their ability to block growth signaling associated with EGFR or p185<sup>neu</sup>, cancer cells have the ability to evade the growth inhibitory effect of these drugs by activating alternative signaling pathways. Moreover, these drugs are reversible inhibitors indicating that the tumour cells may resume proliferation following drug clearance. Therefore, for an effective therapy, combination with a drug capable of killing the cell by a different mechanism (e.g., DNA damage or inhibition of DNA synthesis) is required. However, despite this overwhelming reality of cancer therapy, the development of mono-targeted drugs through high throughput screening or rational drug design remains the most generally adopted strategy. Over the past several years, we have developed a paradigm shifting strategy that seeks to design a single molecule with multiple functions termed "combi-molecule" [17-22]. These molecules despite their combination-based design were not developed with the purpose of eventually replacing the traditional chemotherapy but rather complementing it. Albeit, we demonstrated that many

prototypes (e.g., SMA41, FD137) showed stronger anti-proliferative activity than classical combinations of drugs with the same mechanism of action [20, 23-26].

As outlined in Figure 2.1A, the combi-molecules (see I-Alk) were designed to bind to EGFR on their own and to decompose into another EGFR inhibitor (I) plus a DNA alkylating species (Alk). Previous studies from our laboratory have demonstrated that indeed the combi-molecules (e.g., SMA41, Fig. 2.1A) could directly block EGFR in short exposure assay in vitro at room temperature in serum containing media [18]. Additionally, we demonstrated that they are capable of blocking EGFR phosphorylation and significantly damaging DNA in human tumour cells in vitro and in vivo indicating that our combi-molecules induce a bi-functional activity in whole cells [22, 27]. Using the fluorescence of the generated inhibitor I (excitation 294 nm, emission 451 nm) and <sup>14</sup>C radiolabeled alkyl moiety of SMA41, we previously confirmed that the combi-molecule could indeed decompose in the intracellular compartment into an EGFR inhibitor (I) and a methyldiazonium species (Alk) that damages DNA [27, 28]. While the fluorescence property of the aminoquinazoline (I) permitted the observation of its subcellular distribution or localization, that of the short-lived <sup>14</sup>C methyldiazonium could not be imaged [28]. Here we designed a novel probe, AL237, in which the fluorescent dansyl tag is attached to a 3-alkyl triazene moiety (Fig. 2.1B, I-Alk-Dansyl), which when hydrolysed will release a fluorescent alkylating agent (see Alk-Dansyl). Alkylation of DNA by this fluorescent alkylating molecule (see Fig. 2.1B) would lead to green nuclei (excitation 340 nm, emission around 525 nm) and the release of the aminoquinazoline (I, FD105, excitation 294 nm, emission 451 nm) would generate blue areas in the cells. Thus, fluorescence microscopy would allow us to image the complete fragmentation of the combi-molecule and its co-localization with one of its targets EGFR, using immunofluorescence. Here, we test these hypotheses with AL237 and correlate its biodistribution profile with its dual mechanism of action. For purpose of comparison, a nonconjugated dansylated alkyl agent, N-dansylaziridine was used (see structure in Fig. 2.5C). The latter, as previously reported, can only alkylate nucleic acids [29]. It is to be noted that this study does not seek to establish the growth inhibitory potency of AL237 but rather to demonstrate its binary EGFR-DNA targeting property and to be used as a probe to image the subcellular localization of the two bioactive degradation products responsible for its EGFR-DNA binary targeting mechanism.

#### 2.3. MATERIALS AND METHODS

#### 2.3.1. Cell culture

MDA-MB-468 human breast carcinomas were obtained from the American Tissue Culture Collection (ATCC, Manassas, VA). Mouse fibroblast cells NIH 3T3 used as control or NIH 3T3her14 (transfected with erbB1/EGFR gene) and NIH 3T3neu (transfected with erbB2 gene) were provided by Dr. Moulay Aloui-Jamali (Montreal Jewish General Hospital, Montreal, Canada). All cells were maintained in DMEM supplemented with 10% FBS, 10 mM HEPES, 2 mM L-gutamine and antibiotics (all reagent purchased from Wisent Inc., St-Bruno, Canada) as previously described [18]. Cells were maintained at exponential growth at 37°C in a humidified environment with 5% CO<sub>2</sub>. In all assays cells were plated 24 h before drug administration.

#### 2.3.2. Drug treatment

AL237 and JDA41 were synthesized in our laboratory. The methods used for AL237 and JDA41 complete synthesis were described elsewhere [22, 30]. N-dansylaziridine was purchased from Biomol (Plymouth Meeting, PA), Temozolomide and Iressa were purchased from the

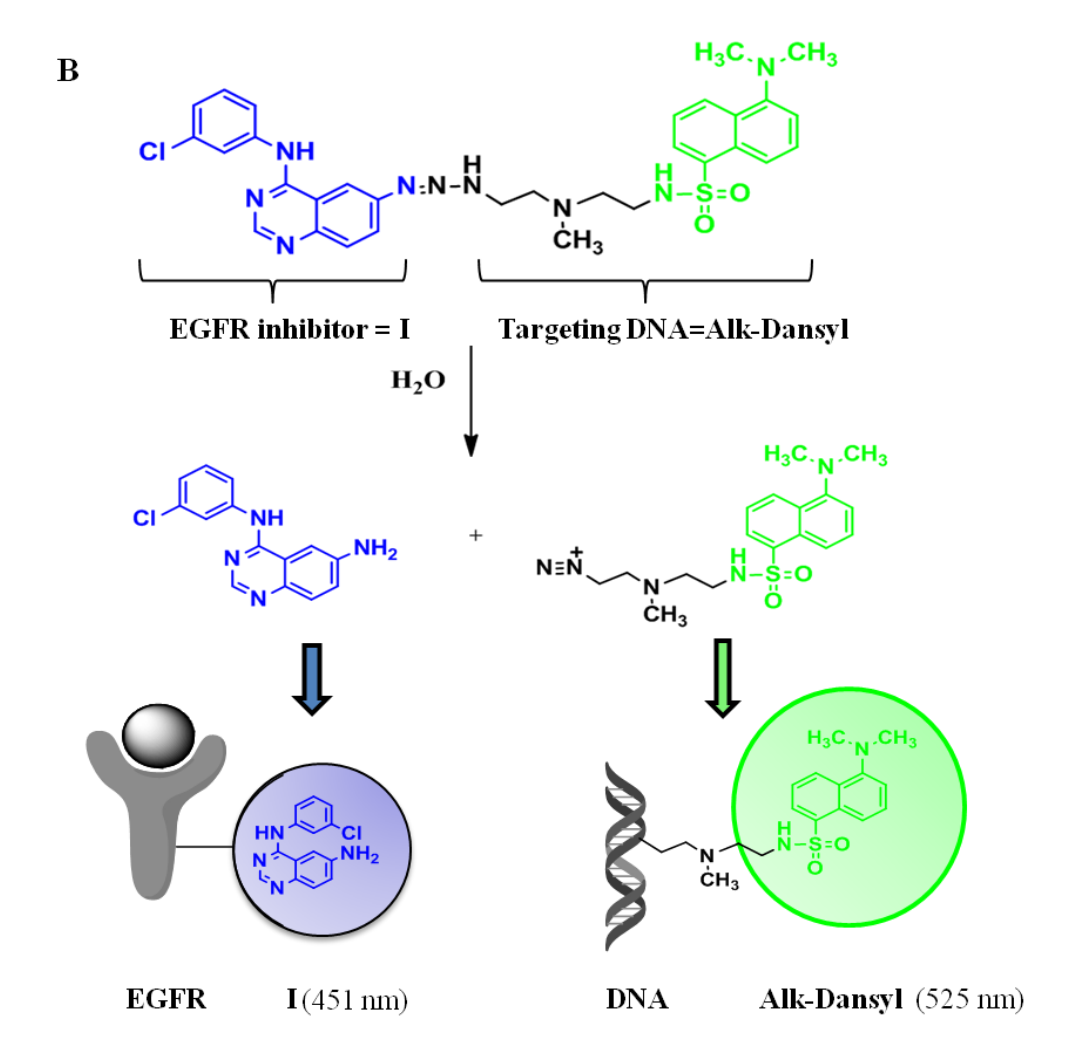


**Figure 2.1**. Structure and stepwise decomposition of AL237.

**A**, AL237 (I-Alk-Dansyl) hydrolyzes to generate EGFR inhibitor (I, FD105) and dansylated alkylating DNA species (Alk-Dansyl). The entire AL237 molecule and the dansylated DNA damaging species both emit at 525 nm (green). **B**, Schematic representation of the combitargeting concept of a single agent directed at two targets in the cell.

hospital pharmacy and extracted from pills in our laboratory. EGF was obtained from Roche Molecular Diagnostics (Laval, QC). In all assays, drugs were dissolved in DMSO and subsequently diluted in phenol-red/FBS-free DMEM before added to cells. The concentration of DMSO never exceeded 0.2% (v/v) during treatment.

#### 2.3.3. Growth inhibition assay

Cells were plated in 96-well flat-bottomed microtiter plates at 5,000 cells/well (NIH 3T3her14, NIH 3T3neu, MDA-MB-468) or 10,000 cells/well (NIH 3T3). After 24 h cells were exposed to different drug concentrations for four days. Briefly, following drug treatment, cells were fixed with 10% ice-cold trichloroacetic acid for 60 min at 4°C, stained with sulforhodamine B (SRB 0.4%) for 4 h at room temperature, rinsed with 1% acetic acid and allowed to dry overnight [31]. The SRB optical density was recorded at 492 nm using a Bio-Rad microplate reader. The results were analyzed by GraphPad Prism (GraphPad Software, Inc., San Diego, CA) and the sigmoidal dose response curve was used to determine IC<sub>50</sub>. Each point represents the average of at least three independent experiments run in triplicate.

#### 2.3.4. *In vitro* Enzyme Assay

The EGFR and src kinase assays are similar to one described previously [27]. Briefly, the kinase reaction was performed in 96-well plates using 4.5 ng/well EGFR or src (Biomol, PA). Following drug addition (range 0.0001-10 µM), phosphorylation of the EGFR was initiated by supplementing the reaction with ATP. The phosphorylated substrate was detected using a HRP-conjugated anti-phosphotyrosine antibody (Santa Cruz Biotechnology, CA) and the colorimetric reaction was monitored at 450 nm using a Bio-Rad reader. The results were analyzed by GraphPad Prism and IC<sub>50</sub> were calculated.

#### 2.3.5. Western Blot Analysis

Cells were grown to 80% confluence in six-well plates, serum starved for 24 h (serum-free DMEM), followed by a 2 h incubation with AL237 at the indicated concentrations. Cells were washed from the drug with PBS, then cells were stimulated with EGF (50 ng/ml) for 15 min. Cells were collected and lysed in ice-cold protein extraction buffer for 30 min (20 mM Tris-HCl pH 7.5, 1% NP-40, 10 mM EDTA, 150 mM NaCl, 20 mM NaF, 1mM Na vanadate, complete protease inhibitor cocktail (Roche Molecular Diagnostics, Laval, Qc)). Equal amounts of proteins were separated on 10% SDS-polyacrylamide gels, then transferred to a PVDF membrane (Immobilon-P, Millipore). Membranes were blocked with 5% milk in TBST (20 mM Tris-HCl, 137 mM NaCl, 0.1% Tween 20) for 3 h. Primary antibodies used for immunodetection were dissolved in antibody buffer (5 mM Tris-HCl pH 7.5, 150 mM NaCl, 0.05% (v/v) Tween 20, 0.05% (w/v) Na azide, 0.25% (w/v) gelatine) or TBST buffer as follows: anti-phospho-tyrosine (clone 4G10, Upstate; 1:1000), anti-EGFR (sc-03, Santa Cruz; 1:1000), anti-phospho-EGFR (Tyr<sup>1068</sup>, 1:1000), anti-XRCC1 (33-2-5, ThermoFisher Scientific; 1:1000), anti-ERCC1 (clone 3H11, ThermoFisher Scientific; 1:1000), anti-phospho-γH2AX (1:1000, Abcam, Cambridge, MA). Anti-phospho-ERK1,2 (Thr<sup>202</sup>/Tyr<sup>204</sup>; 1:4000), anti-ERK1,2 (p44/p42 MAP kinase; 1:2500), anti-phospho-BAD (Ser<sup>112</sup>; 1:1000), anti-BAD (1:250) were obtained from Cell Signaling Technology (Beverly, MA). Anti-tubulin-α (clone DM1A, NeoMarkers; 1:2000) was used as a loading control. Secondary HRP-conjugated antibodies were obtained from Jackson ImmunoResearch Laboratories (West Grove, PA). The bands were visualized using ECL (Amersham Bioscience). Western blot experiments were performed at least twice from two independent cell treatments.

#### 2.3.6. Alkaline comet assay

Cells were exposed to AL237 or N-dansylaziridine (0, 6.25, 12.5, 25, 50, 100 µM) for 2 h and the alkaline comet assay was performed as previously described [27, 32]. During this procedure, cells were protected from direct light to minimize DNA damage. Comets were visualized at 10X magnification using Leica microscope after staining with SYBR Gold (1:10,000, Molecular Probes, Eugene, OR). DNA damage was quantified using Comet Assay IV software (Perceptive Instruments, UK) and the degree of DNA damage was expressed as tail moments. Minimum 50 comets were analyzed for each cell treatment and the mean tail moments were calculated from three independent experiments.

#### 2.3.7. Neutral comet assay

Cells were treated and collected as in the alkaline comet assay, embedded in agarose at the same cell density and lysed with a neutral buffer for 2 h at room temperature (154 mM NaCl, 10 mM Tris-HCl pH 7.8, 10 mM EDTA, 0.5% (v/v) N-lauroyl-sarcosine, pH 8.0). Gels were soaked for 30 min in neutral TBE buffer (90 mM Tris-HCl pH 7.8, 90 mM Boric acid, 2 mM EDTA) and electrophorezed for 20 min at 20V [33, 34]. Modification of the assay permitted to retain the fluorescent dansyl tag to the sites of DNA adducts and allowed to observe nuclei without using a specific DNA staining dye.

#### 2.3.8. Intracellular fluorescence by UV flow cytometry

NIH 3T3, NIH 3T3her14 and NIH 3T3neu were plated at  $0.5 \times 10^6$  cells per well in six-well plates, allowed to adhere overnight and treated with AL237 (0, 6.25, 12.5, 25, 50, 100  $\mu$ M) for 45 min. Cells were collected, washed and resuspended in 300  $\mu$ l PBS supplemented with 1% FBS to minimize cell clumping. Cellular fluorescence levels were measured using a Becton-

Dickinson LSR flow cytometer (BD Biosciences, San Jose, CA). Cells were excited with 340 nm light emitting laser and the AL237 hydrolyzed fragments were detected as follows: the aminoquinazoline emitted at 451 nm (blue) and the dansylated DNA damaging species emitted at 525 nm (green). Fluorescence levels determined by FACS were analyzed with GraphPad Prism software and the accumulated fluorescence for each cell line was expressed as percent mean fluorescence over control. Four independent experiments were performed in duplicate.

# 2.3.9. Nuclear fluorescence UV flow cytometry

NIH3T3, NIH 3T3her14 and NIH 3T3neu were plated at 0.5 x10<sup>6</sup> cells per well in six-well plates, incubated overnight and exposed for 45 min to AL237 or N-dansylaziridine (0, 6.25, 12.5, 25, 50, 100 μM). After washing with PBS, cells were incubated in 300 μl of Vindelov solution for 15 min at 37°C (10 mM Tris-HCl pH 7.5; 10 mM NaCl, 0.1% Nonidet P40 (v/v); 100 μg/ml; RnaseA 50 units/ml) [35]. Nuclei were excited with 340 nm light emitting laser and the aminoquinazoline fragment of AL237 detected by emitting at 451 nm (blue) and the dansylated DNA damaging species or entire combi-molecule emitting at 525 nm (green) on a BD LSR flow cytometer. A minimum of 10,000 cell nuclei were acquired per sample, and each drug concentration was performed in duplicate. The fluorescence levels were quantified with CellQuest Pro software (Becton Dickinson, San Jose, CA), and results are reported as percent fluorescence over control from three independent experiments.

#### 2.3.10. Immunofluorescence of EGFR and phospho-tyrosine

MDA-MB-468 cells were plated at 60% confluence on a micro cover glass (VWR, Mississauga, ON) placed in a 24-well plate. Cells were starved overnight followed by treatment with 25  $\mu$ M AL237 for 2 h, and then stimulated with 50 ng/ml EGF for 15 min. Subsequently,

cells were washed twice with PBS, fixed with 100% ice-cold methanol at -20°C for 5 min, followed by 1h blocking with 5% normal goat serum. Double-immunostaining was performed using directly-coupled mouse anti-phospho-tyrosine-FITC (1:100), mouse anti-EGFR-PE (1:100), or the appropriate IgG-PE or IgG-FITC conjugated controls (1:100, purchased from Santa Cruz Biotechnology Inc., CA). Thereafter, cells were washed twice with PBS, stained with 5 ng/ml DAPI solution (Sigma, St. Louis, MO) and mounted with a gel mounting media (Fisher Scientific, Ottawa, ON). Immunofluorescence images were captured with Leica microscope (Leica, Wetzlar, Germany) using the appropriate filters and analyzed with Leica application suite software (LAS).

#### 2.3.11. Live cell fluorescence imaging of AL237 in NIH 3T3 cells

NIH 3T3, NIH 3T3her14 and NIH 3T3neu were plated at 70% confluence in six-well plates, allowed to adhere overnight and treated with 25  $\mu$ M AL237 for 2 h. At the indicated time points cells were washed with PBS twice and images were saved with Leica DFC300FX camera with the appropriate filters.

# 2.3.12. Immunofluorescence of phospho-γH2AX

MDA-MB-468 cells were plated on slides, incubated overnight, followed by a treatment with 25 μM and 50 μM of AL237 for 2 h. Cells were fixed with 4% paraformaldehyde for 20 min and permeabilized with 0.1% Triton X-100 for 10 min, followed by 1h blocking with 5% normal goat serum. Slides were incubated with mouse anti-phospho-γH2AX antibody (Abcam, Cambridge, MA) for 3h and anti mouse FITC-labeled secondary antibody (Sigma, St. Louis, MO) for 1 h. Typical for double strand DNA breaks phospho-γH2AX foci were observed on a fluorescent Leica microscope at 40X.

# 2.3.13. Annexin V/PI binding assay

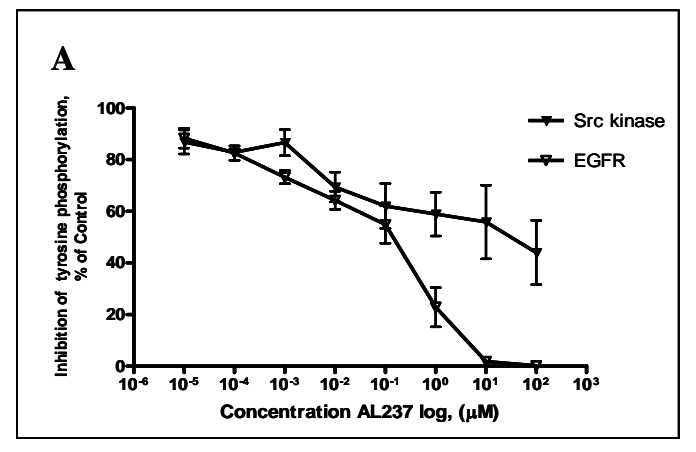
MDA-MB-468 cells were plated in a 6-well plate and treated with a dose range of each drug for 48 h. Thereafter, cells were harvested and incubated with Annexin V-FITC and propidium iodide (PI) using the apoptosis detection kit (BenderMedSystems Inc, USA) following the protocol provided by the supplier. Annexin V-FITC and PI binding were analyzed with a Becton-Dickinson FACScan. Data were collected using logarithmic amplification of both the FL1 (FITC) and FL2 (PI) channels. Quadrant analysis of co-ordinate dot plots was performed with CellQuestPro software.

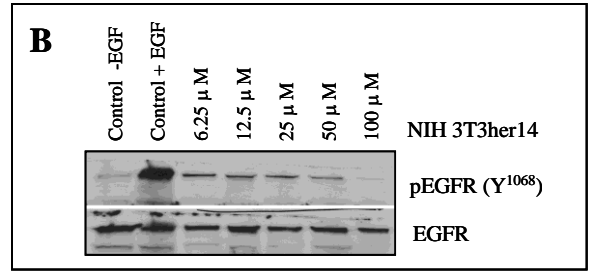
# **2.4. RESULTS**

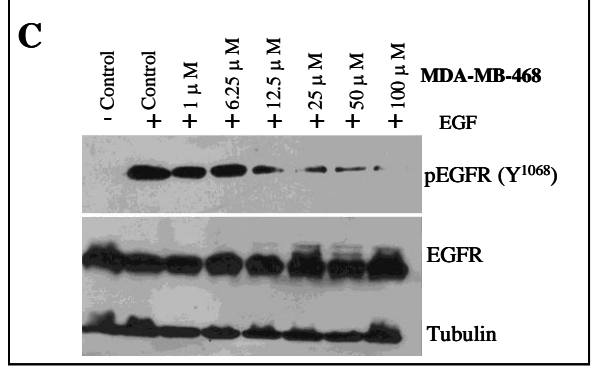
#### 2.4.1. Analysis of binary EGFR-DNA targeting potentials

# 2.4.1.1. Inhibition of EGFR phosphorylation

AL237 being a bulky molecule, we first determined whether the long spacer attached to the 6-position of the quinazoline ring affects its ability to inhibit receptor phosphorylation in purified EGFR enzyme assay. Our results showed that AL237 was capable of inhibiting EGFR phosphorylation with an  $IC_{50}$ =0.27  $\mu$ M. Moreover, we have addressed AL237 selective EGFR binding by measuring inhibition of tyrosine phosphorylation on a src kinase. The result indicates that, despite its significant bulkiness, AL237 binds strongly to the ATP-binding site of EGFR and it is a selective EGFR inhibitor (Fig. 2.2A). Indeed, varieties of similar compounds with bulky side chains have been synthesized in our laboratory and have been shown to retain strong EGFR binding affinity [23, 36, 37]. It is also known that most anilinoquinazolines show unspecific binding to the ErbB2 gene product, which is the closest family member of EGFR [13]







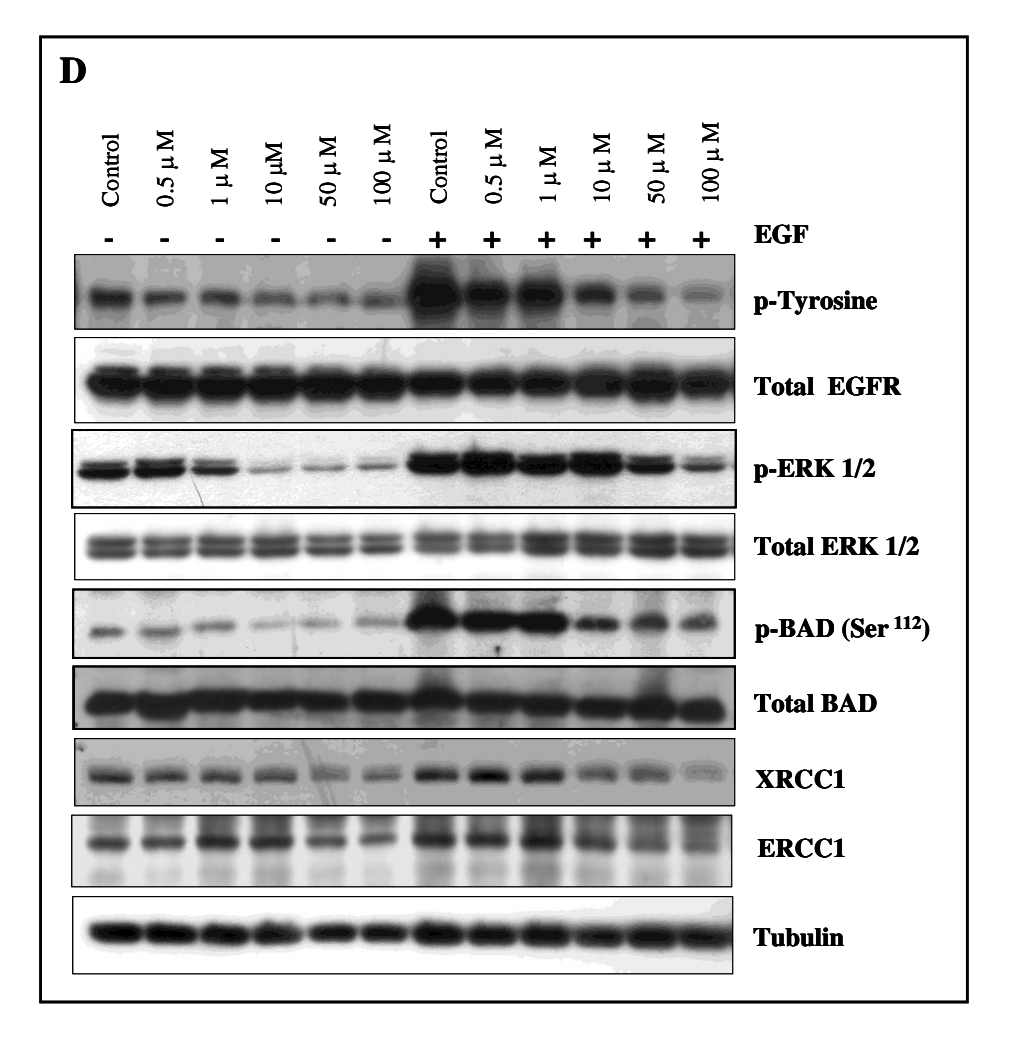


**Figure 2.2**. AL237 inhibits EGFR phosphorylation and downstream signaling.

A, Inhibition of EGFR and src tyrosine phosphorylation by AL237 was measured by in vitro binding assay. Each point represents mean ± SD of three independent experiments run in duplicate. **B**, inhibition of EGFR phosphorylation by AL237 was analyzed in NIH 3T3 cells transfected with EGFR (NIH 3T3her14) by Western blot. Cellular proteins were isolated after exposure to increasing AL237 concentrations for 2 h, followed by EGF stimulation (50 ng/ml). C, MDA-MB-468 cellular proteins (50 µg) were analyzed for phospho-EGFR inhibition after treatment with the indicated doses of AL237 for 2 h, followed by EGF stimulation. Membranes were incubated with anti-phospho-EGFR (tyrosine 1068) antibody. **D,** MDA-MB-468 cells were starved overnight, treated with the indicated concentrations of AL237 for 2 h, thereafter stimulated or not stimulated with EGF (50 ng/ml) for 15 min. Afterwards, cellular proteins were analyzed by Western blot for the effect of AL237 on phospho-ERK1, 2 and phospho-BAD (serine<sup>112</sup>) protein levels followed by incubation with anti-ERK1,2 and anti-BAD antibodies. Blots were also incubated with antibodies against ERCC1 and XRCC1 to detect DNA repair proteins and anti-tubulin antibody was used to control for equal loading. Western blots were repeated twice and similar results from two independent treatments were obtained.

More importantly, to verify the ability of AL237 to block EGFR phosphorylation in whole cells, we analyzed phospho-EGFR levels (Tyr<sup>1068</sup>) in the two panels of EGFR expressing cells.

AL237 induced  $\sim 100\%$  inhibition of EGFR phosphorylation at 6.25  $\mu$ M in NIH 3T3 EGFR transfectant (Fig. 2.2B) and at 12.5  $\mu$ M in the MDA-MB-468 cells (Fig. 2.2C).

# 2.4.1.2. Inhibition of downstream signaling

After analyzing the effect of AL237 on EGFR phosphorylation, we further studied its role on downstream signaling in MDA-MB-468 cells by Western blotting. Cells were treated with and without EGF to determine EGF-dependent EGFR inhibition by AL237 on downstream signaling. Inhibition of EGF-induced phosphorylation of EGFR was accompanied by reduced p44/p42 MAP kinases (ERK1/2) and BAD (Ser<sup>112</sup>) phosphorylation (Fig. 2.2D). EGF-induced signaling was also accompanied by a slight down-regulation of XRCC1 and ERCC1, two DNA repair proteins involved in the repair of AL237-induced DNA damage (Fig. 2.2D).

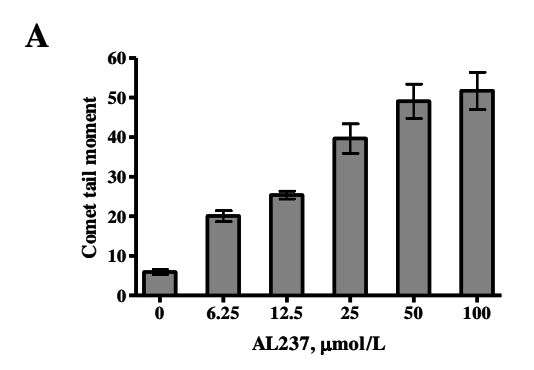
# 2.4.1.3. Induction of DNA damage in MDA-MB-468 breast cancer cells

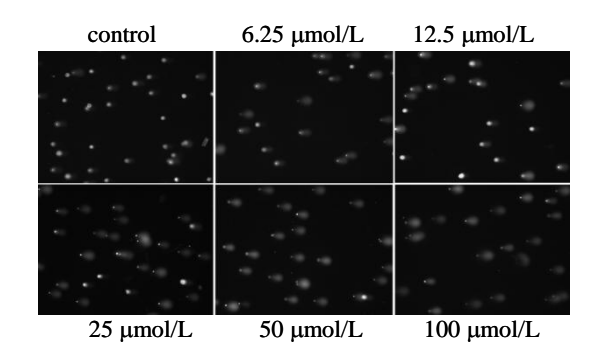
To test the DNA damaging potency of our combi-molecule and the ability to alkylate DNA, cells were treated with AL237 for 2 h. DNA damage was assessed by the alkaline comet assay and quantified by measuring comet tail moment using Comet Assay IV software (Fig. 2.3A). Strong dose-dependent DNA damage was measured with increasing AL237 concentrations and SYBR gold-stained nuclei with typical comet tail formation were imaged (Fig. 2.3A). To verify if the DNA alkylated adducts formed by AL237 resulted in the formation of double strand DNA breaks and the typical  $\gamma$ H2AX foci indicative of the assembly of DNA repair protein complexes, we analyzed phospho- $\gamma$ H2AX activation by Western blotting and immunofluorescence. We observed a dose-dependent increase in  $\gamma$ H2AX protein

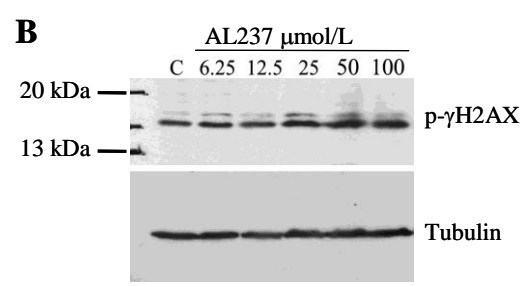
phosphorylation and the formation of 5 to 10 phospho- $\gamma$ H2AX foci per nucleus as compared to untreated cells (Fig. 2.3B). This moderate increase in  $\gamma$ H2AX phosphorylation reflects the inability of alkylating lesions to induce high levels of  $\gamma$ H2AX accumulation or DNA double strand breaks [38, 39]. Overall, the observed strong DNA damaging potency of AL237 and its ability to block cell signaling associated with EGF stimulation confirmed that it behaved as a true combi-molecule. Having shown its dual targeting, the higher cytotoxicity induced by the combi-molecule was addressed by quantitating the levels of apoptosis after 48 h.

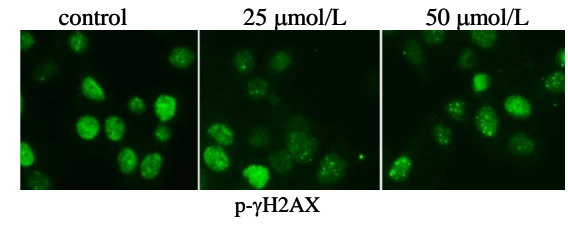
# 2.4.1.4. Induction of apoptosis in MDA-MB-468 breast cancer cells

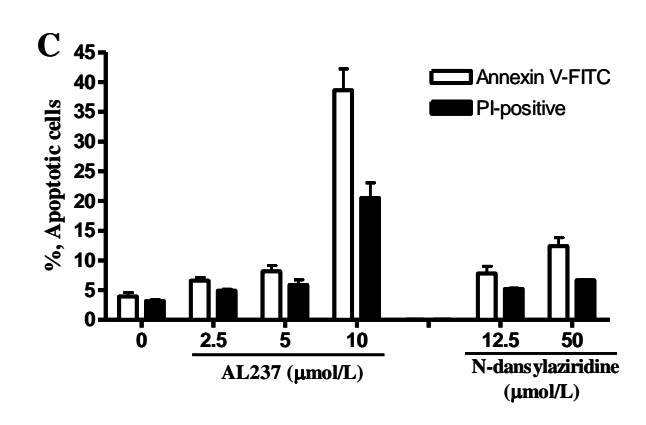
Annexin V-FITC and PI staining were used to distinguish viable (PI-/FITC-), early apoptotic (PI-/FITC+), late apoptotic (PI+/FITC+) and necrotic (PI+/FITC-) cells after 48 h of exposure to the combi-molecule. We observed a strong and a dose-dependent increase in apoptosis by AL237 at IC<sub>50</sub> range reaching as high as 60% apoptotic cells 48 h post-treatment (Fig. 2.3C). In contrast, much lower levels were observed when cells were exposed to 100 μM Temozolomide (9%), 25 μM N-dansylaziridine (12.5%), or combinations of 25 μM Temozolomide and 25 μM Iressa (35%) (Fig. 2.4). Thus, the combined EGFR TK inhibition and DNA damaging properties of AL237 were sufficient to confer high levels of apoptosis in MDA-MB-468 cells. Next, we used AL237 to determine its selective growth inhibition in EGFR/ErbB2-expressing cells and to image the release of its bioactive species in the intracellular compartment.











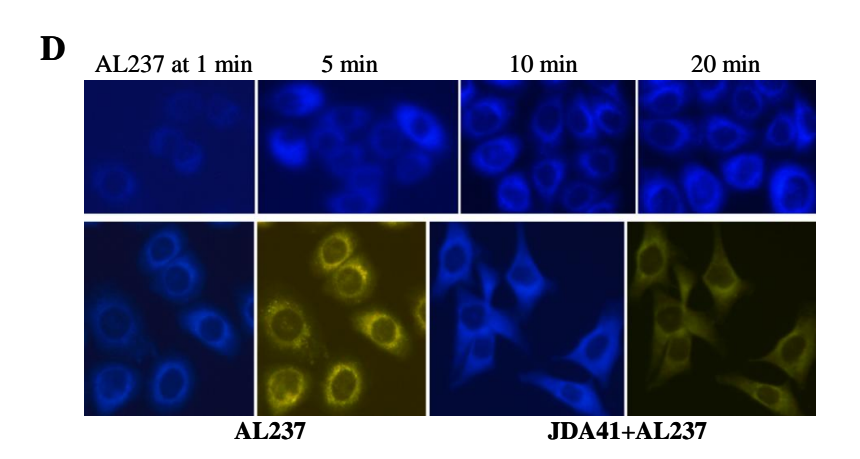


Figure 2.3. DNA damage induced by AL237 in MDA-MB-468.

A, Cells were exposed to AL237 for 2 h followed by assessment of drug-induced DNA damage using an alkaline comet assay. Comets tail moments were quantitated by comet IV software (Perceptive Instruments). Each bar represents the average comet tail moment calculated from 50 comets based on three independent experiments for each concentration (0, 6.25, 12.5, 25, 50, 100 μM). Representative images of DNA comets stained with SYBR Gold dye and visualized by fluorescence microscopy at 10X were shown for each dose. B, Extracts from cells treated for 2 h with increasing concentrations of AL237 were analyzed by Western blot with antiphospho γH2AX antibody. Membrane was probed with anti-tubulin antibody as a loading control. MDA-MB-468 cells were preincubated on a slide, treated with 0, 25 µM or 50 µM of AL237 and analyzed for phospho yH2AX foci. Cells were observed at Leica fluorescent microscope (40X) by indirect immunofluorescence using primary mouse anti-phospho γH2AX antibodies, followed by FITC-labeled anti-mouse antibody. C, Annexin V/PI stained MDA-MB-468 cells were analyzed by FACS 48 h after treatment with AL237 and N-dansylaziridine. **D**, Fluorescence distribution of AL237-EGFR-binding aminoquinazoline species at 25 μM was imaged over time in MDA-MB-468 cells (upper panel). Fluorescence distribution of AL237 hydrolyzed degradation products were observed either alone (lower left panels) or in the presence of equimolar concentrations (25 µM) with a competitive EGFR binding nonfluorescent molecule JDA41 (lower right panels) at 20 min.

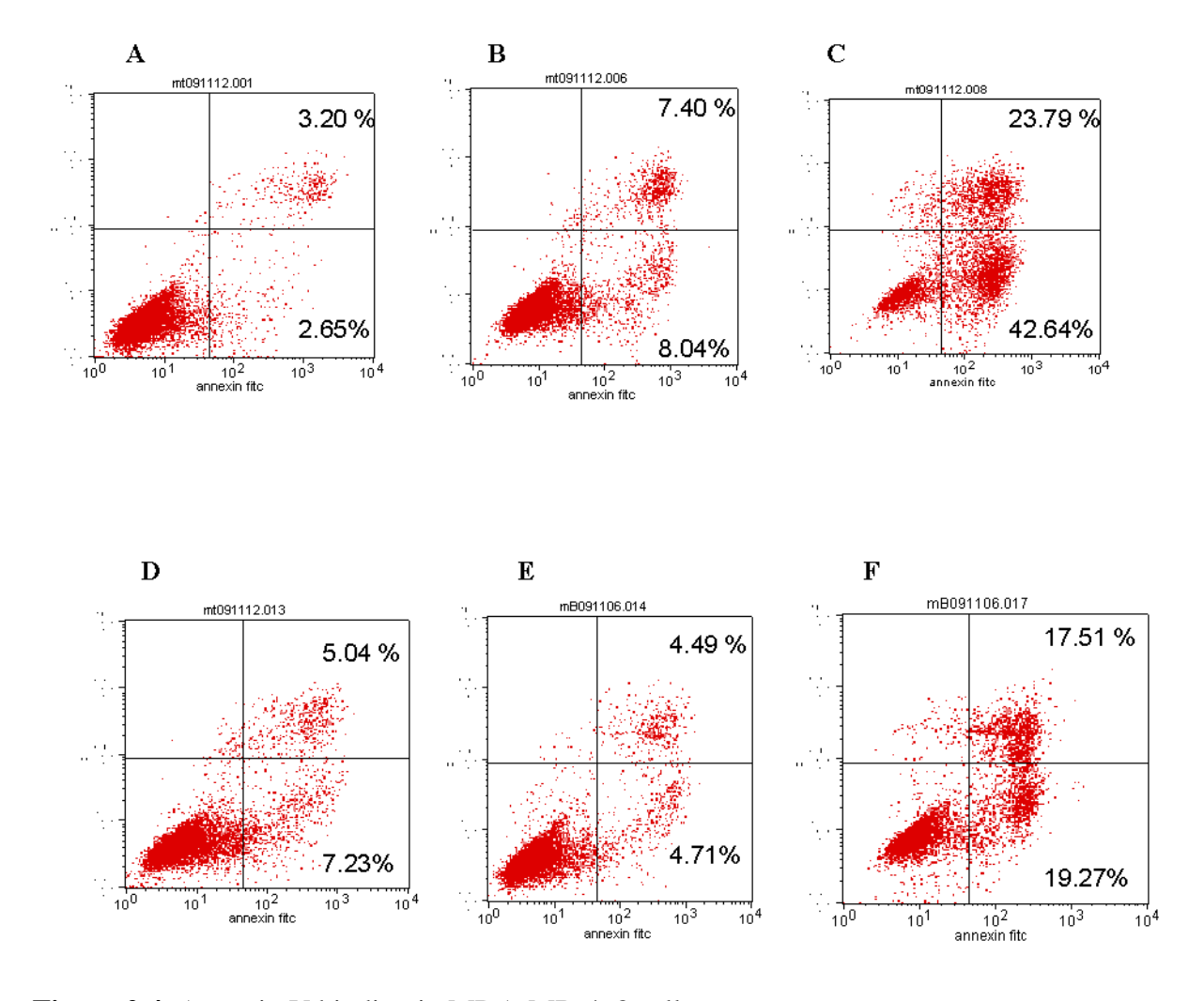


Figure 2.4. Annexin V binding in MDA-MB-468 cells.

Cells were treated for 48 h with a dose range of the following drugs. Dot plots show (**A**) untreated cells, (**B**) treated with 5  $\mu$ M AL237, (**C**) 10  $\mu$ M AL237, (**D**) 25  $\mu$ M of N-dansylaziridine, (**E**) 100  $\mu$ M of Temozolomide or (**F**) equimolar concentrations of Iressa (25  $\mu$ M) and Temozolomide (25  $\mu$ M).

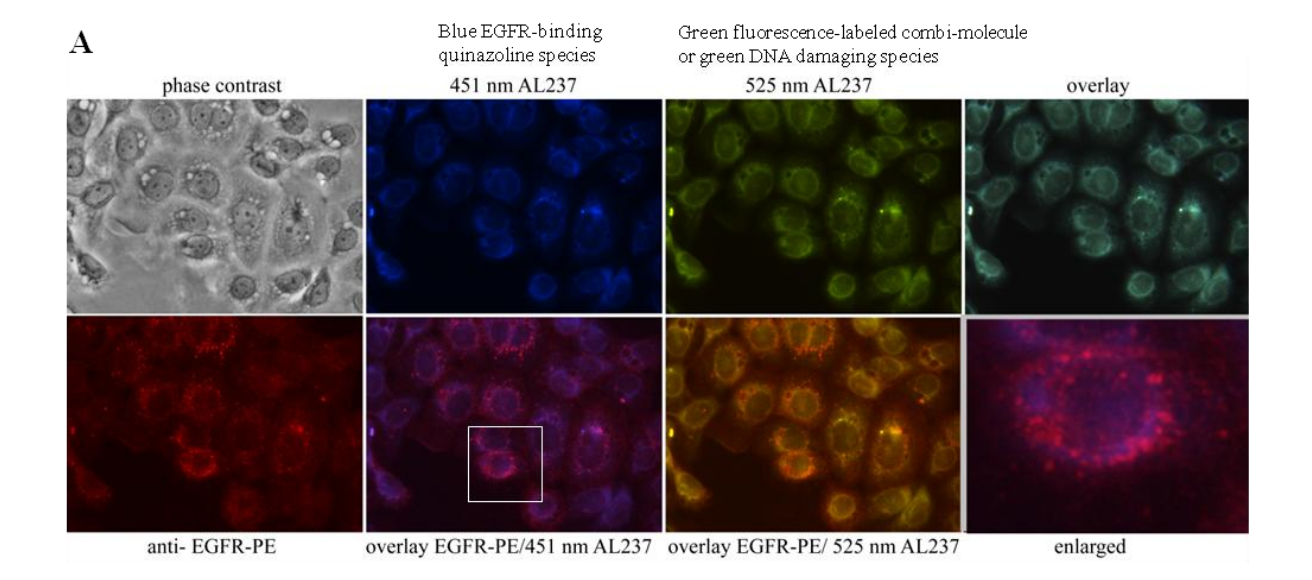
# 2.4.2. Imaging of AL237 in MDA-MB-468 human breast cancer cells and NIH 3T3 transfectants

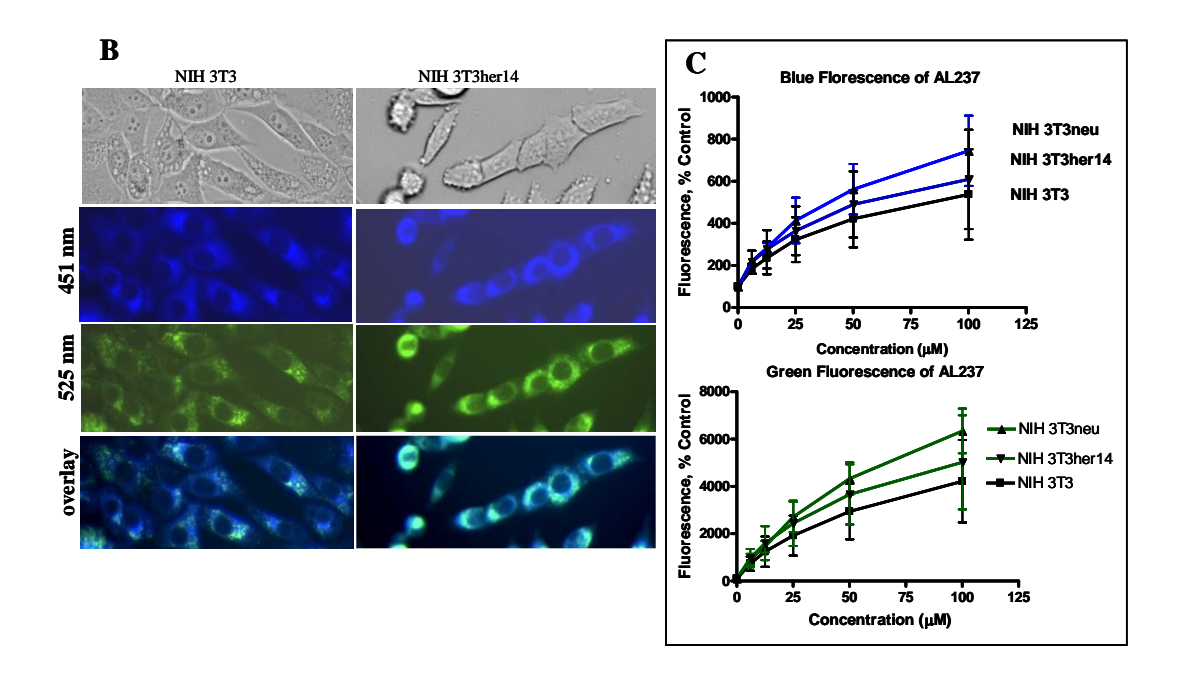
#### 2.4.2.1. Imaging of MDA-MB-468 cells treated with AL237

Fluorescence emission released by AL237 was analyzed in MDA-MB-468 cells at different time points using 25  $\mu$ M of the drug. The two hydrolyzed degradation products were detectable in the cells as early as 5 minutes after addition, reaching a maximum 20 min later (Fig. 2.3D, top). We observed the blue fluorescence associated with the aminoquinazoline FD105 (451 nm) and the green flluorescence associates with the DNA-damaging dansylated moiety (525 nm) in the cytoplasm and in the vicinity of the nucleus. While the entire molecule can still fluoresce in green, the detection of blue FD105 fragment is indicative of a degradation of the molecule which as reported elsewhere has a half-life of 22 min [30]. Whether the combi-molecule was partially or completely decomposed the green fluorescence was consistently localized in the perinuclear area (Fig. 2.3D, bottom left). To challenge the EGFR-directed localization of the combi-molecule in the perinucalear region, we used JDA41 (IC50=0.081  $\mu$ M) a non-fluorescent EGFR TK inhibitor [22]. The results showed that competitive exposure of AL237 (IC50=0.27  $\mu$ M) with JDA41 delocalized the latter into the cytoplasm, indicating that the perinuclear colocalization may be directed by EGFR binding (Fig. 2.3D, bottom right).

# 2.4.2.2. Qualitative analyses of isogenic NIH 3T3 EGFR/ErbB2 transfectants

AL237-released green and blue fluorescence were also observed in an isogenic context using NIH 3T3, NIH 3T3her14 (transfected with EGFR), NIH 3T3neu (transfected with erbB2). As we demonstrated on the merged images in MDA-MB-468 cells (Fig. 2.5A, top right), in NIH 3T3 cells, the blue and green fluorescence produced by AL237 or its decomposition products





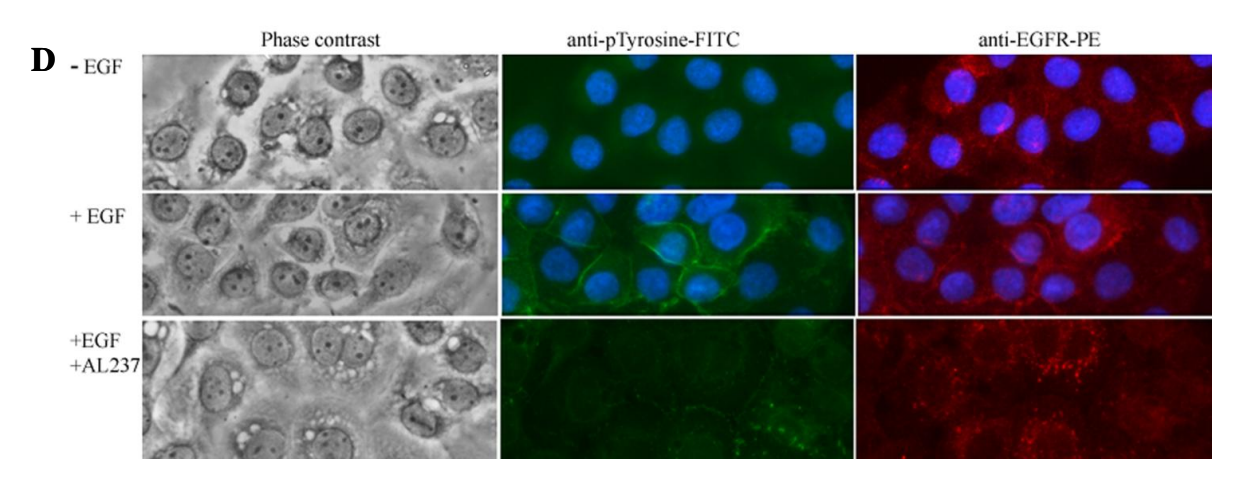


**Figure 2.5.** Cellular fluorescence of AL237 and EGFR in MDA-MB-468 and NIH 3T3, NIH 3T3her14, NIH 3T3neu cells.

A, AL237 was hydrolyzed to an aminoquinazoline fragment which emitted at 451 nm (blue), while the entire AL237 molecule and the dansylated DNA damaging species both emitted at 525 nm (green). Direct drug fluorescence was analyzed in MDA-MB-468 cells after 2 h drug treatment with 25 µM AL237 (upper panel). Each fluorescent fragments was detected using individual filters on Leica fluorescent microscope (40X magnification) and the overlaid image was generated to observe co-localization the two hydrolyzed AL237 fragments (upper right panel). Following drug treatment, MDA-MB-468 cells were immunostained with EGFR-PE labeled antibody (red, lower left panel). Merged images of AL237 (blue, EGFR inhibitor fragment) with EGFR (red) were assembled to outline the area of co-localization (magenta color) and an enlarged cell is represented (lower right panel). The DNA-targeting fragment of AL237 (green) was also overlaid with EGFR to observe the level of co-localization at the perinuclear and nuclear regions. B, NIH 3T3 and NIH 3T3her14 live-cells were imaged to observe biodistribution of the molecule in EGFR and non-EGFR expressing cells. This qualitative analysis was complemented by a quantitative fluorescence measurement of each AL237 species at a single cell level. C, NIH 3T3, NIH 3T3her14 and NIH 3T3neu cells were exposed to the drug for 45 min, washed with PBS, and thereafter each fragment fluorescence was measured by flow cytometry: The accumulated drug-associated fluorescence was measured from 10,000 cells, and then normalized over the background cell fluorescence in the control. Blue fluorescence of the aminoquinazoline species (upper graph) and green fluorescence of the dansylated alkyldiazonium fragment (lower graph) were quantified for each cell type. Each

point is the average value of three independent experiments performed for each cell line in duplicate at each drug concentration. **D**, MDA-MB-468 cells were treated with 25 µM AL237 for 2 h, followed by EGF stimulation, methanol fixed and directly stained with anti-EGFR-PE and anti-phosphotyrosine-FITC antibodies. DAPI stain was used to define nuclei (*upper and middle panels*), but it was omitted from the samples that are drug treated since DAPI-stained nuclei also emitted strong green fluorescence, which interfered with AL237 fluorescence (*lower panel*).

were similarly co-localized in the perinuclear area or in the vicinity of the nucleus (Fig. 2.5B). Interestingly, in the isogenic cells, AL237 or its degradation products were co-localized, with a more pronounced perinuclear distribution in EGFR and ErbB2 expressing cells than in their wild type counterpart. Moreover, quantitative flow cytometric analysis of NIH 3T3, NIH 3T3her14 and NIH 3T3neu cells further confirmed at a single cell level that AL237 decomposed in the cells and released its two fluorescent degradation products: blue fluorescence corresponding to the aminoquinazoline moiety (Fig. 2.5C, top graph) and green fluorescence due to the entire molecule and/ or the released dansylated DNA damaging species (Fig. 2.5C, bottom graph).

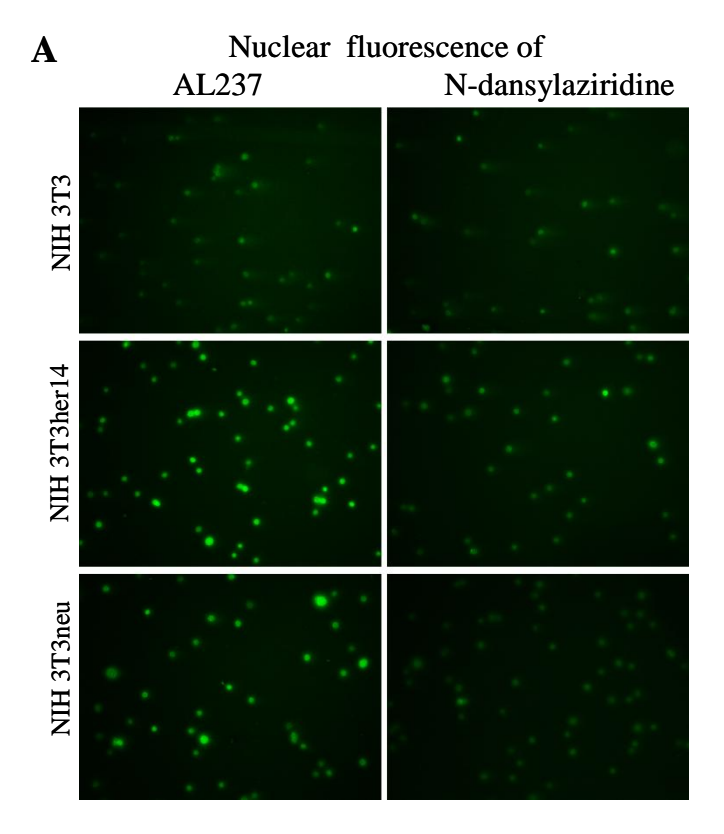
# 2.4.2.3. Co-localization of EGFR and AL237 in MDA-MB-468 cells

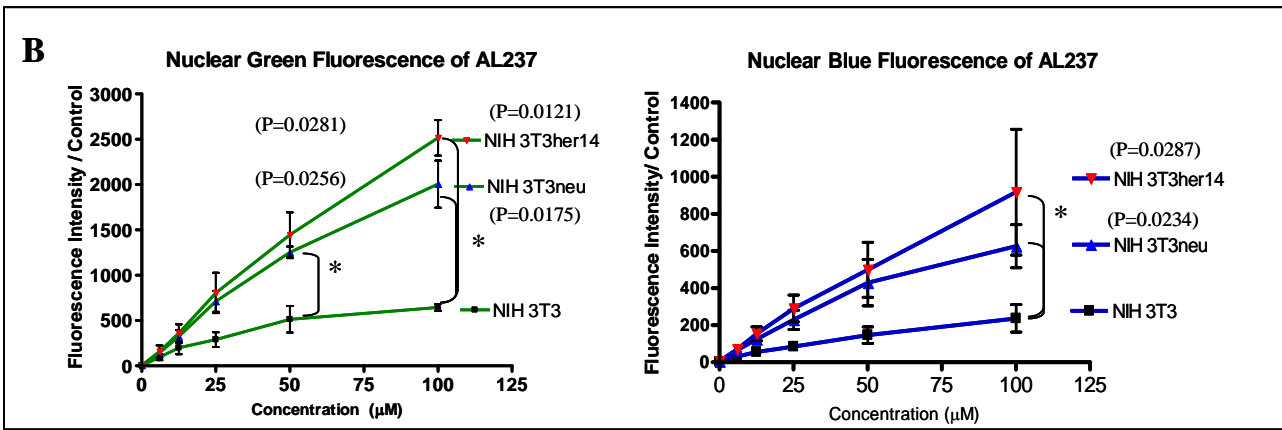
To verify whether AL237 binds to EGFR, we used direct immunofluorescence by staining MDA-MB-468 cells with PE-labeled EGFR and FITC-labeled-phospho-tyrosine antibodies. After EGF-stimulation, we observed activated EGFR at the plasma membrane (Fig. 2.5D, middle) which was strongly inhibited after the cells were exposed for 2 h to 25 μM of AL237, a dose at which EGFR phosphorylation was also shown to be significantly depleted using Western blot analysis (see Fig. 2.2B, C). While in EGF-stimulated cells, the EGFR showed a more membrane localization, in AL237-treated cells, it was redistributed in the cytoplasm in endosome-like structures primarily concentrated around the perinuclear region (Fig. 2.5A, D, bottom right). The localization of the fluorescence is in agreement with the ability of the released blue aminoquinazoline (see Fig. 2.1) to bind to EGFR TK and also with that of the green dansylated alkylating species to alkylate DNA.

#### 2.4.3. Selective nuclear localization and growth inhibition

# 2.4.3.1. Quantitative and qualitative nuclear analysis

When total subcellular fluorescence was analyzed in the isogenic cells, although the trend was towards greater fluorescence in cells transfected with EGFR and its closest homologue ErbB2, the differences in fluorescence intensity were not statistically significant when compared with the wild type (P>0.05, Fig. 2.4C). However, we believed that if the primary localisation of AL237 in the perinuclear region was partially due to its binding to EGFR or related proteins, concomitantly released dansylated alkylating species that covalently bind to DNA might induce high levels of green fluorescence in the nuclei of these cells. Hence, we attempted to detect the levels of green fluorescence directly bound to DNA using a neutral comet assay and flow cytometric analysis of nuclei isolated by the Vindelov method [35]. Under neutral conditions, we expected the alkylated dansyl species to remain bound to nuclei, thereby allowing direct imaging of the adducted DNA. For purpose of comparison, N-dansylaziridine, a dansylated alkylating agent deprived of the quinazoline moiety required for binding to EGFR was used. As depicted in Figure 2.6, strong green fluorescence intensity was observed from nuclei of cells treated with AL237 (Fig. 2.6A, left), with higher intensity in EGFR and ErbB2-transfected cells. Intensities were lower with N-dansylaziridine and not selectively stronger in the transfectants (Fig. 2.6A, right). Quantitative flow cytometric analysis confirmed that AL237 released significantly higher levels of fluorescence in the NIH 3T3her14 and NIH 3T3neu nuclei than in their NIH 3T3 wild type counterpart (Fig. 2.6B). Two- to three-fold difference in green fluorescence intensity was observed between NIH 3T3 and ErbB2 or EGFR. Statistical analysis was performed with a two-tailed unpaired t-test between NIH 3T3 and ErbB2 (at 50  $\mu$ M, P=0.0256; 100  $\mu$ M, P=0.0175) and between NIH 3T3 and EGFR (at 50  $\mu$ M, P=0.0281;





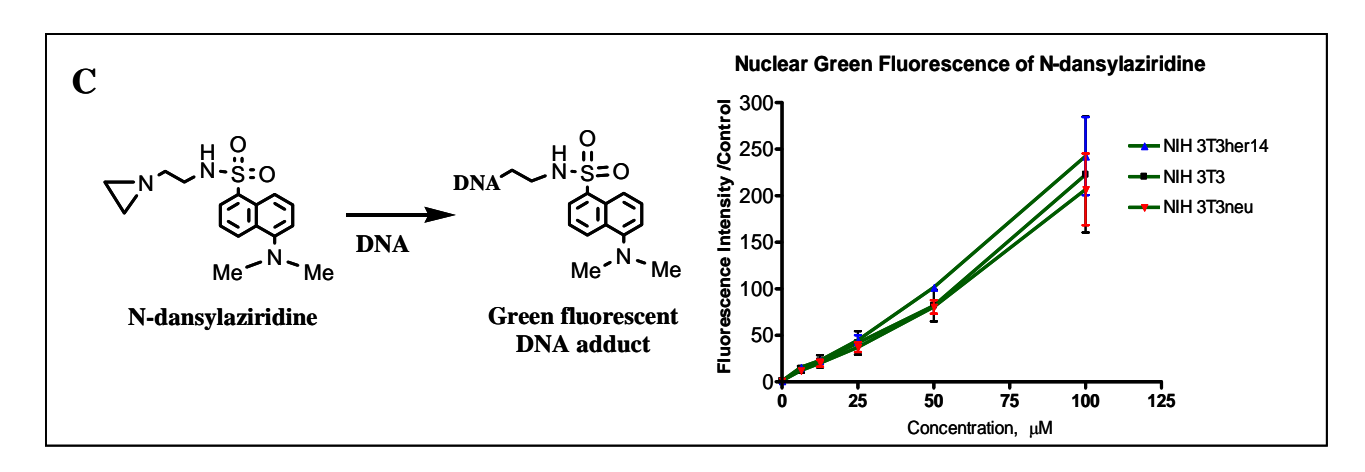


**Figure 2.6.** Nuclear accumulation of AL237 and N-dansylaziridine in NIH 3T3, NIH 3T3her14 and NIH 3T3neu cells.

A, cells were treated with 100 µM AL237 or N-dansylaziridine for 2h. After cells were lysed and electrophoresis under neutral conditions, the nuclei of all three cell lines were analyzed by fluorescence microscopy (10X magnification) for the accumulation of either the dansylated fragment of AL237 (*left panels*) or N-dansylaziridine control (*right panels*). **B**, flow cytometry analysis of NIH 3T3 cells and the transfectants treated with five doses of AL237 for 45 min. Cells were washed twice with PBS then lysed with Vindelov's solution for single nuclei isolation. C, schematic of N-dansylaziridine used as a control and flow cytometry analysis for its nuclear accumulation in NIH 3T3 cells and the transfectants. Minimum 10,000 cell nuclei fluorescence was measured and represented as mean fluorescence normalised over the control. AL237 green fluorescence and quinazoline derived blue fluorescence (B) and N-dansylaziridine fluorescence (C) were calculated as mean  $\pm$  SD determined from four independent experiments performed in duplicates for each drug concentration. Statistical analysis was performed with a two-tailed unpaired t-test, statistical significance P<0.05 (between NIH 3T3 and NIH 3T3neu at 50 μM (P=0.0256), 100 μM (P=0.0175); between NIH 3T3 and NIH 3T3her14 at 50 μM (P=0.0281), 100 μM (P=0.0121) for green fluorescence. Statistical analysis for blue fluorescence intensity was significant at 100 µM dose (P=0.0287) and (P=0.0234).

100  $\mu$ M, P=0.0121). Similarly, higher blue fluorescence intensity in the nuclei of the transfectants was observed and the difference when compared with the wild type cells was statistically significant at the highest dose (100  $\mu$ M, P=0.0287 and P=0.0234). Importantly, no selective green fluorescence distribution was observed in nuclei from isogenic cells treated with N-dansylaziridine (Fig. 2.6C) that does not contain an EGFR targeting moiety. This is an indirect evidence supporting the implication of EGFR in the selective nuclear accumulation of AL237.

# 2.4.3.2. Selective growth inhibition of EGFR expressing MDA-MB-468 and NIH 3T3 cells

To determine whether the binary EGFR/DNA targeting property of AL237 that showed selective biodistribution in EGFR/ErbB2 transfectants, would translate into increased growth inhibitory potency on EGFR-expressing cells, we tested its growth inhibitory effect on MDA-MB-468 and NIH 3T3 transfectants (Fig. 2.7). AL237 showed 5-fold stronger inhibition on EGFR- and ErbB2-expressing cells than in control NIH 3T3 cells (P<0.05, unpaired *t* test; Fig. 2.7A). AL237 also induced strong growth inhibition in the MDA-MB-468 cells that overexpress EGFR (Fig. 2.7B).

#### 2.5. DISCUSSION

The combi-molecules are a novel type of structures designed to block divergent targets in tumour cells. The growth of refractory tumours is driven by multiple signaling disorders that often cannot be blocked by the use of a single drug. The combi-molecule approach is the first that seeks to create molecules capable of blocking at least two divergent targets in the cells by allowing the intact molecules to block one target on their own and to degrade into other species

IC <sub>50</sub> of AL237, μmol/L	
NIH 3T3	$14.0 \pm 0.24$
NIH 3T3her14	$3.1 \pm 0.25$
NIH 3T3neu	$2.8 \pm 0.32$
MDA-MB-468	$5.2 \pm 0.16$
A  100  75  0  101  102  Concentration, μM	B 100 75 75 25 10-1 100 101 102 103 Concentration μM

Figure 2.7. Selective growth inhibition by AL237 in NIH 3T3 and MDA-MB-468 cells.

The IC<sub>50</sub> of AL237 in NIH 3T3 wild type and transfectants (A) and in MDA-MB-468 cells (B) were determined by SRB assay and values were averaged from three independent experiments ran in triplicates.

directed at the same or different targets [18, 20, 23, 26, 40-43]. In order to gain insight into the subcellular distribution and degradation of combi-molecules, we designed a new prototype termed AL237 to: (a) be fluorescent on its own; (b) degrade under physiological conditions to FD105 (an EGFR inhibitor) that fluoresces in the blue and a DNA alkylating fragment that fluoresces in the green (see Fig.2.1). Thus, this was designed to not only allow us to visualize the release of the EGFR inhibitor in the cells but also to image the concomitantly generated DNA damaging species. Since the green fluorescence released from the dansyl moiety attached to the intact combi-molecule is undistinguishable from that emitted by the alkylating dansyl species, the co-localization of blue and green fluorescence suggests that both the intact molecule and its dissociated DNA alkylating dansylated species may be released concomitantly and primarily in the same locations. The high intensity of the green fluorescence in the perinuclear area indicates that the combi-molecules might be primarily localized and decompose to release both the aminoquinazoline inhibitor of EGFR FD105 and the DNA damaging species therein. A fraction of the combi-molecule might also decompose in the nucleus since blue fluorescence was also detected therein. The fact that good co-localization was seen between the blue fluorescence of FD105 and red fluorescence associated with anti-EGFR antibody, lends support to the ability of the released blue FD105 to bind to EGFR. Correspondingly, the poor co-localization observed for the green fluorescence associated with the dansylated alkylating DNA damaging agent with EGFR was in agreement with the inability of the latter species to bind to EGFR but rather to DNA in the nuclei.

Previous work with the <sup>14</sup>C-methyl labeled combi-molecules demonstrated preferential perinuclear distribution of SMA42, an analogue of FD105, released from the model combi-molecule SMA41 [24]. The corresponding <sup>14</sup>C-labeled alkyl group was bound to all three major macromolecules of the cells (DNA, RNA and protein) [27]. Here, the fluorescence labeled alkyl

group presents the advantage of being observable by fluorescence microscopy and being quantified by fluorescence intensity per cell or nucleus by flow cytometry. The results obtained from immunofluorescence and flow cytometric analyses indicate that the combi-molecule and its derived species, despite being abundantly distributed in the perinuclear or partially in the nuclear region is available at high enough concentrations to block EGFR TK activity at the level of the plasma membrane, down-regulate the MAP kinase pathway and prevent downstream induction of DNA repair genes such as the XRCC1 and ERCC1. Thus, it suggests that the combi-molecules simultaneously damages DNA, impairs its repair mechanism and also the phosphorylation of the pro-apoptotic protein BAD. Unfortunately, we were not able to image the membrane localization of AL237, perhaps due to insufficiently high population of bound combi-molecules in the latter area. However, the fact that phosphorylation of EGFR was strongly inhibited by AL237 is an indirect evidence of the presence of a fraction of the intact molecule or its derived quinazoline at the level of the membrane. It should be noted that, whereas the data suggests that EGFR overexpression is associated with elevated nucleus binding of the dansylated DNA moiety, the compound through its DNA damaging moiety is capable of damaging tumour cells that do not express EGFR although to a lesser extent as exemplified by the NIH 3T3 wild type. This suggests that subpopulation of non-EGFRexpressing cells present in heterogeneous tumours may also be killed by the combi-moecule through its DNA damaging arm.

Importantly, we showed that the dansyl moiety is strongly bound to the nucleus, which is in agreement with the high levels of DNA damage observed by the comet assay and a slight increase in  $\gamma$ H2AX phosphorylation and foci formation. The rather moderate increase in  $\gamma$ H2AX phosphorylation is due to the inability of alkylating lesions to induce significant levels

of DNA double strand breaks. In term of nuclear staining, the most striking observation was the significant difference in fluorescence intensity observed between the NIH 3T3 transfectants and their wild type counterpart. This is consistent with our previous observation of selectively high levels of DNA damage induced by the combi-molecule SMA41 in NIH3T3 cells transfected with EGFR when compared with its wild type [44]. A similar observation was made in MDA-MB-435 cells transfected with EGFR or ErbB2 [45]. In this study, nuclei of cells transfected with EGFR or its closest homologue ErbB2 emitted higher green and blue fluorescence intensity then those of NIH 3T3 wild type. This can be rationalized in light of the high levels of EGFR observed in the perinuclear region. Perhaps EGFR and related proteins localized in the perinuclear region serve as anchorage from which the free dansyl alkyldiazonium moiety (see figure 1) can diffuse towards genomic DNA. Indeed, many reports not only described perinuclear distribution of EGFR but also its nuclear translocation [46-50]. Recent studies by Dittmann et al. [50] showed that EGFR translocates to the nucleus in response to radiationinduced DNA lesions, and more importantly, the nuclear EGFR is shown to be involved in DNA repair. Our observations that N-dansylaziridine, which does not contain a quinazoline EGFR targeting moiety, does not emit higher fluorescence intensity in the transfectants, is an indirect evidence of the implication of EGFR and related proteins in the selectivity of nuclear staining by AL237.

This study conclusively demonstrated that the combi-molecule AL237 is indeed an agent that:
(a) penetrates the cells and primarily localizes in the perinuclear region, (b) releases species that block signaling associated with EGFR activation, (c) damages DNA and (d) significantly inhibits tumour cell growth. Thus, it behaved as a valid agent to image the distribution of not only the EGFR inhibitory but also the DNA binding species.

#### 2.6. ACKNOWLEDGMENTS

We are grateful to National Cancer Institute of Canada (NCIC research grant 018475). We also thank the Canadian Institutes of Cancer Research (Grant FRN 49440) for financial support. We are grateful to the MUHC Research Institute for an equipment grant that supported the acquisition of our Leica fluorescence microscope. MT is supported by Fonds de la Recherche en Santé du Québec doctoral training award.

#### 2.7. CONNECTING TEXT

Several combi-molecules have been synthesized in the past to verify the combi-targeting postulates, i.e. effect of "mix-targeting" EGFR and DNA in human tumour cells. While cells transfected with EGFR or HER2 have been used to analyze their EGFR/HER2 targeting, no previous study examined the effects of P-gp expression status on their anti-proliferate activity. More importantly, designing combi-molecules to be functional requires the incorporation of several pharmacophores that may significantly increase their size. Therefore, examining the effect of efflux protein on their intracellular accumulation was critical for future design.

The study described in the next chapter explored the transport of AL237 (MW=632) and AL194 (MW=575), differing by the length of the spacer between triazene-quinazoline and the fluorescence-label dansylaziridine. One space is short and neutral, ethano linker, and the other contains a longer and basic N-methylethanediamine spacer. From previous structure-activity studies, we observed that the length of the spacer and the central methylamino nitrogen were critical for the binding affinity of the combi-molecule for the ATP binding site of EGFR. Having in mind that the decomposition of the combi-molecules inside the cell is an important advantage to overcome the efflux mechanism, in Chapter 3 we proposed to study two

fluorescent molecules with different rate of hydrolysis. We also aimed to address the ability of bulky molecules to diffuse inside the cell and to deliver two bioactive species. We sought to determine whether the instability of the combi-molecule in the intracellular compartment might deplete the rate of efflux of the intact combi-molecules, thereby reducing the incidence of tumour cell resistance associated to by P-glycoprotein overexpression.

#### 2.8 REFERENCES

- 1. Slamon, D.J., et al., *Human breast cancer: correlation of relapse and survival with amplification of the HER-2/neu oncogene.* Science (Washington, DC, United States), 1987. **235**(4785): p. 177-82.
- 2. Aaronson, S.A., *Growth factors and cancer*. Science, 1991. **254**(5035): p. 1146-53.
- 3. Modjtahedi, H. and C. Dean, *The receptor for EGF and its ligands: expression, prognostic value and target for therapy in cancer (review)*. International Journal of Oncology, 1994. **4**(2): p. 277-96.
- 4. Normanno, N., et al., *Epidermal growth factor receptor (EGFR) signaling in cancer*. Gene, 2006. **366**(1): p. 2-16.
- 5. Mendelsohn, J., *Epidermal growth factor receptor inhibition by a monoclonal antibody as anticancer therapy.* Clin Cancer Res, 1997. **3**(12 Pt 2): p. 2703-7.
- 6. Ciardiello, F. and G. Tortora, *A novel approach in the treatment of cancer: targeting the epidermal growth factor receptor.* Clin Cancer Res, 2001. **7**(10): p. 2958-70.
- 7. Albanell, J. and P. Gascon, *Small molecules with EGFR-TK inhibitor activity*. Current Drug Targets, 2005. **6**(3): p. 259-274.
- 8. Bos, M., et al., *PD153035*, a tyrosine kinase inhibitor, prevents epidermal growth factor receptor activation and inhibits growth of cancer cells in a receptor number-dependent manner. Clin Cancer Res., 1997. **3**(11): p. 2099-106.
- 9. Moyer, J.D., et al., *Induction of apoptosis and cell cycle arrest by CP-358774, an inhibitor of epidermal growth factor receptor tyrosine kinase.* Cancer Research, 1997. **57**(21): p. 4838-4848.
- 10. Barker, A.J., et al., Studies leading to the identification of ZD1839 (iressa): an orally active, selective epidermal growth factor receptor tyrosine kinase inhibitor targeted to the treatment of cancer. Bioorganic & Medicinal Chemistry Letters, 2001. 11(14): p. 1911-1914.
- 11. Rusnak, D.W., et al., The effects of the novel, reversible epidermal growth factor receptor/ErbB-2 tyrosine kinase inhibitor, GW2016, on the growth of human normal and tumor-derived cell lines in vitro and in vivo. Mol Cancer Ther, 2001. 1(2): p. 85-94.
- 12. Normanno, N., et al., *Target-based agents against ErbB receptors and their ligands: a novel approach to cancer treatment.* Endocr Relat Cancer., 2003. **10**(1): p. 1-21.
- 13. Wissner, A., et al., Syntheses and EGFR and HER-2 kinase inhibitory activities of 4-anilinoquinoline-3-carbonitriles: analogues of three important 4-anilinoquinazolines

- *currently undergoing clinical evaluation as therapeutic antitumor agents.* Bioorganic & Medicinal Chemistry Letters, 2002. **12**(20): p. 2893-2897.
- 14. Moy, B. and P.E. Goss, *Lapatinib: current status and future directions in breast cancer*. Oncologist, 2006. **11**(10): p. 1047-57.
- 15. Huang, S., et al., Dual-agent molecular targeting of the epidermal growth factor receptor (EGFR): combining anti-EGFR antibody with tyrosine kinase inhibitor. Cancer Res, 2004. **64**(15): p. 5355-62.
- 16. Baumann, M., et al., EGFR-targeted anti-cancer drugs in radiotherapy: Preclinical evaluation of mechanisms. Radiotherapy and Oncology, 2007. **83**(3): p. 238-248.
- 17. Katsoulas, A., et al., Combi-targeting concept: an optimized single-molecule dual-targeting model for the treatment of chronic myelogenous leukemia. Molecular Cancer Therapeutics, 2008. **7**(5): p. 1033-1043.
- 18. Matheson, S.L., J. McNamee, and B.J. Jean-Claude, *Design of a chimeric 3-methyl-1,2,3-triazene with mixed receptor tyrosine kinase and DNA damaging properties: a novel tumor targeting strategy.* J. Pharmacol. Exp. Ther., 2001. **296**(3): p. 832-840.
- 19. Brahimi, F., et al., *Inhibition of epidermal growth factor receptor-mediated signaling by* "Combi-triazene" BJ2000, a new probe for Combi-Targeting postulates. J Pharmacol Exp Ther, 2002. **303**(1): p. 238-46.
- 20. Qiu, Q., et al., *The combi-targeting concept: a novel 3,3-disubstituted nitrosourea with EGFR tyrosine kinase inhibitory properties.* Cancer Chemotherapy and Pharmacology, 2003. **51**(1): p. 1-10.
- 21. Qiu, Q., et al., Type II combi-molecules: design and binary targeting properties of the novel triazolinium-containing molecules JDD36 and JDE05. Anticancer Drugs, 2007. **18**(2): p. 171-7.
- 22. Qiu, Q., et al., *The Combi-Targeting Concept: In vitro and In vivo Fragmentation of a Stable Combi-Nitrosourea Engineered to Interact with the Epidermal Growth Factor Receptor while Remaining DNA Reactive.* Clin. Cancer Res., 2007. **13**(1): p. 331-340.
- 23. Banerjee, R., et al., Synthesis of a prodrug designed to release multiple inhibitors of the epidermal growth factor receptor tyrosine kinase and an alkylating agent: a novel tumor targeting concept. J Med Chem, 2003. **46**(25): p. 5546-51.
- 24. Matheson, S.L., F. Brahimi, and B.J. Jean-Claude, *The combi-targeting concept: intracellular fragmentation of the binary epidermal growth factor (EGFR)/DNA targeting "combi-triazene" SMA41*. Biochemical Pharmacology, 2004. **67**(6): p. 1131-1138.
- 25. Qiu, Q., et al., *Inhibition of cell signaling by the combi-nitrosourea FD137 in the androgen independent DU145 prostate cancer cell line*. Prostate, 2004. **59**(1): p. 13-21.

- 26. Domarkas, J., et al., *The combi-targeting concept: synthesis of stable nitrosoureas designed to inhibit the epidermal growth factor receptor (EGFR)*. J Med Chem, 2006. **49**(12): p. 3544-52.
- 27. Matheson, S.L., et al., *The combi-targeting concept: Dissection of the binary mechanism of action of the combi-triazene SMA41 in vitro and antitumor activity in vivo.* J. Pharmacol. Exp. Ther., 2004. **311**(3): p. 1163-1170.
- 28. Matheson, S.L., S. Mzengeza, and B.J. Jean-Claude, *Synthesis of 1-[4-(m-tolylamino)-6-quinazolinyl]-3-[14C]methyltriazene: a radiolabeled probe for the combi-targeting concept.* J. Labelled Comp. Rad., 2003. **46**(8): p. 729-735.
- 29. Broo, K., et al., *Viral capsid mobility: a dynamic conduit for inactivation*. Proc Natl Acad Sci U S A, 2001. **98**(5): p. 2274-7.
- 30. Larroque-Lombard, A.L., et al., Synthesis and uptake of fluorescence-labeled Combimolecules by P-glycoprotein-proficient and -deficient uterine sarcoma cells MES-SA and MES-SA/DX5. J Med Chem, 2010. **53**(5): p. 2104-13.
- 31. Skehan, P., et al., *New colorimetric cytotoxicity assay for anticancer-drug screening*. J Natl Cancer Inst., 1990. **82**(13): p. 1107-1112.
- 32. McNamee, J.P., et al., *Comet assay: rapid processing of multiple samples.* Mutat Res, 2000. **466**(1): p. 63-69.
- 33. Olive, P.L. and J.P. Banath, *The comet assay: a method to measure DNA damage in individual cells.* Nat Protoc, 2006. **1**(1): p. 23-29.
- 34. Wojewodzka, M., I. Buraczewska, and M. Kruszewski, *A modified neutral comet assay:* elimination of lysis at high temperature and validation of the assay with anti-single-stranded DNA antibody. Mutat Res, 2002. **518**(1): p. 9-20.
- 35. Vindelov, L.L., Flow microfluorometric analysis of nuclear DNA in cells from solid tumors and cell suspensions. A new method for rapid isolation and straining of nuclei. Virchows Arch B Cell Pathol, 1977. **24**(3): p. 227-42.
- 36. Rachid, Z., et al., Novel Nitrogen Mustard-Armed Combi-Molecules for the Selective Targeting of Epidermal Growth Factor Receptor Overexperessing Solid Tumors: Discovery of an Unusual Structure-Activity Relationship. J. Med. Chem., 2007. **50**(11): p. 2605-2608.
- 37. Larroque, A.-L., et al., Synthesis of water soluble bis-triazenoquinazolines: an unusual predicted mode of binding to the epidermal growth factor receptor tyrosine kinase. Chemical Biology & Drug Design, 2008. **71**(4): p. 374-379.
- 38. Huang, X., H.D. Halicka, and Z. Darzynkiewicz, *Detection of histone H2AX phosphorylation on Ser-139 as an indicator of DNA damage (DNA double-strand breaks)*. Curr Protoc Cytom, 2004. **Chapter 7**: p. Unit 7 27.

- 39. Kinner, A., et al., Gamma-H2AX in recognition and signaling of DNA double-strand breaks in the context of chromatin. Nucleic Acids Res, 2008. **36**(17): p. 5678-94.
- 40. Banerjee, R., et al., Synthesis of a Prodrug Designed To Release Multiple Inhibitors of the Epidermal Growth Factor Receptor Tyrosine Kinase and an Alkylating Agent: A Novel Tumor Targeting Concept. J. Med. Chem., 2003. **46**(25): p. 5546-5551.
- 41. Rachid, Z., et al., *The Combi-Targeting Concept: Chemical Dissection of the Dual Targeting Properties of a Series of "Combi-Triazenes"*. J. Med. Chem., 2003. **46**(20): p. 4313-4321.
- 42. Brahimi, F., et al., Multiple mechanisms of action of ZR2002 in human breast cancer cells: a novel combi-molecule designed to block signaling mediated by the ERB family of oncogenes and to damage genomic DNA. Int J Cancer, 2004. 112(3): p. 484-91.
- 43. Qiu, Q., et al., The combi-targeting concept: in vitro and in vivo fragmentation of a stable combi-nitrosourea engineered to interact with the epidermal growth factor receptor while remaining DNA reactive. Clin Cancer Res, 2007. **13**(1): p. 331-40.
- 44. Matheson, S.L., J.P. McNamee, and B.J. Jean-Claude, *Differential responses of EGFR-AGT-expressing cells to the "combi-triazene" SMA41*. Cancer Chemoth. Pharm., 2003. **51**(1): p. 11-20.
- 45. Banerjee, R., et al., *The combi-targeting concept: selective targeting of the epidermal growth factor receptor- and Her2-expressing cancer cells by the complex combi-molecule RB24*. J Pharmacol Exp Ther, 2010. **334**(1): p. 9-20.
- 46. Lin, S.-Y., et al., *Nuclear localization of EGF receptor and its potential new role as a transcription factor.* Nature Cell Biology, 2001. **3**(9): p. 802-808.
- 47. Lo, H.W., et al., *Novel prognostic value of nuclear epidermal growth factor receptor in breast cancer.* Cancer Res, 2005. **65**(1): p. 338-48.
- 48. Lo, H.W., S.C. Hsu, and M.C. Hung, *EGFR signaling pathway in breast cancers: from traditional signal transduction to direct nuclear translocalization.* Breast Cancer Res Treat, 2006. **95**(3): p. 211-8.
- 49. Kim, J., et al., *The phosphoinositide kinase PIKfyve mediates epidermal growth factor receptor trafficking to the nucleus.* Cancer Res, 2007. **67**(19): p. 9229-37.
- 50. Dittmann, K., et al., *Radiation-induced lipid peroxidation activates src kinase and triggers nuclear EGFR transport.* Radiother Oncol, 2009. **92**(3): p. 379-82.

## **Chapter 3**

# Synthesis and Uptake of Fluorescence-Labeled combi-molecules by P-Glycoprotein-Proficient and -Deficient Uterine Sarcoma Cells MES-SA and MES-SA/DX5

Anne-Laure Larroque-Lombard<sup>1</sup>§, Margarita Todorova<sup>1</sup>§, Nahid Golabi<sup>1</sup>, Christopher

Williams<sup>2</sup>, and Bertrand B. Jean-Claude<sup>1</sup>

<sup>1</sup>Cancer Drug Research Laboratory, Department of Medicine, Division of Medical Oncology, McGill University Health Center/Royal Victoria Hospital, 687 Pine Avenue West Rm M-719, Montreal, Quebec, H3A 1A1 Canada.

<sup>2</sup>Chemical Computing Group Inc., 1010 Sherbrooke Street West, Suite 910, Montreal, QC H3A 2R7, Canada.

§ The two authors contributed equally to this manuscript.

#### 3.1. ABSTRACT

Here, we report on the first synthesis of fluorescent-labeled EGFR-DNA targeting combimolecules and studied the influence of P-glycoprotein status of human sarcoma MES-SA cells
on their growth inhibitory effect and cellular uptake. The results showed that **6**, bearing a longer
spacer between the quinazoline ring and the dansyl group was more stable and more cytotoxic
than **4**. In contrast to the latter, it induced significant levels of DNA damage in human tumour
cells. Moreover, in contrast to doxorubicin, a drug known to be actively effluxed by P-gp, the
more stable combi-molecule **6** induced almost identical levels of drug uptake and DNA damage
in P-gp-proficient and -deficient cells. Likewise, in contrast to doxorubicin, **4** and **6** exerted
equal levels of antiproliferative activity against the two cell types. The results *in toto* suggest
that despite their size, the antiproliferative effects of **4** and **6** were independent of P-gp status of
the cells.

#### **KEYWORDS**

Combi-molecules, EGFR inhibitor, DNA damaging species, dansylated fluorescent labeling, multidrug resistance.

#### 3.2. INTRODUCTION

At the advanced stages, solid tumours express a variety of receptors and signaling proteins that not only drive their progression but also render them resistant to tumour drugs. One mechanism of multidrug resistance (MDR) is the expression of reflux pump [e.g., P-glycoprotein (P-gp)] that transports drugs out of the cells, and this is responsible for drug resistance and treatment failure in approximately 90% of cancer patients [1-7]. Also, some mutations in key signaling proteins are often responsible for chemoresistance. Several attempts to modulate MDR led to a limited degree of success in the clinic, and the design of agents that diffuse into the cells regardless of their P-gp status or that selectively kill P-gp-expressing cells have become new drug development strategy [8].

Recently, to circumvent problems associated with target heterogeneity in advanced cancers, we developed novel types of drugs capable of inhibiting refractory tumour cell growth by blocking divergent targets such as the epidermal growth factor receptor (EGFR) and genomic DNA. Many prototypes of these agents termed combi-molecules have been shown to block the growth of human cancer cells with disordered signaling [9-14]. While their ability to concomitantly damage DNA and to induce high levels of apoptosis was demonstrated, the influence of transport pump-mediated MDR, on the potency of these multitargeted molecules was yet to be explored. To analyze their intracellular uptake and dependence on MDR status, we designed fluorescence-labeled prototypes 4 (AL194) and 6 (AL237) and studied their differential uptake by two human uterine sarcoma cell lines (MES-SA and MES-SA/DX5) that do not express EGFR, the primary target of these combi-molecules [15, 16]. The use of cells deprived of EGFR was to avoid any interference of EGFR or related proteins with the retention or subcellular distribution of the molecules. We have now shown elsewhere that EGFR expression

influences their subcellular distribution [17]. Importantly, in contrast to the parental MES-SA cell line, the MES-SA/DX5 has been shown to express P-gp and to be resistant to doxorubicin and paclitaxel [18-20].

The new combi-molecules reported herein were designed to degrade into an aminoquinazoline, fluorescing in the blue, and a dansylated DNA-damaging moiety, fluorescing in the green, thereby facilitating the analysis of drug uptake by fluorescence microscopy and flow cytometry. The IC<sub>50</sub> for EGFR tyrosine kinase inhibition by **4** and **6** were 1.4 and 0.6 μM, respectively, and their binary EGFR-DNA targeting properties are extensively discussed in a separate report [17]. Here, we describe the synthesis of the two combi-molecules, one with a short neutral ethano linker and the other with a longer and basic N-methylethanediamine spacer. We compared their differential uptake in MES-SA cells with that of doxorubicin, by fluorescence microscopy and flow cytometry. In contrast to the clinical anti-cancer drug doxorubicin, the potency of these bulky molecules was independent on the P-gp status of the two cell types. It should be noted that the purpose of this study was not to compare the potency of the fluorescent molecules with that of doxorubicin, a strong DNA intercalator and topoisomerase II inhibitor, but was rather to analyze their differential uptake in comparison with that of doxorubicin, a highly P-gp dependent drug.

#### 3.3. RESULTS AND DISCUSSION

#### 3.3.1. Chemistry

The synthesis of compound **4** and **6** proceeded according to Figure 3.1 and 3.2 respectively. Commercially available 9-fluorenylmethyl N-(2-aminoethyl)carbamate hydrochloride was treated with dansyl chloride in a biphasic ethyl acetate/aqueous potassium carbonate solution to

give 1 (Fig. 3.1). Compound 1 was deprotected with morpholine in DMF to give the amino compound 2. In parallel, the aminoquinazoline was diazotized in dry acetonitrile with nitrosonium tetrafluoroborate to provide the diazonium salt 3 as described previously [14]. Diazonium salt 3 was coupled with 2 in the presence of triethylamine *in situ* to give the desired compound 4. Several attempts to purify 4 by column chromatography failed due to on-column degradation, which we believe could be due to the conversion of 4 to a product resulting from loss of nitrogen. Successful purification was achieved by serial trituration of compound 4 with methylene chloride, ether and petroleum ether to give a pure red-brown powder. The compound was characterized by NMR and MS, and its purity confirmed by elemental analysis.

The synthesis of compound **6** proceeded in a similar fashion. An excess of commercially available N-(2-aminoethyl)-N-methylethanediamine was treated with dansyl chloride to give **5** in ethyl acetate at 0°C (Fig. 3.2) and this product was coupled with the diazonium salt of quinazoline **3** to give **6**. The purification of **6** was as difficult as that of **4**. All attempts to purify this compound by column chromatography failed. Serial trituration provided a pure red-brown powder that was analytically pure. The structure of **6** was further confirmed by NMR and MS.

#### 3.3.2. Half-life in a serum-containing medium

The sole structural difference between **4** and **6** is in the nature of the linker. The linker in **4** is an ethylene group between the sulfonamido moiety of the dansyl and the N3 of the triazene, leaving no possibility for intramolecular hydrogen bonding. By contrast, the dansyl in **6** is separated by 6-bond length and contains a methylamino groups at 3 bond lengths away from the N3 of the triazene, leaving the possibility for intramolecular hydrogen bonding. Interestingly, **4** was 5-fold less stable than **6** with a half-life as short as 5 min (Table 3.1). Perhaps, the

H<sub>3</sub>C CH<sub>3</sub>

H<sub>3</sub>C CH<sub>3</sub>

H<sub>3</sub>C CH<sub>3</sub>

H<sub>3</sub>C CH<sub>3</sub>

H<sub>3</sub>C CH<sub>3</sub>

$$O = S - CI$$
 $O = S - N$ 
 $O$ 

Figure 3.1 Synthesis of compound 4.

i) N-Fmoc-ethylenediamine, EtOAc,  $H_2O$ ,  $K_2CO_3$ , 0 °C, ii) morpholine, DMF, rt; iii) diazonium 3,  $Et_3N$ ,  $CH_3CN/Et_2O$ , -5 °C.

Figure 3.2. Synthesis of compound 6.

i) N-(2-aminoethyl)-N-methylethanediamine, EtOAc, 0 °C; ii) diazonium 3, Et $_3$ N, CH $_3$ CN/Et $_2$ O, -5°C.

**Table 3.1** Half-life of compound 4 and 6 in a serum-containing medium.

Compound	4	6
<b>t</b> ½ (min) *Data are	4.96 ± 0.04*	21.72± 0.27*
means of three experiment s in triplicate	105 100 90 90 90 90 90 90 90 90 90 90 90 90 9	105 100 95 100 95 100 95 100 100 100 100 100 100 100 10

intramolecular interaction between the N-methylamino group and the triazene, plays a significant stabilizing role. We have already evoked a similar interaction for explaining the stability of **7** (Fig. 3.2), a stable dimethyaminoethyl triazene with a  $t_{1/2}$ =108 min that showed significant antitumour activity *in vivo* [10, 21]. To further elaborate on the importance of the N-methylamino group on the stability of **6**, we undertook a molecular modeling study using AM1 semi-empirical calculation.

As outlined in Figure 3.5, conformer 1 containing H-bond is computed to be ~2 kcal/mol more stable than conformer 2, which lacks the H-bond. Conformer 1 has the proposed H-bond (2.62 Å distance) that stabilizes it. The H-bond is absent in conformer 2, as the hydrogen and the amine nitrogen are *trans* to one another at a distance of 4.08 Å. Compound 4, which is not able to adopt H-bond-stabilizing conformations, is less stable. However, in aqueous solution, the superior stability of 6 is better rationalized in terms of the equilibria depicted in Figures 3.3 and 3.4. Because the central nitrogen in 6 is being protonated at physiological pH, the transition state to the formation of the doubly charged species F should have higher energy when compared with 4 under physiological conditions.

#### 3.3.3. Differential growth inhibitory activity

The potency of the two dansylated compounds was compared in MES-SA cells that do not express P-gp. MES-SA cells are also deprived of EGFR expression [15]. Therefore, the EGFR inhibitory activity of the quinazoline side chain would not influence the growth inhibitory effect of compounds **4** and **6**. The results showed that **6** was 3-fold more potent than **4** (Fig. 3.6A). Perhaps the rapid decomposition of **4** compromised its optimal cellular delivery. We also observed a 2-fold stronger potency for **6** in the MDA-MB-468 breast cancer cells that express

**Figure 3.3.** Degradation pathway of compound **6** in physiological conditions.

$$\begin{array}{c} \text{H}_3\text{C} \\ \text{N} \\ \text{O} = \\ \text{S} \\ \text{N} \\ \text{N} \\ \text{A} \\ \\ \text{N} \\$$

Figure 3.4. Degradation pathway of compound 4 in physiological conditions.

EGFR but do not express P-gp, indicating that **6** was more potent than **4** regardless of the P-gp and the EGFR status of the cells (Fig. 3.6B) [22, 23].

Because our primary goal was to compare the cellular penetration of the two compounds in P-gp-proficient and -deficient cells, we tested their effect on both MES-SA (P-gp-deficient) and its derived MES-SA/DX5 (P-gp-proficient) cells. The latter cell line expresses high levels of P-gp and is resistant to doxorubicin. Using the SRB assay, we showed a 20-fold difference between the sensitivity of MES-SA and MES-SA/DX5 to doxorubicin. In contrast, no significant difference (P>0.05) was seen for both 4 and 6 in their potency against the two cell lines. Combi-molecule 6 was equally potent in both cell lines and 4 was 1.6-fold more potent against MES-SA/DX5 than MES-SA, indicating an even greater potency in the cells that express P-gp.

#### 3.3.4. Cellular uptake

To verify whether the differential responses correlated with cell penetration, we exploited the fluorescent properties of doxorubicin and those of compounds **4** and **6** to analyze their intracellular content by fluorescence microscopy and flow cytometry. We have previously used flow cytometry to analyze doxorubicin and compound **6** internalization in human breast tumour cells [17, 24]. Fluorescence microscopy in the parental cell line showed a homogeneous distribution of doxorubicin (Fig. 3.7A, upper panel) throughout the cell population. By contrast, in the MES-SA/DX5 cells (Fig. 3.7A, lower panel), the distribution was heterogeneous with a fraction of the cell population emitting high fluorescence and another with poor to no internalization of doxorubicin. As shown in Figure 3.8A, **4** and **6** penetrate the cells and decompose inside the cells to generate its bioactive species: EGFR inhibitor, blue fluorescence, and a DNA-damaging species, green fluorescence.

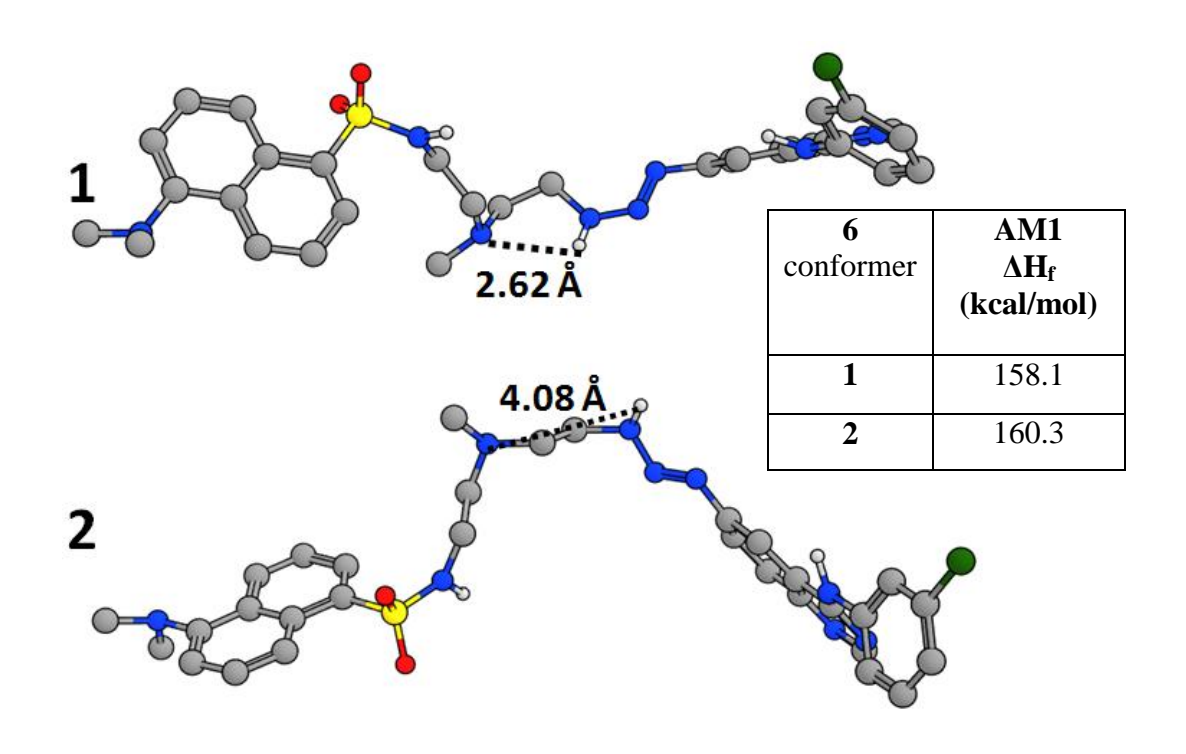


**Figure 3.5**. Molecular modeling using AM1 semi-empirical calculation of 6. The H-N distances are given in Å.

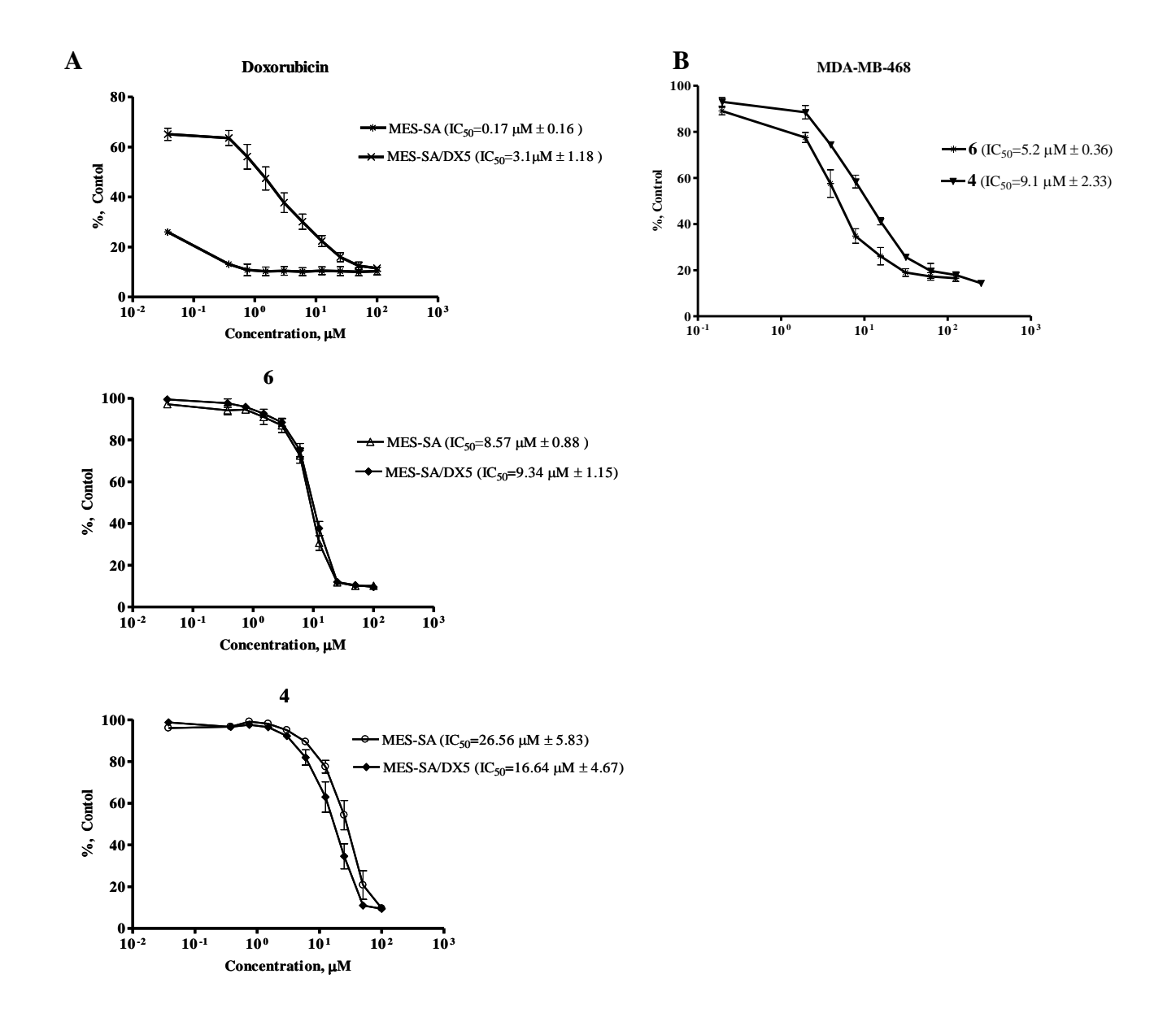


Figure 3.6. Growth inhibition of doxorubicin, 4 and 6 by SRB assay.

**A**, Comparison of antiproliferative activity of doxorubicin, **4** or **6** in MES-SA and MES-SA/DX5 cells after 96 hours. **B**, Growth inhibition of **4** and **6** in human breast MDA-MB-468 cells. Each point represents an average of two independent experiments performed in triplicate.

The two colors were observed at similar intensity in both cell types. Flow cytometric analysis permitted the quantification of the proportion of cells that did not internalize doxorubicin (Fig. 3.7B) and the combi-molecules (Fig. 3.8B). For the more potent compound **6**, at a dose range starting with the IC<sub>50</sub> for growth inhibition, no differential internalization between the two cell types was seen. In contrast, 40% of the cell population could not internalize doxorubicin at this dose range.

#### **3.3.5. DNA damage**

The DNA damaging property of compounds 4 and 6 was assessed by alkaline comet assay. The visualization of DNA comet tails in both cell lines using fluorescence microscopy showed that 6 was a strong DNA damaging agent, while 4 was not able to induce DNA damage (Fig. 3.9). This result is consistent with the stability of the two molecules and also that of the putative dansylated alkyldiazonium released after degradation. The rapid decomposition of 4 seems again to limit its activity. Moreover, 6 damaged DNA in both cell lines with the same intensity, independently of P-gp status, which is in agreement with the growth inhibitory results, and also indicate that the combi-molecule can penetrate and decompose inside the cells to deliver the DNA-damaging moiety (green fluorescence, Fig. 3.8A). The levels of DNA damage induced by doxorubicin were also analyzed in the two cell types, and a differential response was seen with doxorubicin inducing a 2-fold greater number of DNA-damaged cells in the MES-SA population when compared with MES-SA/DX5 (Fig. 3.7C). Cells with a higher comet tail moment than the control were scored as damaged, and the data were presented as percent of cells with damaged DNA. This result was consistent with the differential level of doxorubicin uptake observed between these two cell types.

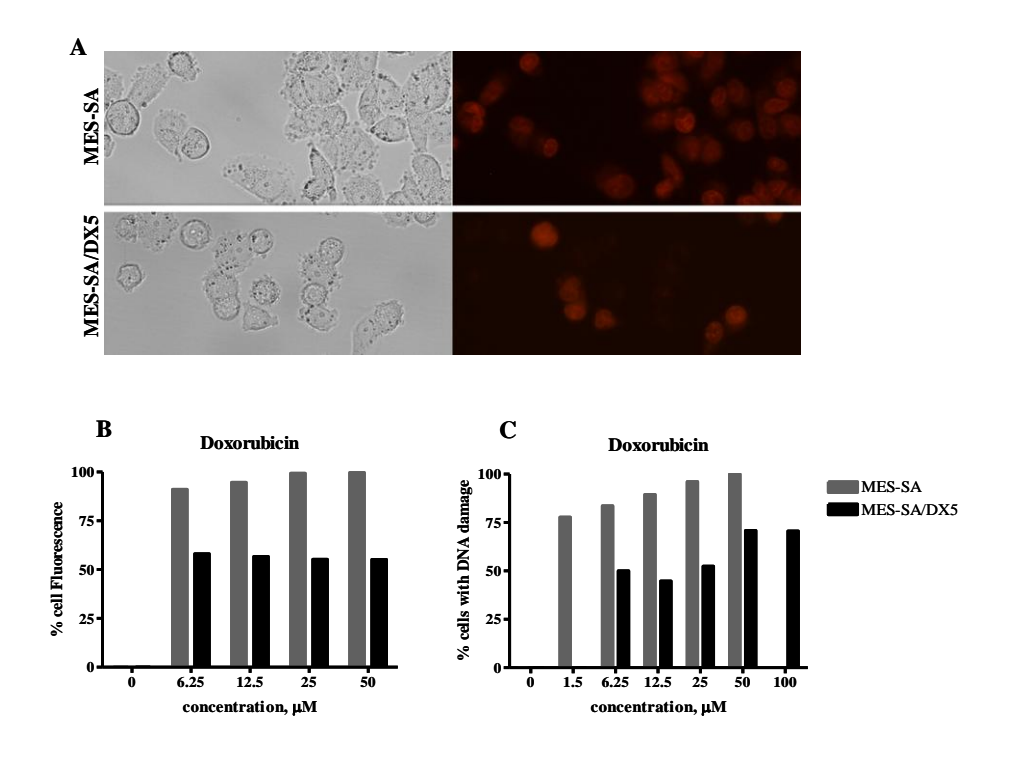


Figure 3.7. Cellular fluorescence and DNA damage by doxorubicin

A, Intracellular accumulation of doxorubicin in P-gp positive and negative cells was determined by fluorescence microscopy. Cells were incubated with 25 μM of doxorubicin for 2 h, washed with PBS and fluorescence was visualized with a Leica fluorescent microscope (40X magnification). B, Cellular fluorescence of doxorubicin by FACS. The levels of accumulated fluorescence for doxorubicin (0, 6.25, 12.5, 25, 50 μM) were quantified in MES-SA and MES-SA/DX5 cells after 2 h. C, DNA damage induced by doxorubicin in MES-SA (0, 1.5, 6.25, 12.5, 25, 50 μM) and MES-SA/DX5 (0, 6.25, 12.5, 25, 50, 100 μM) cells. Cells were exposed for 2 h to doxorubicin and DNA damage was measured using an alkaline comet assay. Fifty cells were scored from each dose and the comet tail moment was calculated by comet IV software (Perceptive Instruments). Cells with a comet tail moment greater than that in the control were scored positive and expressed as percent of cells with damaged DNA.

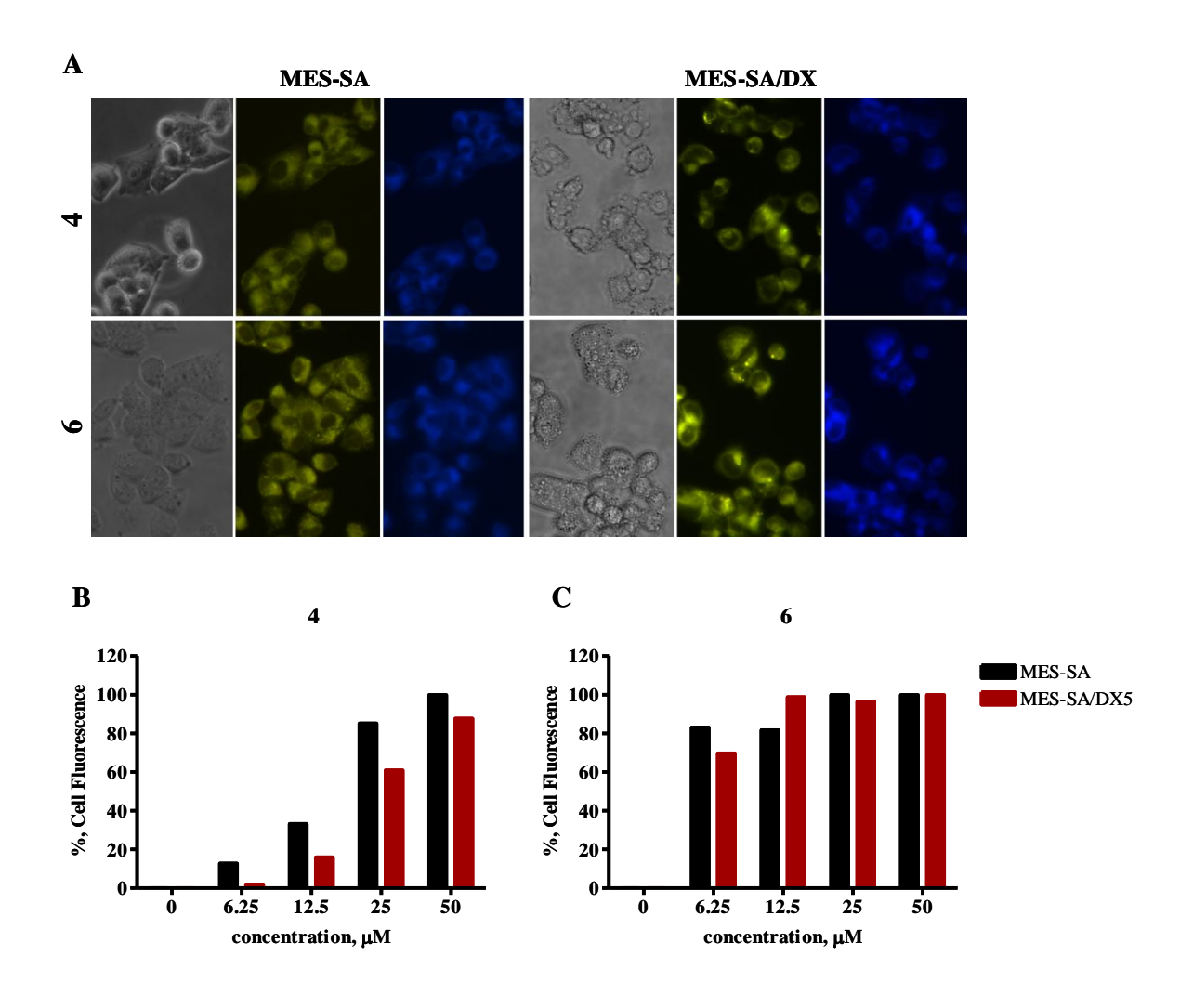
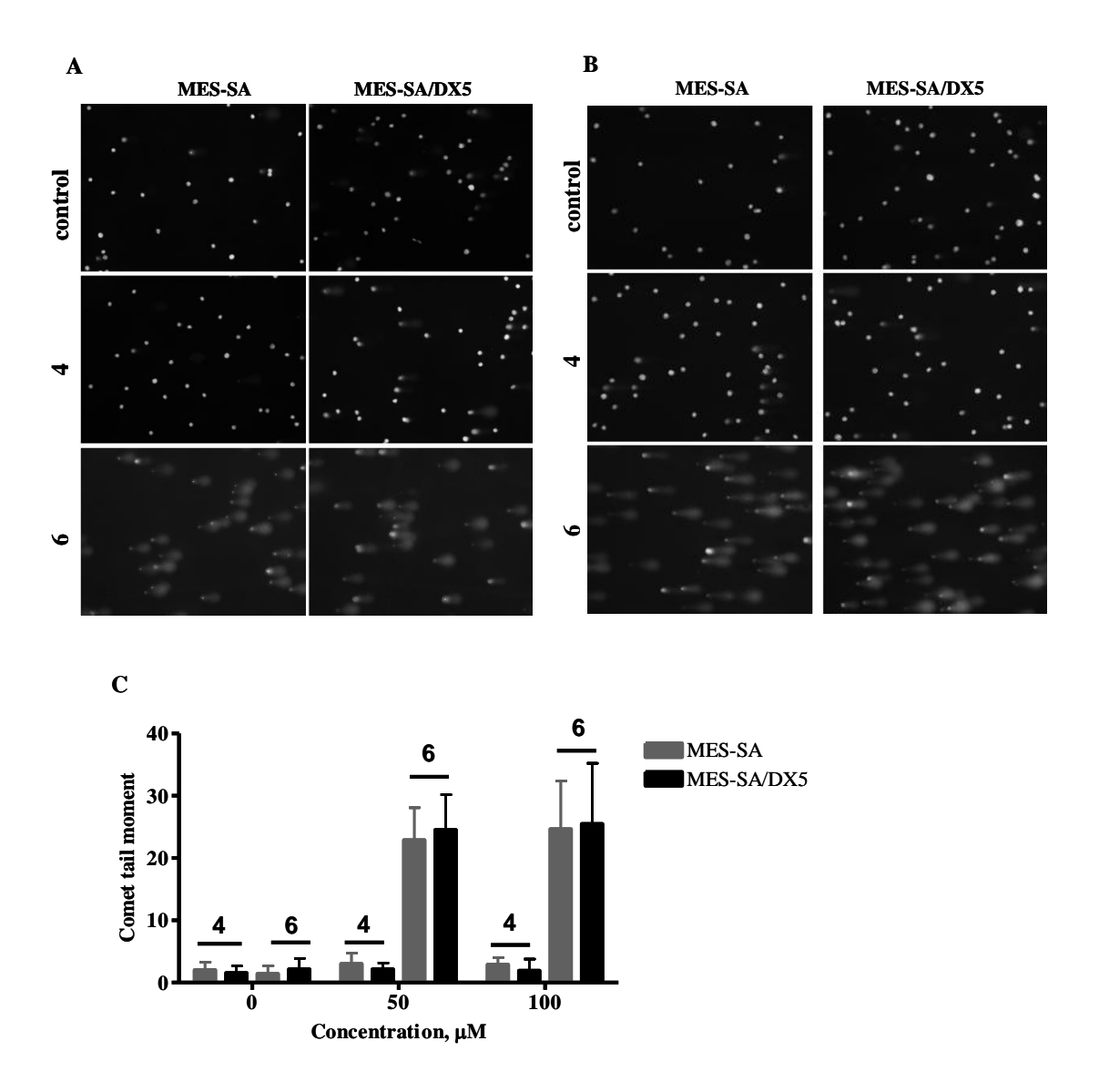


Figure 3.8. Cellular uptake of 4 and 6 by fluorescence microscopy and FACS.

**A,** MES-SA and MES-SA/DX5 cells were incubated with **4** and **6** for 2 h and imaging was performed with Leica fluorescent microscope (40X magnification). Visualization of **4** and **6** degradation species: blue aminoquinazoline and green dansylated species were imaged using individual filters; **B,** Cellular fluorescence of **4** and **C,** Cellular fluorescence of **6** by FACS. The levels of accumulated fluorescence for **4** and **6** (0, 6.25, 12.5, 25, 50 μM) were quantified in MES-SA and MES-SA/DX5 cells by FACS and results were analyzed with GraphPad Prism software.



**Figure 3.9.** DNA damage induced by **4** and **6**. DNA damage was analyzed with 50 (**A**) and 100μM (**B**) of **4** and **6**. MES-SA and MES-SA/DX5 cells were exposed to each combi-molecule for 2 h followed by assessment of drug-induced DNA damage using an alkaline comet assay. Visualization of DNA comets in both cell lines by fluorescence microscopy (10X magnification) after staining with SYBR Gold. **C**, Fifty comets were scored and the comet tail moment quantified by comet IV software (Perceptive Instruments). Two independent experiments were averaged for each cell line and data were analyzed with GraphPad Prism software.

#### 3.4. CONCLUSION

At the advanced stages of many cancers, drug transport is significantly affected by several mechanisms including P-gp-mediated drug efflux [1-5]. This presents a daunting challenge to drug development against advanced cancers. The combi-molecules are designed to possess multiple targeting properties with the purpose of simultaneously blocking several signaling networks in the cells. To this end, several pharmacophores must be appended to one single core structure. Therefore, this leads to the branching of pharmacophores through bulky linkers that often affect the size of the resulting molecules and as a result, their transport into the cells. It is now well known that the greater is the size of an agent is, the more likely that its transport mechanism across the cell membrane will be influenced by efflux proteins. Here, we discovered that at least one mechanism of drug efflux may not prevent cell penetration by two prototypical combi-molecules designed to block EGFR-DNA and carrying a bulky fluorescence-labeled moiety. Although the molecular mechanism of such an important observation requires further elucidation, we believe that the fact that the combi-molecules are designed to decompose inside the cells in order to generate their bioactive species might be a mean by which the rapid efflux of the intact structure was impeded.

#### 3.5. EXPERIMENTAL SECTION

#### **3.5.1.** Chemistry

 $^{1}$ H NMR spectra and  $^{13}$ C NMR spectra were recorded on a Varian 300 MHz spectrometer. Chemical shifts are given as  $\delta$  values in parts per million (ppm) and are referenced to the residual solvent proton or carbon peak. Mass spectrometry was performed by the McGill University Mass spectroscopy Center and electrospray ionization (ESI) spectra were performed

on a Finnigan LC QDUO spectrometer. Data are reported as m/z (intensity relative to base peak = 100). Elemental analyses were carried out by GCL & Chemisar Laboratories, Guelph, Ontario, Canada. The analyses were done two times. All chemicals were purchased from Sigma-Aldrich. Dansyl chloride was purchased from Alfa Aesar, N-(2-aminoethyl)-N-methylethanediamine from Wako Pure Chemical Industries, Ltd and mono-Fmocethylenediamine hydrochloride from Novabiochem. The purity of all compounds tested were >95% as determined by elemental analysis.

#### 3.5.1.1. Compound 1, 2-dansyl-9-fluorenylmethyl N-(2-aminoethyl)carbamate

9-Fluorenylmethyl N-(2-aminoethyl)carbamate hydrochloride (500 mg, 1.57 mmol) was dissolved in water saturated with potassium carbonate and ethyl acetate (50 mL/50 mL). The mixture was cooled to 0 °C and a solution of dansyl chloride (3 eq.) in ethyl acetate was added dropwise. The reaction mixture was stirred and the temperature was raised to room temperature. After four hours, the organic layer was separated, washed with brine twice and dried with magnesium sulphate, filtered and evaporated to provide a yellow-green oil which was purified by trituration in ethyl ether. White pure solid of compound **1** was obtained after filtration (742 mg, 92%). <sup>1</sup>H NMR (300 MHz, *DMSO-*  $d_6$ ):  $\delta$  ppm 2.75 (m, 2H), 2.80 (s, 6H), 2.95 (m, 2H), 4.21 (m, 3H), 7.25 (m, 4H), 7.37 (m, 2H), 7.59 (m, 4H), 7.85 (d, J =7.5 Hz, 1H), 7.99 (m, 1H), 8.08 (d, J =7.5 Hz, 1H), 8.24 (d, J =8.1 Hz, 1H), 8.45 (d, J =8.7 Hz, 1H).

#### 3.5.1.2. Compound 2, Dansyl-N-(2-aminoethyl)amide

The Fmoc group was removed with morpholine/DMF 1/1 (2 mL), 30 min at room temperature. The reaction mixture was evaporated and the crude product was extracted with ethyl acetate and acidic water phase (pH 2). The aqueous phase was alkalinized to pH 5 and extracted with

ethyl acetate to eliminate the secondary products from the aqueous layer. The pH was increased to 10, and this aqueous layer was extracted again with ethyl acetate. The organic layer was dried and the magnesium sulphate filtered and evaporated to provide pure free amine **2** (148 mg, 87%).  $^{1}$ H NMR (300 MHz, *DMSO-d*<sub>6</sub>):  $\delta$  ppm 2.45 (m, 2H), 2.75 (m, 2H), 2.81 (s, 6H), 7.24 (d, J =7.2 Hz, 1H), 7.59 (q, J =7.5 Hz, 2H), 8.09 (d, J =7.2 Hz, 1H), 8.28 (d, J =8.4 Hz, 1H), 8.45 (d, J =8.7 Hz, 1H).

#### 3.5.1.3. Compound 5, Dansyl-N-(2-[(2-aminoethyl)-N-methylamino]-ethyl)amide

Dansyl chloride (1 g, 3.71 mmol) was dissolved in 20 mL of ethyl acetate and was added dropwise to a cold solution of N-(2-aminoethyl)-N-methylethanediamine (2.38 mL, 5 eq.) in 80 mL of ethyl acetate. The reaction mixture was stirred at 0 °C under argon. After two hours, the solution was extracted with neutral water and acidic water (pH 2-3). This acidic water was alkalinized and was extracted with ethyl acetate two times. The organic layer was dried with magnesium sulphate, filtered and evaporated to provide a yellow oil which was purified by crystallization in a minimum of ethyl acetate. White pure crystals of compound 5 was obtained (1.117 g, 86%). H NMR (300 MHz, *DMSO- d*<sub>6</sub>):  $\delta$  ppm 1.92 (s, 3H), 2.13 (t, J = 6.3 Hz, 2H), 2.21 (t, J = 6.7 Hz, 2H), 2.40 (t, J = 6.1 Hz, 2H), 2.81 (s, 6H), 2.84 (t, J = 6.9 Hz, 2H), 7.21 (d, J = 7.5 Hz, 1H), 7.58 (m, 2H), 8.11 (d, J = 7.2 Hz, 1H), 8.27 (d, J = 8.4 Hz, 1H), 8.43 (d, J = 8.1 Hz, 1H).

#### 3.5.1.4. Compound 4

The diazonium compound **3** was synthesized as described in reference [14]: amino-anilinoquinazoline (50 mg, 0.184 mmol) was dissolved in dry acetonitrile (5 mL) under argon and, cooled to -5 °C. Nitrosonium tetrafluoroborate (2 eq.) in acetonitrile was added directly.

After 30 min at -5 °C, the resulting clear orange solution was added dropwise to another solution of compound **2** (1 eq.) in acetonitrile with triethylamine (2 eq.) at 0 °C, after which the mixture was extracted with ethyl acetate and brine. The organic layer was dried with potassium carbonate and evaporated to provide a brown residue, which was purified by serial trituration: firstly the crude product was dissolved in a minimum of methylene chloride and precipitate with petroleum ether and after was triturated in ether/petroleum ether ½ to give after filtration a red-brown solid (93 mg, 88%). H NMR (300 MHz,  $DMSO-d_0$ ):  $\delta$  ppm 2.77 (s, 6H), 3.10 (m, 2H), 3.59 (m, 2H), 7.13 (d, J = 8.4 Hz, 1H), 7.22 (d, J = 7.5 Hz, 1H), 7.39 (m, 1H), 7.59 (m, 2H), 7.73 (d, J = 8.7 Hz, 1H), 7.86 (m, 2H), 8.13 (m, 2H), 8.27 (d, J = 8.7 Hz, 1H), 8.35 (s, 1H), 8.43 (d, J = 9.0 Hz, 1H), 8.58 (s, 1H), 9.89 (s, 1H), 10.59 (m, 1H);  $^{13}$ C NMR (75 MHz,  $DMSO-d_0$ ):  $\delta$  ppm 158.13, 153.92, 152.05, 149.23, 148.90, 141.70, 136.29, 133.36, 130.71, 130.23, 129.74, 129.70, 129.50, 129.08, 128.61, 125.68, 124.28, 123.58, 121.89, 120.84, 119.71, 116.28, 115.82, 115.18, 51.72, 46.31, 45.72 (2C); ESI m/z 572.9 (MH+ with  $^{35}$ Cl). Anal. (C<sub>28</sub>H<sub>27</sub>ClN<sub>8</sub>O<sub>2</sub>S) C, H, N.

#### 3.5.1.5. Compound 6

The diazonium compound **3** was still synthesized as described previously[14]. Amino-anilinoquinazoline (608 mg, 2.246 mmol) was dissolved in dry acetonitrile (80 mL) under argon and, cooled to -5 °C. Nitrosonium tetrafluoroborate (2 eq.) in acetonitrile was added directly. After 30 min at -5 °C, the resulting clear solution was added dropwise to another solution of compound 5 (1 eq.) in acetonitrile with triethylamine (2 eq.) at 0 °C, after which the mixture was extracted with ethyl acetate and brine. The organic layer was dried with potassium carbonate and evaporated to provide a brown residue, which was purified by serial trituration. The crude product was dissolved in a minimum of methylene chloride and precipitated with

petroleum ether, after which it was triturated in ether/petroleum ether 1/4 to give after filtration a red-brown solid (1.2 g, 85%). H NMR (300 MHz, DMSO-  $d_6$ ):  $\delta$  ppm 1.99 (s, 3H), 2.32 (m, 2H), 2.52 (m, 2H), 2.77 (s, 6H), 2.90 (m, 2H), 3.53 (m, 2H), 7.12 to 7.21(m, 2H), 7.39 (m, 1H), 7.55 (m, 2H), 7.75 to 7.97 (m, 4H), 8.12 (m, 2H), 8.30 (d, J = 8.4 Hz, 1H), 8.40 (m, 1H), 8.43 (s, 1H), 8.60 (s, 1H);  $^{13}$ C NMR (75 MHz, DMSO-  $d_6$ ):  $\delta$  ppm 158.10, 153.83, 152.01, 149.73, 148.78, 141.75, 136.69, 133.37, 130.72, 130.07, 129.76, 129.69, 129.56, 128.92, 128.54, 125.40, 124.25, 123.55, 121.83, 120.79, 119.77, 116.37, 115.76, 115.29, 57.04 (2C), 53.84, 46.40, 45.72 (2C), 41.51; ESI m/z 632.1 (MH $^+$  with  $^{35}$ Cl). Anal. (C<sub>31</sub>H<sub>34</sub>ClN<sub>9</sub>O<sub>2</sub>S) C, H, N.

#### 3.5.2. Half-lives

The half-lives of **4** and **6** under physiological conditions were studied by UV spectrophotometer, Farmacia Biotech Ultrospec 2000. The compounds were dissolved in minimum volume of DMSO and diluted with DMEM supplemented with 10% FBS, and absorbance were read at 335 nm for **4**, and 350 nm for **6** in a quartz UV cell maintained at 37 °C with circulating water bath. The experiment was repeated 3 times for each compound. The half-life was estimated by a one-phase exponential decay curve-fit method using the GraphPad software package (GraphPad software, Inc., San Diego, CA). The thermometer was Traceable VWR digital with ± 0.005 °C accuracy.

#### 3.5.3. Molecular modeling

Molecular modeling was performed with MOE software (version 2006.08) available from Chemical Computing Group Inc., 1010 Sherbrooke Street West, Montreal, Quebec, Canada www.chemcomp.com.

#### **3.5.4. Biology**

#### 3.5.4.1. Cell culture

All three cell lines were purchased from the American Type Culture collection (ATCC, Manassas, VA). Human uterine sarcoma cells, MES-SA and MES-SA/DX5 (ATCC: CRL-1976 and CRL-1977 respectively) were maintained in McCoy 5A medium and human breast cancer cells MDA-MB-468 were cultured in DMEM. All media were supplemented with 10% FBS, 1.5 mM L-glutamine (Wisent Inc., St-Bruno, Canada) and 100 μg/ml penicillin/streptomycin (GibcoBRL; Gaithersburg, MD). Cells were grown exponentially at 37 °C in a humidified atmosphere of 95% air and 5% carbon dioxide. In all assays cells were plated 24 h before drug treatment.

#### 3.5.4.2. Drug treatment

Compounds **4** and **6** were synthesized in our laboratory, and doxorubicin hydrochloride was purchased from the hospital drug store (Mayne Pharma Inc., Montreal). In all assays, molecules were dissolved in DMSO (50 mM stock solution) and doxorubicin was dissolved in sterile water (2 mg/ml stock solution) and subsequently diluted in McCoy 5A medium before being added to cells. The concentration of DMSO never exceeded 0.1% (v/v) during treatment.

#### 3.5.4.3. Growth inhibition assay

MES-SA, MES-SA/DX5, and MDA-MB-468 cells were plated at a density of 5000 cells/well in 96-well flat-bottomed microtiter plates (100  $\mu$ L of cell/well). Cells were allowed to attach overnight and then were treated with different drug concentrations for 96 h. Thereafter, cells were fixed using 50  $\mu$ L 50% trichloroacetic acid for 60 min at 4 °C, washed four times with

water, stained with sulforhodamine B (SRB 0.4%) for 2 h at room temperature, rinsed four times with 1% acetic acid and allowed to dry [25]. The resulting colored residue was dissolved in 200 μL Tris base (10 mM, pH 10.0) and optical density was recorded at a wavelength of 492 nm using a Bio-Rad microplate reader (model 2550). The results were analyzed by GraphPad Prism (GraphPad Software, Inc., San Diego, CA) and the sigmoidal dose-response curve was used to determine 50% cell growth inhibitory concentration (IC<sub>50</sub>). Each point represents the average of at least three independent experiments run in triplicate.

#### 3.5.4.4. DNA damage by alkaline comet assay

The alkaline comet assay was performed as previously described [26-28]. Briefly, cells were exposed to doxorubicin (0, 1.5, 6.25, 12.5, 25, 50 μM), 4 and 6 (0, 50, 100 μM) for two hours, harvested by trypsinization, collected in ice-cold PBS by centrifugation at 3000 rpm for 5 min, and then resuspended in PBS at 1x10<sup>6</sup> cells/mL. Cells were mixed with low melting point agarose (0.7%) in PBS at 37 °C (final dilution 1:10), followed by layering the agarose/cells suspension on GelBond film (Lonza, Rockland, ME). Agarose/cell suspension was allowed to solidify for 10 min and then immediately placed in lysis buffer [2.5 M NaCl, 100 mM tetrasodium EDTA, 10 mM Tris-base, 1% (w/v) N-lauroyl-sarcosine, 10% (v/v) DMSO, and 1% (v/v) triton X-100, pH 10.0] overnight at 4 °C. Thereafter, the gels were rinsed with distilled water, equilibrated in alkaline electrophoresis buffer [300 mM NaOH, 10 mM tetra-sodium EDTA, 7 mM 8-hydroxyquinoline, 2% (v/v) DMSO, pH 13.0] for 30 min at room temperature, and electrophoresed at 20V for 25 min in fresh eletrophoresis buffer. The gels were subsequently neutralized in 1 M ammonium acetate and then dehydrated in 100% ethanol overnight. Comets were visualized at 10x magnification using Leica fluorescent microscope after staining with SYBR Gold (1:10,000, Molecular Probes, Eugene, OR) for 45 min.

#### 3.5.4.5. Fluorescence microscopy

Fluorescent properties of molecules were used to image drug transport efficiency and intracellular accumulation. MES-SA and MES-SA/DX5 cells ere plated at 70% confluence in six-well plates, allowed to adhere overnight and treated with 0, 25 and 50  $\mu$ M 4, 6 or doxorubicin. After 2 hours cells were washed twice with PBS and were directly imaged at 40x using Leica fluorescent microscope (Leica DFC300FX camera) without fixation.

#### 3.5.4.6. Flow cytometry analysis of intracellular drug fluorescence

MES-SA and MES-SA/DX5 cells were plated at 0.5x10<sup>6</sup> cells per well in six-well plates, allowed to adhere overnight and incubated in the presence of **4** and **6** or doxorubicin (0, 1.25, 6.25, 12.5, 25, 50 μM) for 2 h. Cells were collected by trypsinization, washed twice with PBS, pelleted by centrifugation and resuspended in 300 μL PBS supplemented with 1% FBS to prevent cell clumping. Intracellular fluorescence levels were measured using a BD LSR flow cytometer (BD Biosciences, San Jose, CA). For **4** and **6**, fluorescence was detected at two wavelengths for the two fluorescent products hydrolyzed in the cell: the aminoquinazoline [excitation at 340 nm, emission at 451 nm (blue)] and the dansylated DNA damaging species [excitation at 340 nm, emission at 525 nm (green)]. To test the transport efficiency of P-gp-proficient cells (MES-SA/DX5) in comparison with the parental MES-SA P-gp-deficient cells, we quantified the fluorescence levels of doxorubicin [excitation at 480 nm, emission at 560-590 nm (red)] and recorded the percentage of doxorubicin-positive P-gp-expressing cells (MES-SA/DX5). FACS results were analyzed with GraphPad Prism software.

#### 3.6. ACKNOWLEDGMENTS

We would like to thank the National Cancer Institute of Canada (NCIC grant 018475); Canadian Institutes of Cancer Research (Grant FRN 49440); Fonds de la Recherche en Santé du Québec doctoral award (M. Todorova) for financial support. We gratefully acknowledge Mr. Nadim K. Saade from the Department of Chemistry, McGill University, for mass spectra.

#### 3.7. CONNECTING TEXT

Previous SAR analysis explored the possibility to obtain large combi-molecules with improved stability, solubility and high affinity for EGFR [29, 30]. A subsequent challenge undertaken by Larroque et al. [31] addressed the design and synthesis of bulky bis-triazenoquinazolines using morpholino linker with a retention of the basic nitrogen required for optimal binding to EGFR [29]. As previously demonstrated central nitrogen of the spacer forms a hydrogen bond with Asp-776 of the ATP site of EGFR EGFR. We now have taken this design one step further by replacing one of quinazoline moiety of the bis-quinazoline structure by a bulky dansyl fluorophore and as demonstrated in Chapter 2 the resulting molecule AL237 lent itself to the analysis of the subcellular distribution of the sub-fragments of the combi-molecules. In addition, this study brought insight on large combi-molecule transport, localization with their cellular targets, EGFR and DNA, and more importantly it confirmed their biological activity. Having now good understanding of the important factors necessary to achieve threecompartment combi-molecules with good solubility and favourable steric conformations for strong EGFR binding, we designed a novel triple-targeting molecule in which the dansyl moiety of AL237 was replaced by a flavone ring, leading to two novel molecules AL232 and AL414. The purpose of adding the flavone ring was to allow the triplex combi-molecules to release PD98059, a known MEK inhibitor.

We have previously shown that dual EGFR-DNA targeting agents are able to induce high apoptosis and superior potency when compared with individual EGFR inhibitors and in combinations with alkylating agents. Despite the unique activity of combi-molecules, their potency is mitigated by the DNA repair capacity of the cells [32]. While inflicting significant DNA damage in tumour cells, they often activate alternative antiapoptotic pathways such as the stress response pathway in which MEK is a key player [33]. Even though we were able to downregulate EGFR activation and EGFR-associated DNA repair and survival pathways, these molecules are not able to block the activation of the DNA repair enzymes through the stress response pathway in which MEK plays a major role.

With this premise, we attempted to synthesize a three compartment combi-molecules designed to contain an EGFR targeting quinazoline, an aminoethylaminoethyltriazene hydrolyzing to the DNA alkylating diazonium, and an aminoflavone moiety programmed to be converted to the known MEK inhibitor PD98059. We hypothesized that the molecule would hydrolyze or would be metabolically cleaved inside the cell or in order to release three bioactive components. Therefore in Chapter 4 we describe the attempt to induce tandem targeting by inhibiting EGFR and MEK signaling while damaging DNA. While the molecule was successfully synthesized, metabolic studies showed that the free MEK inhibitor was not released. Nevertheless, the study set premise for further design and development of triplex combi-molecules containing in addition to a DNA + an EGFR targeting fragment, an additional component targeting the MEK signaling.

#### 3.8. REFERENCES

- 1. Ramachandra, M., et al., *Human P-Glycoprotein Exhibits Reduced Affinity for Substrates during a Catalytic Transition State*. Biochemistry, 1998. **37**(14): p. 5010-5019.
- 2. Sharom, F.J., *The P-glycoprotein efflux pump: how does it transport drugs?* J. Membr. Biol., 1997. **160**(3): p. 161-175.
- 3. Szakacs, G., et al., *Targeting multidrug resistance in cancer*. Nat. Rev. Drug Discovery, 2006. **5**(3): p. 219-234.
- 4. Longley, D.B. and P.G. Johnston, *Molecular mechanisms of drug resistance*. J. Pathol., 2005. **205**(2): p. 275-292.
- 5. Loo, T.W. and D.M. Clarke, *Recent progress in understanding the mechanism of P-glycoprotein-mediated drug efflux.* J. Membr. Biol., 2005. **206**(3): p. 173-185.
- 6. Aller, S.G., et al., Structure of P-Glycoprotein Reveals a Molecular Basis for Poly-Specific Drug Binding. Science (Washington, DC, U. S.), 2009. **323**(5922): p. 1718-1722.
- 7. Perez, E.A., et al., Schedule-dependent synergism of edatrexate and cisplatin in combination in the A549 lung-cancer cell line as assessed by median-effect analysis. Cancer Chemother Pharmacol, 1993. **33**(3): p. 245-250.
- 8. Turk, D., et al., *Identification of Compounds Selectively Killing Multidrug-Resistant Cancer Cells.* Cancer Res, 2009. **69**: p. 8293-8301.
- 9. Brahimi, F., et al., *Inhibition of epidermal growth factor receptor-mediated signaling by "Combi-Triazene" BJ2000, a new probe for Combi-Targeting postulates.* J. Pharmacol. Exp. Ther., 2002. **303**(1): p. 238-246.
- 10. Brahimi, F., et al., Mechanism of action of a novel "combi-triazene" engineered to possess a polar functional group on the alkylating moiety: Evidence for enhancement of potency. Biochem. Pharm., 2005. **70**(4): p. 511-519.
- 11. Brahimi, F., et al., Multiple mechanisms of action of ZR2002 in human breast cancer cells: A novel combi-molecule designed to block signaling mediated by the ERB family of oncogenes and to damage genomic DNA. Int. J. Cancer, 2004. 112(3): p. 484-491.
- 12. Domarkas, J., et al., *The Combi-Targeting Concept: Synthesis of Stable Nitrosoureas Designed to Inhibit the Epidermal Growth Factor Receptor (EGFR)*. J. Med. Chem., 2006. **49**(12): p. 3544-3552.
- 13. Banerjee, R., et al., Synthesis of a Prodrug Designed To Release Multiple Inhibitors of the Epidermal Growth Factor Receptor Tyrosine Kinase and an Alkylating Agent: A Novel Tumor Targeting Concept. J. Med. Chem., 2003. **46**(25): p. 5546-5551.

- 14. Rachid, Z., et al., *The Combi-Targeting Concept: Chemical Dissection of the Dual Targeting Properties of a Series of "Combi-Triazenes"*. J. Med. Chem., 2003. **46**(20): p. 4313-4321.
- 15. Yip, W.L., et al., Targeted delivery and enhanced cytotoxicity of cetuximab-saporin by photochemical internalization in EGFR-positive cancer cells. Mol. Pharm., 2007. **4**(2): p. 241-451.
- 16. Todorova, M.I., et al., Subcellular distribution of a fluorescence-labeled combimolecule designed to block epidermal growth factor receptor tyrosine kinase and damage DNA with a green fluorescent species. Mol Cancer Ther, 2010. **9**(4): p. 869-82.
- 17. Todorova, M., et al., Cellular imaging and signaling to AL237, a fluorescent-labeled probe for the combi-targeting approach to tumor targeting. Molecular Cancer Therapeutics, 2009. in press.
- 18. Harker, W.G., F.R. MacKintosh, and B.I. Sikic, *Development and characterization of a human sarcoma cell line, MES-SA, sensitive to multiple drugs.* Cancer Res, 1983. **43**(10): p. 4943-4950.
- 19. Harker, W.G. and B.I. Sikic, *Multidrug (pleiotropic) resistance in doxorubicin-selected variants of the human sarcoma cell line MES-SA*. Cancer Res, 1985. **45**(9): p. 4091-4096.
- 20. Koo, J.S., et al., Quinoline derivative KB3-1 potentiates paclitaxel induced cytotoxicity and cycle arrest via multidrug resistance reversal in MES-SA/DX5 cancer cells. Life Sci, 2008. 83(21-22): p. 700-708.
- 21. Merayo, N., et al., *The combi-targeting concept: evidence for the formation of a novel inhibitor in vivo*. Anti-Cancer Drugs, 2006. **17**(2): p. 165-171.
- 22. Wang, H., A.E. Giuliano, and M.C. Cabot, Enhanced de novo ceramide generation through activation of serine palmitoyltransferase by the P-glycoprotein antagonist SDZ PSC 833 in breast cancer cells. Mol Cancer Ther, 2002. 1(9): p. 719-26.
- 23. Liem, A.A., et al., *Doxorubicin and vinorelbine act independently via p53 expression and p38 activation respectively in breast cancer cell lines.* Br J Cancer, 2003. **88**(8): p. 1281-4.
- 24. Panasci, L., et al., Sensitization to doxorubicin resistance in breast cancer cell lines by tamoxifen and megestrol acetate. Biochemical Pharmacology, 1996. **52**(7): p. 1097-1102.
- 25. Skehan, P., et al., *New colorimetric cytotoxicity assay for anticancer-drug screening*. J Natl Cancer Inst., 1990. **82**(13): p. 1107-1112.
- 26. Matheson, S.L., et al., *The combi-targeting concept: Dissection of the binary mechanism of action of the combi-triazene SMA41 in vitro and antitumor activity in vivo.* J. Pharmacol. Exp. Ther., 2004. **311**(3): p. 1163-1170.

- 27. Olive, P.L. and J.P. Banath, *The comet assay: a method to measure DNA damage in individual cells.* Nat Protoc, 2006. **1**(1): p. 23-29.
- 28. McNamee, J.P., et al., *Comet assay: rapid processing of multiple samples.* Mutat Res, 2000. **466**(1): p. 63-69.
- 29. Larroque, A.-L., et al., Synthesis of water soluble bis-triazenoquinazolines: an unusual predicted mode of binding to the epidermal growth factor receptor tyrosine kinase. Chemical Biology & Drug Design, 2008. **71**(4): p. 374-379.
- 30. Rachid, Z., et al., Novel Nitrogen Mustard-Armed Combi-Molecules for the Selective Targeting of Epidermal Growth Factor Receptor Overexperessing Solid Tumors: Discovery of an Unusual Structure-Activity Relationship. J. Med. Chem., 2007. **50**(11): p. 2605-2608.
- 31. Larroque-Lombard, A.L., et al., Synthesis and uptake of fluorescence-labeled Combimolecules by P-glycoprotein-proficient and -deficient uterine sarcoma cells MES-SA and MES-SA/DX5. J Med Chem, 2010. **53**(5): p. 2104-13.
- 32. Matheson, S.L., J.P. McNamee, and B.J. Jean-Claude, *Differential responses of EGFR-AGT-expressing cells to the "combi-triazene" SMA41*. Cancer Chemoth. Pharm., 2003. **51**(1): p. 11-20.
- 33. Banerjee, R., A novel small molecule-based multi-targeting approach for the selective therapy of epidermal growth factor receptor (EGFR)- or Her2-expressing carcinomas Ph. D. dissertation, Faculty of Medicine, 2006.

## **Chapter 4**

# Synthesis and Studies on Three-Compartement Flavone-containing Combimolecules Designed to Target EGFR, DNA and MEK

Anne-Laure Larroque-Lombard $^{\dagger \S}$ , Margarita Todorova $^{\dagger \S}$ , Qiu Qiyu $^{\dagger}$ , and Bertrand Jean-Claude $^{\dagger *}$ 

<sup>†</sup>Cancer Drug Research Laboratory, Department of Medicine, Division of Medical Oncology,
McGill University Health Center/Royal Victoria Hospital, 687 Pine Avenue West Rm M-719,
Montreal, Quebec, H3A 1A1 Canada.

<sup>\*</sup> Tel: 514 842-1231, ext 35841. Fax: 514 843-1475. E-mail: <a href="mailto:bertrandj.jean-claude@mcgill.ca">bertrandj.jean-claude@mcgill.ca</a>.

<sup>§</sup> The two authors contributed equally to this manuscript.

#### 4.1 ABSTRACT

Previous work on multifunctional combi-molecule showed the feasibility of an agent capable of carrying an epidermal growth factor receptor (EGFR) inhibitor with a DNA damaging function and a fluorescent dansyl tag. Using a similar approach, we built a complex combi-molecule containing an EGFR targeting quinazoline, an aminoethylaminoethyltriazene compartment designed to be hydrolyzed into a DNA alkylating diazonium and an aminoflavone moiety programmed to be converted to the known MEK inhibitor PD98059 by intracellular and enzymatic hydrolysis. Two complex molecules were synthesized: one with a short aminoethyl spacer, AL232 and the other AL414 with a longer aminoethylamino ethyl spacer containing a protonable nitrogen positioned at a distance that was previously shown to allow a hydrogen bond with the EGFR receptor. As predicted from previous structure-activity studies, AL414 was a more potent inhibitor of EGFR tyrosine kinase than AL232. Both combi-molecules blocked EGFR phosphorylation in whole cells and downregulated extracellular signalingregulated kinases (ERK1,2), which were direct substrates of MEK. However, only AL414 was capable of inducing DNA damage. Thus, it was taken in vivo for metabolic analysis. The results showed that 3 h after injection, AL414 was hydrolyzed to FD105, an EGFR inhibitor, which was further acetylated into an N-acetyl metabolite FD105Ac by N-acetyltransferase (NAT), an even more potent inhibitor of EGFR. The detected flavone derivative was PD98059 linked to the hydroxyalkyl moiety resulting from the decomposition of the alkyldiazonium species and no intact PD98059 was observed. Independent synthesis of the latter metabolite and further in vitro analysis showed that it was deprived of antiproliferative activity. Analysis of ERK1,2 in non EGFR-expressing cells showed a rather moderate inhibition of ERK1,2 phosphorylation indicating that perhaps the observed downregulation of phospho-ERK1/2 under EGFstimulation was primarily due through EGFR TK inhibition.

#### **4.2 INTRODUCTION**

Solid tumour cells are often characterized by overexpression of several receptors and dysfunction of related signal transduction pathways. One such receptor is the epidermal growth factor receptor (EGFR), the expression of which is associated with tumour invasiveness, aggressive proliferation and reduced sensitivity to antitumour drugs [1]. Agents designed to block the tyrosine kinase function of EGFR induce potent antitumour activity in xenograft models and two such molecules Iressa<sup>TM</sup> and Tarceva<sup>TM</sup> are now used in the clinical management of various solid tumours [2-4]. However the spectrum of activity of the latter agents is very narrow and their clinical potency as single agent is rather moderate [5]. Combination with cytotoxic agents is currently an actively explored strategy to potentiate the action of EGFR inhibitors [6-8]. Recently, we developed a novel strategy to enhance the potency of EGFR inhibitors by designing them to contain a triazene function that upon degradation release a DNA damaging moiety [9-11]. These agents termed "combi-molecules" have been shown to induce enhanced apoptosis and superior potency when compared with individual EGFR inhibitors and their combinations with other alkylating agents [12, 13]. However, despite their unique activity, their potency is mitigated by the DNA repair capacity of the cells [14, 15].

"Combi-molecules" are dual targeted agents capable of blocking EGFR-mediated signaling and damaging DNA. The mechanism of their potency is based on their ability to downregulate antiapoptotic signaling and DNA repair while inflicting significant DNA damage to tumour cells [9, 13, 16]. However, they are unable to down-regulate DNA repair proteins induced through the stress response pathway in which MEK is a key player in tumour cells [15, 17-21]. Moreover, MEK phosphorylation is associated with activation of Bad and the antiapoptotic pathway in response to various stressors [22]. To this end, we designed and synthesized novel

molecules capable of not only blocking EGFR and damaging DNA but also inhibiting MEK. Here we describe the first drug design to induce tandem targeting of MEK, DNA and EGFR. Based upon previous chemistry developed to create 3-compartment molecules [23, 24], which carry in addition to the DNA and EGFR targeting moieties, a fluorescent tag, we designed AL232 and AL414. As outlined in figure 4.1 the combi-molecules (see example with AL414) were "programmed" to release FD105, an EGFR inhibitor and an alkyldiazonium species designed to damage DNA (path a) and a flavone derivative (species 1) that would ultimately release PD98059 upon metabolism (path b-c) [13, 25-27].

The flavone-linked diazonium was expected to be further metabolized in the liver to release an intact PD98059, a MEK inhibitor. Here, we describe the synthesis of this type of agents, analyze their degradation products *in vivo* and determine their effect on DNA damage, ERK1,2 (MEK substrates) phosphorylation and their antiproliferative potency.

#### **4.3 RESULTS**

# 4.3.1. Chemistry

The synthesis of AL414 utilizes an adaptation of strategy developed to synthesize the fluorescent-labeled combi-molecule AL237 [23]. The complete pharmacophore-carrying arm was built with a terminal amine that is coupled with the diazonium salt of the aminoquinazoline to generate the triazene at the final step (Fig. 4.2). Briefly, PD98059 was treated with an excess of bis-chlorocarbonate 1 to give carbonate 2. Interestingly the resulting chlorocarbonate was stable enough to be purified by column chromatography. Treatment of the flavone-linked chlorocarbonate with amine 3 prepared using previously described methodology [28, 29] gave

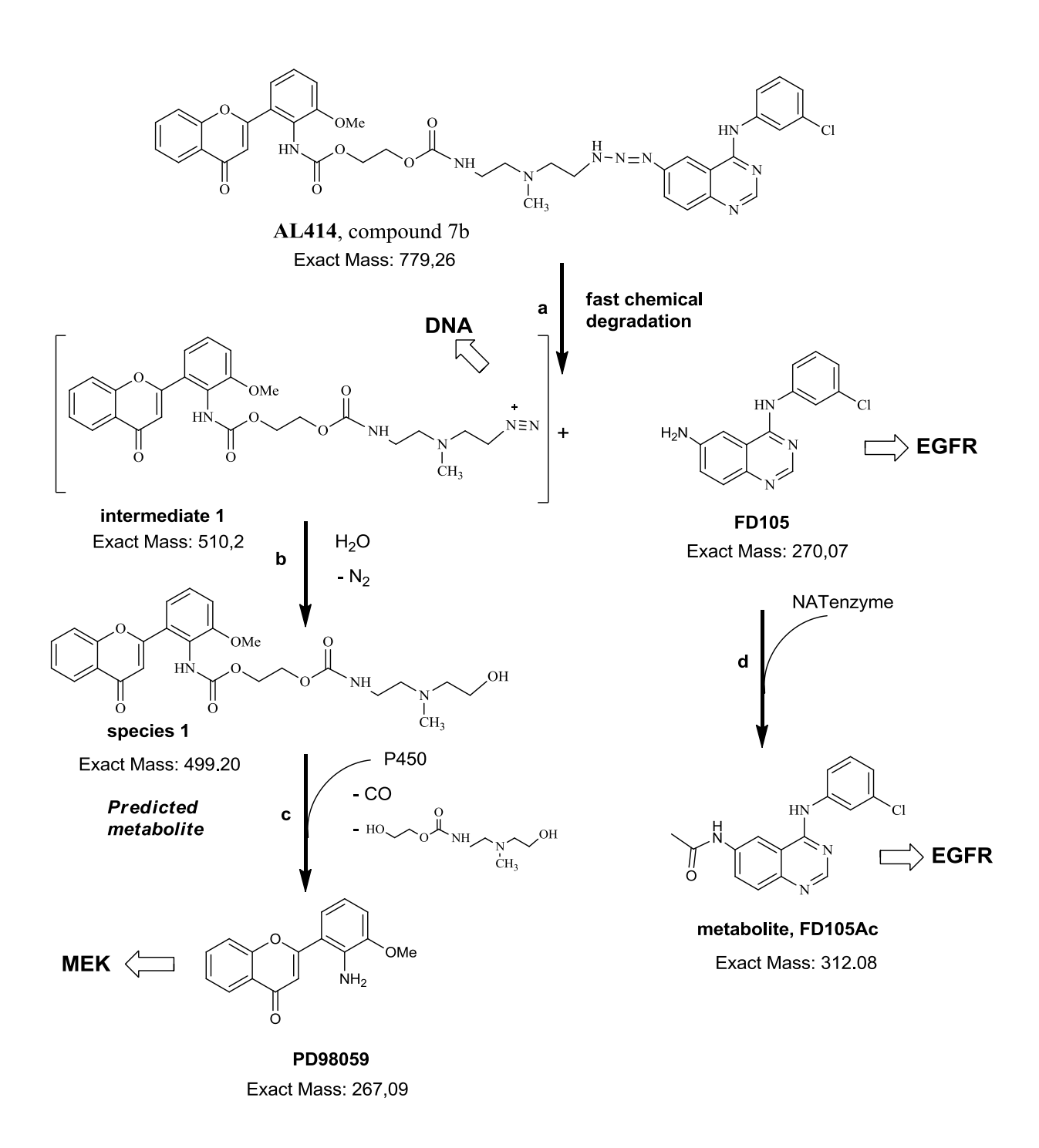


Figure 4.1. Biodegradation of the combi-molecule AL414.

PD98059 1 2 ii 
$$\frac{1}{3}$$
 NHBoc  $\frac{1}{3}$  NHBo

Figure 4.2. Synthesis pathway of AL232 and AL414.

i) excess of bis-chlorocarbonate **1**, CH<sub>2</sub>Cl<sub>2</sub>, 0°C to rt, 18 h, ii) amine **3**, CH<sub>2</sub>Cl<sub>2</sub>, 0°C to rt, 2 h, iii) HCl 1.25 M in MeOH, 18 h, 0°C to rt, iv) Et<sub>3</sub>N, CH<sub>3</sub>CN, -5°C, 30 min.

Figure 4.3. Synthesis pathway of compound 9.

i) excess of bis-chlorocarbonate 1,  $CH_2Cl_2$ , 0°C to rt, 18 h, ii) commercial aminoalcohol **8**,  $CH_2Cl_2$ , 0°C to rt, 2 h.

the Boc-protected compound **4**. The amino group of **4** was unveiled under acidic condition to give **5**, which was coupled to the diazonium salt **6** [10] under basic condition to give **7a** (AL232) and **7b** (AL414) as brown powders. The isolated combi-molecules were purified by trituration. Compound **9** was obtained using the same intermediate **2** which is coupled to commercial aminoalcohol **8** to give **9** purified by preparative TLC (Fig. 4.3).

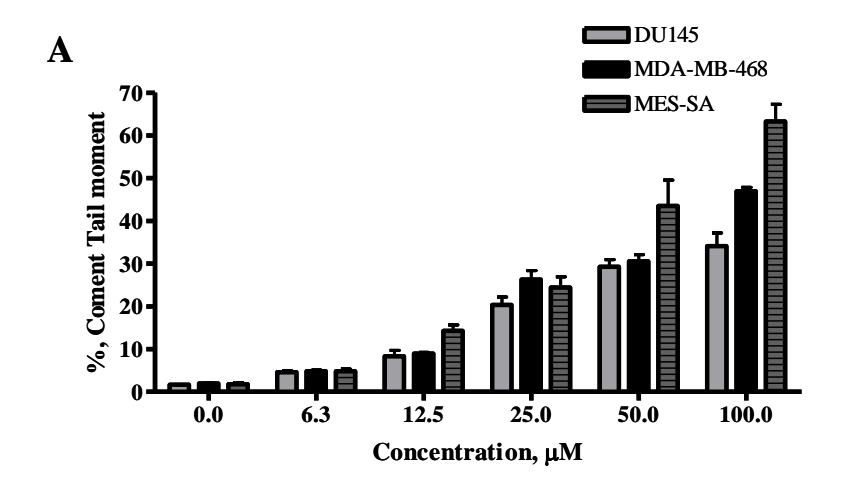
## **4.3.2. DNA damage**

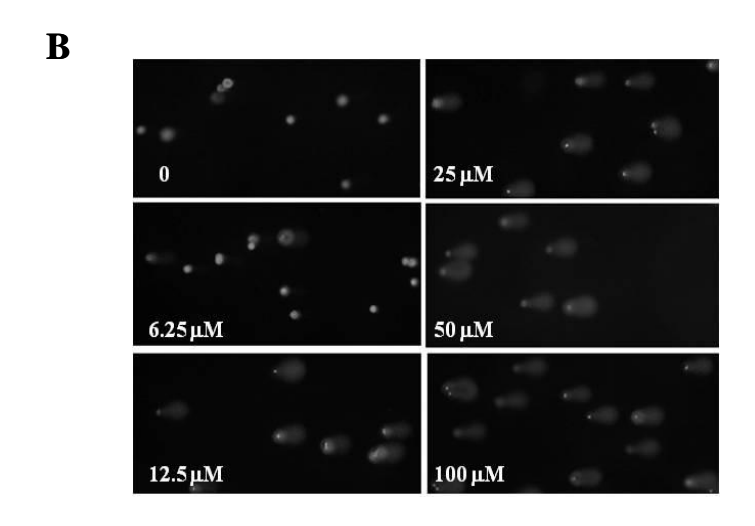
To first test for the ability of AL414 and AL232 to alkylate DNA by releasing the diazonium moiety upon hydrolysis, we performed an alkaline comet assay. The DNA damaging properties of AL232 and AL414 were tested in DU145 prostate, MDA-MB-468 breast and MES-SA uterine sarcoma cancer cells. The extent of DNA damage induced was determined after 2 h treatment with increasing concentrations (0, 6.25, 12.5, 25, 50, 100 µM). Despite the significant bulkiness of its flavone linker arm, AL414 induced high levels of DNA damage in all three cell lines in a dose dependent manner (Fig. 4.4A). However, AL232 was incapable of damaging DNA. The comets were observed by fluorescence microscopy and representative images from MES-SA uterine sarcoma and DU145 prostate carcinoma cells treated with AL414 were presented (Fig. 4.4B and C).

# 4.3.3. EGFR and MEK targeting

# 4.3.3.1. EGFR phosphorylation

As the aminoflavone moiety brought a degree of bulkiness to each combi-molecule, it was important to determine to what extent it affected EGFR inhibitory potency. Inhibition of EGFR phosphorylation was analyzed by *in vitro* enzyme assay and the  $IC_{50}$  concentration for inhibition of receptor TK activity determined to be AL414 ( $IC_{50}$ =0.102  $\mu$ M) and AL232





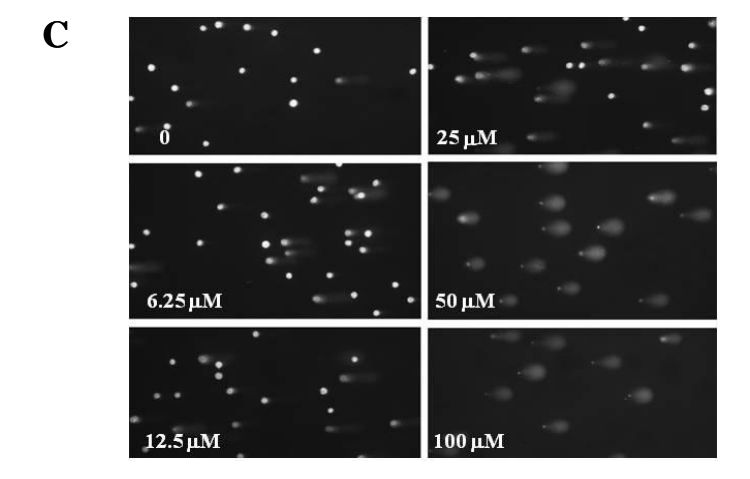


Figure 4.4. DNA damage by AL414 in MDA-MB-468, DU145 and MES-SA cells.

(A) Cells were exposed to AL414 for 2 h followed by assessment of drug-induced DNA damage using an alkaline comet assay. Comets tail moments were quantitated by comet IV software (Perceptive Instruments). Each bar represents the average comet tail moment calculated from 50 comets from two independent experiments for each concentration (0, 6.25, 12.5, 25, 50, 100 μM). Representative images from (B) MES-SA sarcoma and (C) DU145 prostate cancer cells DNA comets stained with SYBR Gold dye and visualized by fluorescence microscopy at 10X were shown for each dose.

 $(IC_{50}=0.211 \mu M)$  (Fig. 4.5A). The cell-base analysis of DU145 treated cells also demonstrated dose-dependent inhibition of EGFR phosphorylation (Fig. 4.5B, C).

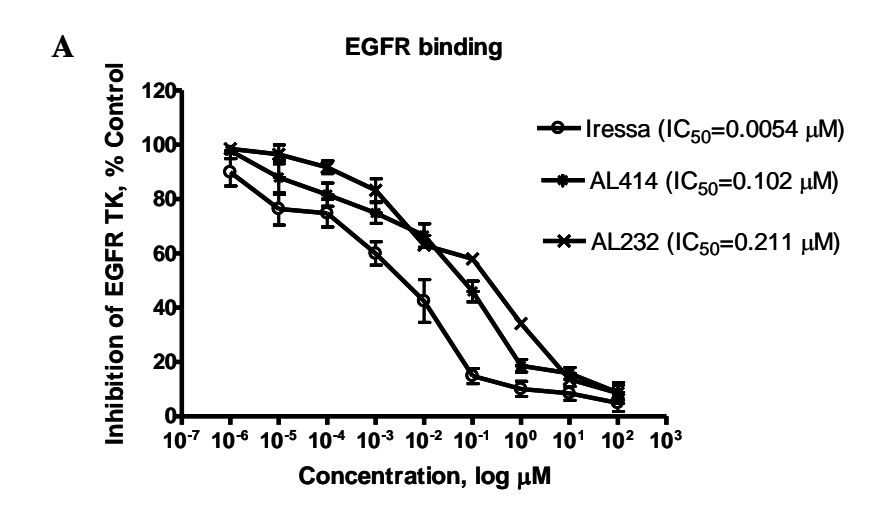
# 4.3.3.2 MEK/ERK1,2 inhibition

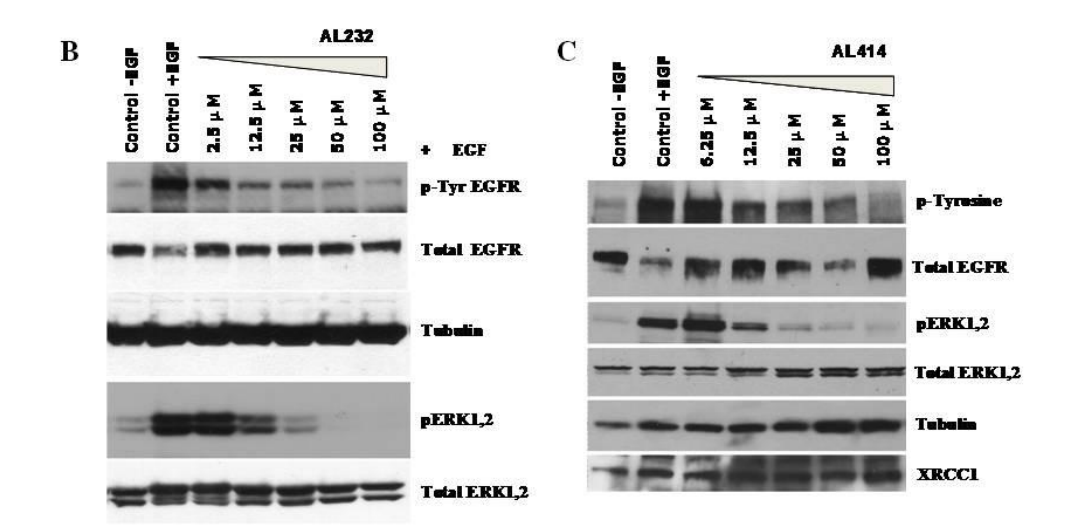
The ability of AL414 to block MEK was indirectly determined through phosphorylation of its substrate ERK1,2. The results from western blot analysis with pERK antibody showed that AL232 and AL414 were capable of inducing a dose-dependent downregulation of ERK1,2 phosphorylation in DU145 cells, but this may have been through the down-regulation of EGF-stimulated MAPK pathway (Fig. 4.5B,C). We therefore analyzed the ability of the latter compounds to down-regulate MEK in non EGFR-expressing MES-SA uterine sarcoma cells in order to determine whether inhibition of ERK1,2 phosphorylation was primarily due to EGFR downregulation (Fig. 4.5D). Only a moderate inhibition of ERK1,2 phosphorylation was induced, indicating that perhaps the free PD98059 was not released as an intact metabolite inside the cells.

# 4.3.4. Selective growth inhibition and cell death by apoptosis

The selective growth inhibition was determined in isogenic NIH 3T3 panel of EGFR/ ErbB2 expressing cells. We observed 10-fold selective antiproliferative advantage of the compounds on cells with high EGFR/ErbB2 overexpression as compared with wild type NIH 3T3 cells (Fig. 4.6). AL414 growth inhibition potency was also evaluated on several other cells lines and we established that the IC $_{50}$  ranged from 2 to 25  $\mu$ M on cells with different levels of EGFR expression (Table 4.1).

The ability of AL414 to induce apoptosis was measured by annexin V/PI binding assay. The apoptotic effect of AL414 on DU145 cells observed after 48 h was determined to be up to 40 % (Fig. 4.7).





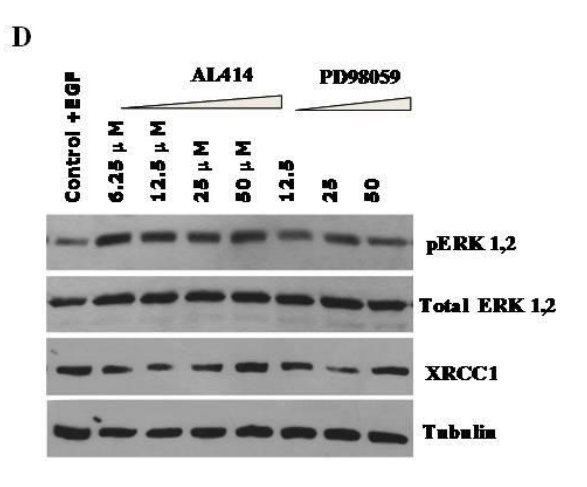
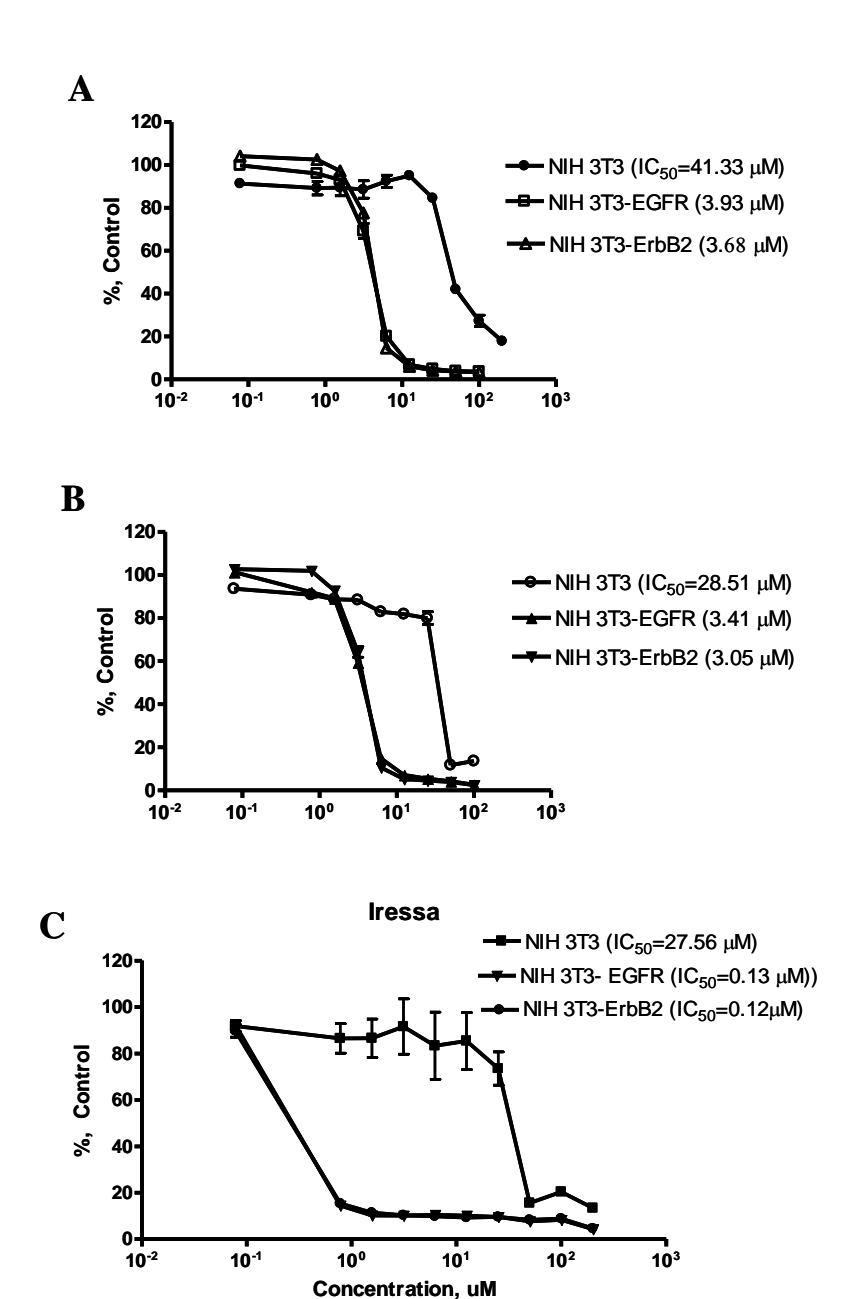
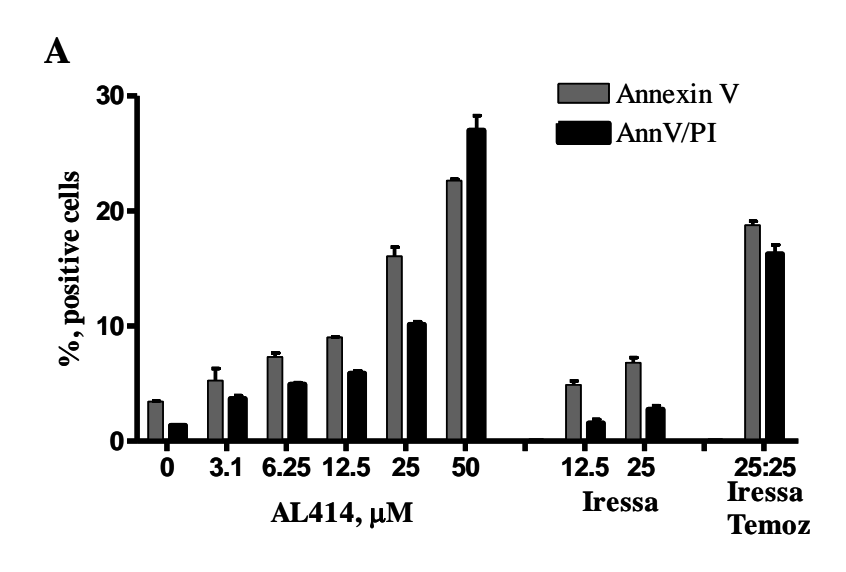
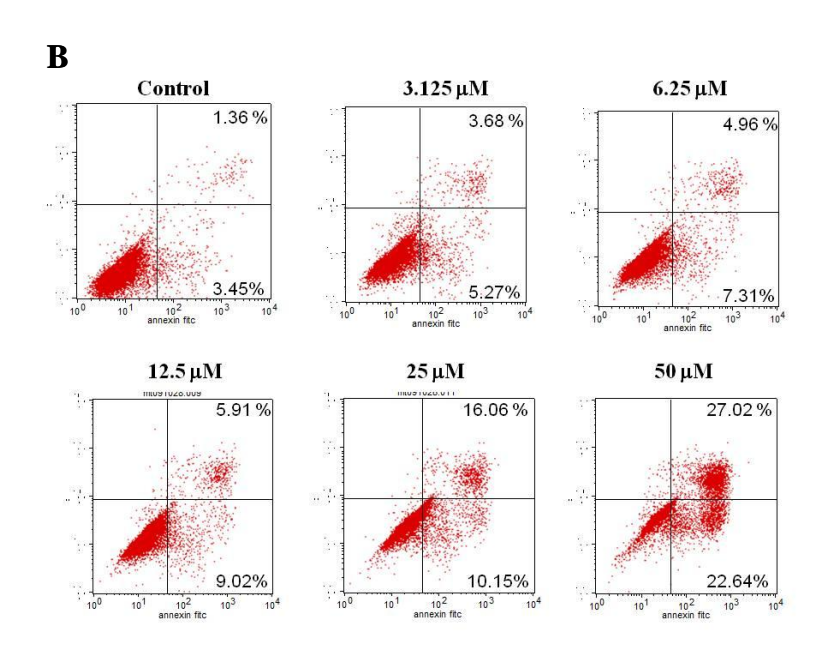


Figure 4.5. Inhibition of EGFR phosphorylation and downstream activation. (A), inhibition of EGFR TK activity by AL414, AL232 and Iressa by *in vitro* enzyme assay. Each point represents mean ± SD of three independent experiments run in duplicate. (B, C), extracts from DU145 cells were analyzed for phospho-tyrosine and phospho-ERK1,2 inhibition after treatment with the indicated doses of AL232 and AL414 for 2 h. Membranes were incubated with anti-EGFR, anti-ERK1,2, anti-XRCC1 antibodies. Anti-tubulin antibody was used for equal loading. (D), P-glycoprotein positive, EGFR negative MES-SA human uterine sarcoma cells were treated with different concentrations of AL414 and PD98059 for 2 h and cell extract analyzed for phospho-ERK1,2 and XRCC1 accumulation using specific antibodies and antitubilin as a loading control.



**Figure 4.6.** Selective growth inhibition by AL414, AL232 and Iressa. Mouse fibroblasts cells, transfected with EGFR or ErbB2 genes, were treated for 6 days with (**A**) AL232, (**B**) AL414, (**C**) Iressa and compared with the non-transfected parental NIH 3T3 cells. Cell growth inhibition was determined by SRB assay and the IC<sub>50</sub> concentration calculated from three independent experiments performed in triplicates.





**Figure 4.7.** Apoptosis by Annexin V binding assay in DU145 cells. Cells were treated for 48 h with a dose range of AL414, two concentrations of Iressa, and equimolar concentrations of Iressa (25  $\mu$ M) and Temozolomide (25  $\mu$ M). (A) Percent early apoptotic (Annexin V) and late apoptotic (Annexin V/PI)-positive cells were represented in histograms from two independent experiments. (B) Dot plots show untreated or treated cells with the indicated concentrations.

#### 4.3.5. *In vivo* metabolism

The ultimate goal of the synthesis of AL414 being for tumour therapy *in vivo*, we analyzed its fate in plasma, lung and liver of CD-1 mice following intraperitoneal (i.p.) administration. The results showed that AL414 was converted into FD105 in plasma (Fig. 4.8). As previously reported for other combi-molecules, the N-acetylated metabolite of FD105 was also detected [25]. A metabolite of PD98059 deriving from PD98059 remaining attached to the linker was also detected in liver and lung. There was no evidence for free PD98059 in the plasma of the animal. The *in vivo* degradation pathway of AL414 was shown in Figure 4.1, path a-b, d.

# **4.3.6.** Activity of species 1 (compound 9)

To test the activity of species **1** obtained from *in vivo* studies (Fig. 4.1, path a, b), we synthesized compound **9** (shown in Fig. 4.3) in order to verify if PD98059 linked to a spacer can still inhibit MEK activity. Potency of compound **9** was tested by a growth inhibition SRB assay in DU145, MDA-MB-468 and HT29 cells. We determined that the IC<sub>50</sub> was in the 100 μM range, thus demonstrating that this compound **9** was not an active species. The results confirmed the data observed previously *in vitro* that the ERK1,2 phosphorylation inhibition was only due to EGFR downregulation induced by the EGFR inhibitor moiety.

#### 4.4. DISCUSSION AND CONCLUSION

The target heterogeneity and multiplicity of cancer have stimulated interest in developing multitargeted drugs. Cancer cells are protected by a variety of signaling networks that allow them to evade cytotoxic lesions. Because of the multiple redundancies in activated pathways, we designed molecules directed at targets as divergent as possible (e.g. receptors and genomic DNA). Here we described the first attempt to use our molecular engineering strategy to graft

**Table 4.1.** Growth inhibitory potency of AL414 on a panel of EGFR and non-EGFR expressing cancer cell lines.

Cell line	DU145	SKBR3	T47D	A549	HT29	MES-SA	MES- SA/DX5
IC <sub>50</sub> μmol/L	$11.33 \pm 0.8$	$10.98 \pm 1.1$	$25.62 \pm 2.09$	41.49 ± 4.6	$10.81 \pm 0.91$	24.47 ± 3.2	$29.10 \pm 2.6$
EGFR status	+	+	+	+	+	-	-

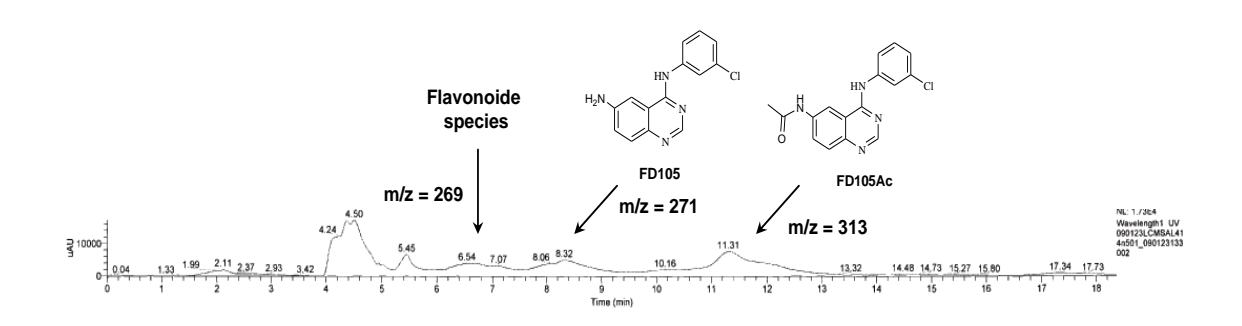


Figure 4.8. LC/MS spectrum of AL414 metabolites observed in mouse plasma.

a MEK directed flavonoid onto the combi-molecular system. The successful synthesis of the designed molecule has permitted the analysis of its fate *in vitro* and *in vivo*. *In vitro* its ability to damage DNA and to block EGFR is an indirect evidence of its internalization inside the cells. Intermediate 1 (Fig. 4.1) is so unstable and also being a charged species does not have the properties required to penetrate into the intracellular compartment. Therefore DNA damage may result from the intracellular decomposition of the intact combi-molecule.

The mechanistic rationale underlying the design of such molecule was in addition to damaging DNA, to block MEK-mediated signal transduction through the stress response pathway, thereby inducing full blown activity of the DNA lesions. The results observed suggest that the released derivative of MEK cannot bind to its active site. To ascertain this even, the primary PD98059 related metabolite was synthesized and tested. The results showed that no inhibition of MEK activity was seen in DU145 cells.

Moreover, to test whether liver enzyme could cleave species **1** (Fig. 4.1), AL414 was administered *in vivo*. While FD105 and its N-acetylated metabolite FD105Ac were observed in the presence of NAT activity (Fig. 4.1, path a and d), free PD98059 was not identified. Perhaps the bulkiness and steric hindrance imposed by o-methoxy group prevented hydrolysis.

The results presented herein showed that the flavone containing 3-compartment combimolecule despite its size could penetrate the cells and inflict at least a dual growth inhibitory hit to the cells. Further studies are ongoing to replace the carbamate linker by a self-hydrolysable chain capable of delivering PD98059 intact.

#### 4.5. EXPERIMENTAL SECTION

# **4.5.1.** Chemistry

 $^{1}$ H NMR spectra and  $^{13}$ C NMR spectra were recorded on a Varian 300 MHz spectrometer. Chemical shifts are given as  $\delta$  values in parts per million (ppm) and are referenced to the residual solvent proton or carbon peak. Mass spectrometry was performed by the McGill University Mass spectroscopy Center and electrospray ionization (ESI) spectra were performed on a Finnigan LC QDUO spectrometer. Data are reported as m/z (intensity relative to base peak = 100). All chemicals were purchased from Sigma-Aldrich. N-(2-aminoethyl)-N-methylethanediamine from Wako Pure Chemical Industries, Ltd.

#### **4.5.1.1. Compound 7a** (AL232)

The diazonium compound **6** was still synthesized as described in reference [10]: 2.3 mg of 4-anilino-6-aminoquinazoline FD105 (4.53.10<sup>-5</sup> mol) was dissolved in dry acetonitrile (5 mL) under argon and, cooled to -5°C. Nitrosonium tetrafluoroborate (2 eq.) in acetonitrile was added directly. After 30 min at -5°C, the resulting clear solution was added dropwise to another solution of compound **5a** (1 eq.) in acetonitrile with triethylamine (2 eq.) at 0°C, after which the mixture was extracted with ethyl acetate and brine. The organic layer was dried with potassium carbonate and evaporated to provide a brown residue, which was purified by trituration in ether/petroleum ether 1/4 to give after filtration a red-brown solid (20 g, 60%). H NMR (300 MHz,  $DMSO-d_6$ )  $\delta$  ppm 3.64 (m, 2H), 3.79 (m, 2H), 3.82 (s, 3H), 4.03 (m, 4H), 6.53 (s, 1H), 7.14 (m, 1H), 7.21 to 7.52 (m, 5H), 7.59 (d, J = 8.0 Hz 1H), 7.70 to 7.98 (m, 4H), 8.04 (d, J = 8 Hz, 1H), 8.14 (sl, 1H), 8.44 (s, 1H), 8.59 (s, 1H), 8.66 (s, 1H), 8.93 (sl, 1H), 9.91 (s, 1H), 10.67 (s, 1H), ESI m/z 723.2 (MH<sup>+</sup> with  $^{35}$ Cl).

# 4.5.1.2. Compound 7b (AL414)

The diazonium compound **6** was still synthesized as described in reference [10]: 56.5 mg of 4-anilino-6-aminoquinazoline FD105 (2.09. $10^{-4}$  mol) was dissolved in dry acetonitrile (5 mL) under argon and, cooled to -5°C. Nitrosonium tetrafluoroborate (2 eq.) in acetonitrile was added directly. After 30 min at -5°C, the resulting clear solution was added dropwise to another solution of compound **5b** (1 eq.) in acetonitrile with triethylamine (2 eq.) at 0°C, after which the mixture was extracted with ethyl acetate and brine. The organic layer was dried with potassium carbonate and evaporated to provide a brown residue, which was purified by trituration in ether/petroleum ether 1/4 to give after filtration a red-brown solid (118 g, 73%). H NMR (300 MHz, *DMSO-d*<sub>6</sub>)  $\delta$  ppm 2.20 (s, 3H), 2.43 (m, 2H), 2.65 (m, 2H), 3.09 (m, 2H), 3.63 (m, 2H), 3.82 (s, 3H), 4.03 (sl, 4H), 6.52 (s, 1H), 7.14 (d, J = 7.5 Hz 1H), 7.24 to 7.60 (m, 5H), 7.58 (d, J = 8.4 Hz 1H),7.73 to 7.93 (m, 4H), 8.4 (d, J = 9.6 Hz 1H), 8.42 (s, 1H), 8.58 (s, 1H); 8.85 (s, 1H), 9.89 (s, 1H), 10.61 (s, 1H). ESI m/z 780.0 (MH<sup>+</sup> with <sup>35</sup>Cl).

### 4.5.1.3. Compound 9

A solution of intermediate **2** (25 mg,  $5.99.10^{-5}$  mol) in dry tetrahydrofuran (1 mL) was added dropwise in a cold solution of commercial hydroxylamine **8** in tetrahydrofuran (1 mL). The mixture was stirred under argon for 4h. The reaction mixture was filtered and the filtrate was evaporated to give 34 mg of crude product, which was purified by preparative TLC (alumina plate,  $CH_2Cl_2/MeOH$  95/5) to give pure compound **9** (17 mg, 60%). H NMR (300 MHz,  $CDCl_3$ )  $\delta$  ppm 2.75 (s, 3H), 3.14 (m, 4H), 3.57 (m, 1H), 3.88 (m, 2H), 3.92 (s, 3H), 4.17 (sl, 6H), 6.73 (s, 1H), 7.08 (m, 2H), 7.31 (m, 1H), 7.42 (m, 2H), 7.54 (d, J = 8 Hz, 1H), 7.70 (m, 1H), 8.19 (d, J = 8 Hz, 1H). ESI m/z 500.2 (MH<sup>+</sup>).

## **4.5.2 Biology**

#### 4.5.2.1. Cell culture

The following cell lines were obtained from the American Type Culture Collection: MDA-MB-468, T47D, SKBR3 human breast carcinomas, DU145 human prostate, A549 human lung carcinoma, MES-SA (CRL-1976) human uterine sarcomas. Mouse fibroblast cells NIH 3T3 used as control or NIH 3T3her14 (transfected with erbB1/EGFR gene) and NIH 3T3neu (transfected with erbB2 gene) were provided by Dr. Moulay Aloui-Jamali (Montreal Jewish General Hospital, Montreal, Canada). All cells were maintained in Dulbecco Modified Eagle's Medium (DMEM) supplemented with 10% FBS, 10 mM HEPES, 2 mM L-glutamine and 100 µg/ml penicillin/streptomycin (all reagent purchased from Wisent Inc., St-Bruno, Canada) as previously described. In all assays cells were plated 24h before drug treatment.

# 4.5.2.2. Drug treatment

AL232 and AL414 were synthesized in our laboratory and Iressa<sup>®</sup> (AstraZeneca) was purchased from our hospital pharmacy and extracted in our laboratory. EGF was obtained from Roche Molecular Diagnostics (Laval, QC). In all assays, drugs were dissolved in DMSO and subsequently diluted in phenol-red-free/FBS-free DMEM before added to cells. The concentration of DMSO never exceeded 0.2% (v/v) during treatment.

#### 4.5.2.3. Growth inhibition assay

Cells were plated at a density of 5000 cells/well in 96-well flat-bottomed microtiter plates (Costar, Corning, NY). Cells were incubated overnight and then treated with the drug for 96 hours. Following drug treatment, cells were fixed, stained with sulforhodamine B (SRB 0.4%) as described elsewhere [30]. The final dried colored residue was dissolved in Tris base (10 mM, pH 10.0), then optical density was measured at 492 nm with microplate reader ELx808 (BioTek Instruments). The results were analyzed by GraphPad Prism (GraphPad Software, Inc., San

Diego, CA) and the sigmoidal dose response curve was used to determine 50% cell growth inhibitory concentration ( $IC_{50}$ ). Each point represents the average of at least three independent experiments run in triplicate.

# 4.5.2.4. DNA damage by alkaline comet assay

The alkaline comet assay was performed as previously described [31-33]. Briefly, cells were exposed to increasing concentrations of AL232 and AL414 for two hours. Cells were trypsinized, washed with PBS and resuspended in PBS at 1x10<sup>6</sup> cells/ml. Cells were mixed with low melting point agarose (0.7%), gels allowed to solidify, then incubated overnight at 4°C with lysis buffer (2.5 M NaCl, 100 mM tetra-sodium EDTA, 10 mM Tris-base, 1% (w/v) Nlauroyl-sarcosine, 10% (v/v) DMSO, and 1% (v/v) triton X-100, pH 10.0). Thereafter, the gels were equilibrated in alkaline electrophoresis buffer (300 mM NaOH, 10 mM tetra-sodium EDTA, 7 mM 8-hydroxyquinoline, 2% (v/v) DMSO, pH 13.0) for 30 min at room temperature and run in fresh eletrophoresis buffer at 20V for 25 min. Comets were visualized at 10X magnification using Leica Microsystems microscope after staining with SYBR Gold (1:10,000, Molecular Probes, Eugene, OR) for 45 min. DNA damage was quantitated using Comet Assay IV (Perceptive Instruments, UK) with minimum 50 comets analyzed for each drug concentration. The degree of DNA damage was expressed as a tail moment parameter (i.e., the distance between the barycenter of the head and the tail of the comet multiplied by the percentage of DNA within the tail of the comet) and the mean tail moment was reported for each cell line.

# 4.5.2.5. In vitro Enzyme Assay

The EGFR kinase assay is similar to the one described previously. Nunc Maxisorp 96-well plates were incubated overnight at 37°C with poly (L-glutamic acid–L-tyrosine, 4:1) (PGT) in PBS. The kinase reaction was performed by using 4.5 ng/well EGFR from Biomol (Plymouth

Meeting, PA). Following drug addition, phosphorylation was initiated by the addition of ATP. A typical assay was performed at drug concentrations ranging from 0.0001-10 μM. The reaction was terminated by aspiration of the reaction mixture and phosphorylated substrate was detected with HRP-conjugated anti-phosphotyrosine antibody (Santa Cruz Biotechnology, CA). The signals were developed by the addition of 3,3′,5,5′-tetramethylbenzidine peroxidase substrate (Kierkegaard and Perry Laboratories, Gaithersberg, MD) and the colorimetric reaction stopped by adding equal volume of H<sub>2</sub>SO<sub>4</sub> (0.09 M) to each well. The plates were read at 450 nm using a microplate reader ELx808 (BioTek Instruments). The results were analyzed by GraphPad Prism (GraphPad Prism Software, Inc., San Diego, CA) and IC<sub>50</sub> calculated.

# 4.5.2.6. Western blot analysis

Cells were starved overnight, treated for two hours with AL232 and AL414, followed by stimulation with EGF (50ng/ml) for 15 min. with the indicated concentrations. Cells were incubated with lysis buffer (20 mM Tris-HCl pH 7.5, 1% NP-40, 10 mM EDTA, 150 mM NaCl, 20 mM NaF, 1mM Na vanadate, supplemented with a tablet of Roche inhibitors) and the protein extracts analyzed by Western blots with the following antibodies: anti-phospho-tyrosine (clone 4G10, Upstate; 1:1000), anti-EGFR (SC-03, Santa Cruz; 1:1000), anti-XRCC1 (33-2-5, ThermoFisher Scientific; 1:1000). Anti-phospho-ERK1,2 (Thr<sup>202</sup>/Tyr<sup>204</sup>; 1:4000) and anti-ERK1,2 (p44/p42 MAP kinase; 1:2500) were obtained from Cell Signaling Technology (Beverly, MA). Anti-tubulin-α (clone DM1A, NeoMarkers; 1:2000) was used as a loading control. Secondary goat anti-rabbit IgG-HRP and goat anti-mouse IgG-HRP were obtained from Jackson ImmunoResearch Laboratories (West Grove, PA). Western blot experiments were performed at least twice from two independent cell treatments and similar results were obtained.

# 4.5.2.7. Annexin V/PI binding assay

DU145 cells were plated in a 6-well plate and treated with a dose range of each drug for 48 h. Thereafter, they were harvested and incubated with Annexin V-FITC and propidium iodide (PI) using apoptosis detection kit (BD Bioscience Pharmingen, USA) following the supplier's protocol. Annexin V-FITC/ PI stained cells were analyzed with a Becton-Dickinson FACScan. Data were collected using logarithmic amplification of both the FL1 (FITC) and FL2 (PI) channels. Quadrant analysis of co-ordinate dot plots was performed with CellQuestPro software.

# 4.5.2.8. In vivo analysis by LC/MS

The animals (male CD-1 nude mice, three per group) bearing DU145 xenografts were given 100 mg/kg doses by i.p. injection. Three hours after injection, mice were sacrificed to analyze the plasma, the organs (brain, liver and kidney) and tumour by LC/MS. The blood samples were collected in heparinized tubes and centrifuged for 8 min at 3,000 rpm and plasma was separated with a micropipette and stored at -80°C. Plasma aliquots (50 μL) were mixed with acetonitrile (100 μL) to precipitate the proteins, and the mixture was centrifuged for 5 min at 6,000 rpm. The tumours and organs were removed, weighed, and homogenized. The homogenates were re-suspended in acetonitrile and centrifuged at 10,000 rpm for 8 min at 4°C, and the supernatants collected. Following evaporation to dryness, the samples were reconstituted in acetonitrile and analyzed by liquid chromatography-mass spectrometry. HPLC was performed using a Thermoquest P4000 with a UV3000 detector and AS300 autosampler, Ascentis<sup>TM</sup> C18, Supelco column (15 cm x 4.6 mm, 5 μm), Acetonitrile/Water 1/1

flux 0.7 mL/min. and the effluent introduced into a Finnigan LC QDUO mass spectrometer. All

solutions were filtered before injection into the HPLC. The injection volumes were kept at 15  $\mu$ L throughout the study.

#### 4.6. CONNECTING TEXT

Our previous studies were directed at bringing insights into the potency and mechanism of action of type I combi-molecules. Indeed, we have determined that the degradation of these EGFR-DNA targeting agents occurs at the perinuclear region and that the latter distribution strongly correlates with the EGFR status of the cells. Furthermore, this corresponds to increased delivery of the DNA damaging agents in the nuclei of EGFR-expressing cells, thus enhanced the potency and DNA-targeting property of the molecules on these cells. The subsequent study in Chapter 5 was directed at investigating the mechanism of action of type II combi-molecules, which were designed to execute binary targeting properties without requirement for hydrolysis. These agents containing a hemi-mustard DNA-damaging moiety attached to the quinazoline EGFR inhibitory moiety, have demonstrated greater EGFR-DNA targeting potency than type I combi-molecules. To address the mechanism underlying the strong DNA damaging and apoptotic activities, we studied their potency in cells which exhibit strong activation of growthand survival-promoting proteins. Ovarian cancer cells are often characterized by overexpression of EGFR and AKT-activated pathways. This confer them reduced sensitivity to classical DNA alkylating agents. Therefore, they were chosen for investigating the mechanism of action of the exquisitely potent type II molecules.

#### 4.7. REFERENCES

- 1. Jorissen, R.N., et al., *Epidermal growth factor receptor: mechanisms of activation and signalling.* Exp Cell Res, 2003. **284**(1): p. 31-53.
- 2. Dai, Q., et al., Enhanced sensitivity to the HER1/epidermal growth factor receptor tyrosine kinase inhibitor erlotinib hydrochloride in chemotherapy-resistant tumor cell lines. Clin Cancer Res, 2005. 11(4): p. 1572-8.
- 3. Fukuoka, M., et al., Multi-institutional randomized phase II trial of gefitinib for previously treated patients with advanced non-small-cell lung cancer (The IDEAL 1 Trial) [corrected]. J Clin Oncol, 2003. **21**(12): p. 2237-46.
- 4. Gordon, A.N., et al., Efficacy and safety of erlotinib HCl, an epidermal growth factor receptor (HER1/EGFR) tyrosine kinase inhibitor, in patients with advanced ovarian carcinoma: results from a phase II multicenter study. Int J Gynecol Cancer, 2005. 15(5): p. 785-92.
- 5. Gaikwad, A., et al., *In vitro evaluation of the effects of gefitinib on the cytotoxic activity of selected anticancer agents in a panel of human endometrial cancer cell lines.* J Oncol Pharm Pract, 2009. **15**(1): p. 35-44.
- 6. Konner, J., et al., A phase II study of cetuximab/paclitaxel/carboplatin for the initial treatment of advanced-stage ovarian, primary peritoneal, or fallopian tube cancer. Gynecol Oncol, 2008. **110**(2): p. 140-5.
- 7. Lacroix, L., et al., Response of ovarian carcinomas to gefitinib-carboplatin-paclitaxel combination is not associated with EGFR kinase domain somatic mutations. Int J Cancer, 2006. 118(4): p. 1068-9.
- 8. Raju, U., et al., Flavopiridol, a cyclin-dependent kinase inhibitor, enhances radiosensitivity of ovarian carcinoma cells. Cancer Res, 2003. **63**(12): p. 3263-7.
- 9. Banerjee, R., et al., *The combi-targeting concept: selective targeting of the epidermal growth factor receptor- and Her2-expressing cancer cells by the complex combi-molecule RB24*. J Pharmacol Exp Ther, 2010. **334**(1): p. 9-20.
- 10. Rachid, Z., et al., *The Combi-Targeting Concept: Chemical Dissection of the Dual Targeting Properties of a Series of "Combi-Triazenes"*. J. Med. Chem., 2003. **46**(20): p. 4313-4321.
- 11. Matheson, S.L., et al., *The combi-targeting concept: Dissection of the binary mechanism of action of the combi-triazene SMA41 in vitro and antitumor activity in vivo.* J. Pharmacol. Exp. Ther., 2004. **311**(3): p. 1163-1170.
- 12. Matheson, S.L., et al., *The combi-targeting concept: dissection of the binary mechanism of action of the combi-triazene SMA41 in vitro and antitumor activity in vivo.* J Pharmacol Exp Ther, 2004. **311**(3): p. 1163-70.

- 13. Brahimi, F., et al., Mechanism of action of a novel "combi-triazene" engineered to possess a polar functional group on the alkylating moiety: Evidence for enhancement of potency. Biochem. Pharm., 2005. **70**(4): p. 511-519.
- 14. Wynne, P., et al., Enhanced repair of DNA interstrand crosslinking in ovarian cancer cells from patients following treatment with platinum-based chemotherapy. Br J Cancer, 2007. **97**(7): p. 927-33.
- 15. Kennedy, R.D. and A.D. D'Andrea, *DNA repair pathways in clinical practice: lessons from pediatric cancer susceptibility syndromes.* J Clin Oncol, 2006. **24**(23): p. 3799-808.
- 16. Matheson, S., et al., *Combi-molecules: a global approach towards better chemoselectivity of cytotoxic agents and chemoresistance of refractory tumors.* Bulletin du Cancer, 2004. **91**(12): p. 911-915.
- 17. Banerjee, R., A novel small molecule-based multi-targeting approach for the selective therapy of epidermal growth factor receptor (EGFR)- or Her2-expressing carcinomas Ph. D. dissertation, Faculty of Medicine, 2006.
- 18. Kharbanda, S., et al., *Activation of MEK kinase 1 by the c-Abl protein tyrosine kinase in response to DNA damage.* Mol Cell Biol, 2000. **20**(14): p. 4979-89.
- 19. Upadhyay, D., et al., Fibroblast growth factor-10 attenuates H2O2-induced alveolar epithelial cell DNA damage: role of MAPK activation and DNA repair. Am J Respir Cell Mol Biol, 2004. **31**(1): p. 107-13.
- 20. Alessi, D.R., et al., *PD 098059 is a specific inhibitor of the activation of mitogen-activated protein kinase kinase in vitro and in vivo.* J Biol Chem, 1995. **270**(46): p. 27489-94.
- 21. Dent, P., et al., *MAPK pathways in radiation responses*. Oncogene, 2003. **22**(37): p. 5885-5896.
- 22. Yacoub, A., et al., Epidermal growth factor and ionizing radiation up-regulate the DNA repair genes XRCC1 and ERCC1 in DU145 and LNCaP prostate carcinoma through MAPK signaling. Radiat Res., 2003. **159**(4): p. 439-52.
- 23. Todorova, M.I., et al., Subcellular distribution of a fluorescence-labeled combimolecule designed to block epidermal growth factor receptor tyrosine kinase and damage DNA with a green fluorescent species. Mol Cancer Ther, 2010. **9**(4): p. 869-82.
- 24. Larroque-Lombard, A.L., et al., Synthesis and uptake of fluorescence-labeled Combimolecules by P-glycoprotein-proficient and -deficient uterine sarcoma cells MES-SA and MES-SA/DX5. J Med Chem, 2010. **53**(5): p. 2104-13.
- 25. Merayo, N., et al., *The combi-targeting concept: evidence for the formation of a novel inhibitor in vivo*. Anti-Cancer Drugs, 2006. **17**(2): p. 165-171.

- 26. Cushman, M., et al., Synthesis and protein-tyrosine kinase inhibitory activities of flavonoid analogues. J Med Chem, 1991. **34**(2): p. 798-806.
- 27. Cushman, M., et al., Synthesis and biochemical evaluation of a series of aminoflavones as potential inhibitors of protein-tyrosine kinases p56lck, EGFr, and p60v-src. J Med Chem, 1994. **37**(20): p. 3353-62.
- 28. Hay, M.P., et al., *DNA-Targeted 1,2,4-Benzotriazine 1,4-Dioxides: Potent Analogues of the Hypoxia-Selective Cytotoxin Tirapazamine*. Journal of Medicinal Chemistry, 2004. **47**(2): p. 475-488.
- 29. Guy, J., et al., Convergent preparation and photophysical characterization of dimaleimide dansyl fluorogens: elucidation of the maleimide fluorescence quenching mechanism. J Am Chem Soc, 2007. **129**(39): p. 11969-77.
- 30. Skehan, P., et al., *New colorimetric cytotoxicity assay for anticancer-drug screening*. J Natl Cancer Inst., 1990. **82**(13): p. 1107-1112.
- 31. Olive, P.L. and J.P. Banath, *The comet assay: a method to measure DNA damage in individual cells.* Nat Protoc, 2006. **1**(1): p. 23-29.
- 32. Matheson, S.L., J. McNamee, and B.J. Jean-Claude, *Design of a chimeric 3-methyl-1,2,3-triazene with mixed receptor tyrosine kinase and DNA damaging properties: a novel tumor targeting strategy.* J. Pharmacol. Exp. Ther., 2001. **296**(3): p. 832-840.
- 33. McNamee, J.P., et al., *Comet assay: rapid processing of multiple samples.* Mutat Res, 2000. **466**(1): p. 63-69.

# Chapter 5

# Cytokinetics of Potent Type II EGFR-DNA Targeting Combi-molecules in Ovarian Cancer Cells

Margarita Todorova<sup>1</sup>, Zakaria Rachid<sup>1</sup>, and Bertrand Jean-Claude<sup>1</sup>

<sup>1</sup>Cancer Drug Research Laboratory, Department of Medicine, Division of Medical Oncology, McGill University Health Center/Royal Victoria Hospital, 687 Pine Avenue West Room M-7.19, Montreal, Quebec, H3A 1A1 Canada

#### 5.1. ABSTRACT

**Objective.** The treatment of ovarian cancer is largely based on cytotoxic therapy. Here, we studied the potency of molecules not only designed to damage DNA but also block the epidermal growth factor receptor (EGFR), which is overexpressed in epithelial ovarian cancer.

**Methods**. The novel agents containing a quinazoline moiety and a hemi-mustard tail were tested against human ovarian cancer cells, TOV112D, TOV21G, OV90 and OVCAR-3, expressing varied levels of EGFR. Their potency was evaluated by analyzing cell growth inhibition, DNA damaging potential, cell cycle arrest, apoptosis, inhibition of EGFR/ERK and AKT signaling, using a number of assays including comet for DNA damage, annexin V binding for apoptosis and western blotting.

**Results.** We observed that the hybrid agents were *ca.* 75-120 fold more potent than gefitinib against the human ovarian cancer cells. Studies on one such agent ZR2008, revealed that it could damage DNA at unusually low concentration (0.5-1 μM), induce c-Jun NH2 kinase (JNK) activation, down-regulate survivin, and activate p53 in the p53 wt expressing TOV21G cells. It blocked EGFR, ERK1,2 and AKT phosphorylation in a dose-dependent manner and arrested cell cycle in G1-S in all the cell lines. However, the levels of apoptosis and growth inhibition were similar in cells where AKT remained activated.

Conclusions. The results *in toto* suggest that ZR2008 down-regulates growth signaling pathways and blocks AKT phosphorylation where EGFR TK inhibition is observed. More importantly, induction of apoptosis was independent of the AKT phosphorylation status of the cells, perhaps due to ZR2008 ability to down-regulate survivin.

#### **5.2. INTRODUCTION**

Ovarian tumours are characterized by a variety of mutation and overexpression of signal transduction proteins [1, 2]. One such dysfunction is the expression of EGFR and its closest homologue ErbB2 that ranges from 35-70 % among different ovarian cancer types [3-6]. Amplification or overexpression of these proteins is associated with aggressive tumour progression and poor patient survival [7-9]. While EGFR can heterodimerize with several members of ErbB2 family, its expression alone has been correlated with poor outcome in women with advanced stage ovarian cancer, following surgery and combination therapy. EGFR expression has been also reported to be associated with ovarian cancer metastasis by mechanisms related to interference with other molecular pathways [10, 11].

Phosphorylation of tyrosine residues 845, 992, 1045 1068, 1145 of EGFR leads to receptor activation of downstream signaling (Ras/Raf/MAPK pathway) and activation of PI3K pathway (PI3K/AKT/BAD) that ultimately blocks apoptosis [12-14]. It was therefore believed that blockade of EGFR phosphorylation could translate into growth inhibition and apoptosis. This has now been demonstrated with small molecule EGFR tyrosine kinase inhibitors and their efficacy has been proven both *in vitro* and in the clinic [15-18]. Two low molecular weight tyrosine kinase inhibitors gefitinib (Iressa®, Astra Zeneca) and erlotinib (Tarceva®, OSI/Genentech) have shown significant clinical activity against non small cell lung carcinoma (NSCLC) and this has been shown to correlate with their ability to bind to the ATP site of EGFR, block its autophosphorylation and subsequent down-stream signaling [19]. Despite the significant potency observed for quinazoline inhibitors against NSCLC, their potency as single agents in ovarian cancer remains to be proven with the currently undergoing phase II clinical trials [20-22]. Studies currently evaluating the effect of EGFR or ErbB2 monoclonal antibodies

in patients with recurrent ovarian cancer have shown minimal activity and limited response as single agents [24-26]. More significant clinical response is observed in ovarian cancer patients overexpressing EGFR when treatment with gefitinib is combined with administration of carboplatin or taxol [27-29]. Recently, the success of EGFR inhibitors in combination with cytotoxic agents and the documented potency of alkylators against ovarian carcinoma prompted us to evaluate the activity of novel mixed EGFR-DNA targeting agents termed "combimolecules" against human ovarian cancer cells [21, 30, 31]. The structure of these EGFR-DNA targeting molecules was kept at the same molecular size as gefitinib or Tarceva to facilitate tumour penetration while retaining their ability to induce tandem targeting of EGFR and DNA. Such molecules (e.g. ZR series, Figure 1) were designed to contain like gefitinib an anilinoquinazoline moiety and unlike gefitinib a hemi-mustard tail [32]. We predicted that the half-mustard DNA-damaging arm instead of the classical bis-chlorethylating moiety, that characterizes the nitrogen mustards, would induce less toxicity *in vivo*.

EGFR expression being associated with activation of the anti-apoptotic PI3K pathway, we surmised that blockade of EGFR-mediated signaling in the ovarian cancer cells would lead to down-regulation of anti-apoptotic signaling, thereby rendering these cells more sensitive to the DNA damage induced by EGFR-DNA targeting drugs. To verify this hypothesis, a set of human ovarian cell lines with varied levels of expression of EGFR was analyzed and the most potent drug of the series was used for studying the mechanism of cell-killing induced by mixtargeting EGFR-DNA agents.

#### 5.3. MATERIAL AND METHODS

#### 5.3.1. Cell culture

The following cell lines used derived from different epithelial ovarian tumours: TOV-21G (clear cell carcinoma), TOV-112D (endometrioid adenocarcinoma) or OV-90 (malignant ascites), were generously provided by Dr. Anne-Marie Mes-Masson (CHUM, Notre-Dame Hospital Research Centre, Montreal, Qc) [33] and OVCAR-3 (serous carcinoma, HTB-161) was purchased from ATCC (Manassas, VA). Cells were maintained in OSE media supplemented with 10% FBS, 1.5 mM L-glutamine and 100 µg/ml penicillin/streptomycin (GibcoBRL; Gaithersburg, MD). Cells were grown exponentially at 37°C in a humidified 95% air and 5% CO<sub>2</sub>. In all assays cells were plated 24 h before drug treatment.

# **5.3.2.** Drug treatment

ZR2003, ZR2008 and ZRMS were synthesized in our laboratory. Synthesis of ZR2003 and ZR2008 was reported previously and ZRMS will be reported elsewhere [32]. In all assays, molecules were dissolved in DMSO (50 mM stock solution) and subsequently diluted in OSE medium prior adding it to cells. The concentration of DMSO never exceeded 0.2% (v/v) during treatment.

# **5.3.3.** Growth inhibition assay

Ovarian cells were plated at a density of 5000 cells/well in 96-well flat-bottomed high-attachment plates and allowed to adhere overnight. Growth inhibition of ZR2003, ZR2008 and ZRMS were compared with that of gefitinib after 4 days exposure to serial drug dilutions. Briefly, following drug treatment, cells were fixed using 50 µl of cold trichloroacetic acid

(50%) for 60 min at 4°C, stained with sulforhodamine B (SRB 0.4%) for two hours at room temperature, rinsed four times with 1% acetic acid and allowed to dry [34]. The resulting colored residue was dissolved in 200 μl Tris base (10 mM) and optical density recorded at a wavelength of 490 nm using a microplate reader (BioTek Instruments). The results were analyzed by GraphPad Prism (GraphPad Software, Inc., San Diego, CA) and the sigmoidal dose response curve was used to determine 50% cell growth inhibitory concentration (IC<sub>50</sub>). Each point represents the average of at least three independent experiments run in triplicate.

# 5.3.4. *In vitro* enzyme assay

The EGFR kinase assay is similar to the one described previously [35]. The assay was performed with 4.5 ng/well EGFR purchased from Biomol (Plymouth Meeting, PA) and drug dilution was ranging from 0.0001-10 μM. The reaction was initiated by the addition of ATP and inhibition of EGFR phosphorylation measured by using anti-phosphotyrosine HRP-conjugated antibody (Santa Cruz Biotechnology, CA). Plate was analyzed at 450 nm ELISA reader (BioTek Instruments) and results were processed to calculate IC<sub>50</sub> by GraphPad Prism.

# 5.3.5. DNA damage by alkaline comet assay

The alkaline comet assay was performed as previously described [36, 37]. Briefly, cells were exposed to ZR2008 for two hours, harvested by trypsinization, collected in ice-cold PBS by centrifugation at 3,000 rpm for 5 min, and then resuspended in PBS. Cells were mixed with agarose (0.7%) at 37°C (diluted 1:10), followed by layering the agarose/cells suspension on GelBond film (Lonza, Rockland, ME). Cells were lysed overnight at 4°C, then incubated in alkaline electrophoresis buffer (300 mM NaOH, 10 mM tetra-sodium EDTA, 7 mM 8-hydroxyquinoline, 2% (v/v) DMSO, pH 13.0) for 30 min, and electrophoresed at 20V for 25

min. The gels were subsequently neutralized in 1 M ammonium acetate, dehydrated in 100% ethanol overnight, and stained before imaging with SYBR Gold dye (1:10,000, Molecular Probes, Eugene, OR). Comets were visualized at 10X magnification using Leica Microsystems microscope.

# 5.3.6. Annexin V/ Propidium Iodide binding assay

OV90, TOV112D and TOV21G cells were cultured in 6-well plates and treated with a dose range of each drug for 48 h. Thereafter, cells were harvested and incubated with Annexin V-FITC and propidium iodide (PI) using the apoptosis detection kit (BenderMedSystems Inc, USA) following a protocol provided by the supplier. Annexin V-FITC and PI binding were analyzed on Becton-Dickinson FACScan. Data were collected using logarithmic amplification of both the FL1 (FITC) and FL2 (PI) channels. Quadrant analysis of co-ordinate dot plots was performed with CellQuestPro software.

#### 5.3.7. Flow cytometry cell cycle distribution analysis

Ovarian cells were plated at  $0.25 \times 10^6$  cells per well in six-well plates, allowed to adhere overnight and incubated for 24 h with 0.625, 1.25, 2.5  $\mu$ M ZR2008. Thereafter, cells were collected by trypsinization, washed twice with PBS, and fixed in 70% ice-cold ethanol. Prior analysis, cells were washed and incubated for 30 min with PI/RnaseA solution at 37 °C and DNA content for cell cycle profile was analyzed using a BD LSR flow cytometer (BD Biosciences, San Jose, CA). Percent cells in each cell phase were quantified by ModFitLT software.

#### **5.3.8.** Western blot analysis

Cells were grown to 80% confluence in 6-well plates, serum starved for 24 h (OSE medium without FBS), followed by a two-hour incubation with the indicated concentrations of ZR2008. Cells were stimulated with EGF (50 ng/ml) for 15 min, rinsed with ice-cold PBS and collected by gentle scraping in PBS. Cells were lysed in lysis buffer (20 mM Tris-HCl pH 7.5, 1% NP-40, 10 mM EDTA, 150 mM NaCl, 20 mM NaF, 1mM Na vanadate, complete protease inhibitors (Roche, 1 tablet per 10 ml buffer), protein concentration was quantified by Bradford method (BioRad protein dye, Bio-Rad laboratories) and 50 µg of total proteins were resolved on 4-12 % gradient SDS-polyacrylamide gels. Proteins were transferred on PVDF membrane (Immobilon-P, Millipore), which were blocked with 5% milk in TBST (20 mM Tris-HCl, 137 mM NaCl, 0.1 % Tween 20) for 1-3 h. Primary antibodies used for immunodetection were dissolved in antibody buffer as follows: anti-phospho-EGFR (Tyr<sup>1068</sup> sc-19; 1:1000), total EGFR (sc-03; 1:1000), PARP1 (sc-8002, 1:1000) all from Santa Cruz biotechnology (Santa Cruz, CA). Anti-phospho-Erk1,2 (Thr<sup>202</sup>/Tyr<sup>204</sup>; 1:4000), ERK1,2 (p44/p42 MAP kinase; 1:2500), phospho-AKT (Ser<sup>473</sup>; 1:1000), AKT (1:1000), phospho-JNK/SAPK (Thr<sup>183</sup>/Tyr<sup>185</sup>, 1:1000), JNK/SAPK, phospho-p53 (Ser<sup>15</sup>, 1:1000), p53, survivin (1:500) were obtained from Cell Signaling Technology (Beverly, MA). Anti-phosho-γH2AX antibody (Ser<sup>137</sup>; 1:500) was purchased from Abcam (Cambridge, MA) and anti-tubulin-α (clone DM1A; 1:2000, NeoMarkers) was used as a loading control. Secondary goat anti-rabbit IgG-HRP and goat antimouse IgG-HRP were obtained from Jackson ImmunoResearch laboratories (West Grove, PA). The bands were visualized by using enhanced chemiluminescence detection system (ECL, ThermoFisher). Western blot experiments were performed at least twice from two independent cell treatments and similar results were obtained.

#### 5.4. RESULTS

# 5.4.1. Growth inhibitory activity

We first studied the potency of three combi-molecules ZR2003, ZR2008 and ZRMS in the panel of ovarian cancer cells in comparison with gefitinib using the sulforhodamine B assay. As their structures are revealed in Figure 1, the three compounds contain an identical chloro-anilinoquinazoline moiety required for the anchorage in the ATP binding pocket of the EGFR but differing by the type of alkylating groups that they carried. We predicted that ZR2008 containing the bromoethyl group would be the most reactive. The results showed that all combi-molecules have strong growth inhibitory effect on all four cell lines at submicromolar concentrations with levels of potency 75-120-fold superior to that of gefitinib, indicating that the appendage of a half-mustard moiety to the quinazoline ring leads to agents with a significantly more potent cytotoxicity profile than gefitinib (Fig. 5.1A, B, C, D). ZR2008 showed the lowest average IC<sub>50</sub> across all four cell lines [0.50 μM (OV90), 0.21 μM (TOV21G), 0.19 μM (TOV112), 0.15 μM (OVCAR3)] and was therefore selected for subsequent mechanistic studies.

# 5.4.2. EGFR signaling

### 5.4.2.1. Inhibition of EGFR TK activity

The EGFR inhibitory potency of ZR2003, ZR2008 and ZRMS was determined by an isolated enzyme assay (Fig 5.2A). All compounds showed extremely strong ability to block EGFR TK activity *in vitro*. The three compounds have similar EGFR TK inhibitory potency: 3-chloro analogue-ZR2003 (IC<sub>50</sub> = 0.025  $\mu$ M), 3-bromo analogue ZR2008 (IC<sub>50</sub> = 0.023  $\mu$ M) and ZRMS (IC<sub>50</sub> = 0.021  $\mu$ M). The IC<sub>50</sub> values were in the same range as that of gefitinib (0.019  $\mu$ M) [38].

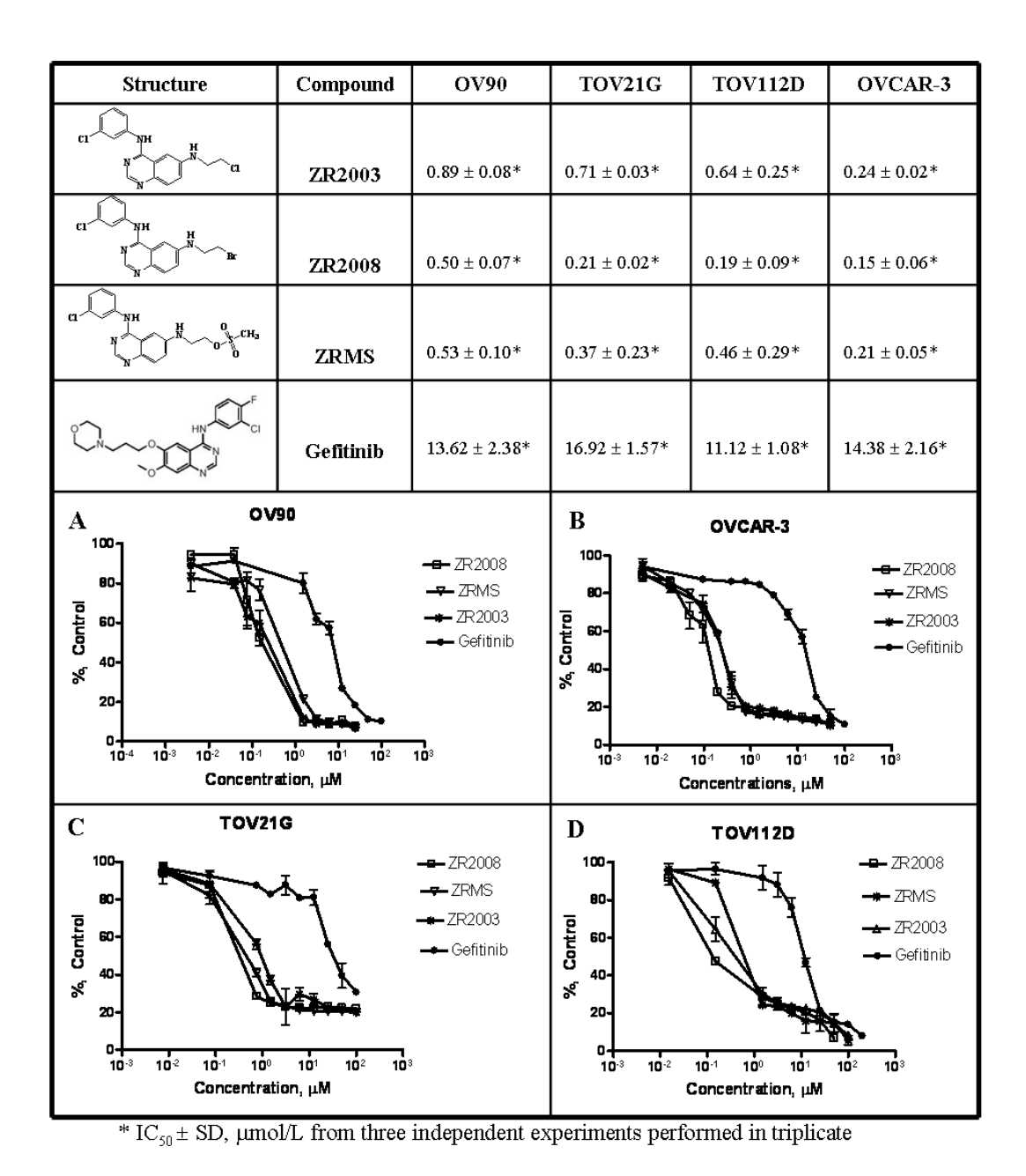


**Figure 5.1.** Antiproliferative effect of ZR2003, ZR2008, ZRMS and gefitinib on four human ovarian cancer cells with different levels of EGFR expression.

Cell growth was measured using SRB assay after cells were exposed to each drug for 96 h. The  $IC_{50} \pm SD$ ,  $\mu mol/L$  was determined from three independent experiments performed in triplicate and growth inhibition curves were shown individually for each cell line: (A) OV90, (B) OVCAR-3, (C) TOV21G, (D) TOV112.

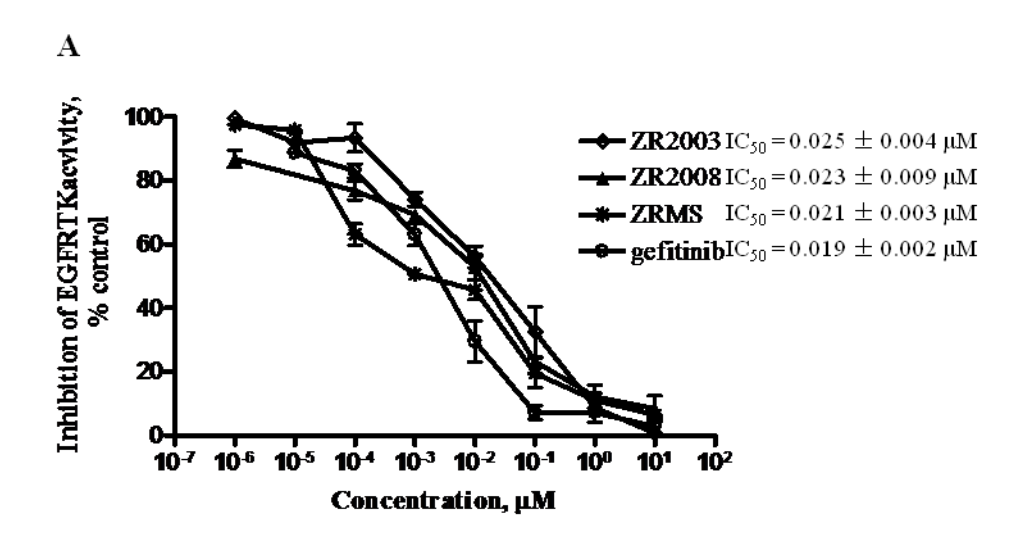
#### 5.4.2.2. EGFR, ERK1,2 and AKT phosphorylation in whole cells

ZR2008 being the most potent across all four ovarian cell lines on cell growth inhibition, was chosen for evaluating EGFR inhibitory potency in the panel of ovarian cells (Fig. 5.2). Very low EGFR activation was seen in OV90 (Fig. 5.2B) and TOV21G (Fig. 5.2C). However, sufficient level of activation of EGFR was detected in TOV112D (Fig. 5.2D) and OVCAR3 (Fig. 5.2E) which permitted an unequivocal examination of inhibition of EGFR phosphorylation. The results showed that ZR2008 could induce a dose-dependent inhibition of EGFR phosphorylation at concentrations as low as 0.6 μM. At IC<sub>50</sub> concentration of gefitinib (12.5 μM), it significantly inhibited EGFR phosphorylation in the latter cells. Inhibition of EGFR in TOV112D and OVCAR3 cells was accompanied by downregulation of AKT and ERK1,2 phosphorylation (Fig. 5.2D, E). In OV90 and TOV21G cells that express barely detectable levels of EGFR, phospho-AKT was not significantly down-regulated, with only moderate inhibition observed at supralethal concentrations (Fig. 5.2B, C).

#### **5.4.3. DNA damage**

# 5.4.3.1. Alkaline comet assay

The DNA damaging property of ZR2008 was evaluated in a whole cell comet assay that permitted the observation of DNA damage *in situ* (Fig. 5.3). An alkaline comet assay was performed to analyze the degree of single and double DNA strand breaks in all four ovarian cancer cells. The results showed that after only two-hour exposure, ZR2008 induced significantly high levels of DNA damage in all cell lines (Fig. 5.3A, B, C, D). DNA breaks were induced at a concentration range rarely observed with classical alkylating agents (0.15-3.25 µM) [39, 40].



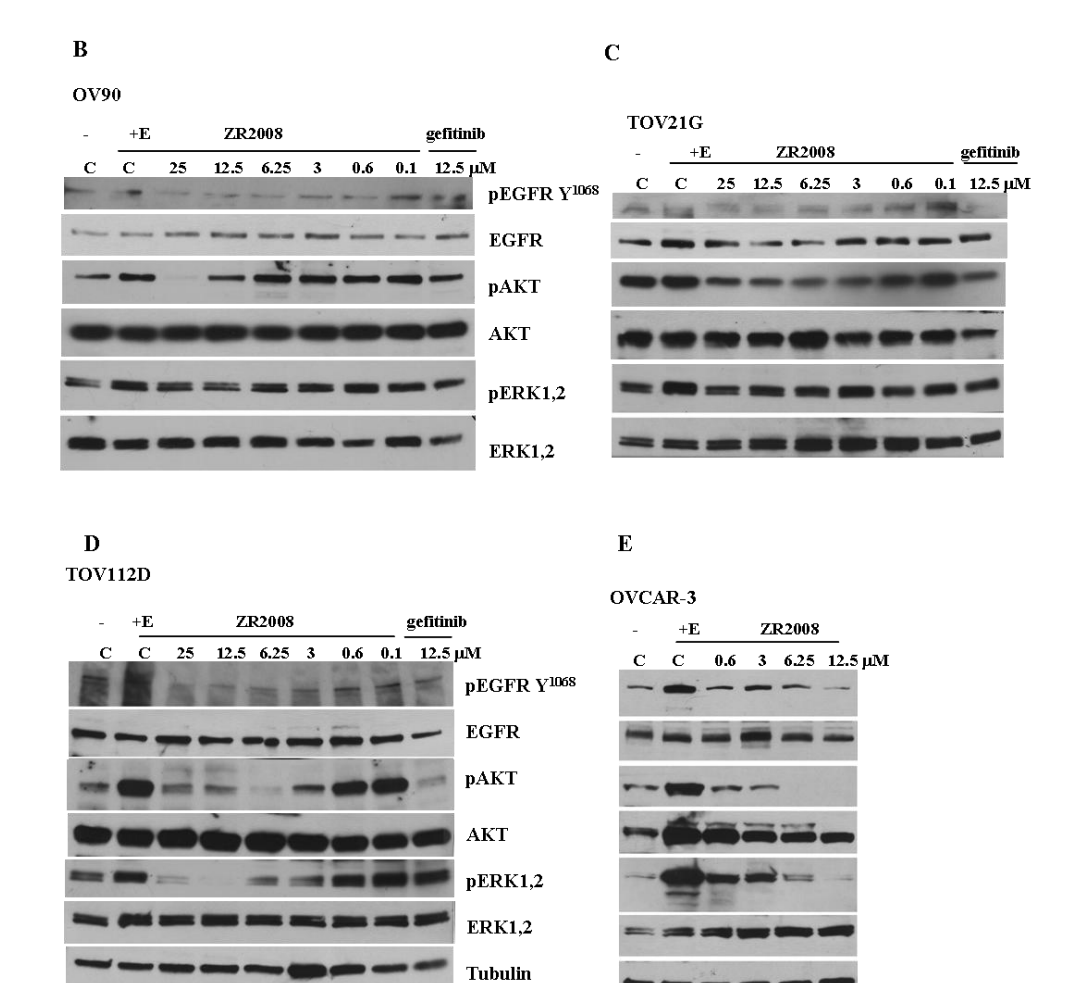


**Figure 5.2.** Inhibition of EGF-induced EGFR phosphorylation and downstream signaling.

(A) Inhibition of EGF-induced EGFR phosphorylation by *in vitro* enzyme assay. ZR2003, ZR008, ZRMS and gefitinib were tested for the ability to inhibit EGFR tyrosine kinase activity. Inhibition of EGFR, ERK1,2 and AKT phosphorylation by ZR2008 was determined in whole cell extracts by western blot. Serum starved OV90 (B), TOV21G (C), TOV112 (D), and OVCAR-3 (E) human ovarian cells were preincubated for 2 h with the indicated concentrations of ZR2008 prior to stimulation with 50 ng/ml EGF for 15 min. Equal amount of cell lysates were loaded and analyzed using anti-phospho EGFR (Tyr<sup>1068</sup>), phosho-AKT (Ser<sup>473</sup>), phospho-ERK1,2 (Thr<sup>202</sup>/Tyr<sup>204</sup>) antibodies. The membranes were stripped, and reprobed with anti-EGFR, anti-AKT, anti-ERK1,2 antibody. Similar results from two independent experiments were obtained and representative images were shown.

# 5.4.3.2. Phosphorylation of histone H2AX

Further analysis of DNA damage induced by ZR2008 was also indirectly assessed by phosphorylation of histone variant H2AX, which is a typical marker of DNA double strand breaks [41]. The results showed that  $\gamma$ H2AX phosphorylation was induced 24 h post-treatment at concentrations as low as 0.15  $\mu$ M in OVCAR3 (Fig. 5.3E, left) and at 0.6  $\mu$ M in TOV112D (Fig 5.3E, right), which is in agreement with the concentration range at which DNA damage was detected by the comet assay.

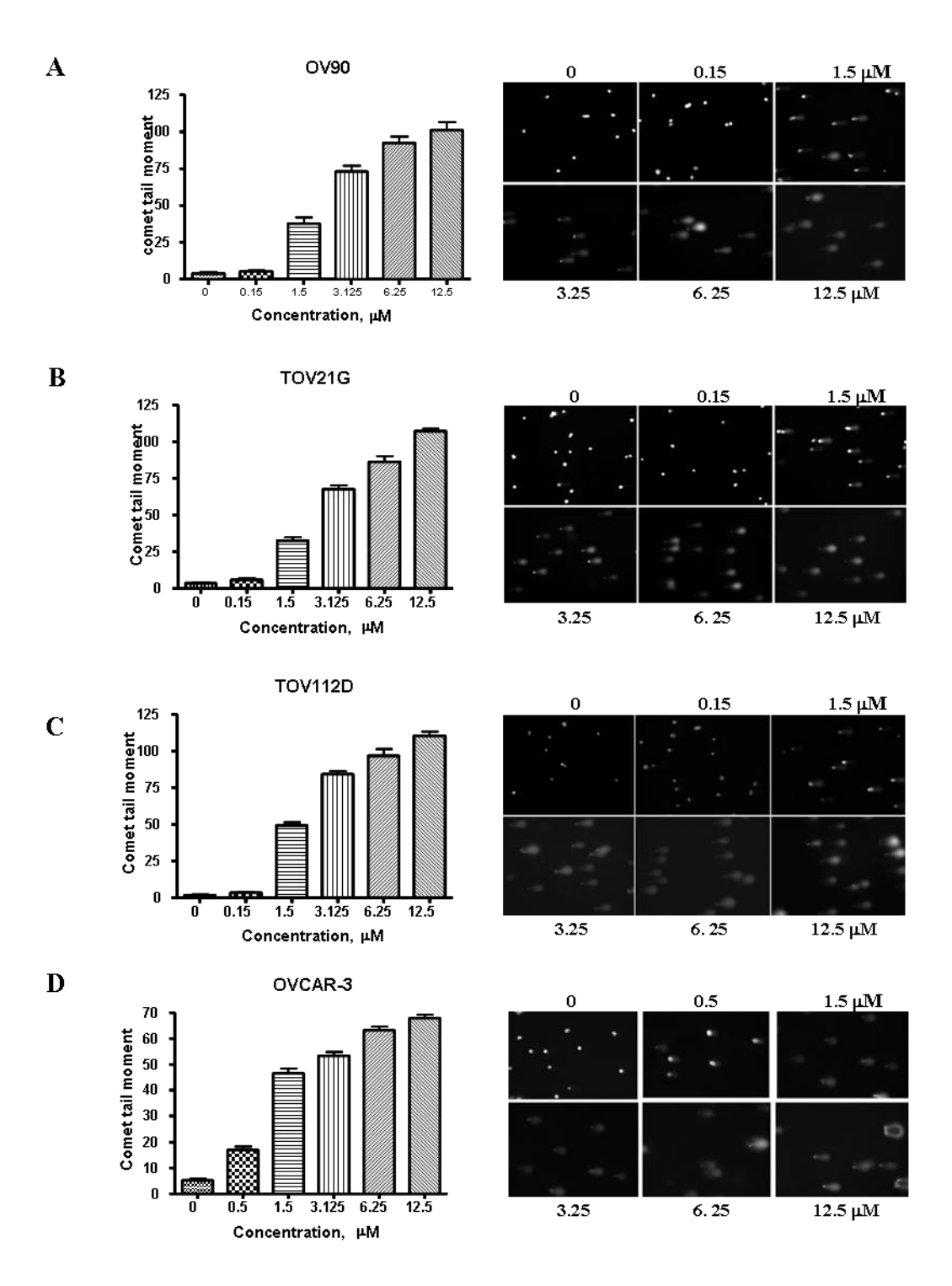
# 5.4.4. Cell cycle arrest and apoptotic response

## 5.4.4.1. Cell Cycle Perturbation

In order to further elucidate the mechanism of action of ZR2008, we analyzed its effect on cell cycle distribution by flow cytometry (Fig. 5.4). The results showed that whether the cells express low or high levels of EGFR, they were significantly arrested in G1 and S. Interestingly, considerable decrease of G2/M population was observed after 24 h treatment with ZR2008 in all cell lines (Fig. 5.4A, B, C, D). In a similar manner, gefitinib significantly arrested the cells in G1 (10-15 % increase) regardless of their EGFR status.

## 5.4.4.2. Activation of the stress response pathway

In order to verify whether the genotoxic stress induced by ZR2008 would trigger activation of the stress response pathway, we analyzed the phospho-Jun N-terminal kinase (JNK) response, known to be activated by DNA damage and to be involved in apoptosis [42]. In all four cell lines JNK was activated in a dose-dependent manner, indicating that the potent DNA lesions have triggered cells stress response (Fig. 5.5A).



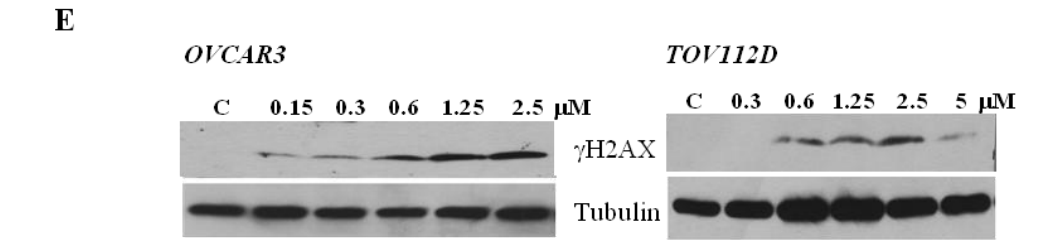
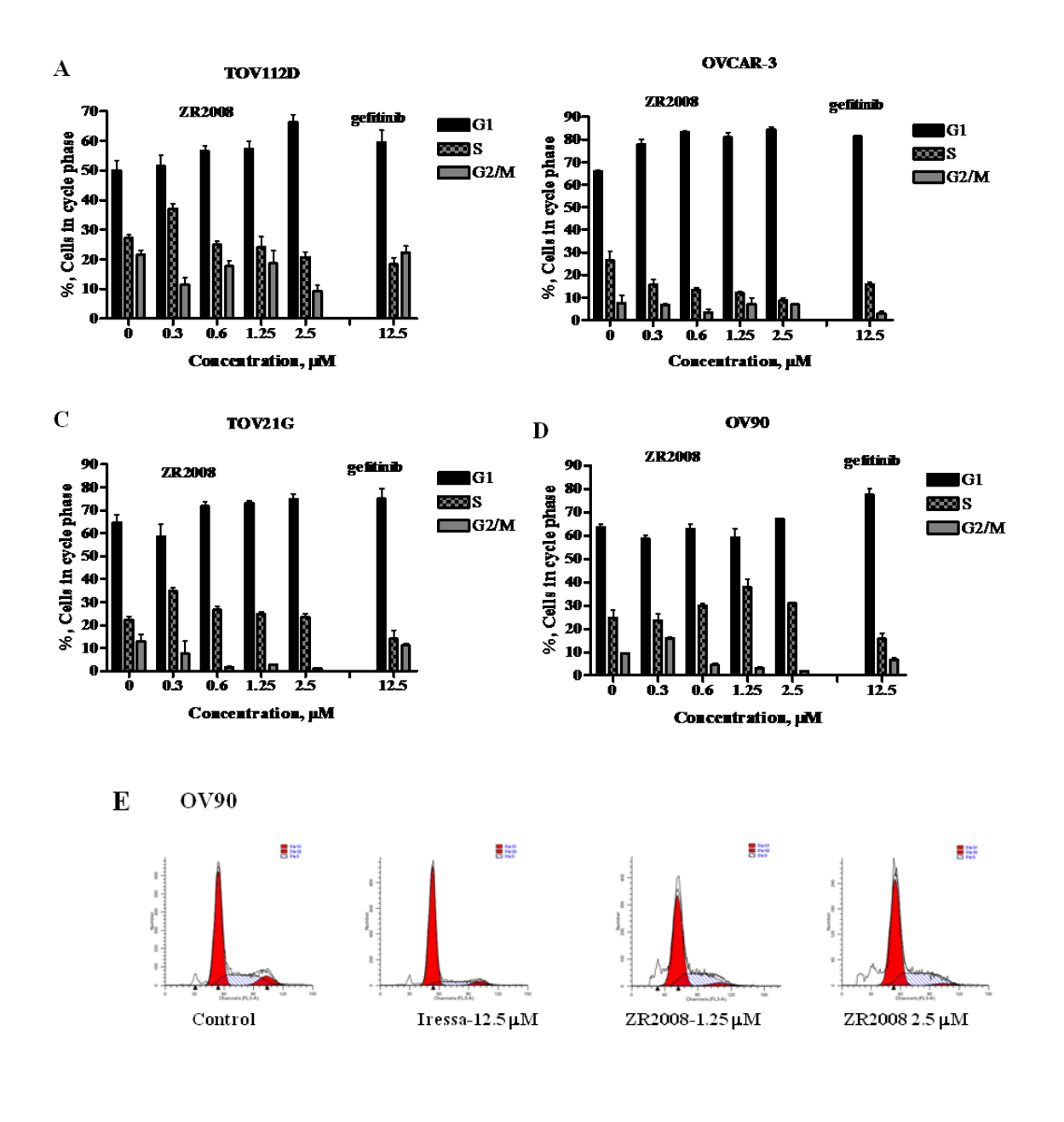
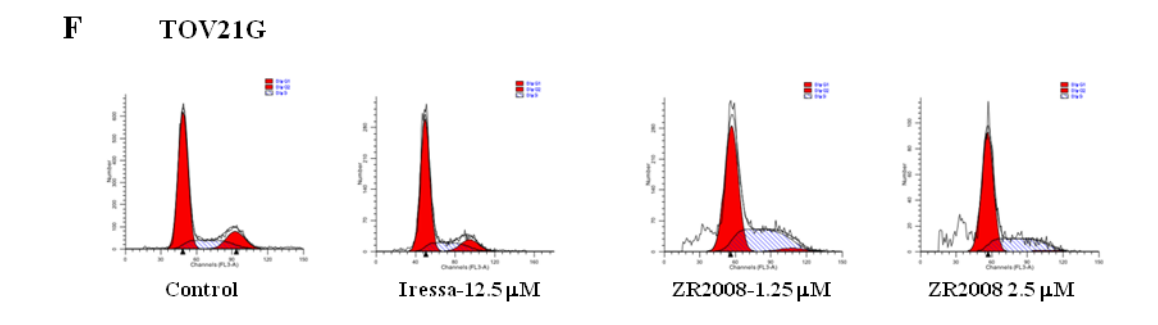


Figure 5.3. Quantitation of DNA damage induced by ZR2008 the panel of ovarian cells.

OV90 (A), TOV21G (B), TOV112D (C), and OVCAR3 (D) cells were exposed to the molecule for 2 h followed by assessment of drug-induced DNA damage using an alkaline comet assay. Comets were analyzed by fluorescence microscopy at 10X magnification after SYBR Gold staining and the comet tail moment was used to report DNA damage after treatment with the indicated dose range of ZR2008. The comet tail moment was calculated by comet IV software (Perceptive Instruments) from two independent experiments and representative comet images from one of the treatments were shown in the panels on the right. (E) Protein extracts from OVCAR3 (left) and TOV112D (right) cells, treated for 24 h with increasing concentrations of ZR2008, were analyzed by Western blot with anti-phospho-γH2AX antibody (1:500) and antitubilin as a loading control.





**Figure 5.4.** Cell cycle distribution after 24 h treatment with ZR2008.

Cells were incubated with four concentrations of ZR2008 [0.3125, 0. 625 (IC<sub>50</sub>), 1.25, 2.5 μM)] or gefitinib (12.5 μM) for 24 h and analyzed by fluorescence activated cell sorting (FACS) after fixation and staining with propidium idodide. Percentages of cells in each cell cycle phase were quantified using ModFitLT software and averaged from two independent experiments. Data from TOV112D (**A**), OVCAR3 (**B**), TOV21G (**C**), and OV90 (**D**) cells were presented as mean ± SEM. Representative cell cycle histograms from OV90 (**E**) and TOV21G (**F**) were showing G1 and mid-S arrest observed with ZR2008 treatment.

# 5.4.4.3. PARP1 cleavage as an indicator of apoptosis

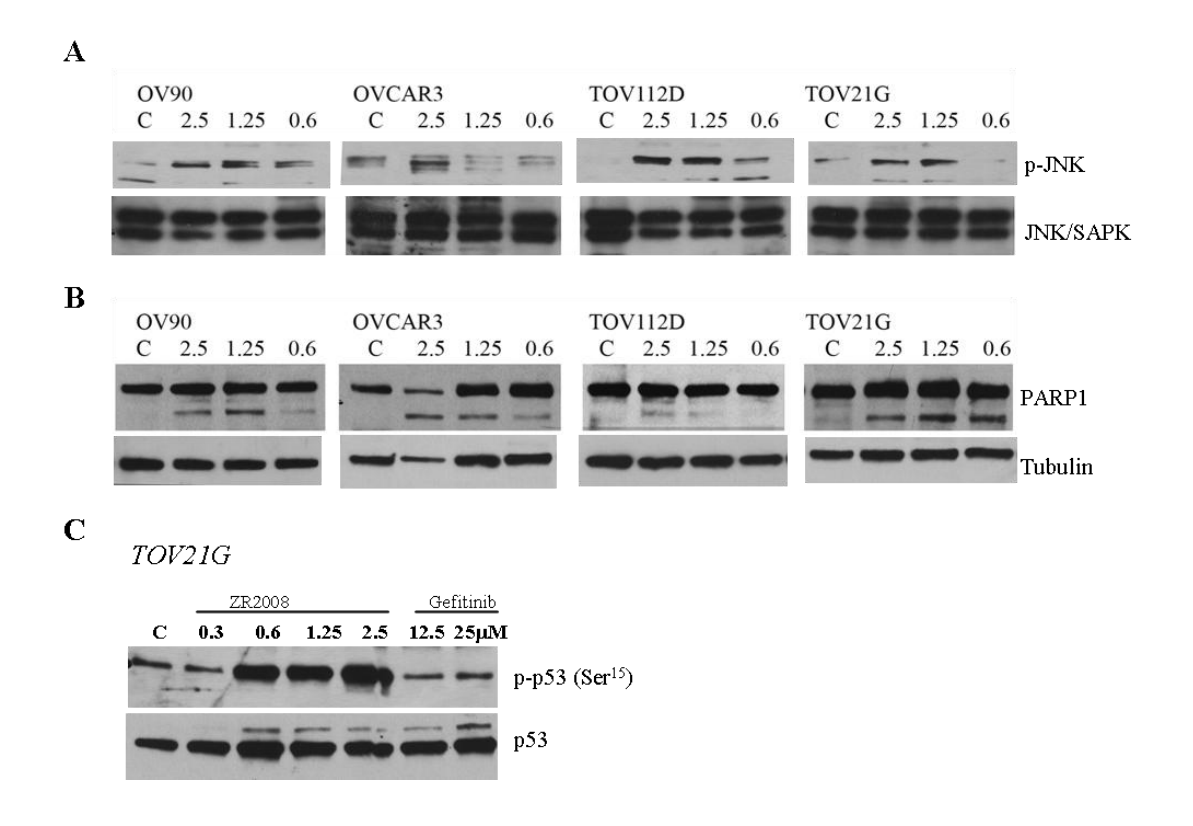
PARP1 cleavage as an indicator of cell death by apoptosis was analyzed by western blot. In all four cell lines treated for 24 h with increasing doses of ZR2008 (0.6, 1.25, 2.5 μM), cleaved 89 kDa PARP1 band was observed in a dose dependent manner (Fig. 5.5B). The results showed a full length 116 kDa PARP1 protein in the control and the appearance of the cleaved PARP1 fragment upon treatment.

# 5.4.4.4. Induction of p53 in TOV21G cells

More importantly, p53 Ser<sup>15</sup> phosphorylation, which is an event triggered by DNA damage, was analyzed in TOV21G cells, the only line expressing wt p53 in the panel [33]. The results showed that both p53 and p53 Ser<sup>15</sup> phosphorylation levels were induced by ZR2008 treatment in a dose-dependent manner (Fig. 5.5C).

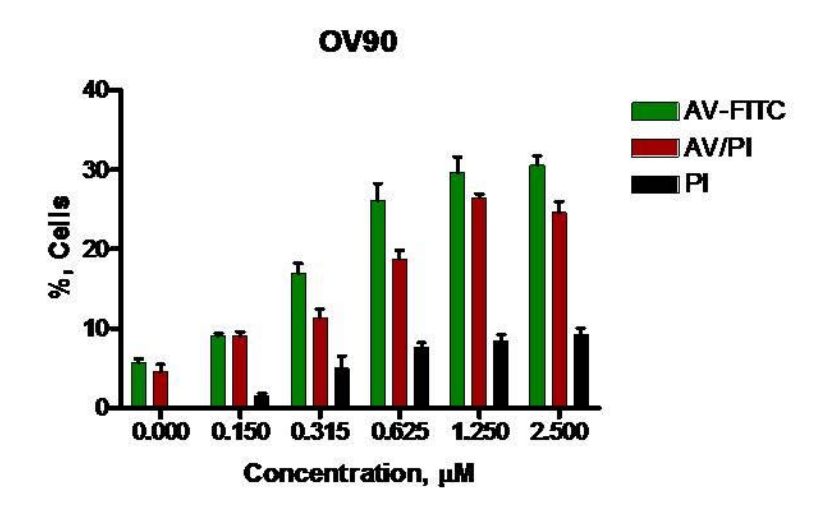
# 5.4.4.5. Apoptosis by Annexin V binding

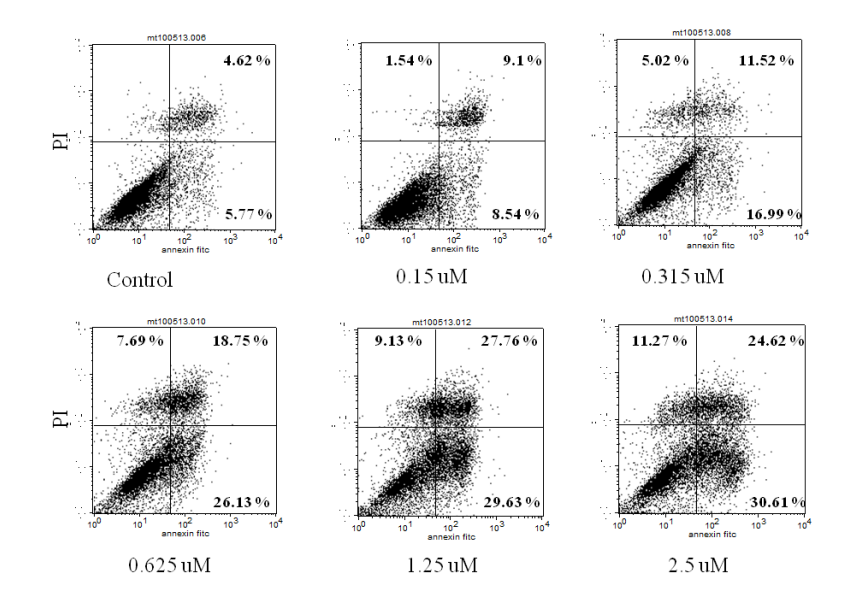
In order to determine whether the tandem inhibition of EGFR signaling and DNA damage translates into apoptosis, Annexin V binding assay was performed. Apoptosis was studied 48 h after drug exposure starting from 2.5 µM concentration as the highest dose tolerated. Significant levels of apoptosis were observed at concentrations as low as 0.3 µM. Regardless of the levels of expression of EGFR or AKT, ZR2008 induced high levels of apoptosis in all ovarian cancer cells at IC<sub>50</sub> concentrations (Fig. 5.6A, B, C). The experiment could not be extended to more then 48 h since by this time, all cells were virtually dead. In contrast, gefitinib induced moderate level of apoptosis in the cell (data not shown), indicating that the addition of a genotoxic tail to the molecules significantly enhanced its cytotoxicity profile.

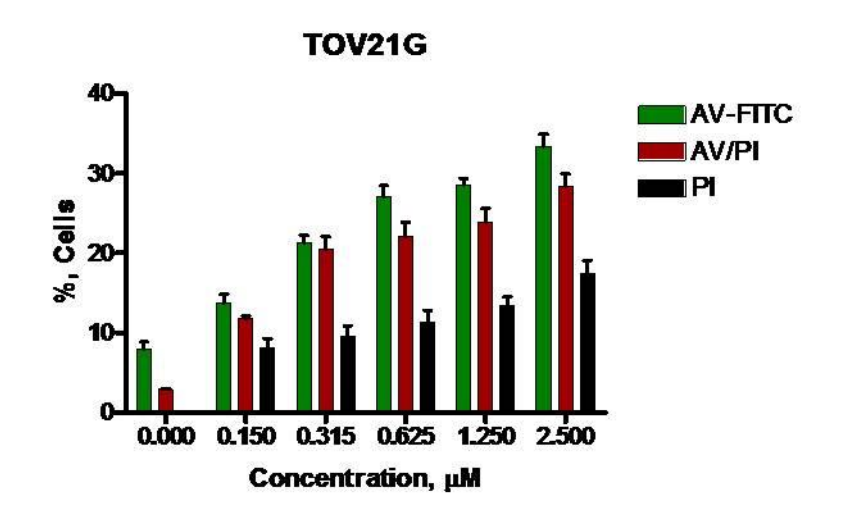


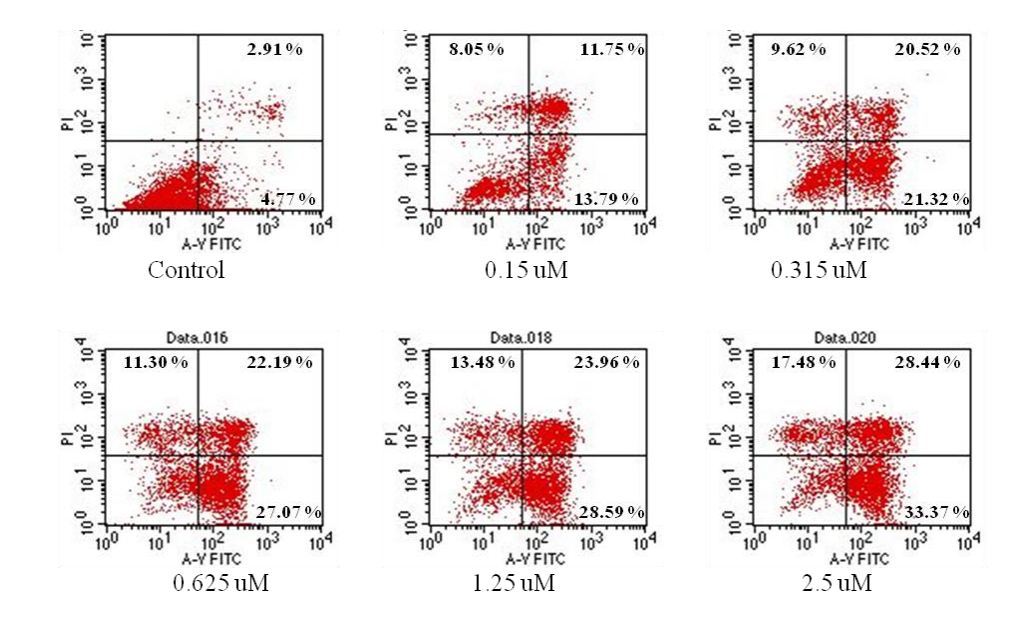
**Figure 5.5.** Activation of apoptotic and stress-induced proteins by ZR2008.

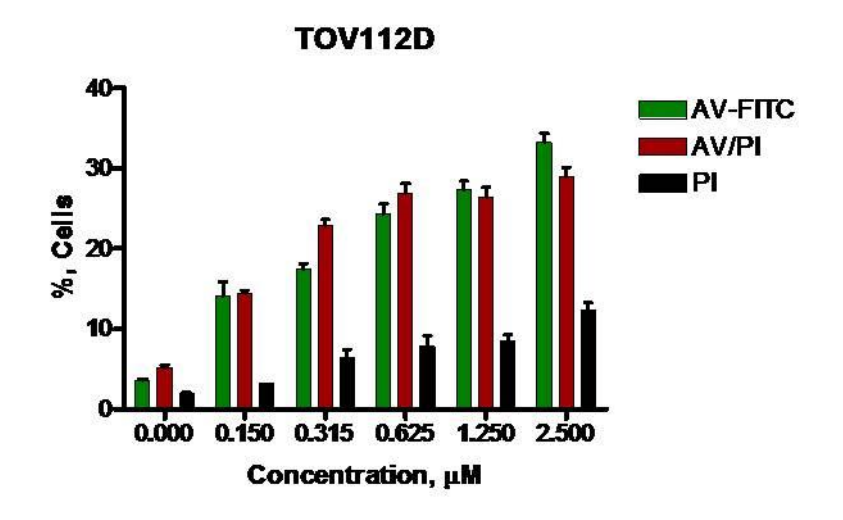
(A) OV90, OVCAR-3, TOV112, and TOV21G ovarian cells were treated with ZR2008 for 24 h and analyzed by Western blot with anti-phospho-JNK/SAPK and anti-JNK/SAPK antibody. (B) Protein extracts from all four ovarian cells treated for 24 h with 0.6, 1.25, 2.5 μM of ZR2008 were analyzed for the appearance of 89 kDa cleaved PARP1 band. (C) TOV21G p53 wt cells were treated with increasing concentration of the ZR2008 and gefitinib (IC<sub>50</sub> concentration) for 24 h. Total protein extracts were analyzed with anti-phospho-p53 (Ser <sup>15</sup>) and p53 antibody (1:1000, Cell Signaling).

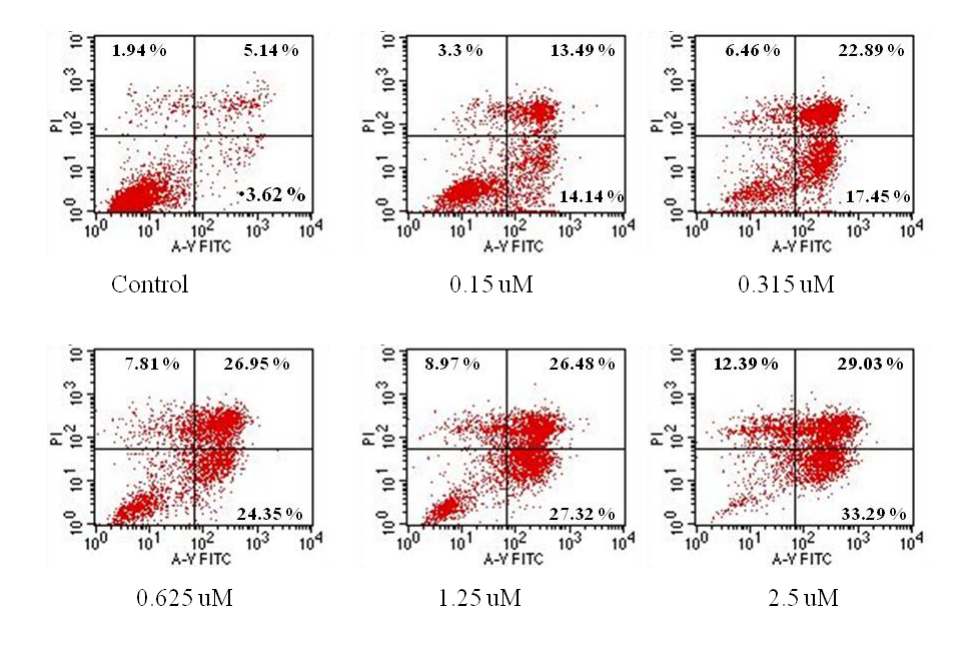












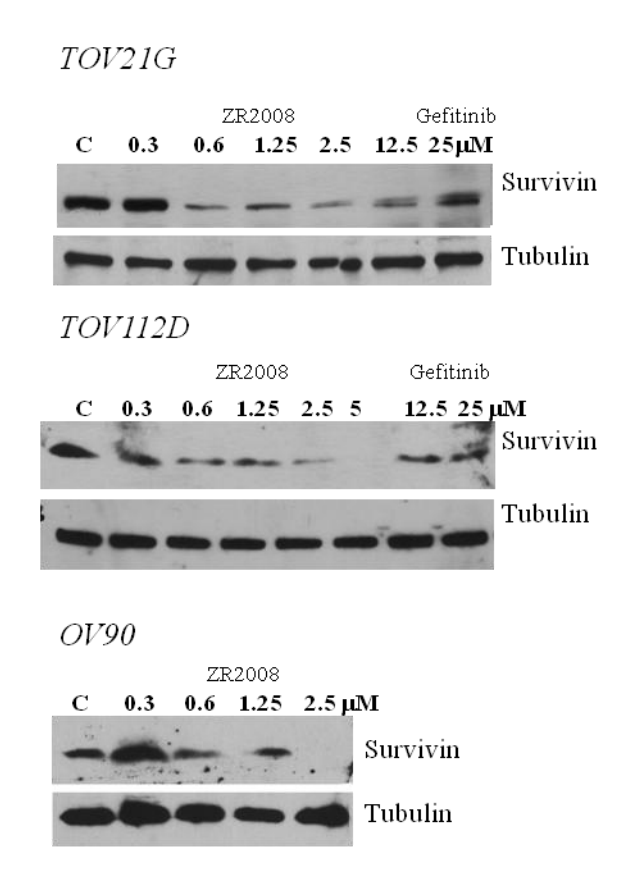


**Figure 5.6.** Induction of cell death by apoptosis in the ovarian cell lines.

OV90 (**A**), TOV21G (**B**), TOV112D (**C**) were incubated with five concentrations of ZR2008 [0.15, 0.325, 0.625 (IC<sub>50</sub>), 1.25, 2.5  $\mu$ M)] for 48 h, stained with Annexin V and PI, and analyzed using a BD LSR flow cytometer. Each point represents the average from two independent experiments performed in triplicate. Results were shown as mean  $\pm$  SE. The dot plot histograms from one the three independent experiments performed were presented below each bar graph. (**D**) Effect of ZR2008 on survivin accumulation after 24 h treatment of TOV21G, TOV112D and OV90 with increasing concentration of ZR2008 (0.3, 0.6, 1.25, 2.5, 5  $\mu$ M). Total cell extracts were analyzed by Western blot with anti-survivin antibody and membranes were reprobed with anti-tubulin antibody as loading control.

#### 5.4.4.6. Survivin accumulation

The strong levels of apoptosis induced by ZR2008 despite the activation of AKT in the cells, stimulated our interest in determining whether it could affect the expression of inhibitor of apoptosis proteins (IAP). We chose to analyze one such member of IAP family, survivin, the expression of which is known to correlate with resistance to DNA damaging agents [43, 44]. Western blot analysis demonstrated a dose-dependent decrease in accumulation of survivin after 24 h treatment with ZR2008 in OV90, TOV21G and TOV112D but not after exposure to gefitinib (Fig. 5.6D). Despite expressing elevated levels of phosphorylated AKT in two of the cell lines (TOV21G and OV90), the cellular depletion of survivin, together with the PARP1 fragmentation observed, was in agreement with the high levels of apoptosis induced by ZR2008.

## 5.5. DISCUSSION

Ovarian cancer has the highest mortality rate of all the gynecological cancers and is the fourth leading cause of cancer death among women in USA. It is usually treated if diagnosed earlier, however in many cases it causes confusing symptoms that progressed unnoticed until the tumour is far too advanced for efficient chemotherapy. At the advance stages, single drug-based chemotherapy often fails and only leads to improved survival when one or more drugs are combined with another cytotoxic agent, usually a DNA damaging agent such as cisplatin. The alkylators are an important class of DNA damaging agents that have been used in the chemotherapy of ovarian cancer for more than 30 years [39]. The best known alkylators used in the clinical management of platinum-resistant ovarian cancer are chlorambucil and melphalan (two aniline mustards) [45-48]. While therapies involving DNA damage or taxanes have now become standard of care, they often fail due to DNA repair-based chemo-resistance [49].

Efforts over the past 20 years have improved our understanding of the biology of epithelial ovarian cancer and have led to the identification of many genes involved in its aggressiveness and progression. One such class of oncogenes is the erbB family. While the importance of AKT activation in the progression and treatment of ovarian cancer is now well established, the role of one member of the erbB family, EGFR in the drug sensitivity of ovarian cancer cells is still controversial.

In the clinic, it has been reported that ovarian cancer patients overexpressing EGFR respond to a treatment with gefitinib when administered in combination with carboplatin or taxol [21, 28]. In contrast, studies designed to correlate ovarian cancer sensitivity to gefitinib showed that there was little correlation between EGFR overexpression and cell sensitivity to the latter drug [50]. The work was not performed under EGF-stimulatory conditions and did outline the fact that cell lines expressing the lowest level of EGFR were the least potent. A discrepancy between the latter study and the current one is our identification of EGFR in TOV211D cells and observation of a dose dependent inhibition of EGFR, subsequent down-regulation of Erk1,2, and inhibition of AKT in the latter cell line. Nevertheless, the average levels of growth inhibition by gefitinib in the cell panel described in the previous study was in the same range as those found in ours (around 10 µM). Here we demonstrated that while ZR2008 was capable of down-regulating EGFR and AKT pathways in EGF-responsive cells, its potency in the ovarian cells with moderate expression of EGFR was in the same range. More importantly, this potency was unaffected in two cell lines where it could only moderately down-regulate AKT phosphorylation. This is a significant result, given the proven role played by AKT in the reduced sensitivity of ovarian tumours to chemotherapy and its constitutive activation in PTEN null cell line that renders them less sensitive to EGFR inhibitors [13].

Importantly, we have shown herein that the mechanism of cell death induced by ZR2008 in all the ovarian cells was apoptosis, which was triggered at IC<sub>50</sub> concentrations. The fact that apoptosis could be triggered without alleviation of AKT phosphorylation suggests for other pro-apoptotic mechanisms involved, independent of receptor activation or related kinases. This mechanism may also be independent of p53 induction since the apoptotic activity of the compounds in the TOV21G cell line (p53wt) was in the same range as in the p53 mutant cells. However, a common observation is that ZR2008 induced JNK phosphorylation in all the cell lines, suggesting that apoptosis could have been triggered through a pathway that involves the latter stress activated protein. While the role of JNK activation in apoptosis is controversial, we recently demonstrated that JNK activation was related to apoptosis induced by the mixed EGFR-DNA damaging molecule RB24 [51].

The potency of ZR2008 was consistently more than 50-fold higher than gefitinib in the cell panel. While this indicates that the hemi-mustard function or the DNA damage that it induces is responsible for such a remarkable difference in potency, it is important to note that in the 10 µM range, gefitinib could induce growth inhibition in all these cells. In a similar manner, ZR2008 ability to block cell growth was corroborated by the induced G1 arrest. Interestingly, in contrast to gefitinib, ZR2008 significantly arrested cells in mid-S phase, an event that could be due to sufficient levels of DNA damage induced to block cell cycle progression. The G1-S arrest could also be related to the observed downregulation of survivin by ZR2008 in TOV21G, TOV112D and OV90 cells. It is now known that overexpression of survivin is associated with resistance to G1 arrest and accelerated S-phase transition upon chemotherapy [52]. Coley *et al.* [53] have also demonstrated a synergistic effect on increased apoptosis and decreased survivin levels when combining an EGFR inhibitor with either cisplatin or paclitaxel in drug resistant

EGFR over-expressing ovarian cancer cells. While the mechanism of decreasing survivin by ZR2008 is not elucidated herein, our results showed that it does not occur through the blockade of the PI3K-AKT pathway. It is also not related to p53-activated pathways since it was down-regulated even in p53 mutant cells. However, in contrast to p53 and AKT status, down-regulation of survivin, observed herein, was in agreement with the massive levels of apoptosis triggered in these cells. The dose-dependent down-regulation of survivin may be the primary mechanism that confers ZR2008 its unique ability to evade the anti-apoptotic signaling mediated by AKT activation in the cells. Whether it ability to down-regulate survivin stems from the tyrosine kinase inhibitory, DNA damaging function or a combination of both properties of ZR2008, remains to be elucidated.

# **5.6. ACKNOWLEDGMENTS**

We thank the Canadian Institute of Health Research (CIHR) for financial support. MT is grateful to the Fond de la Recherche en Santé du Québec (FRSQ) for a doctoral fellowship. We are grateful for the ovarian cancer cell lines kindly provided by Dr. Anne-Marie Mes-Masson, CHUM research center at Notre-Dame Hospital, Montreal. We acknowledge Mitra Heravi for the technical assistance.

#### 5.7. REFERENCES

- 1. de Graeff, P., et al., *The ErbB signalling pathway: protein expression and prognostic value in epithelial ovarian cancer.* Br J Cancer, 2008. **99**(2): p. 341-9.
- 2. Reibenwein, J. and M. Krainer, *Targeting signaling pathways in ovarian cancer*. Expert Opin Ther Targets, 2008. **12**(3): p. 353-65.
- 3. Slamon, D.J., et al., Studies of the HER-2/neu proto-oncogene in human breast and ovarian cancer. Science, 1989. **244**(4905): p. 707-12.
- 4. Ilekis, J.V., et al., Expression of epidermal growth factor and androgen receptors in ovarian cancer. Gynecol Oncol, 1997. **66**(2): p. 250-4.
- 5. Niikura, H., et al., Expression of epidermal growth factor-related proteins and epidermal growth factor receptor in common epithelial ovarian tumors. Int J Gynecol Pathol, 1997. **16**(1): p. 60-8.
- 6. Lafky, J.M., et al., Clinical implications of the ErbB/epidermal growth factor (EGF) receptor family and its ligands in ovarian cancer. Biochim Biophys Acta, 2008. 1785(2): p. 232-65.
- 7. Brustmann, H., Epidermal growth factor receptor expression in serous ovarian carcinoma: an immunohistochemical study with galectin-3 and cyclin D1 and outcome. Int J Gynecol Pathol, 2008. **27**(3): p. 380-9.
- 8. Psyrri, A., et al., Effect of epidermal growth factor receptor expression level on survival in patients with epithelial ovarian cancer. Clin Cancer Res, 2005. **11**(24 Pt 1): p. 8637-43.
- 9. Skirnisdottir, I., B. Sorbe, and T. Seidal, *The growth factor receptors HER-2/neu and EGFR, their relationship, and their effects on the prognosis in early stage (FIGO I-II) epithelial ovarian carcinoma.* Int J Gynecol Cancer, 2001. **11**(2): p. 119-29.
- 10. Qiu, L., et al., Crosstalk between EGFR and TrkB enhances ovarian cancer cell migration and proliferation. Int J Oncol, 2006. **29**(4): p. 1003-11.
- 11. Shield, K., et al., *Multicellular spheroids in ovarian cancer metastases: Biology and pathology*. Gynecol Oncol, 2009. **113**(1): p. 143-8.
- 12. Jorissen, R.N., et al., *Epidermal growth factor receptor: mechanisms of activation and signalling.* Exp Cell Res., 2003. **284**(1): p. 31-53.
- 13. Carnero, A., et al., *The PTEN/PI3K/AKT signalling pathway in cancer, therapeutic implications*. Curr Cancer Drug Targets, 2008. **8**(3): p. 187-98.

- 14. Zhou, C., et al., Inhibition of EGFR/PI3K/AKT cell survival pathway promotes TSA's effect on cell death and migration in human ovarian cancer cells. Int J Oncol, 2006. **29**(1): p. 269-78.
- 15. Smith, J.A., et al., *In vitro evaluation of the effects of gefitinib on the modulation of cytotoxic activity of selected anticancer agents in a panel of human ovarian cancer cell lines.* Cancer Chemother Pharmacol, 2008. **62**(1): p. 51-8.
- 16. Sewell, J.M., et al., *Targeting the EGF receptor in ovarian cancer with the tyrosine kinase inhibitor ZD 1839 ("Iressa")*. Br J Cancer, 2002. **86**(3): p. 456-62.
- 17. Cao, C., et al., *Priming with EGFR tyrosine kinase inhibitor and EGF sensitizes ovarian cancer cells to respond to chemotherapeutical drugs.* Cancer Lett, 2008. **266**(2): p. 249-62.
- 18. Albanell, J. and P. Gascon, *Small molecules with EGFR-TK inhibitor activity*. Current Drug Targets, 2005. **6**(3): p. 259-274.
- 19. Pao, W. and V.A. Miller, *Epidermal growth factor receptor mutations, small-molecule kinase inhibitors, and non-small-cell lung cancer: current knowledge and future directions.* J. Clin. Oncol., 2005. **23**(11): p. 2556-2568.
- 20. Gordon, A.N., et al., Efficacy and safety of erlotinib HCl, an epidermal growth factor receptor (HER1/EGFR) tyrosine kinase inhibitor, in patients with advanced ovarian carcinoma: results from a phase II multicenter study. Int J Gynecol Cancer, 2005. 15(5): p. 785-92.
- 21. Schilder, R.J., et al., *Phase II study of gefitinib in patients with relapsed or persistent ovarian or primary peritoneal carcinoma and evaluation of epidermal growth factor receptor mutations and immunohistochemical expression: a Gynecologic Oncology Group Study.* Clin Cancer Res, 2005. **11**(15): p. 5539-48.
- 22. Fukuoka, M., et al., Multi-institutional randomized phase II trial of gefitinib for previously treated patients with advanced non-small-cell lung cancer (The IDEAL 1 Trial) [corrected]. J Clin Oncol, 2003. **21**(12): p. 2237-46.
- 23. Kimball, K.J., et al., A phase I study of lapatinib in combination with carboplatin in women with platinum sensitive recurrent ovarian carcinoma. Gynecol Oncol, 2008. **111**(1): p. 95-101.
- 24. Gordon, M.S., et al., Clinical activity of pertuzumab (rhuMAb 2C4), a HER dimerization inhibitor, in advanced ovarian cancer: potential predictive relationship with tumor HER2 activation status. J Clin Oncol, 2006. **24**(26): p. 4324-32.
- 25. Schilder, R.J., et al., *Phase II trial of single agent cetuximab in patients with persistent or recurrent epithelial ovarian or primary peritoneal carcinoma with the potential for dose escalation to rash.* Gynecol Oncol, 2009. **113**(1): p. 21-7.

- 26. Seiden, M.V., et al., A phase II trial of EMD72000 (matuzumab), a humanized anti-EGFR monoclonal antibody, in patients with platinum-resistant ovarian and primary peritoneal malignancies. Gynecol Oncol, 2007. **104**(3): p. 727-31.
- 27. Martin, L.P. and R.J. Schilder, *Management of recurrent ovarian carcinoma: current status and future directions.* Semin Oncol, 2009. **36**(2): p. 112-25.
- 28. Pautier, P., et al., *Phase II study of gefitinib in combination with paclitaxel (P) and carboplatin (C) as second-line therapy for ovarian, tubal or peritoneal adenocarcinoma (1839IL/0074)*. Gynecol Oncol. **116**(2): p. 157-62.
- 29. Reed, E., et al., *Paclitaxel, cisplatin, and cyclophosphamide in human ovarian cancer: molecular rationale and early clinical results.* Semin Oncol, 1995. **22**(3 Suppl 6): p. 90-6.
- 30. Lacroix, L., et al., Response of ovarian carcinomas to gefitinib-carboplatin-paclitaxel combination is not associated with EGFR kinase domain somatic mutations. Int J Cancer, 2006. 118(4): p. 1068-9.
- 31. Matheson, S., et al., *Combi-molecules: a global approach towards better chemoselectivity of cytotoxic agents and chemoresistance of refractory tumors.* Bulletin du Cancer, 2004. **91**(12): p. 911-915.
- 32. Rachid, Z., et al., Synthesis of half-mustard combi-molecules with fluorescence properties: correlation with EGFR status. Bioorganic & Medicinal Chemistry Letters, 2005. **15**(4): p. 1135-1138.
- 33. Provencher, D.M., et al., *Characterization of four novel epithelial ovarian cancer cell lines*. In Vitro Cell Dev Biol Anim, 2000. **36**(6): p. 357-61.
- 34. Skehan, P., et al., *New colorimetric cytotoxicity assay for anticancer-drug screening*. J Natl Cancer Inst., 1990. **82**(13): p. 1107-1112.
- 35. Matheson, S.L., J.P. McNamee, and B.J. Jean-Claude, *Differential responses of EGFR-AGT-expressing cells to the "combi-triazene" SMA41*. Cancer Chemoth. Pharm., 2003. **51**(1): p. 11-20.
- 36. McNamee, J.P., et al., *Comet assay: rapid processing of multiple samples.* Mutat Res, 2000. **466**(1): p. 63-69.
- 37. Olive, P.L. and J.P. Banath, *The comet assay: a method to measure DNA damage in individual cells.* Nat Protoc, 2006. **1**(1): p. 23-29.
- 38. Anderson, N.G., et al., *ZD1839* (*Iressa*), a novel epidermal growth factor receptor (EGFR) tyrosine kinase inhibitor, potently inhibits the growth of EGFR-positive cancer cell lines with or without erbB2 overexpression. Int J Cancer, 2001. **94**(6): p. 774-82.

- 39. Lidor, Y.J., et al., Synergistic cytotoxicity of different alkylating agents for epithelial ovarian cancer. Int J Cancer, 1991. **49**(5): p. 704-10.
- 40. Green, J.A. and A.J. Slater, *A study of cis-platinum and ifosfamide in alkylating agent-resistant ovarian cancer.* Gynecol Oncol, 1989. **32**(2): p. 233-5.
- 41. Huang, X., H.D. Halicka, and Z. Darzynkiewicz, *Detection of histone H2AX phosphorylation on Ser-139 as an indicator of DNA damage (DNA double-strand breaks)*. Curr Protoc Cytom, 2004. **Chapter 7**: p. Unit 7 27.
- 42. Ohtsuka, T., et al., Synergistic induction of tumor cell apoptosis by death receptor antibody and chemotherapy agent through JNK/p38 and mitochondrial death pathway. Oncogene, 2003. **22**(13): p. 2034-44.
- 43. Wang, Z., Y. Xie, and H. Wang, *Changes in survivin messenger RNA level during chemotherapy treatment in ovarian cancer cells.* Cancer Biol Ther, 2005. **4**(7): p. 716-9.
- 44. Zaffaroni, N., et al., Expression of the anti-apoptotic gene survivin correlates with taxol resistance in human ovarian cancer. Cell Mol Life Sci, 2002. **59**(8): p. 1406-12.
- 45. McCully, K.S., et al., A reappraisal of the role of chlorambucil in patients with end stage ovarian cancer who have previously been treated with platinum regimens. Scott Med J, 2000. **45**(2): p. 51-3.
- 46. Evans, B.D., et al., Carboplatin and chlorambucil combination chemotherapy as treatment for patients with ovarian cancer. Int J Gynecol Cancer, 1994. **4**(1): p. 66-71.
- 47. Davis-Perry, S., et al., *Melphalan for the treatment of patients with recurrent epithelial ovarian cancer.* Am J Clin Oncol, 2003. **26**(4): p. 429-33.
- 48. Wadler, S., et al., Randomized trial of initial therapy with melphalan versus cisplatin-based combination chemotherapy in patients with advanced ovarian carcinoma: initial and long term results--Eastern Cooperative Oncology Group Study E2878. Cancer, 1996. 77(4): p. 733-42.
- 49. Gornati, D., et al., *Modulation of melphalan and cisplatin cytotoxicity in human ovarian cancer cells resistant to alkylating drugs*. Anticancer Drugs, 1997. **8**(5): p. 509-16.
- 50. Bull Phelps, S.L., et al., *Implications of EGFR inhibition in ovarian cancer cell proliferation*. Gynecol Oncol, 2008. **109**(3): p. 411-7.
- 51. Banerjee, R., et al., *The combi-targeting concept: selective targeting of the epidermal growth factor receptor- and Her2-expressing cancer cells by the complex combi-molecule RB24*. J Pharmacol Exp Ther. **334**(1): p. 9-20.
- 52. Suzuki, A., et al., Survivin initiates cell cycle entry by the competitive interaction with Cdk4/p16(INK4a) and Cdk2/cyclin E complex activation. Oncogene, 2000. **19**(29): p. 3225-34.

53. Coley, H.M., et al., Receptor tyrosine kinase (RTK) inhibition is effective in chemosensitising EGFR-expressing drug resistant human ovarian cancer cell lines when used in combination with cytotoxic agents. Biochem Pharmacol, 2006. **72**(8): p. 941-8.

# Chapter 6

General Discussion and Contribution to Knowledge

## **6.1 GENERAL DISCUSSION AND CONTRIBUTION**

The past decade has seen considerable efforts in the discovery and development of therapeutics that modulate several cancer targets [1-8]. Despite significant developments in the field, only very few drugs have reached the clinical settings. In many cases the new agents have failed to replace the classical ones. However, the combination of these new agents with classical chemotherapeutic drugs has shown great promise. Nevertheless, the mode of combination of two therapeutic agents remained unchallenged. Over the past several years, our group initiated a novel two-drug combination approach of that sought to bridge the gap between classical chemotherapy and modern targeted agents [9-13]. Classical DNA alkylating agents are unspecific agents, the toxicity of which is imputed to the lack of selectivity for tumour targets [14]. In contrast, TKI are targeted agents directed at oncogenes that drive tumour growth, invasion and metastasis. The selectivity of this class of agents has conferred them good tolerability in vivo and they are so well tolerated that they can be administered on a once daily schedule. Thus, we surmise that by appending a cytotoxic tail to such type of inhibitors one might target it to specific kinases that drive tumour growth. In the context of this new approach, we designed molecules termed "combi-molecules" that utilize an alkylating function to target DNA (cytotoxic function) and an EGFR inhibitor (targeting warhead). Several molecules have been synthesized demonstrating the feasibility of this approach termed combi-targeting [15, 16]. Previous analyses of combi-molecules showed that: (a) they can strongly damage DNA and block signaling through EGFR, (b) elicit stress response through JNK pathway activation (c) downregulate the PI3K/AKT pathway, (d) trigger significant levels of apoptosis, (e) confer significant potency in vivo [12, 13, 17, 18].

While combi-molecules were demonstrated to selectively target cells transfected with EGFR and ErbB2 genes, the mechanism of such selectivity still needs to be demonstrated. More importantly, although combi-molecules were designed to degrade into two bioactive species and to hydrolyze upon internalization in the cell, their subcellular localization and decomposition event remained elusive. Classical tumour targeting involved drugs that are rigidly attached to their recognition moiety. One such example of a targeted molecule used in the clinic is estramustine, selected for the treatment of hormone-refractory prostate cancer [19, 20]. The molecule, which contains a nitrogen mustard moiety appended to an estradiol one through a carbamate linker, has been shown to disrupt multiple functions in the cell while remaining intact. It has been reported to interfere with the assembly of microtubule and nuclear matrix and block P-gp efflux pump [21].

## 6.1.1. Contribution 1

Here in the context of this study we have thoroughly investigated the targeting mechanism of AL237, a molecule specifically designed for imaging the distribution of the two fluorescent species deriving from the intact combi-molecule. The principle of type I targeting is such that the molecule is designed to bind to EGFR on its own (*Alk-I*) and to degrade to *Alk*, interacting with DNA and *I*, binding to EGFR. Thus, we labeled the alkyl triazene moiety with fluorescent dansyl group in order to localize the DNA-alkylating moiety. Despite the fact that the entire combi-molecule labeled with a dansyl tag would also fluoresce in the green, the DNA alkylating species released upon hydrolysis is tagged with dansyl and generates green fluorescence in the nucleus. On the other hand, the EGFR inhibitor (*I*) that fluoresces in the blue, was designed to bind to EGFR in the cell wherever it is localized. The use of red-labeled EGFR antibody permitted the verification of the colocalization of the EGFR inhibitory moiety

with EGFR (I, blue or Alk-I, green). Indeed, we have shown that co-localization was seen between the blue fluorescence (I), but not the green (Alk-I) with red fluorescence labeled anti-EGFR antibody, supporting the ability of the released inhibitor (I) to bind to EGFR. Importantly, since the entire combi-molecule fluoresces in the green, it is possible to overlap with the green fluorescence emitted by the DNA damaging moiety. While it was difficult to distinguish between the intact combi-molecule and the DNA damaging species, it should be noted that the molecule was able to hydrolyze in media within  $t_{1/2}$ = 22 min. Since experiments were performed 2 h post-treatment (4 time its half-life), we believe that by this time only the DNA alkylating species or derived products should be detected in the cells.

Using AL237 fluorescence probe, we first demonstrated that the green fluorescence in the nucleus is selectively targeted to cells expressing EGFR and ErbB2. Likewise, the blue fluorescence was selectively targeted in the nucleus of the receptor-expressing cells. Nevertheless, the majority of the blue and green fluorescence were observed in the perinuclear region. The detection of the green fluorescence in the nucleus was a major discovery and allows us to revise the proposed mechanism for tumour targeting by combi-molecule. As outlined in Figure 6.1 the presence of both blue an green fluorescence in the perinuclear region and in the nucleus suggest that the entire molecule can localize and decompose therein to generate the DNA targeting species that fluoresces in the green (*Alk-dansyl*) and *I* that fluoresces in the blue. In terms of intensity of distribution from the cytoplasmic membrane to the nucleus the highest intensity is determined at the perinuclear region where the primary targets are localized. This observation corroborates with the bystander effect suggested by Banarjee *et al.* [18], where the majority of the molecules are localized in the perinuclear region and from where they diffuse to the nucleus. However, our discovery of the blue and green fluorescence in the

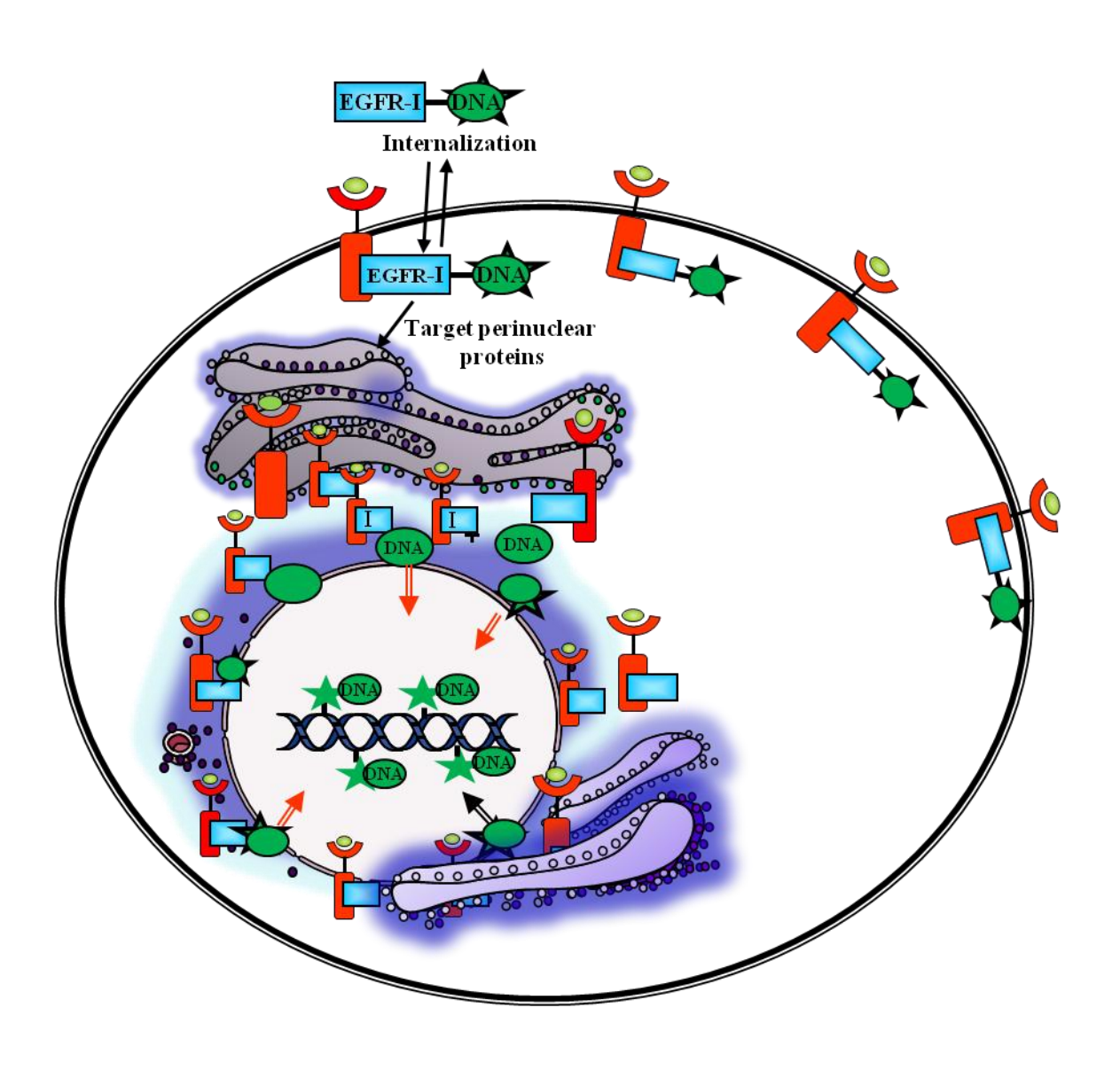


Figure 6.1. Degradation of type I combi-molecules at the perinuclear region.

nucleus allows us to hypothesize that the combi-molecule could also reach the nucleus intact. More importantly, a new revolutionary observation has suggested that EGFR translocates into the nucleus. In addition to our own work, there is now ample evidence of the perinuclear and nuclear localization of EGFR. In early 2000 Lin *et al.* [22] suggested a potential role of EGFR membrane receptor as a transcription factor and later on many additional examples for nuclear EGFR activity and its interactions with several nuclear proteins have been demonstrated [23-26]. Lo and Hung groups [27, 28] showed that EGFR transactivates the following genes (e.g., cyclin D1, iNOS, COX-2, aurora A) and that its abundance in the nucleus phosphorylated PCNA. It is believed that it is involved in the assembly of DNA repair complexes (DNA-PK, MDC1) [29-31]. These results, completed over the last ten years, support the nuclear role of EGFR and add to our observations. Thus, it allows to propose a model that does not only considers EGFR in the perinuclear region but also in the nucleus.

# 6.1.2. Contribution 2

All of the combi-molecules designed in our laboratory, as agents with increased molecular weight, are putative substrates of MDR protein, P-gp. Thus, it was important to elucidate their function in the context of P-gp-expressing cells, which have an active drug efflux mechanism. Until now, an important question for the combi-targeting principle and combi-molecules distribution remained unanswered: the role of P-gp as a molecular determinant for their activity in tumour cells [32]. The ability to trace the fluorescence emitted from the entire molecule or from its two species has been further exploited by defining whether P-gp was a determinant for the cytotoxic potentials of the combi-molecules. It is now known that several molecules of size greater than 500 are effluxed by P-gp. A typical example is taxol (MW=854) and doxorubicin (MW=543) that are actively effluxed by P-gp, thereby leading to reduced cytotoxicity against

the cells. This mechanism, also known as multidrug resistance (MDR), is very common in drug response to anti-tumour agents. We therefore sought to determine whether P-gp expression influenced cell response to AL237 (MW=632 g/mol) and AL194 (MW=575 g/mol). Their fluorescence properties were a major advantage for the combi-targeting concept that permitted the quantification of their intracellular accumulation using fluorescence cell analysis and fluorescence microscopy. These results clearly showed that the potency of AL237 and AL194 were not affected by P-gp despite their high molecular size [33]. This absence of correlation of P-gp expression and cytotoxicity may be explained by the rapid intracellular decomposition of the combi-molecules into its two targeting moiety that are not P-gp substrate. Perhaps, AL237 and AL194 penetrating by passive diffusion are localized at the perinuclear region wherein they rapidly degrade to two species (EGFR inhibitor and DNA alkylator) that are not substrates of Pgp. The absence of differential cytotoxicity between P-gp-positive and P-gp-negative cells of these molecules is an extremely important finding since P-gp expression in the clinic is the molecular determinant for response to clinically used drugs against advanced breast and prostate cancer (e.g., taxol, doxorubicin) [34, 35].

# 6.1.3. Contribution 3

The development and discovery of AL237 has also contributed to the advancement of our drug design strategy [36]. AL237 owes its EGFR binding strength to the central nitrogen in the linker, a critical structure activity relationship, that permits the appendage of bulky pharmacophores to the rest of the combi-molecule [37, 38]. Therefore, we attempted to replace the dansyl moiety in a similar manner with a flavone moiety targeting MEK, a kinase involved in the stress response pathway, which is known to activate DNA repair enzymes [39, 40]. Therefore, we designed and synthesized a three-compartment combi-molecule which upon

hydrolysis was engineered to generate (1) DNA damaging species, (2) the PD98059-like MEK inhibitor, and (3) the aminoquinazoline EGFR inhibitor. The mechanism of blocking MEK activity while damaging DNA was expected to induce a delay in DNA repair, thereby enhancing the cytotoxic potentials of the combi-molecule. The successful synthesis of this 3compartment combi-molecule AL414 has permitted the analysis of its fate in vitro and in vivo. While AL414 has shown a mechanism of action similar to that of AL237, i.e. damaging DNA and blocking EGFR, it did not behave as MEK inhibitor. Even though strong downregulation of ERK1,2 phosphorylation was observed through EGFR inhibition, AL414 was unable to block ERK1,2 phosphoryaltion by MEK inhibition in the absence of EGFR as demonstrated in EGFR-null sarcoma cells. We therefore believed that the free MEK inhibitor PD98059 might not be released from the linker and we further attempted to verify whether metabolic activation in vivo can lead to the latter species formation. Indeed, as LC/MS analysis demonstrated no free PD98059-like species was released but rather an additional metabolite was formed. This study conclusively demonstrated that another type of linker must be thoroughly investigated and designed in order to promote the release of intact MEK inhibitor.

Overall, our studies on the type I combi-molecules demonstrate that the programmed intact structures are partitioned inside the cell into distinct bioactive species, which confer selective targeting of EGFR overexpressing cells, downregulate the MAPK pathway, PI3/AKT kinases pathways and the proteins from the BER and NER (XRCC1 and ERCC1). The pleiotropic effects of combi-molecules culminate in strong apoptosis of cells expressing EGFR and ErbB2 genes.

#### 6.1.4. Contribution 4

The subsequent study was directed at investigating the mechanism of action of type II combimolecules, which were designed to execute binary targeting properties without the requirement for hydrolysis [41]. The prototype of type II combi-molecules, ZR2008, carrying a hemimustard DNA-damaging moiety, was studied in cells derived from a solid tumour traditionally treated with alkylators. Epithelial ovarian cancer cells were characterized by overexpression of signaling proteins involved in EGFR and AKT pathways. The activated EGFR family of receptors stimulate the MAPK pathway to promote growth and the PI3K/AKT pathway promotes cell survival and mechanisms involving key anti-apoptotic molecules. We found that the range of potency of type II combi-molecule was in the submicromolar levels, a range very different from the one observed with type I combi-molecules. We furthermore decided to investigate the mechanism underlying such strong cytotoxic potency and determined that ZR2008 was capable of inducing DNA damage at remarkably low concentration. Moreover, the compound triggered high levels of apoptosis in all 4 different human ovarian cells studied, a response observed independently of their EGFR and AKT status. The ability to induce apoptosis without downregulation of AKT implied the involvement of other pro-apoptotic mechanisms, independent of receptor activation or related kinase-mediated signaling. Our findings suggest that pathways leading to inhibition of survivin could contribute to the mechanisms inducing strong cell death. ZR2008 as a strong EGFR inhibitor and a potent DNAdamaging agent induced G1 early S arrest, two period of the cell cycle when survivin is at its minimum.

Overall, we have demonstrated the potency of ZR2008 to induce strong DNA damage accompanied by G1-mid S cell cycle arrest, which subsequently translated into high levels of

apoptosis in the ovarian cancer cell panel. Conclusively, the data implie the cell inability to repair the damaged DNA and to resume the cell cycle, thus resulting in enhanced cell killing.

## **6.2 CONCLUSIONS**

The work *in toto* described herein contributed to the elucidation of the mechanism of degradation and distribution of combi-molecules that selectively target EGFR-expressing cells. Furthermore, despite the high molecular size of type I combi-molecules, they retained their potency regardless of cells P-gp status, thus concluding that P-gp is not a determinant for their cytotoxic properties. As initiated by AL237 study, where two bulky pharmacophores are spaced by the triazene chain and a basic linker, our design was further extended to molecules carrying three bioactive species. The three-compartment combi-molecules AL414, in spite of its great cytotoxicity and strong EGFR inhibitory potency, was not able to release its third bioactive component. Finally, combi-molecules of type II, carrying a hemi-mustard appended to a quinazoline moiety (EGFR inhibitor, *I*) possess strong mixed EGFR-DNA targeting potentials. These agents are capable of inducing significant levels of apoptosis through mechanisms independent of AKT downregulation. Therefore, novel drugs like ZR2008 may bring new perspectives for treatment of ovarian cancer, which are characterized by constitutive AKT activation and reduced drug sensitivity.

Finally, the two prototypes of combi-molecules used here brought insight into a better characterization of agents for the combi-targeting principle.

#### **6.3 REFERENCES**

- 1. Albanell, J. and P. Gascon, *Small molecules with EGFR-TK inhibitor activity*. Current Drug Targets, 2005. **6**(3): p. 259-274.
- 2. Giaccone, G. and J.A. Rodriguez, *EGFR inhibitors: what have we learned from the treatment of lung cancer?* Nat. Clin. Pract. Oncol., 2005. **2**(11): p. 554-561.
- 3. Zimmermann, G.R., J. Lehar, and C.T. Keith, *Multi-target therapeutics: when the whole is greater than the sum of the parts.* Drug Discov Today, 2007. **12**(1-2): p. 34-42.
- 4. Hennessy, B.T., et al., *Exploiting the PI3K/AKT pathway for cancer drug discovery*. Nat Rev Drug Discov., 2005. **4**(12): p. 988-1004.
- 5. Faivre, S., G. Kroemer, and E. Raymond, *Current development of mTOR inhibitors as anticancer agents*. Nat Rev Drug Discov., 2006. **5**(8): p. 671-88.
- 6. Trachootham, D., J. Alexandre, and P. Huang, *Targeting cancer cells by ROS-mediated mechanisms: a radical therapeutic approach?* Nat Rev Drug Discov, 2009. **8**(7): p. 579-91.
- 7. Zhang, J., P.L. Yang, and N.S. Gray, *Targeting cancer with small molecule kinase inhibitors*. Nature Reviews Cancer, 2009. **9**(1): p. 28-39.
- 8. Altieri, D.C., *Survivin, cancer networks and pathway-directed drug discovery.* Nat Rev Cancer, 2008. **8**(1): p. 61-70.
- 9. Banerjee, R., et al., Synthesis of a Prodrug Designed To Release Multiple Inhibitors of the Epidermal Growth Factor Receptor Tyrosine Kinase and an Alkylating Agent: A Novel Tumor Targeting Concept. J. Med. Chem., 2003. **46**(25): p. 5546-5551.
- 10. Katsoulas, A., et al., Combi-targeting concept: an optimized single-molecule dual-targeting model for the treatment of chronic myelogenous leukemia. Molecular Cancer Therapeutics, 2008. **7**(5): p. 1033-1043.
- 11. Matheson, S.L., J. McNamee, and B.J. Jean-Claude, *Design of a chimeric 3-methyl-1,2,3-triazene with mixed receptor tyrosine kinase and DNA damaging properties: a novel tumor targeting strategy.* J. Pharmacol. Exp. Ther., 2001. **296**(3): p. 832-840.
- 12. Merayo, N., et al., *The combi-targeting concept: evidence for the formation of a novel inhibitor in vivo*. Anti-Cancer Drugs, 2006. **17**(2): p. 165-171.
- 13. Qiu, Q., et al., The Combi-Targeting Concept: In vitro and In vivo Fragmentation of a Stable Combi-Nitrosourea Engineered to Interact with the Epidermal Growth Factor Receptor while Remaining DNA Reactive. Clin. Cancer Res., 2007. **13**(1): p. 331-340.
- 14. Marchesi, F., et al., *Triazene compounds: mechanism of action and related DNA repair systems.* Pharmacol Res, 2007. **56**(4): p. 275-87.

- 15. Matheson, S.L., F. Brahimi, and B.J. Jean-Claude, *The combi-targeting concept: intracellular fragmentation of the binary epidermal growth factor (EGFR)/DNA targeting "combi-triazene" SMA41*. Biochemical Pharmacology, 2004. **67**(6): p. 1131-1138.
- 16. Matheson, S.L., J.P. McNamee, and B.J. Jean-Claude, *Differential responses of EGFR-AGT-expressing cells to the "combi-triazene" SMA41*. Cancer Chemoth. Pharm., 2003. **51**(1): p. 11-20.
- 17. Matheson, S.L., et al., *The combi-targeting concept: Dissection of the binary mechanism of action of the combi-triazene SMA41 in vitro and antitumor activity in vivo.* J. Pharmacol. Exp. Ther., 2004. **311**(3): p. 1163-1170.
- 18. Banerjee, R., et al., *The combi-targeting concept: selective targeting of the epidermal growth factor receptor- and Her2-expressing cancer cells by the complex combi-molecule RB24*. J Pharmacol Exp Ther, 2010. **334**(1): p. 9-20.
- 19. Caffo, O., et al., Estramustine plus docetaxel as second-line therapy in patients with hormone-refractory prostate cancer resistant to docetaxel alone. Urol Oncol. **28**(2): p. 152-6.
- 20. Rosenthal, S.A., et al., *Phase III multi-institutional trial of adjuvant chemotherapy with paclitaxel, estramustine, and oral etoposide combined with long-term androgen suppression therapy and radiotherapy versus long-term androgen suppression plus radiotherapy alone for high-risk prostate cancer: preliminary toxicity analysis of RTOG 99-02.* Int J Radiat Oncol Biol Phys, 2009. **73**(3): p. 672-8.
- 21. Tew, K.D., et al., *Cytotoxicity of estramustine, a steroid-nitrogen mustard derivative, through non-DNA targets.* Mol Pharmacol 1983. **24**(2): p. 324-8.
- 22. Lin, S.Y., et al., *Nuclear localization of EGF receptor and its potential new role as a transcription factor.* Nat Cell Biol, 2001. **3**(9): p. 802-8.
- 23. Lo, H.W., et al., *Novel prognostic value of nuclear epidermal growth factor receptor in breast cancer.* Cancer Res, 2005. **65**(1): p. 338-48.
- 24. Lo, H.W., S.C. Hsu, and M.C. Hung, *EGFR signaling pathway in breast cancers: from traditional signal transduction to direct nuclear translocalization.* Breast Cancer Res Treat, 2006. **95**(3): p. 211-8.
- 25. Kim, J., et al., *The phosphoinositide kinase PIKfyve mediates epidermal growth factor receptor trafficking to the nucleus.* Cancer Res, 2007. **67**(19): p. 9229-37.
- 26. Dittmann, K., et al., *Radiation-induced lipid peroxidation activates src kinase and triggers nuclear EGFR transport.* Radiother Oncol, 2009. **92**(3): p. 379-82.
- 27. Hung, L.-Y., et al., Nuclear epidermal growth factor receptor (EGFR) interacts with signal transducer and activator of transcription 5 (STAT5) in activating Aurora-A gene expression. Nucl. Acids Res., 2008. **36**(13): p. 4337-4351.

- 28. Lo, H.W. and M.C. Hung, *Nuclear EGFR signalling network in cancers: linking EGFR pathway to cell cycle progression, nitric oxide pathway and patient survival.* Br J Cancer, 2006. **94**(2): p. 184-8.
- 29. Lo, H.W., *Nuclear mode of the EGFR signaling network: biology, prognostic value, and therapeutic implications.* Discov Med, 2010. **10**(50): p. 44-51.
- 30. Lo, H.W., et al., Nuclear interaction of EGFR and STAT3 in the activation of the iNOS/NO pathway. Cancer Cell, 2005. **7**(6): p. 575-89.
- 31. Hung, L.Y., et al., Nuclear epidermal growth factor receptor (EGFR) interacts with signal transducer and activator of transcription 5 (STAT5) in activating Aurora-A gene expression. Nucleic Acids Res, 2008. **36**(13): p. 4337-51.
- 32. Aller, S.G., et al., Structure of P-Glycoprotein Reveals a Molecular Basis for Poly-Specific Drug Binding. Science (Washington, DC, U. S.), 2009. **323**(5922): p. 1718-1722.
- 33. Larroque-Lombard, A.L., et al., Synthesis and uptake of fluorescence-labeled Combimolecules by P-glycoprotein-proficient and -deficient uterine sarcoma cells MES-SA and MES-SA/DX5. J Med Chem, 2010. **53**(5): p. 2104-13.
- 34. Mechetner, E., et al., Levels of multidrug resistance (MDR1) P-glycoprotein expression by human breast cancer correlate with in vitro resistance to taxol and doxorubicin. Clin Cancer Res, 1998. **4**(2): p. 389-98.
- 35. Advani, R., et al., A phase I trial of liposomal doxorubicin, paclitaxel and valspodar (PSC-833), an inhibitor of multidrug resistance. Ann Oncol, 2005. **16**(12): p. 1968-73.
- 36. Todorova, M.I., et al., Subcellular distribution of a fluorescence-labeled combimolecule designed to block epidermal growth factor receptor tyrosine kinase and damage DNA with a green fluorescent species. Mol Cancer Ther, 2010. **9**(4): p. 869-82.
- 37. Larroque, A.-L., et al., Synthesis of water soluble bis-triazenoquinazolines: an unusual predicted mode of binding to the epidermal growth factor receptor tyrosine kinase. Chemical Biology & Drug Design, 2008. **71**(4): p. 374-379.
- 38. Rachid, Z., et al., *Optimization of novel combi-molecules: identification of balanced and mixed bcr-abl/DNA targeting properties.* Bioorg Med Chem Lett., 2007. **17**(15): p. 4248-53.
- 39. Yacoub, A., et al., Epidermal growth factor and ionizing radiation up-regulate the DNA repair genes XRCC1 and ERCC1 in DU145 and LNCaP prostate carcinoma through MAPK signaling. Radiation research, 2003. **159**(4): p. 439-52.
- 40. Davis, R.J., Signal transduction by the JNK group of MAP kinases. Cell, 2000. **103**(2): p. 239-52.

41. Rachid, Z., et al., *Synthesis of half-mustard combi-molecules with fluorescence properties: correlation with EGFR status.* Bioorganic & Medicinal Chemistry Letters, 2005. **15**(4): p. 1135-1138.

#### **APPENDIX**

**Appendix 1.** List of cell lines used.

**Appendix 2.** Alkylating agents used in the clinic, information from National Cancer Institute drug dictionary (http://www.cancer.gov/drugdictionary).

**Appendix 3.** Paper published in Molecular Cancer Therapeutics: 2010, **9** (4) p. 869-882.

Appendix 4. Paper published in Journal of Medicinal Chemistry: 2010, 53 (5): p. 2104-13.

**Appendix 5.** Authors signature forms.

**Appendix 6.** Certificate for working with biohazards and chemicals.

.

**Appendix 1.** List of cell lines used

Name of cell line	ATCC catalogue	Origin/mutations harboured	Media
	number		
MDA-MB-468	HTB-132	Human breast carcinoma, PTEN -, DMEM EGFR-high expression	
DU145	HTB-81	Human prostate carcoma, p53 mutant	RPMI
OVCAR-3	HTB-161	Human serous carcinoma	OSE
TOV21G	CRL-11730	Human ovarian epithelial clear cell carcinoma, p53 wild type	OSE
TOV112D	CRL-11731	Human ovarian endometrioid adenocarcinoma	OSE
OV90	CRL-11732	Human ovarian malignant ascites	OSE
MES-SA	CRL-1976	Uterine sarcoma, doxorubicin sensitive, P-gp/ EGFR-negative	McCoy 5A
MES-SA/DX5	CRL-1977	Uterine sarcoma, doxorubicin resistant, P-gp-positive, EGFR-negative	McCoy 5A
NIH 3T3 wild type	CRL-2795	Mouse fibroblast	DMEM
NIH 3T3-her14		EGFR transfected mouse fibroblasts	DMEM
NIH 3T3-neu		ErbB2 transfected mouse fibroblasts	DMEM
HCT116	CCL-247	Colon carcinoma, p53 WT, ras mutant	RPMI
HT29	HTB-38	Colon adenocarcinoma, myc +; ras +; myb +; fos +; p53 +; src -	DMEM

**Appendix 2.** Alkylating agents used in the clinic.

DNA targeting compounds	Effect on DNA and mechanism of action	Clinical trials/ cancers treated
Dacarbazine/ Imidazole	A triazene derivative, alkylates and cross-links DNA during all phases of the cell cycle, resulting in disruption of DNA function, cell cycle arrest, and apoptosis.	III/IV- neuroblastoma III-lymphoma
Temozolomide	A triazene analog of dacarbazine. Alkylating agent converted at physiologic pH to the short-lived active compound, monomethyl triazeno imidazole carboxamide (MTIC). The cytotoxicity of MTIC is due primarily to methylation of DNA at the O6 and N7 positions of guanine, resulting in inhibition of DNA replication. Unlike dacarbazine, which is metabolized to MITC only in the liver, temozolomide is metabolized to MITC at all sites. Temozolomide is administered orally and penetrates well into the central nervous system	III- glioma II/III-NSCLC- brain metastasis II/III-children brain tumours
Adozelesin	An alkylating agent that binds to the DNA minor groove in a sequence-specific manner and forms covalent adducts with adenines, resulting in the inhibition of DNA replication and induction of apoptosis.	Closed II-breast II-SCLC
BCNU/carmustine Lomustine	A nitrosourea that alkylates and cross-links DNA during all phases of the cell cycle, resulting in disruption of DNA function, cell cycle arrest, and apoptosis. This agent also carbamoylates proteins, including <b>DNA repair enzymes</b> , resulting in an enhanced cytotoxic effect. It is highly lipophilic and crosses the blood-brain barrier readily.	III-lymphoma III-gliomas III-glioblastomas II- medulloblastoa ma
Ifosfamide	A synthetic analogue of the nitrogen mustard cyclophosphamide with antineoplastic activity. Ifosfamide alkylates and forms DNA crosslinks, preventing DNA replication. This agent is a prodrug that must be activated through hydroxylation by	IV-Lymphoma, B-ALL III/IV- neuroblastoma

	hepatic microsomal enzymes	III-osteosarcoma
Mitomycin C	Mitomycin C is a methyl-azirino-pyrroloindoledione antineoplastic antibiotic isolated from the bacterium Streptomyces caespitosus and other Streptomyces bacterial species. Bioreduced mitomycin C generates oxygen radicals, alkylates DNA, and produces interstrand DNA cross-links, thereby inhibiting DNA synthesis. Preferentially toxic to hypoxic cells, mitomycin C also inhibits RNA and protein synthesis at high concentrations	IV-liver metastasis of colorectal cancer III-bladder cancer III- hepatocellular carcinoma, metastatic breast cancer
Chlorambucil	An aromatic nitrogen mustard, alkylates and cross- links DNA during all phases of the cell cycle, resulting in disruption of DNA function, cell cycle arrest, and apoptosis	II/III/IV-CLL, NHL, lymphomas
Cyclophosphamide	A synthetic alkylating agent,related to the nitrogen mustards with antineoplastic and immunosuppressive activities. In the liver, it is converted to the active metabolites aldophosphamide and phosphoramide mustard, which bind to DNA, thereby inhibiting DNA replication and initiating cell death.	IV-CLL, ALL II/III-AML, lung, breast II/III-myeloma IV-breast cancer
Bendamustine	A bifunctional mechlorethamine derivative with alkylator and antimetabolite activities. Bendamustine possesses three active moieties: an alkylating group; a benzimidazole ring, which may act as a purine analogue; and a butyric acid side chain. Exact mechanism of action is still unknown, it appears to act primarily as an alkylator. Bendamustine metabolites alkylate and crosslink macromolecules, resulting in DNA, RNA and protein synthesis inhibition, and apoptosis. Bendamustine differs from other alkylators in that it may be more potent in activating p53-dependent stress pathways and inducing apoptosis; it may induce mitotic catastrophe; and it may activate a base excision DNA repair pathway rather than an alkyltransferase DNA repair. Accordingly, this agent	IV-leukemia III-B-CLL, NHL I/II- breast cancer I/II-lung cancer I/II-multiple myeloma

	may be more efficacious and less susceptible to drug resistance than other alkylators	
Melphalan	Orally available phenylalanine derivative of nitrogen mustard. Upon administration, melphalan is converted into highly reactive ethylenimmonium intermediates that induce covalent guanine N7-N7 intra- and intercrosslinks, alkylation of DNA at the N7 position of guanine, N3 of adenine. RNA and proteins may also be alkylated. Subsequently, RNA transcription and protein synthesis are inhibited, resulting in cell growth arrest, overall cytotoxicity against both dividing and non-dividing tumour cells.	III/IV neuroblastoma II/III-myeloma
Mechlorethamine	A nitrogen mustard and an analogue of sulfur mustard, with antineoplastic and immunosuppressive activities. It is metabolized to an unstable, highly reactive ethyleniminium intermediate that alkylates DNA, particularly the N7 position of guanine residues, resulting in DNA base pair mismatching, DNA interstrand crosslinking, the inhibition of DNA repair and synthesis, cell-cycle arrest, and apoptosis.	II, pediatric Hodgkin lymphomas
streptozotocin	A methylnitrosourea isolated from the bacterium Streptomyces achromogenes, alkylates DNA, forming inter-strand DNA cross-links and inhibiting DNA synthesis. Due to its glucose moiety, this agent is readily taken up by pancreatic beta cells, inducing diabetes mellitus at high concentrations. Unlike other nitrosoureas, streptozocin causes little myelosuppression.	II, metastatic neuroendocrine tumours

<sup>\*</sup>Information retrieved from National Cancer Institute, 2010 (<a href="http://www.cancer.gov">http://www.cancer.gov</a>)

Research Article

Molecular Cancer Therapeutics

# Subcellular Distribution of a Fluorescence-Labeled Combi-Molecule Designed to Block Epidermal Growth Factor Receptor Tyrosine Kinase and Damage DNA with a Green Fluorescent Species

Margarita I. Todorova<sup>1</sup>, Anne-Laure Larroque<sup>1</sup>, Sabine Dauphin-Pierre<sup>1</sup>, You-Qiang Fang<sup>1,2</sup>, and Bertrand J. Jean-Claude<sup>1</sup>

#### **Abstract**

To monitor the subcellular distribution of mixed epidermal growth factor (EGF) receptor (EGFR)-DNA targeting drugs termed combi-molecules, we designed AL237, a fluorescent prototype, to degrade into a green fluorescent DNA damaging species and FD105, a blue fluorescent EGFR inhibitor. Here we showed that AL237 damaged DNA in the 12.5 to 50 µmol/L range. Despite its size, it blocked EGFR phosphorylation in an enzyme assay ( $IC_{50} = 0.27 \,\mu\text{mol/L}$ ) and in MDA-MB468 breast cancer cells in the same concentration range as for DNA damage. This translated into inhibition of extracellular signal-regulated kinase 1/2 or BAD phosphorylation and downregulation of DNA repair proteins (XRCC1, ERCC1). Having shown that AL237 was a balanced EGFR-DNA targeting molecule, it was used as an imaging probe to show that (a) green and blue colors were primarily colocalized in the perinuclear and partially in the nucleus in EGFR- or ErbB2-expressing cells, (b) the blue fluorescence associated with FD105, but not the green, was colocalized with anti-EGFR redlabeled antibody, (c) the green fluorescence of nuclei was significantly more intense in NIH 3T3 cells expressing EGFR or ErbB2 than in their wild-type counterparts (P < 0.05). Similarly, the growth inhibitory potency of AL237 was selectively stronger in the transfectants. In summary, the results suggest that AL237 diffuses into the cells and localizes abundantly in the perinuclear region and partially in the nucleus where it degrades into EGFR and DNA targeting species. This bystander-like effect translates into high levels of DNA damage in the nucleus. Sufficient quinazoline levels are released in the cells to block EGF-induced activation of downstream signaling. Mol Cancer Ther; 9(4); 869–82. ©2010 AACR.

#### Introduction

The epidermal growth factor (EGF) receptor (EGFR) and its closest family member p185<sup>neu</sup>, the product of the HER2 gene, are transmembrane receptor tyrosine kinases (TK), which transduce signals associated with tumor cell proliferation (1–4). The variety of approaches currently used to target EGFR includes small monoclonal antibody strategy to block ligand binding and TK inhibitors (5–7). Over the past 10 years, molecules that inhibit

Authors' Affiliations: ¹Cancer Drug Research Laboratory, Department of Medicine, Division of Medical Oncology, McGill University/Royal Victoria Hospital, Montreal, Quebec, Canada and ²Department of Urology of the Third Affiliated Hospital, Sun Yat-Sen University, Guangzhou, China

**Note:** Supplementary material for this article is available at Molecular Cancer Therapeutics Online (http://mct.aacrjournals.org/).

Corresponding Author: Bertrand J. Jean-Claude, Cancer Drug Research Laboratory, Department of Medicine, Division of Medical Oncology, McGill University/Royal Victoria Hospital, 687 Pine Avenue West, Montreal, Quebec, Canada H3A 1A1. Phone: 1-514-934-1934 x 35841; Fax: 1-514-843-1475. E-mail: bertrandj.jean-claude@mcgill.ca

doi: 10.1158/1535-7163.MCT-09-0673

©2010 American Association for Cancer Research.

receptor autophosphorylation and downstream intracellular signaling have been developed and have shown significant antitumor activity in vitro (8-12). Several of them including gefitinib (Iressa), erlotinib (Tarceva), and lapatinib (Tykerb/Tyverb) have been approved for clinical use (13, 14). However, none of these drugs are used in the clinic as single agents in the therapy of advanced cancers (15, 16). Despite their ability to block growth signaling associated with EGFR or p185<sup>neu</sup>, cancer cells have the ability to evade the growth inhibitory effect of these drugs by activating alternative signaling pathways. Moreover, these drugs are reversible inhibitors, indicating that the tumor cells may resume proliferation following drug clearance. Therefore, for an effective therapy, combination with a drug capable of killing the cell by a different mechanism (e.g., DNA damage or inhibition of DNA synthesis) is required. However, despite this overwhelming reality of cancer therapy, the development of mono-targeted drugs through high throughput screening or rational drug design remains the most generally adopted strategy. Over the past several years, we have developed a paradigm shifting strategy that seeks to design a single molecule with multiple functions

termed combi-molecule (17–22). These molecules, despite their combination-based design, were not developed with the purpose of eventually replacing the traditional chemotherapy but rather complementing it. Albeit, we showed that many prototypes (e.g., SMA41, FD137) showed stronger antiproliferative activity than classic combinations of drugs with the same mechanism of action (20, 23–26).

As outlined in Fig. 1A, the combi-molecules (see I-Alk) were designed to bind to EGFR on their own and to decompose into another EGFR inhibitor (I) plus a DNA alkylating species (Alk). Previous studies from our labo-

ratory have shown that indeed the combi-molecules (e.g., SMA41; Fig. 1A) could directly block EGFR in short exposure assay *in vitro* at room temperature in serum-containing media (18). Additionally, we showed that they are capable of blocking EGFR phosphorylation and significantly damaging DNA in human tumor cells *in vitro* and *in vivo*, indicating that our combi-molecules induce a bifunctional activity in whole cells (22, 27). Using the fluorescence of the generated inhibitor I (excitation, 294 nm; emission, 451 nm) and <sup>14</sup>C-radiolabeled alkyl moiety of SMA41, we previously confirmed that the combi-molecule could indeed decompose in the intracellular

Figure 1. A, schematic representation of the combi-targeting concept. B, stepwise decomposition of AL237. I-Alk-Dansyl, to generate EGFR inhibitor (I, FD105) and dansylated alkylating DNA species (Alk-Dansyl). The entire AL237 molecule and the dansylated DNA damaging species both emit at 525 nm (green).

compartment into an EGFR inhibitor (I) and a methyldiazonium species (Alk) that damages DNA (27, 28). Whereas the fluorescence property of the aminoquinazoline (I) permitted the observation of its subcellular distribution or localization, that of the short-lived [14C]methyldiazonium could not be imaged (28). Here we designed a novel probe, AL237, in which the fluorescent dansyl tag is attached to a 3-alkyl triazene moiety (Fig. 1B; I-Alk-Dansyl), which when hydrolysed will release a fluorescent alkylating agent (see Alk-Dansyl). Alkylation of DNA by this fluorescent alkylating molecule (see Fig. 1B) would lead to green nuclei (excitation, 340 nm; emission, ~525 nm), and the release of the aminoquinazoline (I, FD105; excitation, 294 nm; emission, 451 nm) would generate blue areas in the cells. Thus, fluorescence microscopy would allow us to image the complete fragmentation of the combi-molecule and its colocalization with one of its targets, EGFR, using immunofluorescence. Here, we test these hypotheses with AL237 and correlate its biodistribution profile with its dual mechanism of action. For purpose of comparison, a nonconjugated dansylated alkyl agent, N-dansylaziridine, was used (see structure in Fig. 5C). The latter, as previously reported, can only alkylate nucleic acids (29). It is to be noted that this study does not seek to establish the growth inhibitory potency of AL237 but rather to show its binary EGFR-DNA targeting property and to be used as a probe to image the subcellular localization of the two bioactive degradation products responsible for its EGFR-DNA binary targeting mechanism.

#### **Materials and Methods**

#### Cell culture

MDA-MB-468 human breast carcinomas were obtained from American Type Culture Collection. Mouse fibroblast cells NIH 3T3 used as control or NIH 3T3her14 (transfected with erbB1/EGFR gene) and NIH 3T3neu (transfected with erbB2 gene) were provided by Dr. Moulay Aloui-Jamali (Montreal Jewish General Hospital). All cells were maintained in DMEM supplemented with 10% fetal bovine serum, 10 mmol/L HEPES, 2 mmol/L Lgutamine, and antibiotics (all reagents were purchased from Wisent, Inc.) as previously described (18). Cells were maintained at exponential growth at 37°C in a humidified environment with 5% CO<sub>2</sub>. In all assays cells were plated 24 h before drug administration.

#### **Drug treatment**

AL237 and JDA41 were synthesized in our laboratory. The methods used for AL237 and JDA41 complete synthesis were described elsewhere (22, 30). N-dansylaziridine was purchased from Biomol, and Temozolomide and Iressa were purchased from the hospital pharmacy and extracted from pills in our laboratory. EGF was obtained from Roche Molecular Diagnostics. In all assays, drugs were dissolved in DMSO and subsequently diluted in phenol red/fetal bovine serum-free DMEM before added to cells. The concentration of DMSO never exceeded 0.2% (v/v) during treatment.

#### Growth inhibition assay

Cells were plated in 96-well flat-bottomed microtiter plates at 5,000 cells per well (NIH 3T3her14, NIH 3T3neu, MDA-MB-468) or 10,000 cells per well (NIH 3T3). After 24 h cells were exposed to different drug concentrations for 4 d. Briefly, following drug treatment, cells were fixed with 10% ice-cold trichloroacetic acid for 60 min at 4°C, stained with sulforhodamine B (0.4%) for 4 h at room temperature, rinsed with 1% acetic acid, and allowed to dry overnight (31). The sulforhodamine B absorbance was recorded at 492 nm using a Bio-Rad microplate reader. The results were analyzed by GraphPad Prism (GraphPad Software, Inc.), and the sigmoidal dose response curve was used to determine IC<sub>50</sub>. Each point represents the average of at least three independent experiments run in triplicate.

#### In vitro enzyme assay

The EGFR and src kinase assays are similar to one described previously (27). Briefly, the kinase reaction was done in 96-well plates using 4.5 ng/well EGFR or src (Biomol). Following drug addition (range, 0.0001-10 µmol/L), phosphorylation of the EGFR was initiated by supplementing the reaction with ATP. The phosphorylated substrate was detected using a horseradish peroxidase-conjugated anti-phospho-tyrosine antibody (Santa Cruz Biotechnology), and the colorimetric reaction was monitored at 450 nm using a Bio-Rad reader. The results were analyzed by GraphPad Prism, and IC50 was calculated.

#### Western blot analysis

Cells were grown to 80% confluence in six-well plates and serum starved for 24 h (serum-free DMEM), followed by a 2-h incubation with AL237 at the indicated concentrations. Cells were washed from the drug with PBS, and then cells were stimulated with EGF (50 ng/mL) for 15 min. Cells were collected and lysed in ice-cold protein extraction buffer for 30 min [20 mmol/L Tris-HCl (pH 7.5), 1% NP40, 10 mmol/L EDTA, 150 mmol/L NaCl, 20 mmol/L NaF, 1 mmol/L Na vanadate, complete protease inhibitor cocktail (Roche Molecular Diagnostics)]. Equal amounts of proteins were separated on 10% SDS-polyacrylamide gels and then transferred to a polyvinylidene difluoride membrane (Immobilon-P, Millipore). Membranes were blocked with 5% milk in TBST (20 mmol/L Tris-HCl, 137 mmol/L NaCl, 0.1% Tween 20) for 3 h. Primary antibodies used for immunodetection were dissolved in antibody buffer [5 mmol/L Tris-HCl (pH 7.5), 150 mmol/L NaCl, 0.05% (v/v) Tween 20, 0.05% (w/v) Na azide, 0.25% (w/v) gelatin] or TBST buffer as follows: anti-phospho-tyrosine (clone 4G10, Upstate; 1:1,000), anti-EGFR (sc-03, Santa Cruz; 1:1,000), anti-phospho-EGFR (Tyr<sup>1068</sup>, 1:1,000), anti-XRCC1 (33-2-5, ThermoFisher Scientific; 1:1,000), anti-ERCC1 (clone 3H11, ThermoFisher Scientific; 1:1,000), and anti-phospho- $\gamma$ H2AX (1:1,000, Abcam). Anti-phospho-extracellular signal-regulated kinase 1/2 (ERK1/2; Thr<sup>202</sup>/Tyr<sup>204</sup>; 1:4,000), anti-ERK1/2 (p44/p42 mitogen-activated protein kinase; 1:2,500), anti-phospho-BAD (Ser<sup>112</sup>; 1:1,000), anti-BAD (1:250) were obtained from Cell Signaling Technology. Anti-tubulin- $\alpha$  (clone DM1A, NeoMarkers; 1:2,000) was used as a loading control. Secondary horseradish peroxidase–conjugated antibodies were obtained from Jackson ImmunoResearch Laboratories. The bands were visualized using enhanced chemiluminescence (Amersham Bioscience). Western blot experiments were done at least twice from two independent cell treatments.

#### Alkaline comet assay

Cells were exposed to AL237 or N-dansylaziridine (0, 6.25, 12.5, 25, 50, 100  $\mu$ mol/L) for 2 h, and the alkaline comet assay was done as previously described (27, 32). During this procedure, cells were protected from direct light to minimize DNA damage. Comets were visualized at  $10\times$  magnification using Leica microscope after staining with SYBR Gold (1:10,000, Molecular Probes). DNA damage was quantified using Comet Assay IV software (Perceptive Instruments), and the degree of DNA damage was expressed as tail moments. A At minimum, 50 comets were analyzed for each cell treatment and the mean tail moments were calculated from three independent experiments.

#### **Neutral comet assay**

Cells were treated and collected as in the alkaline comet assay, embedded in agarose at the same cell density, and lysed with a neutral buffer for 2 h at room temperature [154 mmol/L NaCl, 10 mmol/L Tris-HCl (pH 7.8), 10 mmol/L EDTA, 0.5% (v/v) *N*-lauroyl-sarcosine (pH 8.0)]. Gels were soaked for 30 min in neutral Tris-borate EDTA buffer [90 mmol/L Tris-HCl (pH 7.8), 90 mmol/L boric acid, 2 mmol/L EDTA] and electrophorezed for 20 min at 20 V (33, 34). Modification of the assay permitted to retain the fluorescent dansyl tag to the sites of DNA adducts and allowed to observe nuclei without using a specific DNA staining dye.

#### Intracellular fluorescence by UV flow cytometry

NIH 3T3, NIH 3T3her14, and NIH 3T3neu were plated at  $0.5 \times 10^6$  cells per well in six-well plates, allowed to adhere overnight, and treated with AL237 (0, 6.25, 12.5, 25, 50, 100 µmol/L) for 45 min. Cells were collected, washed, and resuspended in 300 µL PBS supplemented with 1% fetal bovine serum to minimize cell clumping. Cellular fluorescence levels were measured using a Becton Dickinson LSR flow cytometer (BD Biosciences). Cells were excited with 340-nm light emitting laser, and the AL237 hydrolyzed fragments were detected as follows: the aminoquinazoline emitted at 451 nm (blue) and the dansylated DNA damaging species emitted at 525 nm (green). Fluorescence levels determined by fluorescence-

activated cell sorting were analyzed with GraphPad Prism software, and the accumulated fluorescence for each cell line was expressed as percentage of mean fluorescence over control. Four independent experiments were done in duplicate.

#### Nuclear fluorescence UV flow cytometry

NIH 3T3, NIH 3T3her14, and NIH 3T3neu were plated at  $0.5 \times 10^6$  cells per well in six-well plates, incubated overnight, and exposed for 45 min to AL237 or *N*-dansylaziridine (0, 6.25, 12.5, 25, 50, 100 µmol/L). After washing with PBS, cells were incubated in 300 µL of Vindelov solution for 15 min at 37°C [10 mmol/L Tris-HCl (pH 7.5); 10 mmol/L NaCl, 0.1% Nonidet P40 (v/v); 100 µg/mL; 50 units/mL RnaseA; ref. 35]. Nuclei were analyzed on a BD LSR flow cytometer as described earlier. A minimum of 10,000 cell nuclei were acquired per sample, and each drug concentration was done in duplicate. The fluorescence levels were quantified with Cell-Quest Pro software (Becton Dickinson), and results are reported as percentage fluorescence over control from three independent experiments.

#### Immunofluorescence of EGFR and phospho-tyrosine

MDA-MB-468 cells were plated at 60% confluence on a microcover glass (VWR) placed in a 24-well plate. Cells were starved overnight, followed by treatment with 25  $\mu$ mol/L AL237 for 2 h, and then stimulated with 50 ng/mL EGF for 15 min. Subsequently, cells were washed twice with PBS, fixed with 100% ice-cold methanol at -20°C for 5 min, followed by 1 h blocking with 5% normal goat serum. Double immunostaining was done using directly-coupled mouse anti-phosphotyrosine-FITC (1:100), mouse anti-EGFR-PE (1:100), or the appropriate IgG-PE- or IgG-FITC-conjugated controls (1:100, purchased from Santa Cruz Biotechnology, Inc.). Thereafter, cells were washed twice with PBS, stained with 5 ng/mL 4',6-diamidino-2-phenylindole solution (Sigma), and mounted with a gel mounting media (Fisher Scientific). Immunofluorescence images were captured with Leica microscope (Leica) using the appropriate filters and analyzed with Leica application suite

## Live cell fluorescence imaging of AL237 in NIH 3T3 cells

NIH 3T3, NIH 3T3her14, and NIH 3T3neu were plated at 70% confluence in six-well plates, allowed to adhere overnight, and treated with 25  $\mu$ mol/L AL237 for 2 h. At the indicated time points, cells were washed with PBS twice and images were saved with Leica DFC300FX camera with the appropriate filters.

#### Immunofluorescence of phospho-γH2AX

MDA-MB-468 cells were plated on slides and incubated overnight, followed by a treatment with 25 and 50  $\mu$ mol/L of AL237 for 2 h. Cells were fixed with 4% paraformaldehyde for 20 min and permeabilized with

0.1% Triton X-100 for 10 min, followed by 1 h blocking with 5% normal goat serum. Slides were incubated with mouse anti-phospho- $\gamma$ H2AX antibody (Abcam) for 3 h and antimouse FITC-labeled secondary antibody (Sigma) for 1 h. Typical for double-strand DNA breaks, phospho- $\gamma$ H2AX foci were observed on a fluorescent Leica microscope at 40×.

#### Annexin V/propidium iodide binding assay

MDA-MB-468 cells were plated in a six-well plate and treated with a dose range of each drug for 48 h. Thereafter, cells were harvested and incubated with Annexin V–FITC and propidium iodide (PI) using the apoptosis detection kit (BenderMedSystems, Inc.) following the protocol provided by the supplier. Annexin V–FITC

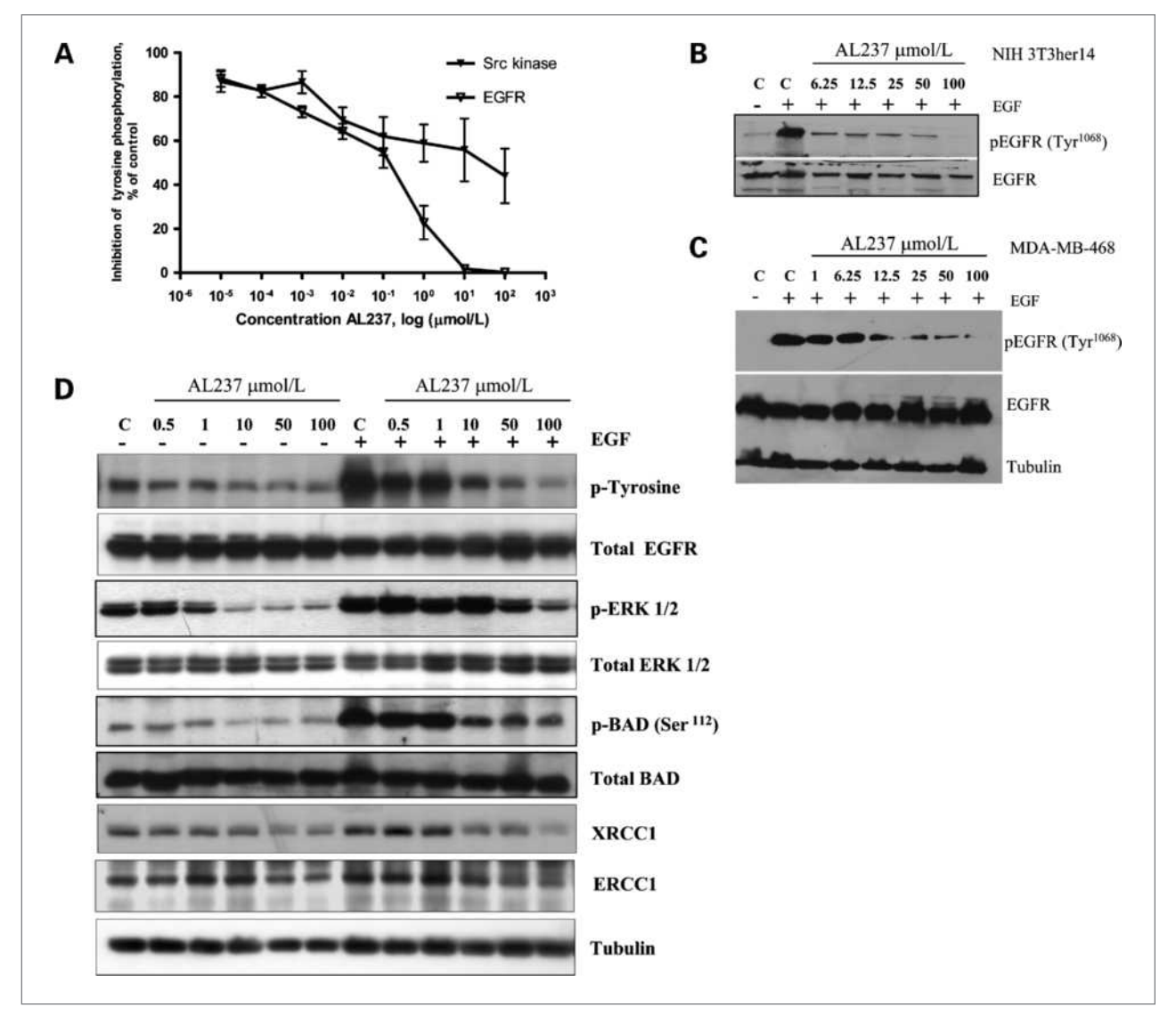


Figure 2. AL237 inhibits EGFR phosphorylation and downstream signaling. A, inhibition of EGFR and src tyrosine phosphorylation by AL237 were measured by *in vitro* binding assay. Points, mean of three independent experiments run in duplicate; bars, SD. B, inhibition of EGFR phosphorylation by AL237 was analyzed in NIH 3T3 cells transfected with EGFR (NIH 3T3her14) by Western blot. Cellular proteins were isolated after exposure to increasing AL237 concentrations for 2 h, followed by EGF stimulation (50 ng/mL). C, MDA-MB-468 cellular proteins (50 µg) were analyzed for phospho-EGFR inhibition after treatment with the indicated doses of AL237 for 2 h, followed by EGF stimulation. Membranes were incubated with anti-phospho-EGFR (Tyr<sup>1068</sup>) antibody. D, MDA-MB-468 cells were starved overnight, treated with the indicated concentrations of AL237 for 2 h, and thereafter stimulated or not stimulated with EGF (50 ng/mL) for 15 min. Afterwards, cellular proteins were analyzed by Western blot for the effect of AL237 on phospho-ERK1/2 and phospho-BAD (Ser<sup>112</sup>) protein levels followed by incubation with anti-ERK1/2 and anti-BAD antibodies. Blots were also incubated with antibodies against ERCC1 and XRCC1 to detect DNA repair proteins, and anti-tubulin antibody was used to control for equal loading. Western blots were repeated twice, and similar results from two independent treatments were obtained.

and PI binding were analyzed with a Becton Dickinson FACScan. Data were collected using logarithmic amplification of both the FL1 (FITC) and FL2 (PI) channels. Quadrant analysis of coordinate dot plots was done with CellQuestPro software.

#### Results

#### Analysis of binary EGFR-DNA targeting potentials

Inhibition of EGFR phosphorylation. For AL237, being a bulky molecule, we first determined whether the long spacer attached to the 6-position of the quinazoline ring affects its ability to inhibit receptor phosphorylation in purified EGFR enzyme assay. Our results showed that AL237 was capable of inhibiting EGFR phosphorylation with an IC<sub>50</sub> of 0.27  $\mu$ mol/L. Moreover, we have addressed AL237 selective EGFR binding by measuring inhibition of tyrosine phosphorylation on a src kinase. The result indicates that, despite its significant bulkiness, AL237 binds strongly to the ATP-binding site of EGFR and is a selective EGFR inhibitor (Fig. 2A). Indeed, varieties of similar compounds with bulky side chains have been synthesized in our laboratory and have been shown to retain strong EGFR binding affinity (23, 36, 37). It is also known that most anilinoquinazolines show unspecific binding to the ErbB2 gene product, which is the closest family member of EGFR (13). More importantly, to verify the ability of AL237 to block EGFR phosphorylation in whole cells, we analyzed phospho-EGFR levels (Tyr<sup>1068</sup>) in the two panels of EGFR-expressing cells. AL237 induced ~100% inhibition of EGFR phosphorylation at 6.25 µmol/L in NIH 3T3 EGFR transfectant (Fig. 2B) and at 12.5  $\mu$ mol/L in the MDA-MB-468 cells (Fig. 2C).

Inhibition of downstream signaling. After analyzing the effect of AL237 on EGFR phosphorylation, we further studied its role on downstream signaling in MDA-MB-468 cells by Western blotting. Cells were treated with and without EGF to determine EGF-dependent EGFR inhibition by AL237 on downstream signaling. Inhibition of EGF-induced phosphorylation of EGFR was accompanied by reduced p44/p42 mitogen-activated protein kinases (ERK1/2) and BAD (Ser<sup>112</sup>) phosphorylation (Fig. 2D). EGF-induced signaling was also accompanied by a slight downregulation of XRCC1 and ERCC1, two DNA repair proteins involved in the repair of AL237-induced DNA damage (Fig. 2D).

Induction of DNA damage in MDA-MB-468 breast cancer cells. To test the DNA damaging potency of our combi-molecule and the ability to alkylate DNA, cells were treated with AL237 for 2 hours. DNA damage was assessed by the alkaline comet assay and quantified by measuring comet tail moment using Comet Assay IV software (Fig. 3A). Strong dose-dependent DNA damage was measured with increasing AL237 concentrations, and SYBR gold-stained nuclei with typical comet tail formation were imaged (Fig. 3A). To verify if the DNA-alkylated adducts formed by AL237 resulted in the formation

of double-strand DNA breaks and the typical γH2AX foci indicative of the assembly of DNA repair protein complexes, we analyzed phospho-yH2AX activation by Western blotting and immunofluorescence. We observed a dose-dependent increase in yH2AX protein phosphorylation and the formation of 5 to 10 phospho-yH2AX foci per nucleus compared with untreated cells (Fig. 3B). This moderate increase in yH2AX phosphorylation reflects the inability of alkylating lesions to induce high levels of γH2AX accumulation or double-strand DNA breaks (38, 39). Overall, the observed strong DNA damaging potency of AL237 and its ability to block cell signaling associated with EGF stimulation confirmed that it behaved as a true combi-molecule. Having shown its dual targeting, the higher cytotoxicity induced by the combimolecule was addressed by quantitating the levels of apoptosis after 48 hours.

Induction of apoptosis in MDA-MB-468 breast cancer cells. Annexin V-FITC and PI staining were used to distinguish viable (PI-/FITC-), early apoptotic (PI-/FITC+), late apoptotic (PI+/FITC+), and necrotic (PI+/FITC-) cells after 48 hours of exposure to the combi-molecule. We observed a strong and a dose-dependent increase in apoptosis by AL237 at IC50 range reaching as high as 60% apoptotic cells 48 hours posttreatment (Fig. 3C). In contrast, much lower levels were observed when cells were exposed to 100 µmol/L Temozolomide (9%), 25 μmol/L N-dansylaziridine (12.5%), or combinations of 25 μmol/L Temozolomide and 25 μmol/L Iressa (35%; see Supplementary Fig. S1). Thus, the combined EGFR TK inhibition and DNA damaging properties of AL237 were sufficient to confer high levels of apoptosis in MDA-MB-468 cells.

Next, we used AL237 to determine its selective growth inhibition in EGFR/ErbB2-expressing cells and to image the release of its bioactive species in the intracellular compartment.

### Imaging of AL237 in MDA-MB-468 human breast cancer cells and NIH 3T3 transfectants

Imaging of MDA-MB-468 cells treated with AL237. Fluorescence emission released by AL237 was analyzed in MDA-MB-468 cells at different time points using 25 μmol/L of the drug. The two hydrolyzed degradation products were detectable in the cells as early as 5 minutes after addition, reaching a maximum 20 minutes later (Fig. 3D, top). We observed the blue fluorescence associated with the aminoquinazoline FD105 (451 nm) and the green fluorescence with the DNA damaging dansylated moiety (525 nm) in the cytoplasm and in the vicinity of the nucleus. Whereas the entire molecule can still fluoresce in green, the detection of blue FD105 fragment is indicative of a degradation of the molecule, which as reported elsewhere has a half-life of 22 minutes (30). Whether the combi-molecule was partially or completely decomposed, the green fluorescence was consistently localized in the perinuclear area (Fig. 3D, bottom left). To challenge the EGFR-directed localization of the

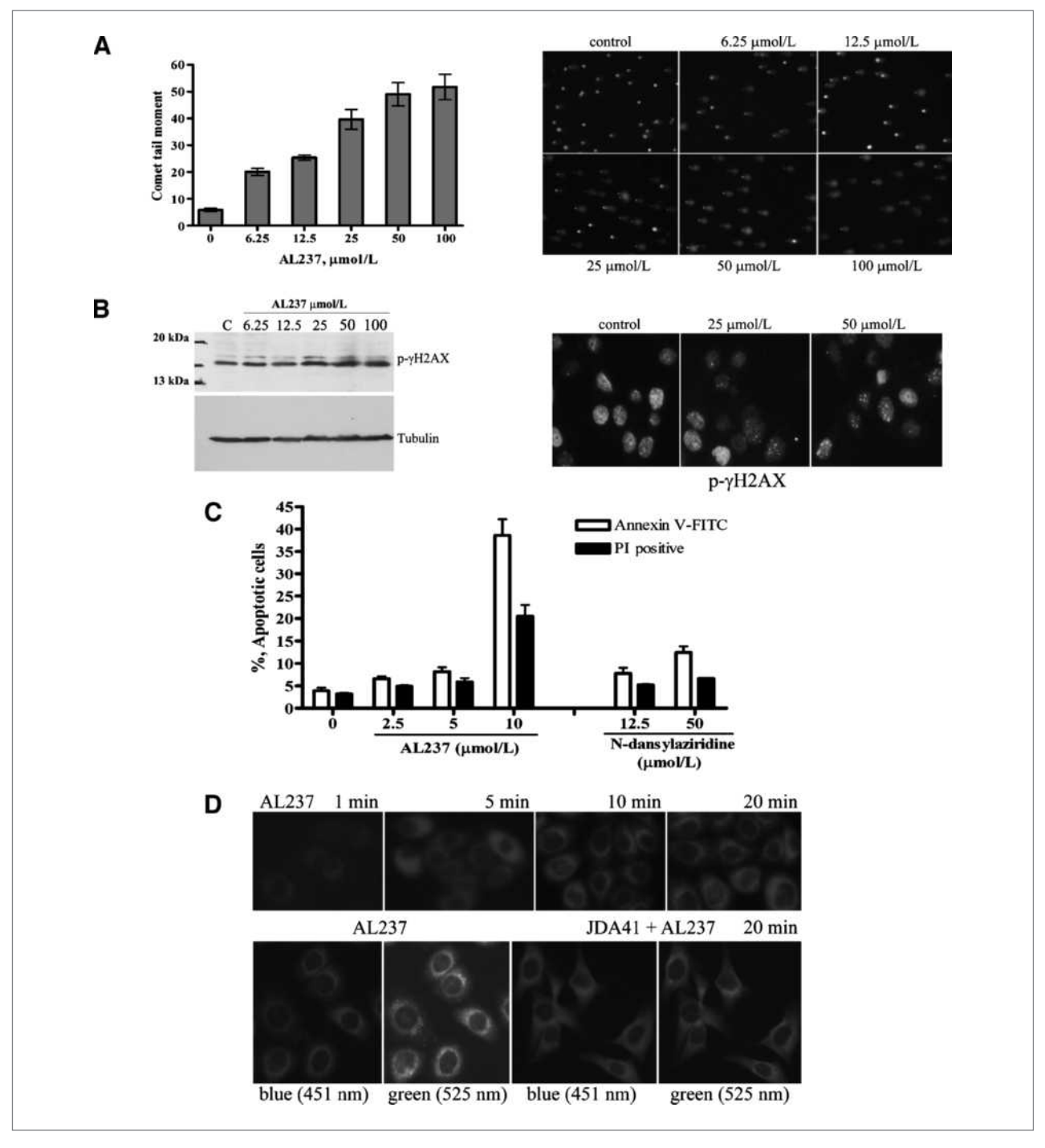
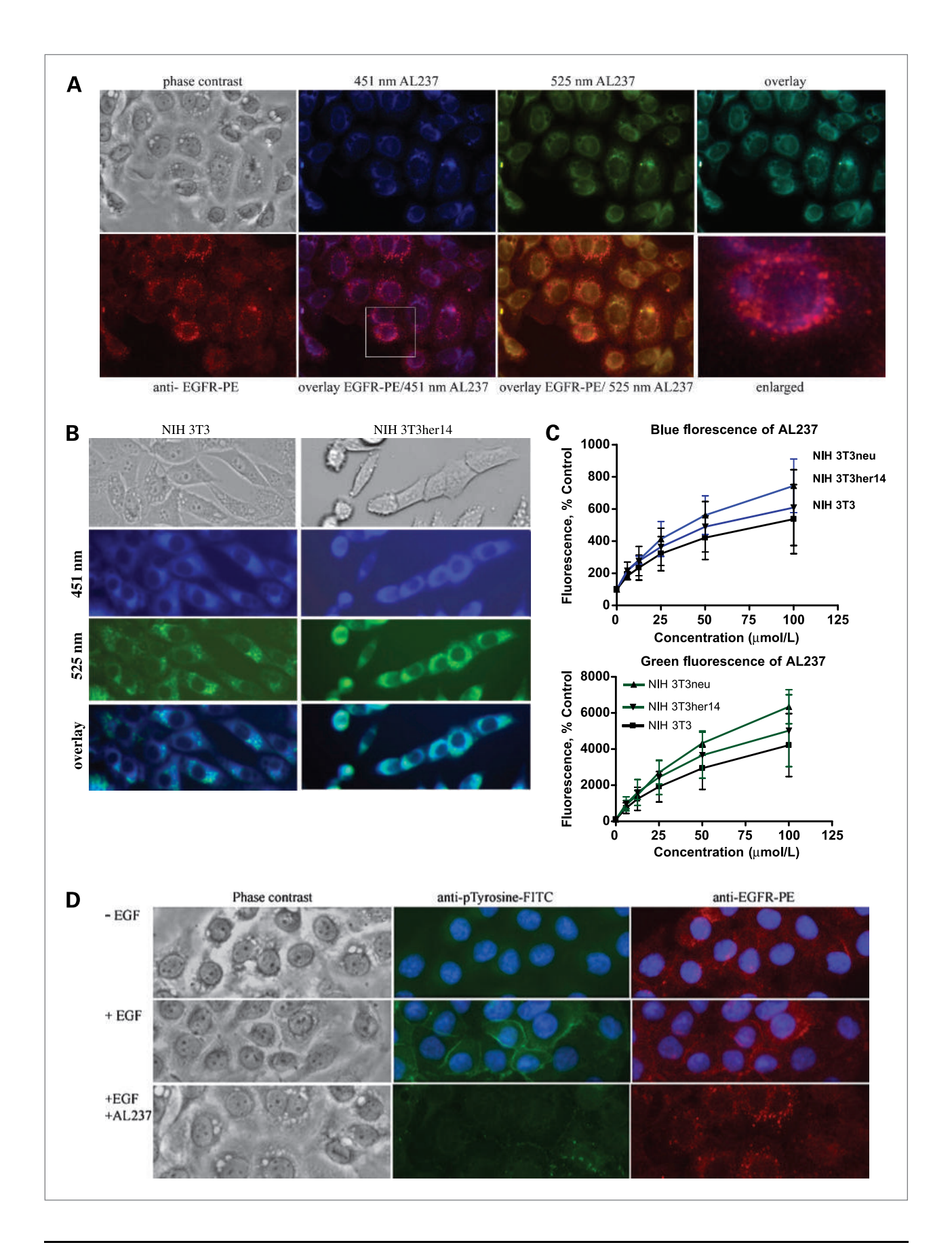


Figure 3. DNA damage induced by AL237 in MDA-MB-468. A, cells were exposed to AL237 for 2 h, followed by assessment of drug-induced DNA damage using an alkaline comet assay. Comet tail moments were quantitated by comet IV software (Perceptive Instruments). Columns, average comet tail moment calculated from 50 comets based on three independent experiments for each concentration (0, 6.25, 12.5, 25, 50, 100 mmol/L). Representative images of DNA comets stained with SYBR Gold dye and visualized by fluorescence microscopy at 10x were shown for each dose. B, extracts from cells treated for 2 h with increasing concentrations of AL237 were analyzed by Western blot with anti-phospho-γH2AX antibody. Membrane was probed with anti-tubulin antibody as a loading control. MDA-MB-468 cells were preincubated on a slide, treated with 0, 25, or 50 μmol/L of AL237, and analyzed for phospho-γH2AX foci. Cells were observed at Leica fluorescent microscope (40x) by indirect immunofluorescence using primary mouse anti-phospho-γH2AX antibodies, followed by FITC-labeled antimouse antibody. C, Annexin V/PI-stained MDA-MB-468 cells were analyzed by fluorescence-activated cell sorting 48 h after treatment with AL237 and N-dansylaziridine. D, fluorescence distribution of AL237-EGFR-binding aminoquinazoline species at 25 μmol/L was imaged over time in MDA-MB-468 cells (top). Fluorescence distribution of AL237 hydrolyzed degradation products were observed either alone (bottom left) or in the presence of equimolar concentrations (25 μmol/L) with a competitive EGFR binding nonfluorescent molecule JDA41 (bottom right) at 20 min.



combi-molecule in the perinucalear region, we used JDA41 (IC<sub>50</sub> = 0.081 mmol/L), a nonfluorescent EGFR TK inhibitor (22). The results showed that competitive exposure of AL237 (IC<sub>50</sub> = 0.27 mmol/L) with JDA41 delocalized the latter into the cytoplasm, indicating that the perinuclear colocalization may be directed by EGFR binding (Fig. 3D, bottom right).

Qualitative analyses of isogenic NIH 3T3 EGFR/ ErbB2 transfectants. AL237-released green and blue fluorescence were also observed in an isogenic context using NIH 3T3, NIH 3T3her14 (transfected with EGFR), and NIH 3T3neu (transfected with erbB2). As we have shown on the merged images in MDA-MB-468 cells (Fig. 4A, top right), in NIH 3T3 cells, the blue and green fluorescence produced by AL237 or its decomposition products were similarly colocalized in the perinuclear area or in the vicinity of the nucleus (Fig. 4B). Interestingly, in the isogenic cells, AL237 or its degradation products were colocalized, with a more pronounced perinuclear distribution in EGFR- and ErbB2-expressing cells than in their wildtype counterpart. Moreover, quantitative flow cytometric analysis of NIH 3T3, NIH 3T3her14, and NIH 3T3neu cells further confirmed at a single-cell level that AL237 decomposed in the cells and released its two fluorescent degradation products: blue fluorescence corresponding to the aminoquinazoline moiety (Fig. 4C, top graph) and green fluorescence due to the entire molecule and/or the released dansylated DNA damaging species (Fig. 4C, bottom graph).

Colocalization of EGFR and AL237 in MDA-MB-468 cells. To verify whether AL237 binds to EGFR, we used direct immunofluorescence by staining MDA-MB-468 cells with PE-labeled EGFR and FITC-labeled phospho-tyrosine antibodies. After EGF stimulation, we observed activated EGFR at the plasma membrane (Fig. 4D, middle), which was strongly inhibited after the cells were exposed for 2 hours to 25 μmol/L of AL237, a dose at which EGFR phosphorylation was also shown to be significantly depleted using Western blot analysis (see Fig. 2B and C). Whereas in EGF-stimulated

cells, the EGFR showed a more membrane localization, in AL237-treated cells, it was redistributed in the cytoplasm in endosome-like structures primarily concentrated around the perinuclear region (Fig. 4A and D, bottom right). The localization of the fluorescence is in agreement with the ability of the released blue aminoquinazoline (see Fig. 1) to bind to EGFR TK and also with that of the green dansylated alkylating species to alkylate DNA.

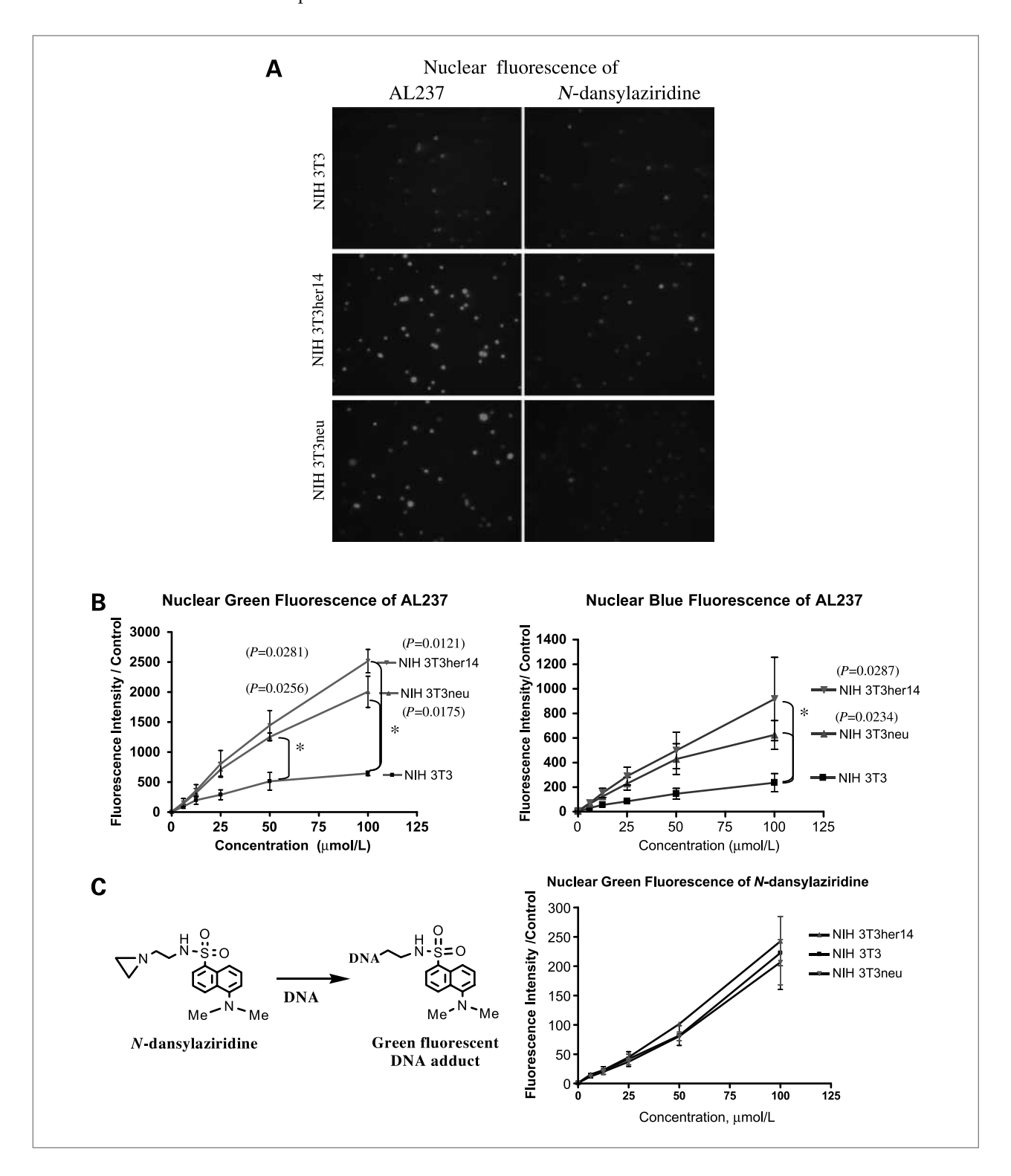
#### Selective nuclear localization and growth inhibition

Quantitative and qualitative nuclear analysis. When total subcellular fluorescence was analyzed in the isogenic cells, although the trend was toward greater fluorescence in cells transfected with EGFR and its closest homologue ErbB2, the differences in fluorescence intensity were not statistically significant when compared with the wild type (P > 0.05; Fig. 4C). However, we believed that if the primary localization of AL237 in the perinuclear region was partially due to its binding to EGFR or related proteins, concomitantly released dansylated alkylating species that covalently bind to DNA might induce high levels of green fluorescence in the nuclei of these cells. Hence, we attempted to detect the levels of green fluorescence directly bound to DNA using a neutral comet assay and flow cytometric analysis of nuclei isolated by the Vindelov method (35). Under neutral conditions, we expected the alkylated dansyl species to remain bound to nuclei, thereby allowing direct imaging of the adducted DNA. For purpose of comparison, N-dansylaziridine, a dansylated alkylating agent deprived of the quinazoline moiety required for binding to EGFR, was used. As depicted in Fig. 5, strong green fluorescence intensity was observed from nuclei of cells treated with AL237 (Fig. 5A, left), with higher intensity in EGFR and ErbB2-transfected cells. Intensities were lower with N-dansylaziridine and not selectively stronger in the transfectants (Fig. 5A, right). Quantitative flow cytometric analysis confirmed that AL237 released significantly higher levels of fluorescence in the NIH

Figure 4. Cellular fluorescence of AL237 and EGFR in MDA-MB-468, NIH 3T3, NIH 3T3her14, and NIH 3T3neu cells. A, AL237 was hydrolyzed to an aminoquinazoline fragment that emitted at 451 nm (blue), whereas the entire AL237 molecule and the dansylated DNA damaging species both emitted at 525 nm (green). Direct drug fluorescence was analyzed in MDA-MB-468 cells after 2 h of drug treatment with 25 µmol/L AL237 (top). Each fluorescent fragment was detected using individual filters on Leica fluorescent microscope (40× magnification), and the overlaid image was generated to observe colocalization of the two hydrolyzed AL237 fragments (top right). Following drug treatment, MDA-MB-468 cells were immunostained with EGFR PE-labeled antibody (red, bottom left). Merged images of AL237 (blue, EGFR inhibitor fragment) with EGFR (red) were assembled to outline the area of colocalization (magenta), and an enlarged cell is represented (bottom right). The DNA-targeting fragment of AL237 (green) was also overlaid with EGFR to observe the level of colocalization at the perinuclear and nuclear regions. B, NIH 3T3 and NIH 3T3her14 live cells were imaged to observe biodistribution of the molecule in EGFR-expressing and non-EGFR-expressing cells. This qualitative analysis was complemented by a quantitative fluorescence measurement of each AL237 species at a single-cell level. C, NIH 3T3, NIH 3T3her14, and NIH 3T3neu cells were exposed to the drug for 45 min and washed with PBS, and thereafter, each fragment fluorescence was measured by flow cytometry: The accumulated drug-associated fluorescence was measured from 10,000 cells and then normalized over the background cell fluorescence in the control. Blue fluorescence of the aminoquinazoline species (top) and green fluorescence of the dansylated alkyldiazonium fragment (bottom) were quantified for each cell type. Each point is the average value of three independent experiments done for each cell line in duplicate at each drug concentration. D, MDA-MB-468 cells were treated with 25 µmol/L AL237 for 2 h, followed by EGF stimulation, methanol fixed, and directly stained with anti-EGFR-PE and anti-phospho-tyrosine-FITC antibodies. 4',6-Diamidino-2-phenylindole stain was used to define nuclei (top and middle), but it was omitted from the samples that were drug treated because 4',6-diamidino-2-phenylindole-stained nuclei also emitted strong green fluorescence, which interfered with AL237 fluorescence (bottom).

3T3her14 and NIH 3T3neu nuclei than in their NIH 3T3 wild-type counterpart (Fig. 5B). Two- to 3-fold differences in green fluorescence intensity were observed between NIH 3T3 and ErbB2 or EGFR. Statistical analysis was done with a two-tailed unpaired t test between

NIH 3T3 and ErbB2 (at 50  $\mu$ mol/L, P = 0.0256; 100  $\mu$ mol/L, P = 0.0175) and between NIH 3T3 and EGFR (at 50  $\mu$ mol/L, P = 0.0281; 100  $\mu$ mol/L, P = 0.0121). Similarly, higher blue fluorescence intensity in the nuclei of the transfectants was observed and the



IC<sub>50</sub> of AL237, µmol/L NIH 3T3  $14.0 \pm 0.24$  $3.1 \pm 0.25$ NIH 3T3her14  $2.8 \pm 0.32$ NIH 3T3neu MDA-MB-468  $5.2 \pm 0.16$ MDA-MB-468 **B**100 -NIH 3T3 Control Control NIH 3T3neu 50 -NIH 3T3her14 % 10<sup>°</sup> 10<sup>°</sup> 10 10 10 10<sup>1</sup> 10 10 Concentration, µmol/L Concentration, µmol/L

Figure 6. Selective growth inhibition by AL237 in NIH 3T3 and MDA-MB-468 cells. IC<sub>50</sub> values of AL237 in NIH 3T3 wild type and transfectants (A) and in MDA-MB-468 cells (B) were determined by sulforhodamine B assay, and values were averaged from three independent experiments ran in triplicates.

difference when compared with the wild-type cells was statistically significant at the highest dose ( $100 \mu mol/L$ , P = 0.0287 and P = 0.0234). Importantly, no selective green fluorescence distribution was observed in nuclei from isogenic cells treated with N-dansylaziridine (Fig. 5C) that does not contain an EGFR targeting moiety. This is an indirect evidence supporting the implication of EGFR in the selective nuclear accumulation of AL237.

Selective growth inhibition of EGFR-expressing MDA-MB-468 and NIH 3T3 cells. To determine whether the binary EGFR/DNA targeting property of AL237 that showed selective biodistribution in EGFR/ErbB2 transfectants would translate into increased growth inhibitory potency on EGFR-expressing cells, we tested its growth inhibitory effect on MDA-MB-468 and NIH 3T3 transfectants (Fig. 6). AL237 showed 5-fold stronger inhibition on EGFR- and ErbB2-expressing cells than in control NIH 3T3 cells (P < 0.05, unpaired t test; Fig. 6A). AL237 also induced strong growth inhibition in the MDA-MB-468 cells that overexpress EGFR (Fig. 6B).

#### **Discussion**

The combi-molecules are a novel type of structures designed to block divergent targets in tumor cells. The growth of refractory tumors is driven by multiple signaling disorders that often cannot be blocked by the use of a single drug. The combi-molecule approach is the first that seeks to create molecules capable of blocking at least two divergent targets in the cells by allowing the intact molecules to block one target on their own and to degrade into other species directed at the same or different targets (18, 20, 22, 23, 26, 40, 41). To gain insight into the subcellular distribution and degradation of combimolecules, we designed a new prototype termed AL237 to (a) be fluorescent on its own and (b) degrade under physiologic conditions to FD105 (an EGFR inhibitor) that fluoresces in the blue and a DNA alkylating fragment that fluoresces in the green (see Fig. 1). Thus, this was designed to not only allow us to visualize the release of the EGFR inhibitor in the cells but also to image

Figure 5. Nuclear accumulation of AL237 and N-dansylaziridine in NIH 3T3, NIH 3T3her14, and NIH 3T3neu cells. A, cells were treated with 100  $\mu$ mol/L AL237 or N-dansylaziridine for 2 h. After cells were lysed and electrophoresed under neutral conditions, the nuclei of all three cell lines were analyzed by fluorescence microscopy (10 $\times$  magnification) for the accumulation of either the dansylated fragment of AL237 (left) or N-dansylaziridine control (right). B, flow cytometry analysis of NIH 3T3 cells and the transfectants treated with five doses of AL237 for 45 min. Cells were washed twice with PBS and then lysed with Vindelov's solution for single nuclei isolation. C, schematic of N-dansylaziridine used as a control and flow cytometry analysis for its nuclear accumulation in NIH 3T3 cells and the transfectants. A minimum of 10,000—cell nuclei fluorescence was measured and represented as mean fluorescence normalized over the control. AL237 green fluorescence and quinazoline-derived blue fluorescence (B) and N-dansylaziridine fluorescence (C) were calculated as mean  $\pm$  SD determined from four independent experiments done in duplicates for each drug concentration. Statistical analysis was done with a two-tailed unpaired t test; statistical significance at P < 0.05 [between NIH 3T3 and NIH 3T3neu at 50  $\mu$ mol/L (P = 0.0256), 100  $\mu$ mol/L (P = 0.0175); between NIH 3T3 and NIH 3T3her14 at 50  $\mu$ mol/L (P = 0.0281), 100  $\mu$ mol/L (P = 0.0121)] for green fluorescence. Statistical analysis for blue fluorescence intensity was significant at 100  $\mu$ mol/L dose (P = 0.0287 and P = 0.0234).

the concomitantly generated DNA damaging species. Because the green fluorescence released from the dansyl moiety attached to the intact combi-molecule is undistinguishable from that emitted by the alkylating dansyl species, the colocalization of blue and green fluorescence suggests that both the intact molecule and its dissociated DNA alkylating dansylated species may be released concomitantly and primarily in the same locations. The high intensity of the green fluorescence in the perinuclear area indicates that the combimolecules might be primarily localized and decompose to release both the aminoquinazoline inhibitor of EGFR FD105 and the DNA damaging species therein. A fraction of the combi-molecule might also decompose in the nucleus, because blue fluorescence was also detected therein. The fact that good colocalization was seen between the blue fluorescence of FD105 and red fluorescence associated with anti-EGFR antibody lends support to the ability of the released blue FD105 to bind to EGFR. Correspondingly, the poor colocalization observed for the green fluorescence associated with the dansylated alkylating DNA damaging agent with EGFR was in agreement with the inability of the latter species to bind to EGFR but rather to DNA in the nuclei.

Previous work with the <sup>14</sup>C-methyl labeled combi-molecules showed preferential perinuclear distribution of SMA42, an analogue of FD105, released from the model combi-molecule SMA41 (24). The corresponding 14C-labeled alkyl group was bound to all three major macromolecules of the cells (DNA, RNA, and protein; ref. 27). Here, the fluorescence-labeled alkyl group presents the advantage of being observable by fluorescence microscopy and being quantified by fluorescence intensity per cell or nucleus by flow cytometry. The results obtained from immunofluorescence and flow cytometric analyses indicate that the combi-molecule and its derived species, despite being abundantly distributed in the perinuclear or partially in the nuclear region, is available at high enough concentrations to block EGFR TK activity at the level of the plasma membrane, downregulate the mitogen-activated protein kinase pathway, and prevent downstream induction of DNA repair genes, such as the XRCC1 and ERCC1. Thus, it suggests that the combi-molecules simultaneously damages DNA and impairs its repair mechanism and also the phosphorylation of the proapoptotic protein BAD. Unfortunately, we were not able to image the membrane localization of AL237, perhaps due to insufficiently high population of bound combi-molecules in the latter area. However, the fact that phosphorylation of EGFR was strongly inhibited by AL237 is an indirect evidence of the presence of a fraction of the intact molecule or its derived quinazoline at the level of the membrane. It should be noted that, whereas the data suggest that EGFR overexpression is associated with elevated nucleus binding of the dansylated DNA moiety, the compound through its DNA damaging moiety is capable of damaging tumor cells that do not express EGFR

although to a lesser extent as exemplified by the NIH 3T3 wild type. This suggests that subpopulation of non–EGFR-expressing cells present in heterogeneous tumors may also be killed by the combi-moecule through its DNA damaging arm.

Importantly, we showed that the dansyl moiety is strongly bound to the nucleus, which is in agreement with the high levels of DNA damage observed by the comet assay and a slight increase in yH2AX phosphorylation and foci formation. The rather moderate increase in γH2AX phosphorylation is due to the inability of alkylating lesions to induce significant levels of double-strand DNA breaks. In term of nuclear staining, the most striking observation was the significant difference in fluorescence intensity observed between the NIH 3T3 transfectants and their wild-type counterpart. This is consistent with our previous observation of selectively high levels of DNA damage induced by the combi-molecule SMA41 in NIH 3T3 cells transfected with EGFR when compared with its wild type (42). A similar observation was made in MDA-MB-435 cells transfected with EGFR or ErbB2 (43). In this study, nuclei of cells transfected with EGFR or its closest homologue ErbB2 emitted higher green and blue fluorescence intensity than those of NIH 3T3 wild type. This can be rationalized in light of the high levels of EGFR observed in the perinuclear region. Perhaps EGFR and related proteins localized in the perinuclear region serve as anchorage from which the free dansyl alkyldiazonium moiety (see Fig. 1) can diffuse toward genomic DNA. Indeed, many reports not only described perinuclear distribution of EGFR but also its nuclear translocation (44-48). Recent studies by Dittmann et al. (48) showed that EGFR translocates to the nucleus in response to radiation-induced DNA lesions, and more importantly, the nuclear EGFR is shown to be involved in DNA repair. Our observations that Ndansylaziridine, which does not contain a quinazoline EGFR targeting moiety, does not emit higher fluorescence intensity in the transfectants is an indirect evidence of the implication of EGFR and related proteins in the selectivity of nuclear staining by AL237.

This study conclusively showed that the combimolecule AL237 is indeed an agent that (a) penetrates the cells and primarily localizes in the perinuclear region, (b) releases species that block signaling associated with EGFR activation, (c) damages DNA, and (d) significantly inhibits tumor cell growth. Thus, it behaved as a valid agent to image the distribution of not only the EGFR inhibitory but also the DNA binding species.

#### **Disclosure of Potential Conflicts of Interest**

No potential conflicts of interest were disclosed.

#### **Acknowledgments**

We thank National Cancer Institute of Canada and Canadian Institutes of Cancer Research for financial support and MUHC Research Institute

for an equipment grant that supported the acquisition of our Leica fluorescence microscope.

#### **Grant Support**

National Cancer Institute of Canada grant 018475, Canadian Institutes of Cancer Research grant FRN 49440, and Fonds de la Recherche en Santé du Québec doctoral award (M. Todorova). M. Todorova is sup-

#### References

- Slamon DJ, Clark GM, Wong SG, et al. Human breast cancer: correlation of relapse and survival with amplification of the HER-2/ neu oncogene. Science (Washington, DC) 1987;235:177–82.
- Aaronson SA. Growth factors and cancer. Science 1991;254: 1146–53.
- Modjtahedi H, Dean C. The receptor for EGF and its ligands: expression, prognostic value and target for therapy in cancer (review). Int J Oncol 1994;4:277–96.
- Normanno N, De Luca A, Bianco C, et al. Epidermal growth factor receptor (EGFR) signaling in cancer. Gene 2006;366:2–16.
- Mendelsohn J. Epidermal growth factor receptor inhibition by a monoclonal antibody as anticancer therapy. Clin Cancer Res 1997; 3:2703–7.
- Ciardiello F, Tortora G. A novel approach in the treatment of cancer: targeting the epidermal growth factor receptor. Clin Cancer Res 2001;7:2958–70.
- Albanell J, Gascon P. Small molecules with EGFR-TK inhibitor activity. Current Drug Targets 2005;6:259–74.
- Bos M, Mendelsohn J, Kim YM, et al. PD153035, a tyrosine kinase inhibitor, prevents epidermal growth factor receptor activation and inhibits growth of cancer cells in a receptor number-dependent manner. Clin Cancer Res 1997;3:2099–106.
- Moyer JD, Barbacci EG, Iwata KK, et al. Induction of apoptosis and cell cycle arrest by CP-358774, an inhibitor of epidermal growth factor receptor tyrosine kinase. Cancer Res 1997;57:4838–48.
- 10. Barker AJ, Gibson KH, Grundy W, et al. Studies leading to the identification of ZD1839 (Iressa): an orally active, selective epidermal growth factor receptor tyrosine kinase inhibitor targeted to the treatment of cancer. Bioorg Med Chem Lett 2001;11:1911–4.
- 11. Rusnak DW, Lackey K, Affleck K, et al. The effects of the novel, reversible epidermal growth factor receptor/ErbB-2 tyrosine kinase inhibitor, GW2016, on the growth of human normal and tumor-derived cell lines in vitro and in vivo. Mol Cancer Ther 2001;1:85–94.
- Normanno N, Bianco C, De Luca A, Maiello MR, Salomon DS. Target-based agents against ErbB receptors and their ligands: a novel approach to cancer treatment. Endocr Relat Cancer 2003;10:1–21.
- 13. Wissner A, Brawner Floyd M, Rabindran SK, et al. Syntheses and EGFR and HER-2 kinase inhibitory activities of 4-anilinoquinoline-3-carbonitriles: analogues of three important 4-anilinoquinazolines currently undergoing clinical evaluation as therapeutic antitumor agents. Bioorg Med Chem Lett 2002;12:2893–7.
- Moy B, Goss PE. Lapatinib: current status and future directions in breast cancer. Oncologist 2006:11:1047–57.
- 15. Huang S, Armstrong EA, Benavente S, Chinnaiyan P, Harari PM. Dual-agent molecular targeting of the epidermal growth factor receptor (EGFR): combining anti-EGFR antibody with tyrosine kinase inhibitor. Cancer Res 2004;64:5355–62.
- Baumann M, Krause M, Dikomey E, et al. EGFR-targeted anti-cancer drugs in radiotherapy: preclinical evaluation of mechanisms. Radiother Oncol 2007;83:238–48.
- Katsoulas A, Rachid Z, McNamee JP, Williams C, Jean-Claude BJ. Combi-targeting concept: an optimized single-molecule dual-targeting model for the treatment of chronic myelogenous leukemia. Mol Cancer Ther 2008;7:1033

  –43.
- Matheson SL, McNamee J, Jean-Claude BJ. Design of a chimeric 3methyl-1,2,3-triazene with mixed receptor tyrosine kinase and DNA damaging properties: a novel tumor targeting strategy. J Pharmacol Exp Ther 2001;296:832–40.

ported by Fonds de la Recherche en Santé du Québec doctoral training award.

The costs of publication of this article were defrayed in part by the payment of page charges. This article must therefore be hereby marked *advertisement* in accordance with 18 U.S.C. Section 1734 solely to indicate this fact

Received 07/23/2009; revised 12/03/2009; accepted 12/23/2009; published OnlineFirst 03/30/2010.

- 19. Brahimi F, Matheson SL, Dudouit F, et al. Inhibition of epidermal growth factor receptor-mediated signaling by "combi-triazene" BJ2000, a new probe for combi-targeting postulates. J Pharmacol Exp Ther 2002;303:238–46.
- Qiu Q, Dudouit F, Matheson SL, et al. The combi-targeting concept: a novel 3,3-disubstituted nitrosourea with EGFR tyrosine kinase inhibitory properties. Cancer Chemother Pharmacol 2003;51:1–10.
- Qiu Q, Domarkas J, Banerjee R, et al. Type II combi-molecules: design and binary targeting properties of the novel triazolinium-containing molecules JDD36 and JDE05. Anticancer Drugs 2007;18:171–7.
- 22. Qiu Q, Domarkas J, Banerjee R, et al. The combi-targeting concept: in vitro and in vivo fragmentation of a stable combi-nitrosourea engineered to interact with the epidermal growth factor receptor while remaining DNA reactive. Clin Cancer Res 2007;13:331–40.
- 23. Banerjee R, Rachid Z, McNamee J, Jean-Claude BJ. Synthesis of a prodrug designed to release multiple inhibitors of the epidermal growth factor receptor tyrosine kinase and an alkylating agent: a novel tumor targeting concept. J Med Chem 2003;46:5546–51.
- 24. Matheson SL, Brahimi F, Jean-Claude BJ. The combi-targeting concept: intracellular fragmentation of the binary epidermal growth factor (EGFR)/DNA targeting "combi-triazene" SMA41. Biochem Pharmacol 2004;67:1131–8.
- Qiu Q, Dudouit F, Banerjee R, McNamee JP, Jean-Claude BJ. Inhibition of cell signaling by the combi-nitrosourea FD137 in the androgen independent DU145 prostate cancer cell line. Prostate 2004;59: 13–21
- Domarkas J, Dudouit F, Williams C, et al. The combi-targeting concept: synthesis of stable nitrosoureas designed to inhibit the epidermal growth factor receptor (EGFR). J Med Chem 2006;49:3544–52.
- 27. Matheson SL, McNamee JP, Wang T, et al. The combi-targeting concept: dissection of the binary mechanism of action of the combi-triazene SMA41 in vitro and antitumor activity in vivo. J Pharmacol Exp Ther 2004;311:1163–70.
- Matheson SL, Mzengeza S, Jean-Claude BJ. Synthesis of 1-[4-(m-tolylamino)-6-quinazolinyl]-3-[14C]methyltriazene: a radiolabeled probe for the combi-targeting concept. J Labelled Comp Rad 2003;46:729–35.
- Broo K, Wei J, Marshall D, et al. Viral capsid mobility: a dynamic conduit for inactivation. Proc Natl Acad Sci U S A 2001;98:2274–7.
- Larroque-Lombard AL, Todorova M, Golabi N, Williams C, Jean-Claude B. Synthesis and differential uptake of fluorescence-labeled combi-molecule bu P-gp-preficient and defficient uterine sarcoma cells MFS-SA and MFS-SA/DX5. J Med Chem 2009. submitted
- Skehan P, Storeng R, Scudiero D, et al. New colorimetric cytotoxicity assay for anticancer-drug screening. J Natl Cancer Inst 1990;82: 1107–12.
- **32.** McNamee JP, McLean JR, Ferrarotto CL, Bellier PV. Comet assay: rapid processing of multiple samples. Mutat Res 2000;466:63–9.
- Olive PL, Banath JP. The comet assay: a method to measure DNA damage in individual cells. Nat Protocols 2006;1:23–9.
- Wojewodzka M, Buraczewska I, Kruszewski M. A modified neutral comet assay: elimination of lysis at high temperature and validation of the assay with anti-single-stranded DNA antibody. Mutat Res 2002;518:9–20.
- Vindelov LL. Flow microfluorometric analysis of nuclear DNA in cells from solid tumors and cell suspensions. A new method for rapid isolation and straining of nuclei. Virchows Arch B Cell Pathol 1977;24: 227–42

- 36. Rachid Z, Brahimi F, Qiu Q, et al. Novel nitrogen mustard-armed combi-molecules for the selective targeting of epidermal growth factor receptor overexperessing solid tumors: discovery of an unusual structure-activity relationship. J Med Chem 2007;50:2605–8.
- Larroque A-L, Peori B, Williams C, et al. Synthesis of water soluble bis-triazenoquinazolines: an unusual predicted mode of binding to the epidermal growth factor receptor tyrosine kinase. Chem Biol Drug Des 2008;71:374–9.
- 38. Huang X, Halicka HD, Darzynkiewicz Z. Detection of histone H2AX phosphorylation on Ser-139 as an indicator of DNA damage (DNA double-strand breaks). Curr Protoc Cytom 2004; Chapter 7: Unit 7 27.
- Kinner A, Wu W, Staudt C, Iliakis G. γ-H2AX in recognition and signaling of DNA double-strand breaks in the context of chromatin. Nucleic Acids Res 2008;36:5678–94.
- Rachid Z, Brahimi F, Katsoulas A, Teoh N, Jean-Claude BJ. The combi-targeting concept: chemical dissection of the dual targeting properties of a series of "combi-triazenes". J Med Chem 2003;46: 4313–21.
- 41. Brahimi F, Rachid Z, Qiu Q, et al. Multiple mechanisms of action of ZR2002 in human breast cancer cells: a novel combi-molecule designed to block signaling mediated by the ERB family of oncogenes and to damage genomic DNA. Int J Cancer 2004;112:484–91.

- **42.** Matheson SL, McNamee JP, Jean-Claude BJ. Differential responses of EGFR-/AGT-expressing cells to the "combi-triazene" SMA41. Cancer Chemoth Pharm 2003;51:11–20.
- 43. Banerjee R, McNamee JP, Jean-Claude BJ. The combi-targeting concept: selective targeting of the epidermal growth factor receptor (EGFR)- and Her2-expressing cancer cells by the complex combimolecule RB24 (NSC 741279). J Pharmacol Exp Ther 2009, Acceptable pending revision.
- Lin S-Y, Makino K, Xia W, et al. Nuclear localization of EGF receptor and its potential new role as a transcription factor. Nature Cell Biology 2001;3:802–8.
- 45. Lo HW, Xia W, Wei Y, et al. Novel prognostic value of nuclear epidermal growth factor receptor in breast cancer. Cancer Res 2005;65: 338–48.
- 46. Lo HW, Hsu SC, Hung MC. EGFR signaling pathway in breast cancers: from traditional signal transduction to direct nuclear translocalization. Breast Cancer Res Treat 2006;95:211–8.
- Kim J, Jahng WJ, Di Vizio D, et al. The phosphoinositide kinase PIKfyve mediates epidermal growth factor receptor trafficking to the nucleus. Cancer Res 2007;67:9229–37.
- 48. Dittmann K, Mayer C, Kehlbach R, Rothmund MC, Peter Rodemann H. Radiation-induced lipid peroxidation activates src kinase and triggers nuclear EGFR transport. Radiother Oncol 2009;92:379–82.

**2104** *J. Med. Chem.* **2010**, *53*, 2104–2113 DOI: 10.1021/jm9016043

Medicinal Chemistry
Article

## Synthesis and Uptake of Fluorescence-Labeled Combi-molecules by P-Glycoprotein-Proficient and -Deficient Uterine Sarcoma Cells MES-SA and MES-SA/DX5

Anne-Laure Larroque-Lombard,<sup>†,§</sup> Margarita Todorova,<sup>†,§</sup> Nahid Golabi,<sup>†</sup> Christopher Williams,<sup>‡</sup> and Bertrand J. Jean-Claude\*,<sup>†</sup>

†Cancer Drug Research Laboratory, Department of Medicine, Division of Medical Oncology, McGill University Health Center/Royal Victoria Hospital, 687 Pine Avenue West Room M-719, Montreal, Quebec, H3A 1A1 Canada, and <sup>‡</sup>Chemical Computing Group Inc., 1010 Sherbrooke Street West, Suite 910, Montreal, Quebec H3A 2R7, Canada. <sup>§</sup>The two authors contributed equally to this paper.

Received October 30, 2009

Here, we report on the first synthesis of fluorescent-labeled epidermal growth factor receptor—DNA targeting combi-molecules, and we studied the influence of P-glycoprotein status of human sarcoma MES-SA cells on their growth inhibitory effect and cellular uptake. The results showed that 6, bearing a longer spacer between the quinazoline ring and the dansyl group, was more stable and more cytotoxic than 4. In contrast to the latter, it induced significant levels of DNA damage in human tumor cells. Moreover, in contrast to doxorubicin, a drug known to be actively effluxed by P-gp, the more stable combi-molecule 6 induced almost identical levels of drug uptake and DNA damage in P-gp-proficient and -deficient cells. Likewise, in contrast to doxorubicin, 4 and 6 exerted equal levels of antiproliferative activity against the two cell types. The results *in toto* suggest that despite their size, the antiproliferative effects of 4 and 6 were independent of P-gp status of the cells.

#### Introduction

At the advanced stages, solid tumors express a variety of receptors and signaling proteins that not only drive their progression but also render them resistant to tumor drugs. One mechanism of multidrug resistance (MDR)<sup>a</sup> is the expression of a reflux pump [e.g., P-glycoprotein (P-gp)] that transports drugs out of the cells, <sup>1-5</sup> and this is responsible for drug resistance and treatment failure in approximately 90% of cancer patients.<sup>6,7</sup> Also, some mutations in key signaling proteins are often responsible for chemoresistance. Several attempts to modulate MDR led to a limited degree of success in the clinic, and the design of agents that diffuse into the cells regardless of their P-gp status or that selectively kill P-gp-expressing cells<sup>8</sup> has become a new drug development strategy.

Recently, to circumvent problems associated with target heterogeneity in advanced cancers, we developed novel types of drugs capable of inhibiting refractory tumor cell growth by blocking divergent targets such as the epidermal growth factor receptor (EGFR) and genomic DNA. Many prototypes of these agents termed combi-molecules have been shown to block the growth of human cancer cells with disordered signaling. While their ability to concomitantly damage DNA and to induce high levels of apoptosis was demonstrated, the influence of transport pump-mediated MDR on the potency of these multitargeted molecules has yet to be explored. To analyze their intracellular uptake and dependence on MDR status, we designed fluorescence-labeled prototypes 4 (AL194) and 6 (AL237)<sup>15</sup> and studied their differential uptake by two human uterine sarcoma cell lines (MES-SA

and MES-SA/DX5) that do not express EGFR, <sup>16</sup> the primary target of these combi-molecules. The use of cells deprived of EGFR was to avoid any interference of EGFR or related proteins with the retention or subcellular distribution of the molecules. We have now shown elsewhere that EGFR expression influences their subcellular distribution. <sup>15</sup> Importantly, in contrast to the parental MES-SA cell line, the MES-SA/DX5 has been shown to express P-gp and to be resistant to doxorubicin and paclitaxel. <sup>17–19</sup>

The new combi-molecules reported herein were designed to degrade into an aminoquinazoline, fluorescing in the blue, and a dansylated DNA-damaging moiety, fluorescing in the green, thereby facilitating the analysis of drug uptake by fluorescence microscopy and flow cytometry. The IC $_{50}$  values for EGFR tyrosine kinase inhibition by 4 and 6 were 1.4 and 0.6  $\mu$ M, respectively, and their binary EGFR—DNA targeting properties are extensively discussed in a separate report. <sup>15</sup>

Here, we describe the synthesis of the two combi-molecules, one with a short neutral ethano linker and the other with a longer and basic *N*-methylethanediamine spacer. We compared their differential uptake in MES-SA cells with that of doxorubicin, by fluorescence microscopy and flow cytometry. In contrast to the clinical anticancer drug doxorubicin, the potency of these bulky molecules was independent of the P-gp status of the two cell types. It should be noted that the purpose of this study was not to compare the potency of the fluorescent molecules with that of doxorubicin, a strong DNA intercalator and topoisomerase II inhibitor, but was rather to analyze their differential uptake in comparison with that of doxorubicin, a highly P-gp-dependent drug.

#### **Results and Discussion**

Chemistry. The synthesis of compound 4 and 6 proceeded according to Schemes 1 and 2, respectively. Commercially

<sup>\*</sup>To whom correspondence should be addressed. Tel: 514-934-1934 ext 35841. Fax: 514-843-1475. E-mail: jacques.jeanclaude@staff.mcgill.ca.

<sup>&</sup>lt;sup>a</sup>Abbreviations: P-gp, P-glycoprotein; EGFR, epidermal growth factor receptor; MDR, multidrug resistance.

#### **Scheme 1.** Synthesis of Compound $4^a$

<sup>a</sup> Reagents and conditions: (i) N-Fmoc-ethylenediamine, EtOAc, H<sub>2</sub>O, K<sub>2</sub>CO<sub>3</sub>, 0 °C. (ii) Morpholine, DMF, room temperature. (iii) Diazonium 3, Et<sub>3</sub>N, CH<sub>3</sub>CN/Et<sub>2</sub>O, -5 °C.

Scheme 2. Synthesis of Compound  $6^a$ 

available 9-fluorenylmethyl N-(2-aminoethyl)carbamate hydrochloride was treated with dansyl chloride in a biphasic ethyl acetate/aqueous potassium carbonate solution to give 1 (Scheme 1). Compound 1 was deprotected with morpholine in DMF to give the amino compound 2. In parallel, the aminoquinazoline was diazotized in dry acetonitrile with nitrosonium tetrafluoroborate to provide the diazonium salt 3 as previously described. 14 Diazonium salt 3 was coupled with 2 in the presence of triethylamine in situ to give the desired compound 4. Several attempts to purify 4 by column chromatography failed due to on-column degradation,

which we believe could be due to the conversion of 4 to a product resulting from loss of nitrogen. Successful purification was achieved by serial trituration of compound 4 with methylene chloride, ether, and petroleum ether to give a pure red-brown powder. The compound was characterized by NMR and MS, and its purity was confirmed by elemental analysis.

The synthesis of compound 6 proceeded in a similar fashion. An excess of commercially available N-(2-aminoethyl)-N-methylethanediamine was treated with dansyl chloride to give 5 in ethyl acetate at 0 °C (Scheme 2), and this

<sup>&</sup>lt;sup>a</sup> Reagents and conditions: (i) N-(2-Aminoethyl)-N-methylethanediamine, EtOAc, 0 °C. (ii) Diazonium 3, Et<sub>3</sub>N, CH<sub>3</sub>CN/Et<sub>2</sub>O, -5 °C.

Table 1. Half-Lives of Compounds 4 and 6 in a Serum-Containing Medium

Compound	4	6
t 1/2 (min)	$4.96 \pm 0.04$ *	21.72 ± 0.27*
	105- 100- 90- 90- 90- 90- 90- 90- 90- 90- 90-	105 100- 95- 90- 90- 90- 90- 90- 90- 90- 90

<sup>\*</sup> Data are means of three experiments in triplicate.

product was coupled with the diazonium salt of quinazoline 3 to give 6. The purification of 6 was as difficult as that of 4. All attempts to purify this compound by column chromatography failed. Serial trituration provided a pure red-brown powder that was analytically pure. The structure of 6 was further confirmed by NMR and MS.

Half-Life in a Serum-Containing Medium. The sole structural difference between 4 and 6 is in the nature of the linker. The linker in 4 is an ethylene group between the sulfonamido moiety of the dansyl and the N3 of the triazene, leaving no possibility for intramolecular hydrogen bonding. By contrast, the dansyl in 6 is separated by six bond lengths and contains a methylamino group three bond lengths away from the N3 of the triazene, leaving the possibility for intramolecular hydrogen bonding. Interestingly, 4 was 5-fold less stable than 6 with a half-life as short as 5 min (Table 1). Perhaps, the intramolecular interaction between the N-methylamino group and the triazene plays a significant stabilizing role. We have already evoked a similar interaction for explaining the stability of 7 (Scheme 2), a stable dimethyaminoethyl triazene with a  $t_{1/2}=108~{\rm min^{10}}$  that showed significant antitumor activity *in vivo.*<sup>20</sup> To further elaborate on the importance of the N-methylamino group on the stability of 6, we undertook a molecular modeling study using AM1 semiempirical calculation.

As outlined in Figure 1, conformer 1 containing a H-bond is computed to be  $\sim$ 2 kcal/mol more stable than conformer 2, which lacks the H-bond. Conformer 1 has the proposed H-bond (2.62 Å distance) that stabilizes it. The H-bond is absent in conformer 2, as the hydrogen and the amine nitrogen are trans to one another at a distance of 4.08 Å. Compound 4, which is not able to adopt H-bond-stabilizing conformations, is less stable. However, in aqueous solution, the superior stability of 6 is better rationalized in terms of the equilibria depicted in Schemes 3 and 4. Because the central nitrogen in 6 is protonated at physiological pH, the transition state to the formation of the doubly charged species F should have a higher energy when compared with that for C in Scheme 4. This may account for the slower rate of hydrolysis for 6 when compared with 4 under physiological conditions.

**Differential Growth Inhibitory Activity.** The potency of the two dansylated compounds was compared in MES-SA cells

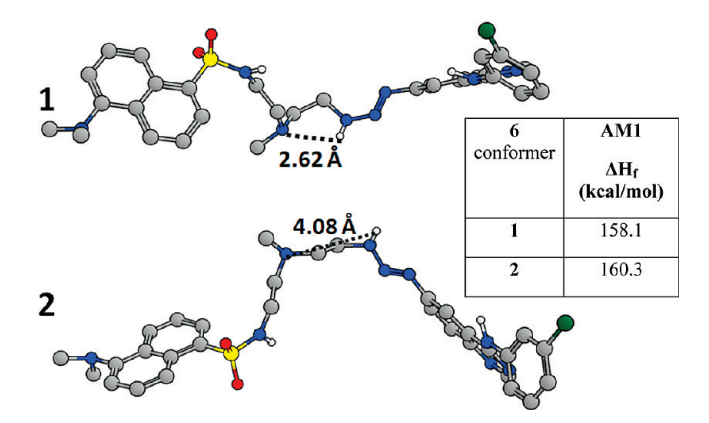


**Figure 1.** Molecular modeling using AM1 semi-empirical calculation of **6**. The H-N distances are given in  $\mathring{A}$ .

that do not express P-gp. MES-SA cells are also deprived of EGFR expression. <sup>16</sup> Therefore, the EGFR inhibitory activity of the quinazoline side chain would not influence the growth inhibitory effect of compounds **4** and **6**. The results showed that **6** was 3-fold more potent than **4** (Figure 2A). Perhaps the rapid decomposition of **4** compromised its optimal cellular delivery. We also observed a 2-fold stronger potency for **6** in the MDA-MB-468 breast cancer cells that express EGFR but do not express P-gp, <sup>21,22</sup> indicating that **6** was more potent than **4** regardless of the P-gp and the EGFR status of the cells (Figure 2B).

Because our primary goal was to compare the cellular penetration of the two compounds in P-gp-proficient and -deficient cells, we tested their effects on both MES-SA (P-gp-deficient) and its derived MES-SA/DX5 (P-gp-proficient) cells. The latter cell line expresses high levels of P-gp and is resistant to doxorubicin. Using the SRB assay, we showed a 20-fold difference between the sensitivity of MES-SA and MES-SA/DX5 to doxorubicin. In contrast, no significant difference (P > 0.05) was seen for both 4 and 6 in their potency against the two cell lines. Combi-molecule 6 was equally potent in both cell lines, and 4 was 1.6-fold more potent against MES-SA/DX5 than MES-SA, indicating an even greater potency in the cells that express P-gp.

Cellular Uptake. To verify whether the differential responses correlated with cell penetration, we exploited the

Scheme 3. Degradation Pathway of Compound 6 in Physiological Conditions

Scheme 4. Degradation Pathway of Compound 4 in Physiological Conditions

fluorescent properties of doxorubicin and those of compounds 4 and 6 to analyze their intracellular content by fluorescence microscopy and flow cytometry. We have previously used flow cytometry to analyze doxorubicin and compound 6 internalization in human breast tumor cells. 15,23

Fluorescence microscopy in the parental cell line showed a homogeneous distribution of doxorubicin (Figure 3A, upper panel) throughout the cell population. By contrast, in the MES-SA/DX5 cells (Figure 3A, lower panel), the distribution was heterogeneous with a fraction of the cell population emitting high fluorescence and another with poor to no

internalization of doxorubicin. As shown in Figure 4A, 4 and 6 penetrate the cells and decompose inside the cells to generate its bioactive species: EGFR inhibitor, blue fluorescence, and a DNA-damaging species, green fluorescence. The two colors were observed at similar intensity in both cell types. Flow cytometric analysis permitted the quantification of the proportion of cells that did not internalize doxorubicin (Figure 3B) and the combi-molecules (Figure 4B). For the more potent compound 6, at a dose range starting with the IC<sub>50</sub> for growth inhibition, no differential internalization between the two cell types was seen. In contrast, 40% of the

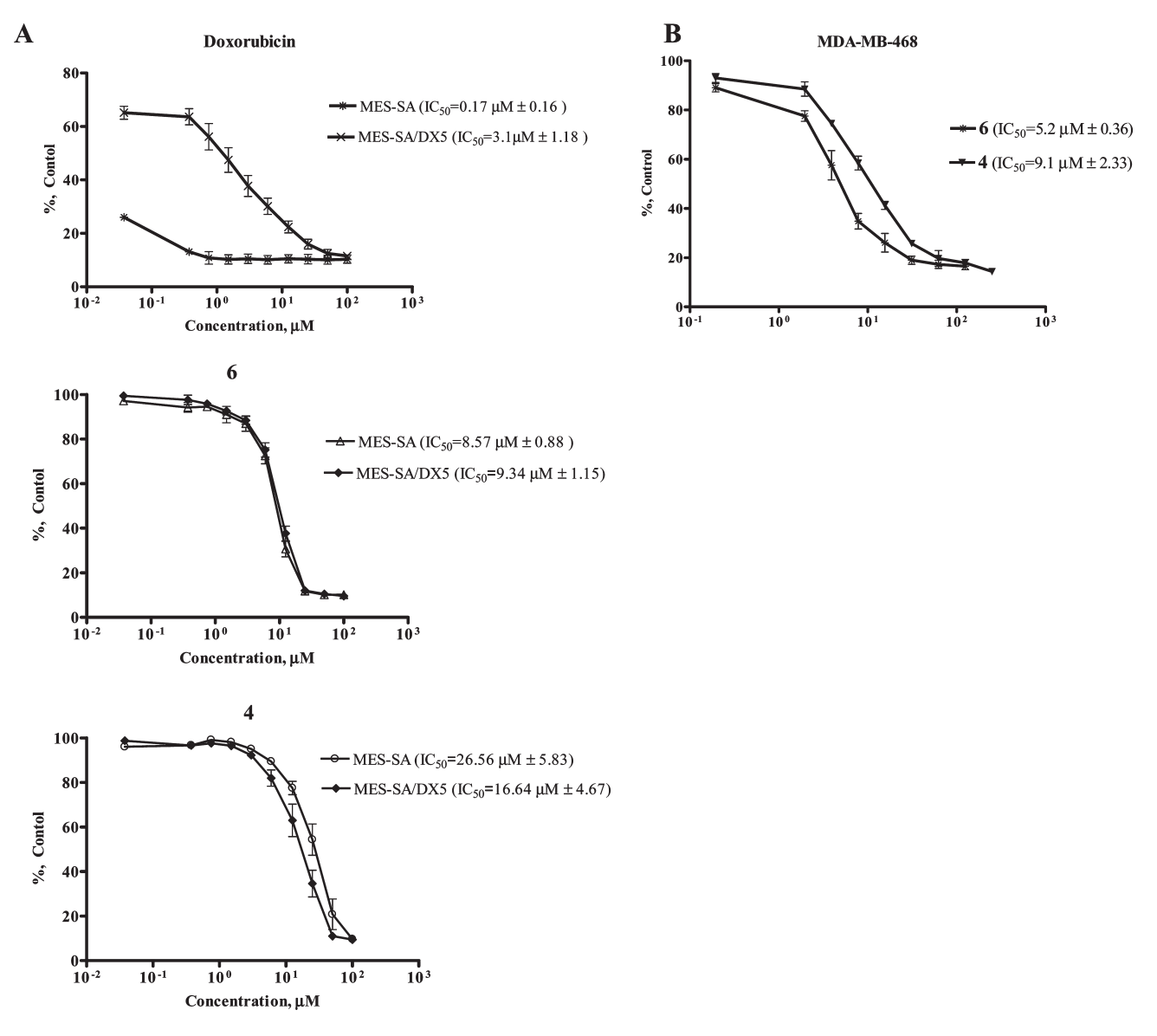


**Figure 2.** Growth inhibition of doxorubicin, **4**, and **6** by SRB assay. (A) Comparison of antiproliferative activity of doxorubicin, **4**, or **6** in MES-SA and MES-SA/DX5 cells after 96 h. (B) Growth inhibition of **4** and **6** in human breast MDA-MB-468 cells. Each point represents an average of two independent experiments performed in triplicate.

cell population could not internalize doxorubicin at this dose range.

DNA Damage. The DNA-damaging property of compounds 4 and 6 was assessed by alkaline comet assay. The visualization of DNA comet tails in both cell lines using fluorescence microscopy showed that 6 was a strong DNAdamaging agent, while 4 was not able to induce DNA damage (Figure 5). This result is consistent with the stability of the two molecules and also that of the putative dansylated alkyldiazonium released after degradation. The rapid decomposition of 4 seems again to limit its activity. Moreover, 6 damaged DNA in both cell lines with the same intensity, independently of P-gp status, which is in agreement with the growth inhibitory results, and also indicated that the combimolecule can penetrate and decompose inside the cells to deliver the DNA-damaging moiety (green fluorescence, Figure 4A). The levels of DNA damage induced by doxorubicin were also analyzed in the two cell types, and a differential response was seen with doxorubicin inducing a 2-fold greater number of DNA-damaged cells in the MES-SA

population when compared with MES-SA/DX5 (Figure 3C). Cells with a higher comet tail moment than the control were scored as damaged, and the data were presented as percent of cells with damaged DNA. This result was consistent with the differential level of doxorubicin uptake observed between these two cell types.

#### Conclusion

At the advanced stages of many cancers, drug transport is significantly affected by several mechanisms including P-gp-mediated drug efflux. <sup>1–5</sup> This presents a daunting challenge to drug development against advanced cancers. The combimolecules are designed to possess multiple targeting properties with the purpose of simultaneously blocking several signaling networks in the cells. To this end, several pharmacophores must be appended to one single core structure. Therefore, this leads to the branching of pharmacophores through bulky linkers that often affect the size of the resulting molecules and, as a result, their transport into the cells. It is now well-known that the greater the size of an agent is, the

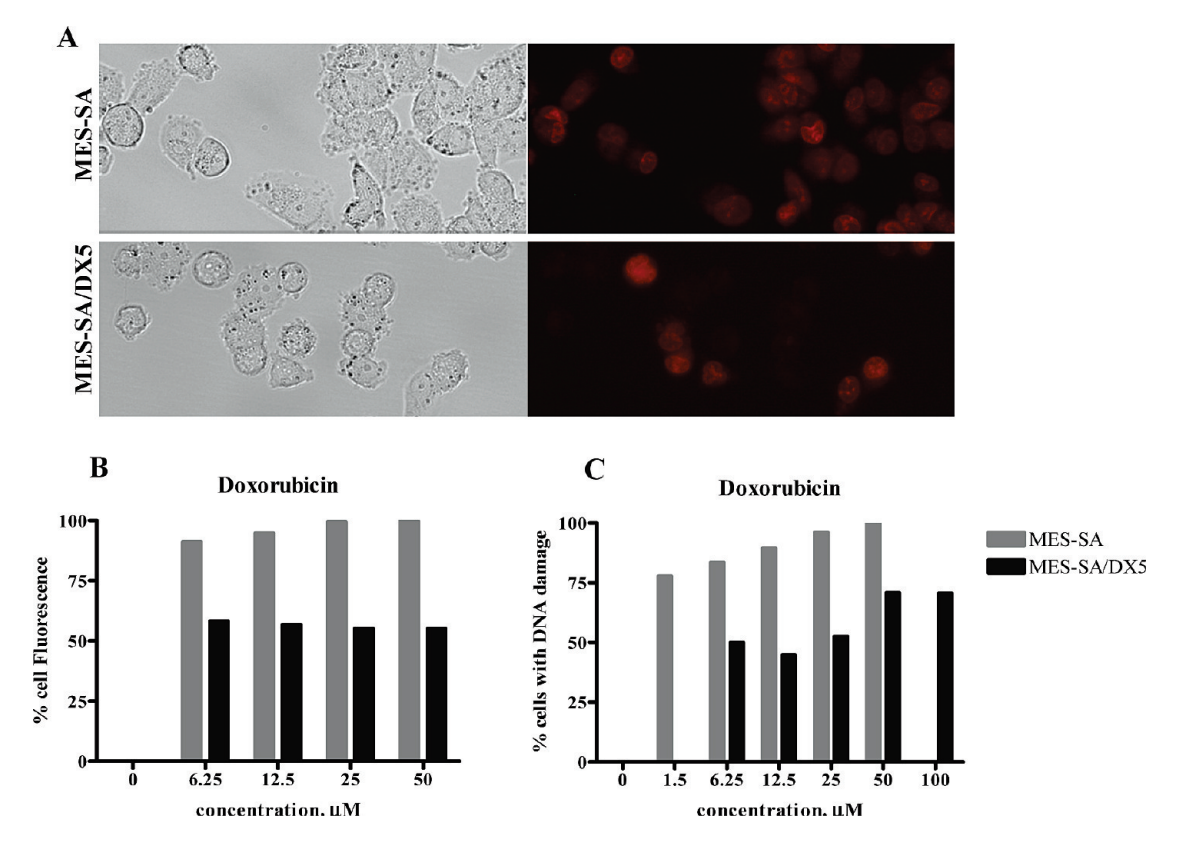


Figure 3. Cellular fluorescence and DNA damage by doxorubicin. (A) Intracellular accumulation of doxorubicin in P-gp-positive and -negative cells was determined by fluorescence microscopy. Cells were incubated with 25  $\mu$ M doxorubicin for 2 h and washed with PBS, and fluorescence was visualized with a Leica fluorescent microscope (40× magnification). (B) Cellular fluorescence of doxorubicin by FACS. The levels of accumulated fluorescence for doxorubicin (0, 6.25, 12.5, 25, and 50 µM) were quantified in MES-SA and MES-SA/DX5 cells after 2 h. (C) DNA damage induced by doxorubicin in MES-SA (0, 1.5, 6.25, 12.5, 25, and 50 \(mu\)M) and MES-SA/DX5 (0, 6.25, 12.5, 25, 50, and 100 \(mu\)M) cells. Cells were exposed for 2 h to doxorubicin, and DNA damage was measured using an alkaline comet assay. Fifty cells were scored from each dose, and the comet tail moment was calculated by comet IV software (Perceptive Instruments). Cells with a comet tail moment greater than that in the control were scored positive and expressed as percent of cells with damaged DNA.

more likely that its transport mechanism across the cell membrane will be influenced by efflux proteins. Here, we discovered that at least one mechanism of drug efflux may not prevent cell penetration by two prototypical combi-molecules designed to block EGFR-DNA and carrying a bulky fluorescence-labeled moiety. Although the molecular mechanism of such an important observation requires further elucidation, we believe that the fact that the combi-molecules are designed to decompose inside the cells to generate their bioactive species might be a mean by which the rapid efflux of the intact structure was impeded.

#### **Experimental Section**

Chemistry. <sup>1</sup>H NMR spectra and <sup>13</sup>C NMR spectra were recorded on a Varian 300 MHz spectrometer. Chemical shifts are given as  $\delta$  values in parts per million (ppm) and are referenced to the residual solvent proton or carbon peak. Mass spectrometry was performed by the McGill University Mass Spectroscopy Center, and electrospray ionization (ESI) spectra were performed on a Finnigan LC QDUO spectrometer. Data are reported as m/z (intensity relative to base peak = 100). Elemental analyses were carried out by GCL & Chemisar Laboratories (Guelph, Ontario, Canada). The analyses were done two times. All chemicals were purchased from Sigma-Aldrich. Dansyl chloride was purchased from Alfa Aesar, N-(2aminoethyl)-N-methylethanediamine was from Wako Pure Chemical Industries, Ltd., and mono-Fmoc-ethylenediamine hydrochloride was from Novabiochem. The purities of all compounds tested were > 95% as determined by elemental analysis.

Compound 1, 2-Dansyl-9-fluorenylmethyl N-(2-Aminoethyl)carbamate. 9-Fluorenylmethyl N-(2-aminoethyl)carbamate hydrochloride (500 mg, 1.57 mmol) was dissolved in water saturated with potassium carbonate and ethyl acetate (50 mL/50 mL). The mixture was cooled to 0 °C, and a solution of dansyl chloride (3 equiv) in ethyl acetate was added dropwise. The reaction mixture was stirred, and the temperature was raised to room temperature. After 4 h, the organic layer was separated, washed with brine twice and dried with magnesium sulfate, filtered, and evaporated to provide a yellowgreen oil, which was purified by trituration in ethyl ether. A white pure solid of compound 1 was obtained after filtration (742 mg, 92%). <sup>1</sup>H NMR (300 MHz, DMSO- $d_6$ ):  $\delta$  ppm 2.75 (m, 2H), 2.80 (s, 6H), 2.95 (m, 2H), 4.21 (m, 3H), 7.25 (m, 4H), 7.37 (m, 2H), 7.59 (m, 4H), 7.85 (d, J = 7.5 Hz, 1H), 7.99 (m, 1H), 8.08 (d, J = 7.5 Hz, 1H)1H), 8.24 (d, J = 8.1 Hz, 1H), 8.45 (d, J = 8.7 Hz, 1H).

Compound 2, Dansyl-N-(2-aminoethyl)amide. The Fmoc group was removed with morpholine/DMF 1/1 (2 mL) for 30 min at room temperature. The reaction mixture was evaporated, and the crude product was extracted with ethyl acetate and acidic water phase (pH 2). The aqueous phase was alkalinized to pH 5 and extracted with ethyl acetate to eliminate the secondary products from the aqueous layer. The pH was increased to 10, and this aqueous layer was extracted again with ethyl acetate. The organic layer was dried, and the magnesium sulfate was filtered and evaporated to provide pure free amine 2 (148 mg, 87%). <sup>1</sup>H NMR (300 MHz, DMSO- $d_6$ ):  $\delta$  ppm 2.45 (m, 2H), 2.75 (m, 2H), 2.81 (s, 6H), 7.24 (d, J = 7.2 Hz, 1H), 7.59 (q, J = 7.5 Hz, 2H, 8.09 (d, J = 7.2 Hz, 1H), 8.28 (d, J = 8.4 Hz, 1H),8.45 (d, J = 8.7 Hz, 1H).

Compound 5, Dansyl-N-(2-[(2-aminoethyl)-N-methylamino]ethyl)amide. Dansyl chloride (1 g, 3.71 mmol) was dissolved in 20 mL

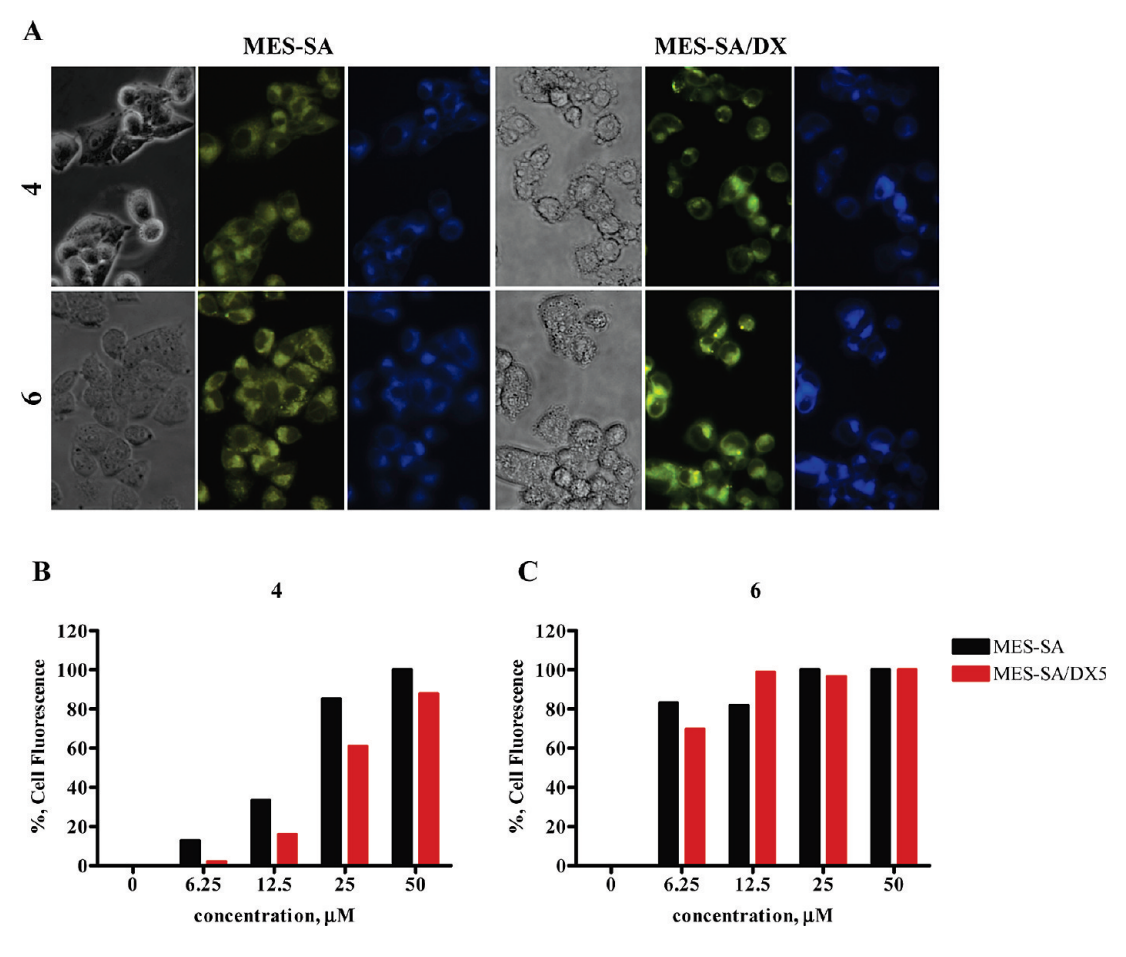


Figure 4. (A) Cellular fluorescence of 4 and 6 by fluorescence microscopy. MES-SA and MES-SA/DX5 cells were incubated with 4 and 6 for 2 h, and imaging was performed with Leica fluorescent microscope ( $40 \times$  magnification). Visualization of 4 and 6 degradation species: Blue aminoquinazoline and green dansylated species were imaged using individual filters. (B) Cellular fluorescence of 4 and 6 by FACS. The levels of accumulated fluorescence for 4 and 6 (0, 6.25, 12.5, 25, and 50  $\mu$ M) were quantified in MES-SA and MES-SA/DX5 cells by FACS, and results were analyzed with GraphPad Prism software.

of ethyl acetate and was added dropwise to a cold solution of N-(2-aminoethyl)-N-methylethanediamine (2.38 mL, 5 equiv) in 80 mL of ethyl acetate. The reaction mixture was stirred at 0 °C under argon. After 2 h, the solution was extracted with neutral water and acidic water (pH 2-3). This acidic water was alkalinized and was extracted with ethyl acetate two times. The organic layer was dried with magnesium sulfate, filtered, and evaporated to provide a yellow oil, which was purified by crystallization in a minimum of ethyl acetate. White pure crystals of compound 5 were obtained (1.117 g, 86%).  $^{1}$ H NMR (300 MHz, DMSO- $d_{6}$ ):  $\delta$  ppm 1.92 (s, 3H), 2.13 (t, J = 6.3 Hz, 2H), 2.21 (t, J = 6.7 Hz, 2H), 2.40 (t, J = 6.1 Hz, 2H), 2.81 (s, 6H), 2.84 (t, J = 6.9 Hz, 2H), 7.21 (d, J = 7.5 Hz, 1H), 7.58 (m, 2H), 8.11 (d, J = 7.2 Hz, 1H), 8.27 (d, J = 8.4 Hz, 1H), 8.43 (d, J = 8.1 Hz, 1H).

Compound 4. The diazonium compound 3 was synthesized as described in ref 14: Amino-anilinoquinazoline (50 mg, 0.184 mmol) was dissolved in dry acetonitrile (5 mL) under argon and cooled to −5 °C. Nitrosonium tetrafluoroborate (2 equiv) in acetonitrile was added directly. After 30 min at −5 °C, the resulting clear orange solution was added dropwise to another solution of compound 2 (1 equiv) in acetonitrile with triethylamine (2 equiv) at 0 °C, after which the mixture was extracted with ethyl acetate and brine. The organic layer was dried with potassium carbonate and evaporated to provide a brown residue, which was purified by serial trituration: First, the crude product was dissolved in a minimum of methylene chloride and precipitated with petroleum ether and after was triturated in ether/petroleum ether 1/4 to give after filtration a red-brown solid (93 mg, 88%).

<sup>1</sup>H NMR (300 MHz, DMSO- $d_6$ ): δ ppm 2.77 (s, 6H), 3.10 (m, 2H), 3.59 (m, 2H), 7.13 (d, J = 8.4 Hz, 1H), 7.22 (d, J = 7.5 Hz, 1H), 7.39 (m, 1H), 7.59 (m, 2H), 7.73 (d, J = 8.7 Hz, 1H), 7.86 (m, 2H), 8.13 (m, 2H), 8.27 (d, J = 8.7 Hz, 1H), 8.35 (s, 1H), 8.43 (d, J = 9.0 Hz, 1H), 8.58 (s, 1H), 9.89 (s, 1H), 10.59 (m, 1H). <sup>13</sup>C NMR (75 MHz, DMSO- $d_6$ ): δ ppm 158.13, 153.92, 152.05, 149.23, 148.90, 141.70, 136.29, 133.36, 130.71, 130.23, 129.74, 129.70, 129.50, 129.08, 128.61, 125.68, 124.28, 123.58, 121.89, 120.84, 119.71, 116.28, 115.82, 115.18, 51.72, 46.31, 45.72 (2C). ESI m/z 572.9 (MH<sup>+</sup> with <sup>35</sup>Cl). Anal. (C<sub>28</sub>H<sub>27</sub>ClN<sub>8</sub>O<sub>2</sub>S) C, H, N.

Compound 6. The diazonium compound 3 was still synthesized as previously described. 14 Amino-anilinoquinazoline (608 mg, 2.246 mmol) was dissolved in dry acetonitrile (80 mL) under argon and cooled to -5 °C. Nitrosonium tetrafluoroborate (2 equiv) in acetonitrile was added directly. After 30 min at -5 °C, the resulting clear solution was added dropwise to another solution of compound 5 (1 equiv) in acetonitrile with triethylamine (2 equiv) at 0 °C, after which the mixture was extracted with ethyl acetate and brine. The organic layer was dried with potassium carbonate and evaporated to provide a brown residue, which was purified by serial trituration. The crude product was dissolved in a minimum of methylene chloride and precipitated with petroleum ether, after which it was triturated in ether/petroleum ether 1/4 to give after filtration a red-brown solid (1.2 g, 85%). <sup>1</sup>H NMR (300 MHz, DMSO-*d*<sub>6</sub>): δ ppm 1.99 (s, 3H), 2.32 (m, 2H), 2.52 (m, 2H), 2.77 (s, 6H), 2.90 (m, 2H), 3.53 (m, 2H), 7.12 to 7.21 (m, 2H), 7.39 (m, 1H), 7.55 (m, 2H), 7.75 to 7.97 (m, 4H), 8.12 (m, 2H), 8.30 (d, J = 8.4 Hz, 1H), 8.40

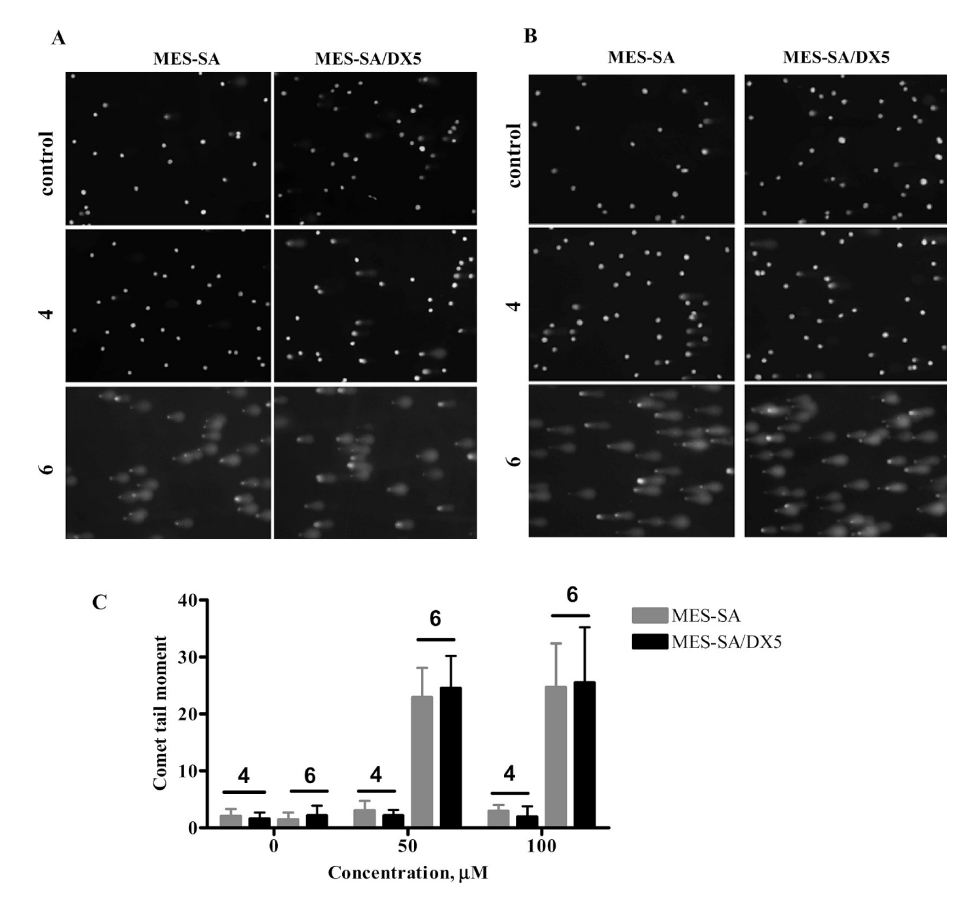


Figure 5. DNA damage induced by 4 and 6 at 50 (A) and 100  $\mu$ M (B). MES-SA and MES-SA/DX5 cells were exposed to each combi-molecule for 2 h followed by assessment of drug-induced DNA damage using an alkaline comet assay. Visualization of DNA comets in both cell lines by fluorescence microscopy (10× magnification) after staining with SYBR Gold. (C) Fifty comets were scored, and the comet tail moment was quantified by comet IV software (Perceptive Instruments). Two independent experiments were averaged for each cell line, and data were analyzed with GraphPad Prism software.

(m, 1H), 8.43 (s, 1H), 8.60 (s, 1H). <sup>13</sup>C NMR (75 MHz, DMSO $d_6$ ):  $\delta$  ppm 158.10, 153.83, 152.01, 149.73, 148.78, 141.75, 136.69, 133.37, 130.72, 130.07, 129.76, 129.69, 129.56, 128.92, 128.54, 125.40, 124.25, 123.55, 121.83, 120.79, 119.77, 116.37, 115.76, 115.29, 57.04 (2C), 53.84, 46.40, 45.72 (2C), 41.51. ESI m/z 632.1 (MH $^+$  with  $^{35}$ Cl). Anal. (C<sub>31</sub>H<sub>34</sub>ClN<sub>9</sub>O<sub>2</sub>S) C, H, N.

Half-Lives. The half-lives of 4 and 6 under physiological conditions were studied by UV spectrophotometer, Farmacia Biotech Ultrospec 2000. The compounds were dissolved in minimum volume of DMSO and diluted with DMEM supplemented with 10% FBS, and the absorbances were read at 335 nm for 4 and 350 nm for 6 in a quartz UV cell maintained at 37 °C with a circulating water bath. The experiment was repeated three times for each compound. The half-life was estimated by a one-phase exponential decay curve-fit method using the Graph-Pad software package (GraphPad software, Inc., San Diego, CA). The thermometer was Traceable VWR digital with  $\pm 0.005$  °C accuracy.

Molecular Modeling. Molecular modeling was performed with MOE software (version 2006.08) available from Chemical Computing Group Inc. (Montreal, Quebec, Canada; www. chemcomp.com).

Biology. Cell Culture. All three cell lines were purchased from the American Type Culture Collection (ATCC, Manassas, VA). Human uterine sarcoma cells, MES-SA, and MES-SA/DX5 (ATCC: CRL-1976 and CRL-1977, respectively) were maintained in McCoy 5A medium, and human breast cancer cells MDA-MB-468 were cultured in DMEM. All media were supplemented with 10% FBS, 1.5 mM L-glutamine (Wisent Inc., St.-Bruno, Canada), and 100 µg/mL penicillin/streptomycin (GibcoBRL, Gaithersburg, MD). Cells were grown exponentially at 37 °C in a humidified atmosphere of 95% air and 5% carbon dioxide. In all assays, cells were plated 24 h before drug treatment.

**Drug Treatment.** Compounds 4 and 6 were synthesized in our laboratory, and doxorubicin hydrochloride was purchased from the hospital drug store (Mayne Pharma Inc., Montreal). In all assays, molecules were dissolved in DMSO (50 mM stock solution), and doxorubicin was dissolved in sterile water (2 mg/mL stock solution) and subsequently diluted in McCoy 5A medium before it was added to cells. The concentration of DMSO never exceeded 0.1% (v/v) during treatment.

Growth Inhibition Assay. MES-SA, MES-SA/DX5, and MDA-MB-468 cells were plated at a density of 5000 cells/well in 96-well flat-bottomed microtiter plates (100  $\mu$ L of cell/well). Cells were allowed to attach overnight and then were treated with different drug concentrations for 96 h. Thereafter, cells were fixed using 50 µL of 50% trichloroacetic acid for 60 min at 4 °C, washed four times with water, stained with sulforhodamine B (SRB 0.4%) for 2 h at room temperature, rinsed four times with 1% acetic acid, and allowed to dry.24 The resulting colored residue was dissolved in 200  $\mu$ L of Tris base (10 mM, pH 10.0), and the optical density was recorded at a wavelength of 492 nm using a Bio-Rad microplate reader (model 2550). The results were analyzed by GraphPad Prism (GraphPad Software, Inc.), and the sigmoidal dose-response curve was used to determine 50% cell growth inhibitory concentration (IC<sub>50</sub>). Each point represents the average of at least three independent experiments run in triplicate.

DNA Damage by Alkaline Comet Assay. The alkaline comet assay was performed as previously described. 25-27 Briefly, cells were exposed to doxorubicin  $(0, 1.5, 6.25, 12.5, 25, \text{ and } 50 \,\mu\text{M})$ ,

4, and 6 (0, 50, and 100  $\mu$ M) for 2 h, harvested by trypsinization, collected in ice-cold PBS by centrifugation at 3000 rpm for 5 min, and then resuspended in PBS at  $1 \times 10^6$  cells/mL. Cells were mixed with low melting point agarose (0.7%) in PBS at 37 °C (final dilution 1:10), followed by layering the agarose/cells suspension on GelBond film (Lonza, Rockland, ME). The agarose/cell suspension was allowed to solidify for 10 min and then immediately placed in lysis buffer [2.5 M NaCl, 100 mM tetra-sodium EDTA, 10 mM Tris-base, 1% (w/v) N-lauroylsarcosine, 10% (v/v) DMSO, and 1% (v/v) triton X-100, pH 10.0] overnight at 4 °C. Thereafter, the gels were rinsed with distilled water, equilibrated in alkaline electrophoresis buffer [300 mM NaOH, 10 mM tetra-sodium EDTA, 7 mM 8-hydroxyquinoline, 2% (v/v) DMSO, pH 13.0] for 30 min at room temperature, and electrophoresed at 20 V for 25 min in fresh eletrophoresis buffer. The gels were subsequently neutralized in 1 M ammonium acetate and then dehydrated in 100% ethanol overnight. Comets were visualized at 10× magnification using Leica fluorescent microscope after staining with SYBR Gold (1:10000, Molecular Probes, Eugene, OR) for 45 min.

**Fluorescence Microscopy.** Fluorescent properties of molecules were used to image drug transport efficiency and intracellular accumulation. MES-SA and MES-SA/DX5 cells were plated at 70% confluence in six-well plates, allowed to adhere overnight, and treated with 0, 25, and 50  $\mu$ M **4**, **6**, or doxorubicin. After 2 h, cells were washed twice with PBS and were directly imaged at  $40\times$  using Leica fluorescent microscope (Leica DFC300FX camera) without fixation.

Flow Cytometry Analysis of Intracellular Drug Fluorescence. MES-SA and MES-SA/DX5 cells were plated at  $0.5 \times 10^6$  cells per well in six-well plates, allowed to adhere overnight, and incubated in the presence of **4** and **6** or doxorubicin (0, 1.25, 6.25, 12.5, 25, and 50  $\mu$ M) for 2 h. Cells were collected by trypsinization, washed twice with PBS, pelleted by centrifugation, and resuspended in 300 µL of PBS supplemented with 1% FBS to prevent cell clumping. Intracellular fluorescence levels were measured using a BD LSR flow cytometer (BD Biosciences, San Jose, CA). For 4 and 6, fluorescence was detected at two wavelengths for the two fluorescent products hydrolyzed in the cell: the aminoquinazoline [excitation at 340 nm and emission at 451 nm (blue)] and the dansylated DNAdamaging species [excitation at 340 nm and emission at 525 nm (green)]. To test the transport efficiency of P-gp-proficient cells (MES-SA/DX5) in comparison with the parental MES-SA P-gp-deficient cells, we quantified the fluorescence levels of doxorubicin [excitation at 480 nm and emission at 560-590 nm (red)] and recorded the percentage of doxorubicin-positive P-pg-expressing cells (MES-SA/DX5). FACS results were analyzed with GraphPad Prism software.

Acknowledgment. We thank the National Cancer Institute of Canada (NCIC Grant 018475), Canadian Institutes of Cancer Research (Grant FRN 49440), and Fonds de la Recherche en Santé du Québec doctoral award (M.T.) for financial support. We gratefully acknowledge Nadim K. Saade from the Department of Chemistry, McGill University, for mass spectra.

#### References

- Ramachandra, M.; Ambudkar, S. V.; Chen, D.; Hrycyna, C. A.; Dey, S.; Gottesman, M. M.; Pastan, I. Human P-Glycoprotein Exhibits Reduced Affinity for Substrates during a Catalytic Transition State. *Biochemistry* 1998, 37, 5010–5019.
- (2) Sharom, F. J. The P-glycoprotein efflux pump: how does it transport drugs? J. Membr. Biol. 1997, 160, 161–175.
- (3) Szakacs, G.; Paterson, J. K.; Ludwig, J. A.; Booth-Genthe, C.; Gottesman, M. M. Targeting multidrug resistance in cancer. *Nat. Rev. Drug Discovery* 2006, 5, 219–234.
- (4) Longley, D. B.; Johnston, P. G. Molecular mechanisms of drug resistance. J. Pathol. 2005, 205, 275–292.

- (5) Loo, T. W.; Clarke, D. M. Recent progress in understanding the mechanism of P-glycoprotein-mediated drug efflux. J. Membr. Biol. 2005, 206, 173–185.
- (6) Aller, S. G.; Yu, J.; Ward, A.; Weng, Y.; Chittaboina, S.; Zhuo, R.; Harrell, P. M.; Trinh, Y. T.; Zhang, Q.; Urbatsch, I. L.; Chang, G. Structure of P-Glycoprotein Reveals a Molecular Basis for Poly-Specific Drug Binding. Science (Washington, DC, U. S.) 2009, 323, 1718–1722.
- (7) Perez, R. P.; Hamilton, T. C.; Ozols, R. F.; Young, R. C. Mechanisms and modulation of resistance to chemotherapy in ovarian cancer. *Cancer* 1993, 71, 1571–80.
- (8) Turk, D.; Hall, M. D.; Chu, B. F.; Ludwig, J. A.; Fales, H. M.; Gottesman, M. M.; Szakacs, G. Identification of Compounds Selectively Killing Multidrug-Resistant Cancer Cells. *Cancer Res.* 2009, 69, 8293–8301.
- (9) Brahimi, F.; Matheson, S. L.; Dudouit, F.; McNamee, J. P.; Tari, A. M.; Jean-Claude, B. J. Inhibition of epidermal growth factor receptor-mediated signaling by "Combi-Triazene" BJ2000, a new probe for Combi-Targeting postulates. J. Pharmacol. Exp. Ther. 2002, 303, 238–246.
- (10) Brahimi, F.; Rachid, Z.; McNamee, J. P.; Alaoui-Jamali, M. A.; Tari, A. M.; Jean-Claude, B. J. Mechanism of action of a novel "combi-triazene" engineered to possess a polar functional group on the alkylating moiety: Evidence for enhancement of potency. *Biochem. Pharmacol.* 2005, 70, 511–519.
- (11) Brahimi, F.; Rachid, Z.; Qiu, Q.; McNamee, J. P.; Li, Y.-J.; Tari, A. M.; Jean-Claude, B. J. Multiple mechanisms of action of ZR2002 in human breast cancer cells: A novel combi-molecule designed to block signaling mediated by the ERB family of oncogenes and to damage genomic DNA. *Int. J. Cancer* 2004, *112*, 484–491.
- damage genomic DNA. *Int. J. Cancer* **2004**, *112*, 484–491.

  (12) Domarkas, J.; Dudouit, F.; Williams, C.; Qiyu, Q.; Banerjee, R.; Brahimi, F.; Jean-Claude, B. J. The Combi-Targeting Concept: Synthesis of Stable Nitrosoureas Designed to Inhibit the Epidermal Growth Factor Receptor (EGFR). *J. Med. Chem.* **2006**, *49*, 3544–3552.
- (13) Banerjee, R.; Rachid, Z.; McNamee, J.; Jean-Claude, B. J. Synthesis of a Prodrug Designed To Release Multiple Inhibitors of the Epidermal Growth Factor Receptor Tyrosine Kinase and an Alkylating Agent: A Novel Tumor Targeting Concept. *J. Med. Chem.* 2003, 46, 5546–5551.
- (14) Rachid, Z.; Brahimi, F.; Katsoulas, A.; Teoh, N.; Jean-Claude, B. J. The Combi-Targeting Concept: Chemical Dissection of the Dual Targeting Properties of a Series of "Combi-Triazenes. J. Med. Chem. 2003, 46, 4313–4321.
- (15) Todorova, M.; Larroque, A.-L.; Dauphin-Pierre, S.; Fang, Y. Q.; Jean-Claude, B. J. Cellular imaging and signaling to AL237, a fluorescent-labeled probe for the combi-targeting approach to tumor targeting. *Mol. Cancer Ther.* 2009, accepted for publication.
- (16) Yip, W. L.; Weyergang, A.; Berg, K.; Tonnesen, H. H.; Selbo, P. K. Targeted delivery and enhanced cytotoxicity of cetuximab-saporin by photochemical internalization in EGFR-positive cancer cells. *Mol. Pharmaceutics* 2007, 4, 241–451.
- (17) Harker, W. G.; MacKintosh, F. R.; Sikic, B. I. Development and characterization of a human sarcoma cell line, MES-SA, sensitive to multiple drugs. *Cancer Res.* 1983, 43, 4943–4950.
- (18) Harker, W. G., Sikic, B. I. Multidrug (pleiotropic) resistance in doxorubicin-selected variants of the human sarcoma cell line MES-SA. *Cancer Res.* 1985, 45, 4091–4096.
- (19) Koo, J. S.; Choi, W. C.; Rhee, Y. H.; Lee, H. J.; Lee, E. O.; Ahn, K. S.; Bae, H. S.; Ahn, K. S.; Kang, J. M.; Choi, S. U.; Kim, M. O.; Lu, J.; Kim, S. H. Quinoline derivative KB3-1 potentiates paclitaxel induced cytotoxicity and cycle arrest via multidrug resistance reversal in MES-SA/DX5 cancer cells. *Life Sci* 2008, 83, 700-708.
- (20) Merayo, N.; Rachid, Z.; Qiu, Q.; Brahimi, F.; Jean-Claude, B. J. The combi-targeting concept: Evidence for the formation of a novel inhibitor in vivo. *Anti-Cancer Drugs* 2006, 17, 165–171.
- (21) Wang, H.; Giuliano, A. E.; Cabot, M. C. Enhanced de novo ceramide generation through activation of serine palmitoyltransferase by the P-glycoprotein antagonist SDZ PSC 833 in breast cancer cells. *Mol. Cancer Ther.* **2002**, *1*, 719–726.
- (22) Liem, A. A.; Appleyard, M. V.; O'Neill, M. A.; Hupp, T. R.; Chamberlain, M. P.; Thompson, A. M. Doxorubicin and vinorelbine act independently via p53 expression and p38 activation respectively in breast cancer cell lines. *Br. J. Cancer* **2003**, *88*, 1281–1284.
- (23) Panasci, L.; Jean-Claude, B. J.; Vasilescu, D.; Mustafa, A.; Damian, S.; Damian, Z.; Georges, E.; Liu, Z.; Batist, G.; Leyland-Jones, B. Sensitization to doxorubicin resistance in breast cancer cell lines by tamoxifen and megestrol acetate. *Biochem. Pharmacol.* 1996, 52, 1097–1102.
- (24) Skehan, P.; Storeng, R.; Scudiero, D.; Monks, A.; McMahon, J.; Vistica, D.; Warren, J. T.; Bokesch, H.; Kenney, S.; Boyd, M. R. New colorimetric cytotoxicity assay for anticancer-drug screening. *J. Natl. Cancer Inst.* **1990**, *82*, 1107–1112.

- (25) Matheson, S. L.; McNamee, J. P.; Wang, T.; Alaoui-Jamali, M. A.; Tari, A. M.; Jean-Claude, B. J. The combi-targeting concept: Dissection of the binary mechanism of action of the combi-triazene SMA41 in vitro and antitumor activity in vivo. J. Pharmacol. Exp. Ther. 2004, 311, 1163–1170.
- (26) Olive, P. L.; Banath, J. P. The comet assay: A method to measure DNA damage in individual cells. *Nat. Protoc.* 2006, *1*, 23–29.
  (27) McNamee, J. P.; McLean, J. R.; Ferrarotto, C. L.; Bellier, P. V. Comet assay: Rapid processing of multiple samples. *Mutat. Res.* 2000, 466, 63–69.